APPLICATIONS OF EFFECTIVE FIELD THEORY AT THE INTERSECTION OF NUCLEAR AND PARTICLE PHYSICS

by

Regina Staropoli de Azevedo

A Dissertation Submitted to the Faculty of the

DEPARTMENT OF PHYSICS

In Partial Fulfillment of the Requirements
For the Degree of

DOCTOR OF PHILOSOPHY

In the Graduate College

THE UNIVERSITY OF ARIZONA

2012

THE UNIVERSITY OF ARIZONA
GRADUATE COLLEGE

As members of the Dissertation Committee, we certify that we have read the dissertation prepared by Regina Staropoli de Azevedo
entitled Applications of Effective Field Theory at the Intersection of Nuclear and Particle Physics
and recommend that it be accepted as fulfilling the dissertation requirement for the Degree of Doctor of Philosophy.

Ubirajara van Kolck — Date: 9 May 2012

Sean Fleming — Date: 9 May 2012

Shufang Su — Date: 9 May 2012

Michael Shupe — Date: 9 May 2012

John Rutherfoord — Date: 9 May 2012

Final approval and acceptance of this dissertation is contingent upon the candidate's submission of the final copies of the dissertation to the Graduate College.
I hereby certify that I have read this dissertation prepared under my direction and recommend that it be accepted as fulfilling the dissertation requirement.

Dissertation Director: Ubirajara van Kolck — Date: 9 May 2012

STATEMENT BY AUTHOR

This dissertation has been submitted in partial fulfillment of requirements for an advanced degree at the University of Arizona and is deposited in the University Library to be made available to borrowers under rules of the Library.

Brief quotations from this dissertation are allowable without special permission, provided that accurate acknowledgment of source is made. Requests for permission for extended quotation from or reproduction of this manuscript in whole or in part may be granted by the head of the major department or the Dean of the Graduate College when in his or her judgment the proposed use of the material is in the interests of scholarship. In all other instances, however, permission must be obtained from the author.

SIGNED: Regina Staropoli de Azevedo

ACKNOWLEDGEMENTS

First of all, I am very grateful to God for giving me strength to face my health problems and to write this dissertation. Without His help, I would not be healed today.

There is a large amount of people without whose support this dissertation would not exist. Hence, it is impossible to thank them all, so those whom I forget, please forgive me.

I am greatly indebted to my advisor, Prof. Bira van Kolck, for teaching me the physics that this dissertation is based upon, and for showing me the beauty of Effective Field Theories approach to problems in QCD. Most of the work in this dissertation would not have been possible without him.

I can not be thankful enough for the collaboration of Emanuele Mereguetti and Bingwei Long, from whom I not only enjoyed the time we spent working together, but also their great friendship. They, both, deserve credit for an ample part of this dissertation. I am particularly grateful to Emanuele for putting up with me in the last four yeas.

I have to mention Dr. Roger Haar, Prof. Ke Chiang (Johnny) Hsieh and Prof. Sean Fleming for not only teaching me a lot of physics, but also for being great friends and for always encouraging me to continue my studies when I doubted myself. And Prof. Michael Shupe and Prof. John Rutherfoord for their great knowledge and kindness. My knowledge in Quantum Field Theory and Nuclear Physics was abroaden thanks to the courses of Prof. Zackaria Chacko, Prof. Shufang Su and Prof. Bruce Barrett.

The Department of Physics has been a friendly environment to me throughout these past seven years. I am blessed to have found friends like Elizabeth Todd, Erica McEvoy, Chiara Paleari, Swati Singh, Micheal Kruse, Sybil DeClark, Michelle Solis, Steve Steinke, Matt Leone, Sam Magill, Robert Gill, and many others, whom made my life a little bit easier. Outside the Department, friends like Margo Haar, Noe Badillo, Elizabeth Riedel, Monica, Martha and Tina Grecchi, Mackenzie Coleman, and all my brazilian friends, they are too many to count, whom told me that I could do it. And I thank the U.S. Department of Energy for the financial support.

And, then, there my parents, Isaura and Darcio. I owe to them more than I could possibly think. Even thoug they never really liked it, they supported my purpose in following my career away from home. I regret that I could not spend more time with them. All of my accomplishments are also their accomplishments

Last, but not least, there is Angel, an angel sent by God to take care of and to comfort me in the moments of despair. Thank you for being one of the most beautiful thing in the world and for just being there.

DEDICATION

To Isaura, Darcio, Ricardo, Rafael and Eliza,
whose every important dates I missed to write this dissertation.
I love you.

TABLE OF CONTENTS

LIST OF FIGURES 8

LIST OF TABLES 11

ABSTRACT 12

CHAPTER 1 INTRODUCTION 14
1.1 HQET, NRQCD and an example of how to use an EFT 16
1.2 Chiral Perturbation Theory 23
1.3 Perturbative Pions and One-Pion Exchange 33
1.4 Soft Collinear Effective Theory 38

CHAPTER 2 PION-PION SCATTERING AND ELECTRON-POSITRON ANNIHILATION IN THE RHO REGION WITH VECTOR SYMMETRY 45
2.1 Introduction 45
2.2 Construction of the Lagrangian 48
2.3 Power Counting Near the Rho Peak 58
2.3.1 $\pi\pi \to \pi\pi$ 60
2.3.2 $e^+e^- \to \pi\pi$ 61
2.4 Main Ingredients 63
2.4.1 Rho Self-Energy 63
2.4.2 Photon-Rho Mixing 66
2.5 Cross Sections 68
2.5.1 $\pi\pi \to \pi\pi$ 68
2.5.2 $e^+e^- \to \pi^+\pi^-$ 70
2.6 Comparison to Data 73
2.6.1 $e^+e^- \to \pi^+\pi^-$ 73
2.6.2 $\pi\pi \to \pi\pi$ 76
2.7 Conclusion 76

CHAPTER 3 RENORMALIZATION OF PION EXCHANGE WITH AUXILIARY FIELDS AND A PERTURBATIVE SOLUTION FOR THE DEUTERON 82
3.1 Introduction 82
3.2 Lagrangian 85
3.3 Two-Nucleon Potential in Momentum Space 86

TABLE OF CONTENTS – Continued

3.4 Two-Nucleon Potential in Coordinate Space 88
3.5 Limiting Cases 90
3.6 Deuteron Binding Energy 93
3.7 Perturbative Solution 95
3.7.1 Sharp cutoff 100
3.7.2 Gaussian cutoff 103
3.8 Conclusions and Outlook 105

CHAPTER 4 EXCLUSIVE DECAYS OF χ_{bJ} AND η_b INTO TWO CHARMED MESONS 107
4.1 Introduction 107
4.2 Degrees of freedom and the Effective Field Theories 110
4.3 NRQCD + SCET 114
4.3.1 Matching 114
4.3.2 Running 116
4.4 pNRQCD + bHQET 122
4.4.1 Matching 122
4.4.2 Running 129
4.5 Decay Rates and Phenomenology 132
4.6 Conclusions 142

CHAPTER 5 CONCLUSION 147

APPENDIX A CONNECTION BETWEEN VECTOR EFT AND CHIRAL PERTURBATION THEORY 151

APPENDIX B PION SELF-ENERGY 154

APPENDIX C DECAYS OF THE RHO 157
C.1 $\rho \to \pi\pi$ 157
C.2 $\rho \to e^+e^-$ 158

APPENDIX D SOLUTION OF THE RUNNING EQUATION IN pNRQCD AND bHQET 160

APPENDIX E BOOST TRANSFORMATION OF THE D-MESON DISTRIBUTION AMPLITUDE 165

REFERENCES 168

LIST OF FIGURES

Figure 2.1 Self-energy $i\Pi^{\mu\nu}$ of the rho meson. A solid (dashed) line represents a rho (pion). Vertices are from the LO Lagrangian. . . 60

Figure 2.2 Dressed rho propagator $iD^{\mu\nu}$, where the self-energy is resummed. 60

Figure 2.3 LO pion-pion scattering amplitude $i\mathcal{T}^{(0)}_{\pi\pi}$ around the rho peak. 61

Figure 2.4 LO amplitude $i\mathcal{T}^{(0)}_{ee}$ for annihilation of a lepton-antilepton pair into two pions around the rho peak. A wavy line (solid line with arrow) represents a photon (fermion), and the shaded blob denotes the time-like pion form factor $F_\pi(s)$. 61

Figure 2.5 Photon-rho mixing $i\Xi^{\mu\nu}$. The circled circle denotes a vertex from the NLO Lagrangian. 62

Figure 2.6 Pion form factor $F_\pi(s)$ in Vector EFT. 62

Figure 2.7 $e^+e^- \to \pi\pi$ cross section, $\sigma_{ee}(nb)$, as a function of the center-of-mass energy, $\sqrt{s}$. The dot-dashed, full, dotted and the thick-dashed lines represent the cross sections obtained in Vector EFT around rho meson, in Vector EFT using "higher-order calculations" in the cross-section kinematics, in Vector EFT using a "higher-order decay width", and in ChPT, respectively. The bullets, squares, triangle, and diamond represent the experimental data AKMETSHIN 07 (Experiment NOVOSIBIRKSK - CMD - 2) [72], ACHASOV 06 (Experiment NOVOSIBIRSK-SND) [73] and BARKOV 85 (Experiment OLYA Part I and Part II) [74], respectively. The error bars are included, but they are very small to be seen. 80

Figure 2.8 $\pi\pi \to \pi\pi$ phase-shift, $\delta^1_1(^o)$, as a function of the center-of-mass energy, $\sqrt{s}$. The dot-dashed, dotted and thick dashed-lines represent the phase-shifts in Vector EFT, using "higher-order-rho-decay width" in Vector EFT, and in ChPT, respectively. The bullets and squares represent the experimental data from Protopopescu [75] and Estabrooks [76], respectively. The error bars are small, but included. 81

Figure 4.1 Matching QCD onto EFT_I. On the r.h.s., the double lines represent the non-relativistic b ($\bar{b}$) (anti)quark, while the dashed lines represent the collinear c ($\bar{c}$) (anti)quark. 114

Figure 4.2 Soft diagrams at one loop. 117

LIST OF FIGURES – Continued

Figure 4.3 Ultrasoft diagrams at one loop. 117
Figure 4.4 Collinear diagrams at one loop. 118
Figure 4.5 Matching NRQCD + SCET onto pNRQCD + bHQET. On the r.h.s. the double solid lines represent heavy b ($\bar{b}$) (anti)quarks, the double dashed lines bHQET c ($\bar{c}$) (anti)quarks, and the single dashed lines collinear light quarks. 123
Figure 4.6 One-loop diagrams in pNRQCD. The first diagram contains insertions of quark-antiquark potentials. In the second diagram the gluon is ultrasoft. 130
Figure 4.7 One-loop diagrams in bHQET. There are three analogous diagrams for the other copy of bHQET. 130
Figure 4.8 $\Gamma(\chi_{b0} \to PP)$ as a function of λ_D, calculated with the distribution amplitudes $\phi^{\rm Exp}$ (*top*) and $\phi^{\rm Braun}$ (*bottom*). The dash dotted and solid lines denote the NLL-resummed decay rate. For comparison, the decay rate without resummation is also shown, denoted by dash double-dotted (*top*) and dashed (*bottom*) lines. For $\phi^{\rm Braun}$ we vary the parameter σ_D from $\sigma_D = 1$ (lower curve) to $\sigma_D = 1.4$ (middle curve) to $\sigma_D = 1.8$ (upper curve). 136
Figure 4.9 $\Gamma(\chi_{b0} \to PP)$ as a function λ_D. The dash dotted line denotes the decay rate calculated with $\phi^{\rm Exp}$, while the three solid lines with $\phi^{\rm Braun}$. For $\phi^{\rm Braun}$ we vary the value of the parameter σ_D from $\sigma_D = 1$ (lower curve) to $\sigma_D = 1.4$ (middle curve) to $\sigma_D = 1.8$ (upper curve). 137
Figure 4.10 *Top*: Scale dependence of $\Gamma(\chi_{b0} \to PP)$ on the matching scale μ_b. We vary μ_b from a central value $\mu_b = 2m_b$ (solid line) to a maximum of $\mu_b = 20$ GeV (dashed line) and a minimum of $\mu_b = 5$ GeV (dotted line). The dashed and dotted lines overlap almost perfectly. *Bottom*: Scale dependence of $\Gamma(\chi_{b0} \to PP)$ on the matching scale μ_c'. We varied μ_c' from a central value of $\mu_c' = m_c$ (solid line) to a maximum of $\mu_c' = 2.5$ GeV (dashed line) and a minimum of $\mu_c' = 1.2$ GeV (dotted line). 139
Figure 4.11 *First two*: $\Gamma(\eta_b \to PV_L + \text{c.c.})$ as a function of λ_D and δ, computed using exponential distribution amplitudes $\phi_P^{\rm Exp}$ and $\phi_{V_L}^{\rm Exp}$. *Last two*: $\Gamma(\eta_b \to PV_L + \text{c.c.})$ as a function of λ_D and $|\sigma_{D_L^*} - \sigma_D|/\sigma$, computed with the Braun distribution amplitudes $\phi_P^{\rm Braun}$ and $\phi_{V_L}^{\rm Braun}$. 145

LIST OF FIGURES – Continued

Figure 4.12 Branching ratios $\mathcal{B}(\chi_{b0} \to PP)$ (*top*) and $\mathcal{B}(\eta_b \to PV_L +$ c.c.) (*bottom*). The latter is computed using the distribution amplitude ϕ^{Braun}. 146

Figure A.1 LO contributions to pion-pion scattering at low energies in (a) ChPT and (b) Vector EFT. 152
Figure A.2 LO pion form factor at low energies. 152

Figure B.1 Pion self-energy $-i\Sigma$ in Vector EFT. 155
Figure B.2 Dressed pion propagator iD in terms of multiple insertions of the pion self-energy. 155

Figure C.1 Decays (a) $\rho \to \pi\pi$ and (b) $\rho \to e^+e^-$ at LO. 158

LIST OF TABLES

1.1 Degrees of freedom in SCET and their respective momentum, scaling with λ. A similar analysis can bound in Ref. [32]. 40

4.1 Degrees of freedom in $\mathrm{EFT_I}$(NRQCD + SCET). w is the $b\bar{b}$ relative velocity in the bottomonium rest frame, while $\lambda \sim m_c/2m_b$ is the SCET expansion parameter. We assume $m_b w \sim m_c$ (or, equivalently, $w \sim \lambda$) and $m_b w^2 \sim m_b \lambda^2 \sim \Lambda_{\mathrm{QCD}}$. 113

4.2 Degrees of freedom in $\mathrm{EFT_{II}}$(pNRQCD + bHQET). The scale Q in bHQET is $Q = n\cdot v' \Lambda_{\mathrm{QCD}}$ for the $\bar{n}$-collinear sector and $Q = \bar{n}\cdot v \Lambda_{\mathrm{QCD}}$ for the n-collinear sector. $n \cdot v'$ and $\bar{n} \cdot v$ are the large light-cone components of the D-meson velocities in the bottomonium rest frame, $n\cdot v' \sim \bar{n}\cdot v \sim 2m_b/m_c$. λ and w are defined as in Tab. 4.1. The scaling of quark and gluon fields collinear in the n direction is obtained by exchanging the p^+ and p^- components of $\bar{n}$-collinear fields 114

ABSTRACT

We apply effective field theory (EFT) techniques to solve problems at the intersection of nuclear and particle physics. In particular, we study three problems that span different energy scales. First, we probe scattering processes, like $\pi\pi$ scattering and e^+e^- annihilation into pions, around the rho mass, $m_\rho \simeq 770$ MeV, which is comparable to the characteristic QCD scale, $M_{\rm QCD} \sim 1$ GeV. Second, we analyze the nucleon-nucleon potential, especially the renormalization of its binding energy, whose momentum scale, $\kappa \sim 45$ MeV, is much smaller than the pion mass, $m_\pi \simeq 140$ MeV, which in turn is much smaller than $M_{\rm QCD}$. Finally, we address a decay problem of a bottomonium into charmed mesons covering two different scales larger than $M_{\rm QCD}$, the bottom mass $m_b \sim 4.5$ GeV and the charm mass $m_c \sim 1.5$ GeV. At energies comparable to $M_{\rm QCD}$, rho mesons with masses parametrically comparable to the pion masses are incorporated in a controlled low-energy EFT of QCD, with the assumption that the latter has a dynamical "vector symmetry". We enlarge the "Vector EFT" of pions and rhos to include electromagnetic gauge invariance, and the connections to vector-meson-dominance models are discussed. We develop a power counting for reactions at energies near the rho mass, which requires selective resummations of the momentum expansion. We calculate the amplitudes for $\pi\pi \to \pi\pi$ and $e^+e^- \to \pi^+\pi^-$ in leading order and compare them with data. At lower energies, we use an EFT with momentum of the order of the mass of the pion, Chiral Perturbation Theory (ChPT), to develop a framework to study the renormalization of the two-nucleon problem. To eliminate the $1/r^3$ singularity in the isovector tensor force from the one-pion-exchange potential in leading order (LO), we add auxiliary-field potentials. The latter could possibly substitute the various counterterms necessary to renormalize the amplitude arising from the one-pion-exchange potential. By treating the short-range interaction of

the nucleon-nucleon potential as the dominant piece, we provide an exact solution of the Schrödinger equation and find the binding energy of the deuteron, B, in a first approximation. The long-range interaction is treated in perturbation theory in order to calculate the first correction to B. At higher energies, we take advantage of the separation between the scales $2m_b \gg m_c \gg M_{\rm QCD}$ and use a sequence of EFTs to develop a framework to study the exclusive two-body decays of bottomonium into two charmed mesons and apply it to study the decays of the C-even bottomonia. We prove that, at LO in the EFT power counting, the decay rate factorizes into the convolution of two perturbative matching coefficients and three non-perturbative matrix elements, one for each hadron. We calculate the relations between the decay rate and non-perturbative bottomonium and D-meson matrix elements at LO, with next-to-leading-log resummation. The phenomenological implications of these relations are discussed.

CHAPTER 1

INTRODUCTION

Quantum Chromodynamics (QCD) is the correct theory of strong interactions that combine quarks and gluons into hadrons and mesons. Many opportunities to comprehend the dynamics of strong interacting systems have been offered since strong interactions at various length scales are explored in nuclear and particle physics experiments. To understand or to estimate the results of these experiments and to find evidence for "new physics", a thorough investigation of strong interactions is necessary.

Phenomenological models that are not formulated from QCD have been used to describe features of strong interactions with some success. This is because specific aspects of quark-gluon dynamics can be ignored at low energies. Even though phenomenological models are successful, they, in most of the cases, involve educated guesswork to examine a particular class of problems. However, there seems to be no correlation among different classes of problems. Different models based on different assumptions about strong interactions may describe well a particular interacting system, yet they usually fail outside the domain they have been designed for.

On the other hand, it is nearly impossible to use QCD to solve low-energy dynamics of hadronic systems because at low energies, of order of the characteristic scale $M_{\rm QCD} \sim 1$ GeV, the strong coupling constant, α_s, becomes large and, thus, a perturbative expansion in α_s becomes impossible. Non-perturbative calculations may be numerically done in lattice QCD. This approach, however, can be expensive and impracticable since powerful computers are needed.

The theories that exploit the existence of various scales of QCD are the Effective Field Theories (EFTs) [1, 2, 3, 4, 5]. The essential premises of EFTs are that they incorporate and take advantage of the existence of multiple scales and that the dynamics of the low-energy physics do not rely on the details of the high-

energy physics. Additionally, EFTs encode the same symmetries of their underlying theory, and have low-energy constants (LECs) that can be determined from either the underlying theory or low-energy experiments.

The main ingredient of an EFT is the construction of the most general Lagrangian that involves the relevant low-energy degrees of freedom. Moreover, the success of EFTs relies on two essential elements related to each other, renormalization-group invariance (RGI) and power counting. In order to separate the low- and high-energy degrees of freedom in calculations of observables it is necessary to introduce a cutoff parameter Λ in momentum space. RGI ensures that observables are independent of Λ.

For the scale of the underlying theory, $M_{\rm HI}$, an EFT with momenta $Q \sim M_{\rm LO} \ll M_{\rm HI}$ is constructed through the Lagrangian with all possible interactions allowed by symmetries of the theory. The Lagrangian can be written as an expansion in powers of $Q/M_{\rm HI}$ with parameters that depend on $M_{\rm HI}$ and Λ. In order to have predictive power the expansion is systematically truncated at an order according to the desired accuracy. If more accurate results of the observables with less dependence on the cutoff are desired, the expansion needs to be truncated at higher order. The ordering of interactions that allows such truncation is called power counting. After truncating the expansions at any desired order the parameters are fitted to some low-energy experimental data, and other observables are predicted. If predictions fail, the power counting is rethought. Such is the case when the perturbative expansion diverges around a resonance, a non-perturbative phenomenon [6, 7, 8]. In order to keep results finite throughout the low-energy region, certain terms need to be resummed in the expansion. The power counting must be extended to the kinematic region around the "resonant degree of freedom" (RDOF), and a non-perturbative treatment of RDOF must be considered, e.g. the RDOF self energy is resummed. Such resummation leads to a dressed propagator that is enhanced compared to the propagator outside the region of the RDOF. Such an example is studied in Chapter 2.

RGI is satisfied order by order because of power counting, which means that at

each order it is necessary that the latter delivers a sufficient amount of operators that absorb any cutoff dependencies. Such operators are, in many publications, called counterterms. Unfortunately, there are problems in which, at a certain order in a proposed power counting, there are not enough counterterms to absorb the Λ dependence of the observables and RGI fails. An example is provided by the renormalization of singular potentials, again a non-perturbative problem [9]. A solution based on adding several counterterms at higher orders was proposed in Ref. [9]. In Chapter 3, an approach based on replacing several counterterms found in Ref. [9] with auxiliary fields is used to eliminate the singularities.

Different types of EFTs can also be used to describe problems with various high-energy scales $Q \gg M_{\rm QCD}$, where the high-energy degrees of freedom, integrated out in perturbation theory, are described by the QCD Lagrangian. However, large logarithms of the ratio between energy scales appear in these kinds of problems spoiling perturbation theory. RGI allows the systematic resummation of such logarithms, which improves the perturbative expansion. Below the high-energy scale Q, non-perturbative effects take place, and still EFT provides a rationale through power counting for non-perturbative contributions. Processes involving various EFTs, with the features mentioned above, are examined in Chapter 4.

In this chapter we discuss some of the EFTs relevant for the rest of the dissertation: heavy-particle EFT and non-relativistic QCD (NRQCD), Chiral Perturbation Theory (ChPT), nuclear EFT, and Soft Collinear Effective Theory (SCET).

1.1 HQET, NRQCD and an example of how to use an EFT

In all the three applications shown in this dissertation we use EFTs of QCD. Since the main ingredient of an EFT is the construction of the most general low-energy Lagrangian that exploits the underlying-theory symmetries and their breaking, we will start this section by describing the QCD Lagrangian. Symmetries and their breaking will be discussed in later sections.

The QCD Lagrangian describes the strong interactions among quarks with num-

ber of quark flavors $N_f = 1, \ldots, 6$ and gluons. They represent fields in the non-Abelian color $SU(3)_c$ gauge group. The QCD Lagrangian with the lowest-dimension operators is given by

$$\begin{aligned}\mathcal{L}_{\rm QCD}(x) &= \bar{q}(x)\left(i\gamma^\mu D_\mu - M - eQ\gamma^\mu A_\mu(x)\right)q(x) - \frac{1}{4}G^a_{\mu\nu}(x)G^{a\,\mu\nu}(x) \\ &- \frac{1}{4}F_{\mu\nu}(x)F^{\mu\nu}(x) - \frac{\theta}{64\pi^2}g_s\epsilon^{\mu\nu\alpha\beta}G^a_{\mu\nu}(x)G^a_{\alpha\beta}(x), \end{aligned} \tag{1.1}$$

where for $N_f = 6$ $q(x) = (u(x)\ d(x)\ s(x)\ c(x)\ b(x)\ t(x))$ is the set containing the quark fields up, down, strange, charm, bottom and top, respectively, $A_\mu(x)$ stands for the photon field, e is the electron charge, θ is a real parameter and the gauge-covariant derivative is

$$D_\mu = \partial_\mu - ig_s G^a_\mu T^a, \tag{1.2}$$

with $G^a_\mu(x)$ being the gluon fields, g_s the strong coupling constant and T^a the eight generators of $SU(3)_c$. Additionally, M is the quark mass matrix for $N_f = 6$ given by $M = \text{Diag}\,(m_u,\ m_d,\ m_s,\ m_c,\ m_b,\ m_t)$ and $Q = \text{Diag}\,(q_u,\ q_d,\ q_s,\ q_c,\ q_b,\ q_t)$ is the quark charge matrix. $G^a_{\mu\nu}$ and $F_{\mu\nu}$ are the gauge-invariant gluon and photon fields strengths given by

$$G^a_{\mu\nu}(x) = \partial_\mu G^a_\nu(x) - \partial_\nu G^a_\mu(x) + g_s f_{abc} G^b_\mu(x) G^c_\nu(x), \tag{1.3}$$

$$F_{\mu\nu}(x) = \partial_\mu F_\nu(x) - \partial_\nu F_\mu(x), \tag{1.4}$$

where f_{abc} is the $SU(3)_c$ structure constants. The θ term is related to an anomaly in the axial $U(1)$ symmetry [10], and can be expressed as a total derivative. Because of the anomaly, the total derivative cannot be neglected since it does represent physical processes via fields known as axions. However, the θ term is not relevant for the applications presented in this section or this dissertation.

In two of the applications, Chapters 3 and 4, we use EFTs to describe systems that involve particles with mass $m \gtrsim M_{\rm QCD}$. Here, two EFTs are used to describe such systems, heavy-particle EFT and non-relativistic QCD.

The first EFT to be discussed is heavy-particle EFT. Heavy particles, baryons and heavy quarks, cannot be treated in a fully relativistic fashion in low-energy EFT

since their masses are much larger than the characteristic QCD scale, $m \gtrsim M_{\rm QCD}$. In Refs. [11, 12], it was proposed that heavy particles be treated as extreme non-relativistic particles interacting with light particles. Since heavy particles are involved in this "new" effective field theory, this approach is called heavy-particle EFT. When the particle is a heavy quark such c or b, we speak of heavy-quark effective theory (HQET). Since the heavy particle (quark or baryon) is approximately on-shell, its momentum can be written as

$$p^\mu = mv^\mu + k^\mu, \tag{1.5}$$

where m is the mass of the heavy particle, v^μ is its 4-velocity satisfying $v_\mu v^\mu = 1$, mv^μ "carries" most of the momentum p^μ and k^μ is the residual momentum that refers to the heavy particle off-shellness. For a heavy quark in a hadron, $m \gg M_{\rm QCD}$ and $k^\mu \sim M_{\rm QCD}$. For a baryon at low energies, $m \sim M_{\rm QCD}$ and $k^\mu \ll M_{\rm QCD}$. In either case, the velocity v^μ does not change by interactions of the heavy particle with light particles involving momentum transfer k^μ, which makes it useful to redefine the particle fields in terms of a label v as

$$\psi(x) = e^{-imv\cdot x}\left(N_v(x) + h_v(x)\right), \tag{1.6}$$

where $\psi(x)$ is the relativistic Dirac spinor of the heavy field, $N_v(x)$ and $h_v(x)$ are the upper and lower components of the spinor given by

$$N_v(x) = e^{imv\cdot x}P_v^+\psi(x) = e^{imv\cdot x}\frac{1+\not{v}}{2}\psi(x), \tag{1.7}$$

$$h_v(x) = e^{imv\cdot x}P_v^-\psi(x) = e^{imv\cdot x}\frac{1-\not{v}}{2}\psi(x), \tag{1.8}$$

with $P_v^+ + P_v^- = 1$.

By using the properties $\not{v}N_v(x) = N_v(x)$ and $\not{v}h_v(x) = -h_v(x)$, the kinetic part of the fermionic part of the Lagrangian (1.1) becomes, in terms of the labeled fields $N_v(x)$, $h_v(x)$ and velocity v,

$$\begin{aligned}\mathcal{L}_v(x) &= \left(\bar{N}_v(x) + \bar{h}_v(x)\right)e^{imv\cdot x}\left(i\left(-im\not{v} + \not{D}\right) - m\right)e^{-imv\cdot x}\left(N_v(x) + h_v(x)\right)\\ &= \bar{N}_v(x)i\not{D}N_v(x) + \bar{h}_v(x)\left(i\not{D} - 2m\right)h_v(x)\\ &\quad + \bar{N}_v(x)i\not{D}h_v(x) + \bar{h}_v(x)i\not{D}N_v(x).\end{aligned} \tag{1.9}$$

The most common form of the Lagrangian, found in heavy-particles references, is found by making the substitution $D^\mu = v \cdot D v^\mu + D^\mu_\perp$. Then, the lowest-order Lagrangian for heavy fields is

$$\mathcal{L}_v(x) \;=\; \bar{N}_v(x)\,(iv\cdot D)\,N_v(x) + \ldots, \tag{1.10}$$

where the dots stand for higher-order interactions of the heavy field $N_v(x)$ given by expansions in powers of $k/m \sim \mathcal{O}(M_{\rm QCD}/m)$. The field $h_v(x)$ was eliminated by a field redefinition found through the equation of motion or through a gaussian integration on the path integral formulation. If $N_v(x)$ refers to heavy-quark fields the Lagrangian in Eq. (1.10) is the HQET Lagrangian, $\mathcal{L}_{\rm HQET}(x)$. Note that if one wishes to work in the heavy-hadron rest frame, where $v^\mu = (1, \vec{0})$, then $D^\mu_\perp = \vec{D}^\mu$, where $\vec{D}^\mu$ is the spatial covariant derivative. Furthemore, observe that from the equation of motion correspondent to the Lagrangian in Eq. (1.10), the energy of a heavy field is zero in its rest frame. The covariant derivative, given by Eq. (1.2), contains interactions of $N_v(x)$ with gluons at any energy scale. Now, the covariant derivative, present in Eq. (1.10), introduces only interactions of $N_v(x)$ with soft gluons, gluons with low momentum, while the hard (large-momentum) gluons are integrated out.

Further, EFT can also be applied to solve problems with two heavy fields, like nucleons, charmonium and bottomonium. In the case of heavy-quark systems, these interactions are described by the non-relativistic QCD Lagrangian. Some important extra scales need to be taken into consideration. $M_{\rm QCD}$ and m are not the only scales involved in the description of the dynamics of the theory, but also other scales like binding energy mv^2 and relative momentum mv. In the case of the heavy quarkonium, for example, the kinetic energy is of order $p^2/2m \sim mv^2$, an important term that is present in the HQET Lagrangian only in the ... of Eq. (1.10). This and other terms are fixed by Lorentz invariance. To obtain the constraints of Lorentz invariance in the non-relativistic Lagrangian for heavy fields, one can use

"reparametrization invariance" [13]: v^μ and D^μ can be reparametrized as

$$v^\mu \to w^\mu = v^\mu + \frac{k^\mu}{m}, \tag{1.11}$$

$$D^\mu \to D'^\mu = D^\mu - ik^\mu, \tag{1.12}$$

where, now,

$$w^2 = \left(v^\mu + \frac{k^\mu}{m}\right)^2 = 1. \tag{1.13}$$

Changing the labels w and D' to v and D, respectively, the Lagrangian is represented by

$$\mathcal{L}_{\rm NR}(x) = \mathcal{L}\left(\bar{N}_v(x), N_v(x), \left(v - \frac{k}{m}\right)^\mu, (iD + k)^\mu\right). \tag{1.14}$$

The reparametrizations of v and D that leave the Lagrangian in Eq. (1.14) invariant are

$$v^\mu \to V^\mu = v^\mu + i\frac{D^\mu}{m}, \tag{1.15}$$

$$D^\mu \to \mathcal{D}^\mu = -imV^\mu = -imv^\mu + D^\mu, \tag{1.16}$$

and the Lagrangian can, therefore, be rewritten as

$$\mathcal{L}_{\rm NR}(x) = \bar{N}_v(x) iV^\mu \cdot \mathcal{D}^\mu N_v(x) = \bar{N}_v(x)\left(iv\cdot D - \frac{D^2}{2m}\right) N_v(x). \tag{1.17}$$

The non-relativistic expansion of the Lagrangian in Eq. (1.17) can be obtained by making the field redefinition

$$N'_v(x) = \left(\sum_{l,j} \frac{1}{m^{l+2j}} b_{lj} \left(iv\cdot D\right)^l D^{2j} m\right) N_v(x), \tag{1.18}$$

where b_{lj} are normalization coefficients. The final expression for the non-relativistic Lagrangian, then, can be wirtten as

$$\mathcal{L}_{\rm NR}(x) = \bar{N}_v(x)\left(iv\cdot D - \frac{D^2 - (v\cdot D)^2}{2m}\right) N_v(x) + \ldots, \tag{1.19}$$

which, in the rest frame, can be recognized as

$$\mathcal{L}_{\rm NR}(x) = \bar{N}_v(x)\left(iD_0 - \frac{\vec{D}^2}{2m}\right) N_v(x) + \ldots. \tag{1.20}$$

If $N_v(x) = N$ is the nucleon field, the Lagrangian in Eq. (1.20) may be extended to include contact terms and pions, described in next sections and Chapter 3. The Lagrangian shown in Eq. (1.20) can also be used to describe interactions among heavy quarks. In this case, $N_v(x)$ stands for the heavy fields, as in Chapter 4. Just as an observation, the reparametrization exists already for one heavy quark theory, HQET, in order to eliminate the redundancy in the theory description by both a velocity and a residual momentum [13].

A simple qualitative example that demonstrates that EFT is a powerful technique to describe low-energy dynamics without any knowledge of the high-energy physics is Rayleigh scattering. A review following Refs. [2, 3] is given here.

Rayleigh scattering is the problem of low-energy photons that scatter from neutral atoms in their ground state. The energy of the photons E_γ is sufficiently small that it does not excite the atom, which has an excitation energy ΔE. The separation between the scales that contributes to the scattering process is

$$E_\gamma \ll \Delta E \ll a_0^{-1} \ll M_{\rm atom}, \tag{1.21}$$

where $M_{\rm atom}$ and a_0^{-1} are the mass and the inverse of the size of the atom, respectively. Since $M_{\rm atom}$ is heavy compared to E_γ and ΔE, atom recoil can be neglected. To describe interacting systems of heavy particles and photons, the heavy-particle Lagrangian in Eq. (1.10) may be used with the covariant derivative substituted by the partial derivative since gluons are not relevant degrees of freedom. The strength tensor of the photon A_μ, $F_{\mu\nu}$, defined in Eq. (1.4) present in the the QCD Lagrangian shown in Eq. (1.1) has to be recovered here, in addition to extra relevant interacting terms. The most general effective heavy-particle Lagrangian, allowed by Lorentz and gauge invariance symmetries, which can be constructed with the relevant degrees of freedom atoms and photons is

$$\begin{aligned} \mathcal{L}_{\rm eff} &= \psi^\dagger \left(iv\cdot\partial\right)\psi - \frac{1}{4}F_{\mu\nu}F^{\mu\nu} + c_1\psi^\dagger\psi F_{\mu\nu}F^{\mu\nu} + c_2\psi^\dagger v^\gamma v^\lambda \psi F_{\mu\gamma}F^\mu_\lambda \\ &\quad + c_3\psi^\dagger v^\gamma \psi \partial_\gamma F_{\mu\nu}F^{\mu\nu} + \cdots, \end{aligned} \tag{1.22}$$

where ψ is the atom field, c_1, c_2 and c_3 are low-energy parameters to be estimated from the underlying-theory Lagrangian. To keep gauge invariance, ψ cannot be

directly coupled to A_μ, only to $F_{\mu\nu}$. The first two terms represent the kinetic terms for atom and photon, respectively. The last three terms represent the interaction of the atom with the electromagnetic fields. The dots stand for all possible interactions.

To recognize the leading-order contributions to the effective Lagrangian, dimensional analysis and power counting must be used. From the unit system that is being used, where the scaling dimensions are $[x] = [t] = -1$ and $[Q] = [E] = [\partial] = 1$, and $[\mathcal{L}] = 4$, the dimensions of the photon strength tensor and of the atom fields are $[F_{\mu\nu}] = 2$ and $[\psi] = 3/2$, respectively. The parameters, then, have dimensions $[c_1] = [c_2] = -3$ and $[c_3] = -4$. Since the first two interacting terms in Eq. (1.22) have the lowest dimensions, they are leading order while the last interaction belongs to a higher-order Lagrangian. In order to determine the size of the coefficients the low-energy effective Lagrangian, Eq. (1.22), must be matched to the underlying-theory Lagrangian. The cross section σ depends only on the size of the atom because low-energy photons do not probe details of the internal structure of the atom. On the other hand, the coefficients c_1 and c_2 completely describe the scattering system. The last two sentences combined leads to an estimate for the size of the low-energy parameters of $c_1 \sim c_2 \sim a_0^3$.

Finally, an analysis of the cross section σ may be done to answer why is the sky blue. The cross section has dimensions of area, $[\sigma] = -2$, and it is proportional to a dimensionless phase space and to the square of the scattering amplitude, obtained from the Lagrangian, Eq. (1.22). For example, in the Lagrangian piece, $c_1\psi^\dagger\psi F_{\mu\nu}F^{\mu\nu}$, each photon field strength contains one derivative acting on the photon field, which corresponds to E_γ. Thus, the scattering amplitude is proportional to $E_\gamma^2 a_0^3$. The same analysis may be done with the other relevant piece in the Lagrangian. The cross section, then, is proportional to

$$\sigma \ \alpha \ E_\gamma^4 a_0^6. \tag{1.23}$$

Since Eq. (1.23) grows as E_γ^4, blue light is scattered more powerfully than red, hence the blue sky.

Eq. (1.23) is not valid at all energy regimes; the high-energy information is lost.

Corrections to Eq. (1.23) may be accounted for by determining the size of the c_3 parameter. For this particular problem $M_{LO} \sim E_\gamma$, and the corrections are given by expansions in $E_\gamma/\Delta E$, since ΔE is the smallest, and thus the most important, high-energy scale. Therefore, the error predicted is of the order $\mathcal{O}\left(E_\gamma/\Delta E\right)$ and

$$\sigma \ \sim \ E_\gamma^4 a_0^6 \left(1 + \mathcal{O}\left(\frac{E_\gamma}{\Delta E}\right)\right). \tag{1.24}$$

Even though the proportionality constant can be determined from, for example, matching the low-energy amplitude to the underlying-theory amplitude, a lot of information is presented in Eq. (1.24) with only a few EFT ingredients.

1.2 Chiral Perturbation Theory

ChPT is the EFT that reproduces strong interactions at low energies, and provides a theoretical framework that will be used in latter discussions. In particular, ChPT is used to describe interactions among light pseudoscalar mesons, pions, including weak and electromagnetic contributions. The choice of the relevant degrees of freedom (d.o.f.s) appropriate for some EFT depends on the separation of energy scales: for example, the large gap between the masses of the pions, $m_\pi \simeq 140$ MeV, and the masses of nucleons, $m_N \simeq 940$ MeV, or heavier mesons, like the vector rho mesons $m_\rho \simeq 770$ MeV, observed in the hadronic spectrum. In the present case, we especially focus on light d.o.f.s. Then, the momentum scale for the ChPT, the soft scale, is $M_{\rm LO} \sim Q \sim m_\pi$ while the momentum scale for the chiral symmetry breaking scale, the hard scale, is $M_{\rm HI} \sim M_{\rm QCD} \sim m_N, m_\rho,$ etc. The construction of ChPT is based on the global chiral, $SU(2)_L \times SU(2)_R$, and the local $U(1)_{V=L+R}$ symmetries of QCD. Thus, this section is dedicated to a brief study of chiral symmetry and its breaking and is specialized for $N_f = 2$.

As a starting point, we consider the limit of massless quarks, also known as the chiral limit. The kinetic term of Eq. (1.1) can be written as a function of left- and right-handed quark fields q_L and q_R as

$$\bar{q}(x) i \not{D} q(x) = \bar{q}_L i \not{D} q_L + \bar{q}_R i \not{D} q_R, \tag{1.25}$$

where

$$q_L = \frac{1-\gamma_5}{2} q \equiv P_L\, q, \qquad q_R = \frac{1+\gamma_5}{2} q \equiv P_R\, q. \tag{1.26}$$

The terms in Eq. (1.25) are invariant under independent global unitary transformations,

$$q_L \to e^{-i\alpha_L^a t^a} q_L \equiv L\, q_L, \qquad q_R \to e^{-i\alpha_R^a t^a} q_R \equiv R\, q_R, \tag{1.27}$$

where α_L^a and α_R^a are three real left and three real right parameters, $t^a = \tau^a/2$ are the three generators of the flavor $SU(2)$ group that satisfy the commutation relation

$$\left[t^a, t^b\right] = i\epsilon^{abc} t^c, \tag{1.28}$$

and L and R belong to $SU(2)_L$ and $SU(2)_R$ groups.

From Noether's theorem, one can obtain three left-handed and three right-handed currents

$$L_\mu^a(x) = \bar{q}_L(x)\gamma_\mu t^a q_L(x), \tag{1.29}$$

$$R_\mu^a(x) = \bar{q}_R(x)\gamma_\mu t^a q_R(x). \tag{1.30}$$

Equivalently, from linear combinations of the transformations L and R, which form vector and axial transformations, $V = L + R$ and $A = L - R$, respectively, one can obtain three vector and three axial currents

$$V_\mu^a(x) = \bar{q}(x)\gamma_\mu t^a q(x), \tag{1.31}$$

$$A_\mu^a(x) = \bar{q}(x)\gamma_\mu \gamma^5 t^a q(x). \tag{1.32}$$

The corresponding conserved charges satisfy the Lie algebra of the chiral $SU(2)_L \times SU(2)_R$ group,

$$\left[Q_L^a, Q_L^b\right] = i\epsilon^{abc} Q_L^c, \qquad \left[Q_R^a, Q_R^b\right] = i\epsilon^{abc} Q_R^c, \qquad \left[Q_L^a, Q_R^b\right] = 0 \tag{1.33}$$

or, for the vector and axial charges,

$$\left[Q_V^a, Q_V^b\right] = i\epsilon^{abc} Q_V^c, \quad \left[Q_A^a, Q_A^b\right] = i\epsilon^{abc} Q_V^c, \quad \left[Q_V^a, Q_A^b\right] = i\epsilon^{abc} Q_A^c. \tag{1.34}$$

Thus in the chiral limit, the global group

$$G \;=\; SU(2)_L \times SU(2)_R, \tag{1.35}$$

is the global chiral symmetry group. And sometimes, due to V and A transformations, the group is erroneously called $SU(2)_V \times SU(2)_A$, even though $SU(2)_A$ is not a group.

In the limit of massless u and d quarks, the Lagrangian shown in Eq. (1.1) has a larger global symmetry group

$$U(2)_L \times U(2)_R = SU(2)_L \times SU(2)_R \times U(1)_V \times U(1)_A, \tag{1.36}$$

where the $U(1)_V$ and $U(1)_A$ transformations are

$$q \;=\; \begin{pmatrix} q_L \\ q_R \end{pmatrix} \rightarrow e^{-i\alpha_V} \begin{pmatrix} q_L \\ q_R \end{pmatrix} \equiv U_V \begin{pmatrix} q_L \\ q_R \end{pmatrix} \tag{1.37}$$

$$q \;=\; \begin{pmatrix} q_L \\ q_R \end{pmatrix} \rightarrow e^{-i\alpha_A\gamma^5} \begin{pmatrix} q_L \\ q_R \end{pmatrix} \equiv U_A \begin{pmatrix} q_L \\ q_R \end{pmatrix}, \tag{1.38}$$

with α_V and α_A the real vector and axial parameters, and U_V and U_A are elements of the group $U(1)_V$ and $U(1)_A$, respectively. The axial current associated with the $U(1)_A$ group is, however, broken by quantum effects, an event called $U(1)_A$ anomaly, thus $U(1)_A$ is not a symmetry of the quantum theory. The $U(1)_V$ symmetry contains an element that transforms both the left- and right-handed quark fields by a phase leading to quark number conservation.

Since the electromagnetic field is introduced in later chapters, I mention here that the electromagnetic term in the QCD Lagrangian in Eq. (1.1) can also be decomposed into left- and right-handed quarks

$$-eA_\mu(x)\bar{q}(x)Q\gamma^\mu q(x) = -eA_\mu(x)\left(\bar{q}_L(x)Q\gamma^\mu q_L(x) + \bar{q}_R(x)Q\gamma^\mu q_R(x)\right). \tag{1.39}$$

where Q is now the quark charge matrix for the $N_f = 2$ case, $Q = \mathrm{Diag}\,(2/3, 1/3)$, and the electromagnetic field A_μ is a gauge field associated with the local $U(1)$ symmetry,

$$U = \exp\left(i\theta t^3\right), \tag{1.40}$$

where θ is a parameter. The $U(1)$ symmetry is kept unbroken and leads to the conservation of electromagnetic current.

Until now, we neglected the quark-mass term, in Eq. (1.1), which can also be decomposed, as well as the kinetic term, as

$$\bar{q}_R(x) M q_L(x) + c.c., \tag{1.41}$$

where a coupling between q_L and q_R is observed, and therefore, such term does not have chiral symmetry. Chiral symmetry is thus not an exact symmetry. The quark mass matrix in Eq. (1.1) can be written as

$$M = \frac{1}{2}(m_u + m_d)\, I + (m_u - m_d)\, t^3. \tag{1.42}$$

If the masses of the u and d were the same, the isospin symmetry $SU(2)_V$ would be exact. However, their masses are $m_u = 2.5^{+0.6}_{-0.8}$ MeV and $m_d = 5^{+0.7}_{-0.9}$ MeV [14], and because of the non-vanishing terms in Eq. (1.42), chiral symmetry is explicitly broken by the mass term. Chiral symmetry is, then, an approximate symmetry. Since the light quark masses, m_u and m_d, are smaller than $M_{\rm QCD} \sim 1$ GeV, they can be treated as a perturbation around zero quark masses.

The chiral symmetry of the Lagrangian could also be realized in the states, in particular, the ground state. In other words, if the QCD ground state, the vacuum $|0\rangle$, is invariant under chiral symmetry, the charges corresponding to chiral symmetry Q^a_I, for $I = L,\ R,\ V,\ A$ annihilate the vacuum,

$$Q^a_I |0\rangle = 0. \tag{1.43}$$

Nonetheless, there are indications that chiral symmetry is not realized in the ground state of QCD due to non-perturbative dynamical effects, thus chiral symmetry is spontaneously broken. The most striking indication lies in the hadronic spectrum, explained next. Assuming, at first, that $Q^a_A|0\rangle = 0$ and $[Q^a_A, H] = 0$, degenerate states with opposite parities are expected to appear in the hadronic spectrum. However, this is contradicted by the fact that hadrons with such degeneracies are not observed. As an example, all the components of the rho (ρ) meson isospin

triplet (ρ^+, ρ^-, ρ^0) have approximately the same mass ($\simeq$ 770 MeV), obeying isospin $SU(2)_V$ symmetry. At the same time the ρ has parity -1 and its closest axial partner with parity $+1$ would be the a_1 meson with mass $\simeq$ 1260 MeV [14]. However, they cannot be considered degenerate states, since the mass splitting between both states, those with negative and positive parities, is about 500 MeV, a number of the same order of the mesons masses. Another example is the pion isospin triplet (π^+, π^-, π^0) with mass $\simeq$ 140 MeV and parity -1. The closest scalar with parity $+1$ is the f_0 meson with mass $\simeq$ 600 MeV, which gives a mass splitting of $\simeq$ 450 MeV larger than the mass of the pion. Other examples of non-degenerate states with opposite parities would be omega w meson $J^P = 1^-$, where J stands for total angular momentum and P for parity, and mass $\simeq$ 780 MeV and f_1 with $J^P = 1^+$ and mass $\sim$ 1285; f_0 with $J^P = 0^+$ and $\simeq$ 975 MeV and η with $J^P = 0^-$ and mass $\simeq$ 1295 MeV; K^* with $J^P = 1^-$ and mass $\simeq$ 890 MeV and K_1 with $J^P = 1^+$ and mass $\simeq$ 1350 MeV [15], all "chiral partners" with mass splittings comparable to their masses, and thus they cannot be considered degenerate.

From the hadronic spectrum, it is observed that the vacuum is annihilated by vector charges,

$$Q_V^a(x)|0\rangle = 0, \tag{1.44}$$

but not annihilated by axial charges,

$$Q_A^a(x)|0\rangle \neq 0, \tag{1.45}$$

which means the vacuum is not invariant under the broken "symmetry" $SU(2)_A$. Thus the chiral symmetry G is spontaneously broken down to its diagonal, the isospin subgroup

$$H = SU(2)_{V=L+R}. \tag{1.46}$$

Since there are three broken generators, there are three massless Goldstone bosons (GB) with parity -1 [16]. They are identified to the isospin triplet of pions, which are not exactly massless since the quark masses explicitly break chiral symmetry.

The next step is to construct the most general effective Lagrangian that describes the low-energy interactions of the relevant degrees of freedom, the Goldstone bosons and photons if included, rather than quarks and gluons. The Lagrangian for hadrons must preserve a nonlinear realization of chiral symmetry developed by Callan, Coleman, Wess and Zumino (CCWZ) [17].

The three Goldstone bosons, associated with pions, are combined into the single matrix ξ that transforms non-linearly under the approximate global chiral symmetry as

$$\xi^2 \to L\xi^2 R^\dagger, \tag{1.47}$$

where

$$\xi = e^{i\pi/f_\pi} = e^{i\pi^a t^a/f_\pi}, \tag{1.48}$$

with $\pi^a(x)$ being the Goldstone bosons associated with the pion isospin triplet, and $f_\pi \simeq 92$ MeV is the pion decay constant.

Just like in QCD, the photon is introduced as a gauge field A_μ associated with the local $U(1)$ symmetry given by Eq. (1.40), which is kept unbroken. Under this symmetry the gauge field transforms as

$$A_\mu t^3 \to U\left(A_\mu t^3 - i\partial_\mu\right)U^\dagger \tag{1.49}$$

and the Goldstone bosons as

$$\xi^2 \to U\xi^2 U^\dagger, \tag{1.50}$$

so that the pion fields π^a change in agreement with their electromagnetic charge. Photons can be included in the effective chiral Lagrangian through the covariant derivative

$$D_\mu \xi^2 = \partial_\mu \xi^2 + ieA_\mu \left[t^3, \xi^2\right] \tag{1.51}$$

and through the field strength (1.4), ensuring that the effective Lagrangian is invariant under $U(1)$ transformations.

Chiral symmetry is broken explicitly by the quark masses, and this breaking can be incorporated in the effective Lagrangian ($\mathcal{L}_{\text{eff}}$) by treating M as a spurion field, which means that we pretend that M transforms under chiral symmetry as

$$M \to RML^{\dagger}, \tag{1.52}$$

a manner that would keep the Lagrangian invariant under chiral symmetry. This symmetry is broken in the sense that M does not transform in such a way. To break G down to H we restrict the spurion field to a constant

$$M \;=\; M^{\dagger} = \begin{pmatrix} m_u & 0 \\ 0 & m_d \end{pmatrix} \equiv \bar{m}\left(1 - 2\varepsilon\, t^3\right), \tag{1.53}$$

which generates the Goldstone-boson masses.

The ChPT Lagrangian is, then, constructed by adding all possible interacting terms that include, in this case, M, ξ, A_μ and obey chiral symmetry. Such Lagrangian has an infinite number of interactions and must be organized as an expansion of small ratios of scales [18]. To count mass terms properly, one should think of such terms in leading order. Because quark-mass terms are treated as a perturbation around the chiral limit, the leading terms should contain only one mass matrix. Besides, leading-order terms should involve the minimum amount of derivatives and, under global chiral rotations, mass terms do not contain derivatives. Thus, the leading-order-mass terms can be written as

$$\frac{f_\pi^2}{4}\mu \mathrm{Tr}\left(M\xi^2 + \xi^{\dagger\,2} M^{\dagger}\right) = \frac{f_\pi^2}{4}\mu\bar{m}\mathrm{Tr}\left(\xi^2 + \xi^{\dagger\,2}\right), \tag{1.54}$$

where f_π, given by Eq. (1.48), is another scale associated with the pions, besides their masses, and μ is a low-energy constant. By expanding ξ and ξ^2, one identifies the square of the masses of the GBs to be proportional to μ and to the average quark mass, $\bar{m}$, which in the chiral limit are zero. In addition, the GBs are degenerate with the vacuum and at zero momentum their interactions disappear. Therefore, the terms in the Lagrangian are ordered in powers of derivatives d and square of pion masses n, i.e. quark masses, through a chiral index

$$\nu = d + 2n - 2, \tag{1.55}$$

as

$$\mathcal{L}_{\rm ChPT} = \sum_{\nu=0}^{\infty} \mathcal{L}^{(\nu)}_{\rm ChPT}. \tag{1.56}$$

The lowest-order ChPT Lagrangian, corresponding to chiral index $\nu = 0$, can then be written as

$$\begin{aligned}
\mathcal{L}^{(0)}_{\rm ChPT} &= \frac{f_\pi^2}{4}{\rm Tr}\left[2\left(\partial_\mu\xi^\dagger\right)\partial^\mu\xi - \xi^{\dagger 2}\left(\partial_\mu\xi\right)\partial^\mu\xi - \xi^2\left(\partial_\mu\xi^\dagger\right)\partial^\mu\xi^\dagger\right] + \frac{f_\pi^2 m_\pi^2}{4}{\rm Tr}\left(\xi^2+\xi^{\dagger 2}\right) \\
&\quad -\frac{1}{4}F_{\mu\nu}F^{\mu\nu} + 2ief_\pi^2 A_\mu {\rm Tr}\left[t^3\left(\xi^\dagger\partial^\mu\xi + \xi\partial^\mu\xi^\dagger\right)\right] \\
&\quad -e^2 f_\pi^2 A_\mu A^\mu {\rm Tr}\left[2t^3\xi t^3\xi^\dagger - \frac{1}{2}\right] \qquad (1.57) \\
&= \frac{1}{2}\left(\partial_\mu\boldsymbol{\pi}\cdot\partial^\mu\boldsymbol{\pi} - m_\pi^2\boldsymbol{\pi}^2\right) - \frac{1}{4}F_{\mu\nu}F^{\mu\nu} - eA_\mu\left(\boldsymbol{\pi}\times\partial^\mu\boldsymbol{\pi}\right)_3 \\
&\quad +\frac{1}{24f_\pi^2}\left[4\boldsymbol{\pi}\cdot\partial_\mu\boldsymbol{\pi}\,\boldsymbol{\pi}\cdot\partial^\mu\boldsymbol{\pi} - \boldsymbol{\pi}^2\left(4\partial_\mu\boldsymbol{\pi}\cdot\partial^\mu\boldsymbol{\pi} - m_\pi^2\boldsymbol{\pi}^2\right)\right] + \ldots \qquad (1.58)
\end{aligned}$$

After constructing the most general effective Lagrangian for pions and photons consistent with the chiral symmetry of QCD, one needs to calculate observables to a desired order. This is accomplished by performing a power counting that validates an order-by-order truncation of observables. Like the Lagrangian, the observables are expanded in powers of $Q/M_{\rm QCD}$. To demonstrate how power counting is done, I will consider, for simplicity, a generic process involving only pions with momenta $Q \sim m_\pi$. Observables are, usually, obtained from Feynman diagrams, whose size can be estimated from dimensionful quantities like Q, $M_{\rm QCD}$, f_π, etc. The power counting may be done without any concerns about the ultraviolet divergences that appear in loop calculations, since they are absorbed in the low-energy constants in the same order as the Lagrangian. In other words, ChPT is renormalizable at each order and thus the observables do not depend on the ultraviolet cutoff Λ.

To power count diagrams, each pion field and each derivative, present in the vertices of the ChPT Lagrangian, contribute with $1/f_\pi$ and Q, respectively. Similarly, vertices that explicitly break chiral symmetry are proportional to $m_\pi^2 \sim Q^2$. For each loop momentum, it is assigned a factor $Q^4/\left(4\pi\right)^2$, where Q^4 counts for the integration volume d^4q, and $(4\pi)^2$ is a factor that is always present in the result after

an explicit calculation is done. When estimating Feynman diagrams, the factors 4π and f_π can be combined into $4\pi f_\pi \sim 1$ GeV, suggesting the use of $M_{\rm QCD} = 4\pi f_\pi$ as an estimate of the chiral symmetry breaking scale. Finally, the pion propagator contributes with $1/Q^2$, since pions are relativistic, and, thus, their energies have sizes comparable to their 3-momenta. In the scheme considered above, each diagram contributes with Q^σ, with

$$\sigma = 2 + 2L + \sum_i V_i \nu_i, \tag{1.59}$$

where i denotes the type of vertices, L and V_i stand for number of loops and number of vertices of the type-i, and ν_i is given by Eq. (1.55). The chiral dimension σ corresponds to Weinberg's power counting of ChPT [18].

Therefore, for a particular process involving only pions, various contributing diagrams can be organized according to Eq. (1.59). The leading-order (LO) diagrams are those with

$$\sigma = \sigma_{\rm min} = 2, \tag{1.60}$$

which means that, in a process involving only pions, the contributions of the lowest-order diagrams are proportional to Q^2. An amplitude, however, should be dimensionless. In order to correct the diagram dimension, it is necessary to take into account the f_π factors, associated to external GBs. Hence, the actual LO amplitude is proportional to

$$\mathcal{T}^{(0)} \sim \frac{Q^\sigma}{f_\pi^g}, \tag{1.61}$$

where g is the number of external GBs. The next-to-leading-order (NLO) diagrams will have index $\sigma = \sigma_{\rm min} + 2$, which can come from the tree-level diagrams with only one vertex containing 4 derivatives, 2 derivatives and m_π^2, or m_π^4 factors, or can come from one-loop diagrams constructed out of leading-order interactions. In both cases, the NLO amplitude, $\mathcal{T}^{(2)}$ is suppressed by the ratio $Q^2/M_{\rm QCD}^2$ compared to the LO amplitude, i. e.

$$\mathcal{T}^{(2)} \sim \mathcal{T}^{(0)} \left(\frac{Q}{M_{\rm QCD}}\right)^2. \tag{1.62}$$

As an explicit example, consider pion-pion ($\pi\pi$) scattering. From the LO Lagrangian, $\mathcal{L}^{(0)}_{\rm ChPT}$, the LO contribution for the scattering amplitude is the tree-level diagram corresponding to the four-pion contact vertex, four pions interacting at one spacetime point, and is of $\mathcal{O}\left(Q^2/f_\pi^2\right)$. The NLO diagrams are suppressed by $Q^2/M^2_{\rm QCD}$, and so on.

If, besides the pions, electromagnetic fields are also involved in ChPT, the simplest tree-level diagram one can have for the $\pi\pi$ scattering is through an exchange of a virtual photon. Such a diagram is proportional to $e^2 \sim 4\pi/137$, which, numerically, contributes in NLO. An example of an interaction involving pions and photons is the electron-positron annihilation into two pions ($e^+e^- \to \pi^+\pi^-$). The LO amplitude corresponds to the tree-level diagram containing an exchange of virtual photons, and is of $\mathcal{O}\left(e/Q\right)$. Again, NLO diagrams are suppressed by $Q^2/M^2_{\rm QCD}$.

Processes, such as $\pi\pi \to \pi\pi$ and $e^+e^- \to \pi^+\pi^-$, at low energies have been described very well by ChPT. Despite successes, ChPT cannot describe the same processes around the rho peak, thus the idea of extending ChPT to include rho mesons as chiral partners of the pions. In Chapter 2, we include vector mesons in a controlled EFT that obeys a vector symmetry of QCD. Vector symmetry is the assumption that there is a limit where QCD has a symmetry larger than chiral symmetry. In this limit the vector mesons are massless — thus it is called the vector limit. Away from the vector limit, the vector mesons become massive. In addition to the vector mesons, we enlarge the vector symmetry to admit electromagnetic gauge invariance. In the construction of the most general effective Lagrangian describing interactions among pions, rhos and photons, it is necessary to perform a diagonalization of the gauge-boson mass matrix to obtain massive pions and rhos and massless photons. We study the same processes mentioned above, $\pi\pi \to \pi\pi$ and $e^+e^- \to \pi^+\pi^-$. One can construct a Vector EFT as an expansion in powers of $Q/M_{\rm QCD}$, where Q denotes external momenta, the pion mass and the rho mass. In processes where $Q \ll m_\rho$, the rho can be integrated out and ChPT is restored. However, when Q is around the rho resonance (peak) region, in which a large cross section is produced, the power counting needs to be extended to this non-

perturbative region in order to take into account the "kinematic" fine-tuning to the resonant peak. At lowest order, we include all interactions that contribute to these processes, which leads to a dressing of the rho propagator. In the loop calculations finite terms were included as well as renormalization-group invariance. Finally, we calculate and analyze the lowest-order cross sections around the rho peak for both processes. A manuscript with the results presented in Chapter 2 is in preparation, and it was done in collaboration with J. R. Morones-Ibarra and U. van Kolck.

1.3 Perturbative Pions and One-Pion Exchange

In the previous section, interactions among Goldstone bosons were studied. Here, the discussion is extended to include in EFT nucleons, non-relativistic objects, consistently with chiral symmetry. More precisely EFT is applied to the nuclear force problem, a nucleon-nucleon (NN) interaction with momenta below or at the pion mass scale, $Q \lesssim m_\pi$. Such application is relevant because of the existence of shallow bound states in nuclear physics, i. e. binding energies of NN interacting systems that are much below than m_π^2/M_{QCD} [19, 20, 21]. Actually, at very low energies the pions can be integrated out and interactions among nucleons can be described by contact terms. Such a theory where only nucleons are taken into account is called "pionless" EFT. In this case, the low-energy observables of the NN interactions can be expanded in powers of Q/m_π. From these contact terms the ones without derivatives correspond to two-nucleon interactions with zero angular momentum, $l = 0$, which exist only in the ${}^1S_0$ and ${}^3S_1$ channels. For systems containing interactions only among nucleons the most general non-relativistic effective Lagrangian is

$$\begin{aligned}\mathcal{L} &= N^\dagger \left(i\partial^0 + \frac{\vec{\nabla}^2}{2m_N} + \dots \right) N \\ &\quad - \frac{1}{(2f_\pi)^2} \left[C_V^{(0)} N^\dagger \boldsymbol{\tau} N \cdot N^\dagger \boldsymbol{\tau} N + C_T^{(0)} N^\dagger \vec{\sigma} \boldsymbol{\tau} N \cdot N^\dagger \vec{\sigma} \boldsymbol{\tau} N \right] + \cdots , \quad (1.63)\end{aligned}$$

where N is the nucleon field, m_N is the mass of the nucleon, $\vec{\sigma}$ and $\boldsymbol{\tau}$ are spin and isospin Pauli matrices, respectively. The dots denote contact interactions with an arbitrary number derivatives and multi-nucleon interactions, in particular, the

three-body force. The first term represents the kinetic energy of the nucleon and the last two terms are the two independent interactions used to describe the ${}^1S_0$ and ${}^3S_1$ channels. In addition, $C_V^{(0)}$ and $C_T^{(0)}$ correspond to spin-singlet and -triplet low-energy unknown constants determined by a fit to low-energy NN data, like ${}^1S_0$ and ${}^3S_1$ phase-shifts.

Even though the pionless EFT describes well interacting nucleons at low energy, the energy scale much below than m_π^2/M_{QCD} is too limited for most nuclear physics problems. As the EFT typical momentum Q reaches the scale of the mass of the pion m_π, $Q \sim m_\pi$, pion fields need to be explicitly included in EFT as extra degrees of freedom — pionful EFT. The lowest-order effective Lagrangian allowed by approximate chiral symmetry that describes interactions among pions and nucleons is given by

$$\begin{aligned} \mathcal{L}_{\pi,N}^{(0)} &= \mathcal{L}_{\mathrm{ChPT}}^{(0)} + \mathcal{L}_{NN}^{(0)} - \frac{1}{2f_\pi} g_A \vec{\nabla}\boldsymbol{\pi} \cdot\cdot N^\dagger \vec{\sigma}\boldsymbol{\tau} N \\ &\quad - \frac{1}{2f_\pi^2} N^\dagger \boldsymbol{\tau} \cdot (\boldsymbol{\pi} \times \partial_0 \boldsymbol{\pi})\, N + \ldots, \end{aligned} \tag{1.64}$$

where $g_A \simeq 1.26$ is the pion-nucleon axial-vector coupling constant, $\mathcal{L}_{NN}^{(0)}$ is the nucleon-nucleon interaction at leading order, and the dots contain irrelevant terms for the derivation of the nuclear force. The Lagrangian, in Eq. (1.64), is obtained according to ChPT chiral index, which is now $\nu' = \nu + f/2$. However, as one can see later, ChPT power counting has to be modified and the Lagrangian should contain, then, some derivative contact interactions [9].

If the number of nucleons A is just 0 or 1, the pionful EFT reduces to ChPT, seen in the last section, where the power counting is based on naive dimensional analysis. When $A = 2$ or more, however, the power counting is more complicated. Amplitudes for multiple-nucleons systems include "reducible" Feynman graphs with intermediate nucleon states, whose loops are integrated over the zeroth component of the four momentum leading to shallow poles at Q^2/M_N. This infrared enhancement creates contributions of $\mathcal{O}\left(M_{\mathrm{QCD}}/Q\right)$ over ChPT (or systems with $A = 0, 1$) [5] that cause the appearance of bound states indicating that the system is of non-perturbative nature, which invalidates Weinberg's power counting.

In Ref. [22], Weinberg proposed a way to generate the amplitude, which consists in summing all irreducible diagrams containing pions — the potential V — and in truncating the potential according to Weinberg's power counting, $\sigma' = \sigma + 2 - 2C - N$, where C is the number of connected pieces and N is the number of nucleons. We stress, here, that Weinberg's power counting is now applied to the potential. The potential is, then, iterated to all orders. Such iteration is the Lippmann-Schwinger (LS) equation, which is equivalent to the Schrödinger equation for the potential V. When the short-range interactions are assumed to obey naive dimensional analysis, the only contributions to the lowest-order potential are the derivativeless contact interactions and the one-pion exchange (OPE). The leading-order potential is then

$$V_{NN}^{(0)}(\vec{q}) = -\left(\frac{1}{2f_\pi}\right)^2 \boldsymbol{\tau}_1 \cdot \boldsymbol{\tau}_2 \left[g_A^2 \frac{\vec{\sigma}_1 \cdot \vec{q}\vec{\sigma}_2 \cdot \vec{q}}{\vec{q}^2 + m_\pi^2} + C_V^{(0)} + C_T^{(0)} \vec{\sigma}_1 \cdot \vec{\sigma}_2 \right], \quad (1.65)$$

where $\vec{q}$ is the transferred momentum.

Even though few-nucleon systems have been successfully described by Weinberg's power counting, Kaplan, Savage and Wise (KSW) claimed that the latter shows some inconsistencies [23]. The LS equation needs to be solved numerically with the introduction of a regulator which limits the momenta to cutoff Λ, separating low- and high-energy physics. This procedure generates a cutoff dependence in observables. Renormalization-group invariance ensures that low-energy physics does not depend on the choice of the regulator, i. e. low-energy observables do not depend on Λ. Therefore, the Λ dependence generated by OPE is absorbed in the coefficients of the contact interactions. Nonetheless, KSW [23] observed that ultraviolet (UV) divergences found in loop diagrams could not be absorbed by the available counterterms and suggested that pion exchange should not be fully iterated but rather be treated in perturbation theory. In this approach, the UV divergences are absorbed by the same, or even, lower-order operators in the expansion. LO and NLO NN phase shifts were successfully calculated [24]. From the results obtained, however, Ref. [25] observed that the KSW expansion does not converge already at relatively low momenta. NN phase shifts were computed at next-to-next-to-leading order ($\mathrm{N^2LO}$) [25], in the KSW scheme, and confirmed that the convergence is, indeed, slow in the

$^1S_0$ channel, but no perturbative convergence was found the spin-triplet $^3S_1 -^3 D_1$ coupled channels for momenta of the order of 100 MeV. Ref. [25] concluded that a singularity, stronger in spin-triplet than in spin-singlet channels, is the cause of the failure of the expansion convergence.

The problem, then, must rely on the comparison between short-range and OPE interactions. At $Q \sim m_\pi$, the OPE potential is of $\mathcal{O}\left(1/f_\pi^2\right)$, and, based on naive dimensional analysis, it was assumed that the coefficients of the LO contact interactions are of $\mathcal{O}\left(1/f_\pi^2\right)$. On the other hand, the contribution of each OPE iteration is of $\mathcal{O}\left(m_N Q/4\pi f_\pi^2\right)$, thus the fully iterated potential leads to virtual or real bound states at $Q \sim f_\pi \sim 100$ MeV, a non-perturbative effect. Still, the problem of the NN potential relies on the renormalization of the OPE, more specifically the problem resides in the tensor-force singularity of the nucleon potential [26]. The singularity can be explicitly seen by taking the Fourier transform of $V_{NN}^{(0)}\left(\vec{q}\right)$ in Eq. (1.65) which is

$$\begin{aligned} V_{\mathrm{OPE}}(r) &= \frac{m_\pi^3}{12\pi}\left(\frac{g_A}{2f_\pi}\right)^2 \boldsymbol{\tau}_1\cdot\boldsymbol{\tau}_2\left[T\left(m_\pi r\right)S_{12}\right. \\ &\qquad \left. +\vec{\sigma}_1\cdot\vec{\sigma}_2\left(Y\left(m_\pi r\right)-\frac{4\pi}{m_\pi^3}\delta^3\left(\vec{r}\right)\right)\right], \quad (1.66) \end{aligned}$$

where the Yukawa potential $Y\left(m_\pi r\right)$ and the tensor force $T\left(m_\pi r\right)$ are

$$Y\left(m_\pi r\right) = \frac{e^{-m_\pi r}}{m_\pi r}, \quad (1.67)$$

$$T\left(m_\pi r\right) = Y\left(m_\pi r\right)\left(1+\frac{3}{m_\pi r}+\frac{3}{\left(m_\pi r\right)^2}\right), \quad (1.68)$$

and the tensor operator is

$$S_{12} = 3\left(\vec{\sigma}_1\cdot\hat{r}\right)\left(\vec{\sigma}_2\cdot\hat{r}\right)-\vec{\sigma}_1\cdot\vec{\sigma}_2. \quad (1.69)$$

The singularity $1/\left(m_\pi r\right)^3$ in the tensor force $T\left(m_\pi r\right)$ is present only in spin-triplet partial waves. Thus the renormalization problem should only appear in spin-triplet channels. Ref. [27] examined the non-perturbative renormalization of the OPE in lowest waves, and concluded that Weinberg's power counting is consistent in a nonperturbative partial calculation. Still, OPE also contributes to higher partial

waves, and a cutoff dependence can be expected in some spin-triplet channels where the potential is attractive [9].

A complete investigation of the cutoff dependence of LO NN higher partial waves can be found in Ref. [9], where the introduction of counterterms that absorb cutoffs produced cutoff-independent phase shifts, at least for Λs up to 1 GeV, hence solving the renormalization issue. A summary of their observations is given here. For the low partial-wave channels, the constants $C_V^{(0)}$ and $C_T^{(0)}$ were fit to ${}^1S_0$, ${}^3S_1$ and ${}^3D_1$ phase shifts, all at 10 MeV. At various laboratory energies, the Λ dependence observed in these phase shifts is very small for $\Lambda \gtrsim 1$ GeV. The phase shifts for spin-singlet channels like ${}^1P_1$, ${}^1D_2$, ${}^1F_3$ and ${}^1G_4$, where the potential does not exhibit singularities, were found to have a very small dependence in the cutoff. The same small Λ dependence was found in spin-triplet channels like ${}^3P_1$ and ${}^3F_3$, where the tensor force is repulsive. All of these results validate Weinberg's power counting for the non-perturbative potential in leading order.

The existence of singularities in spin-triplet channels, like ${}^3P_0$ and ${}^3D_2$, where the tensor force is attractive, generates spurious bound states with binding energies that depend on the cutoff. As a consequence, the phase shifts in certain partial waves also depend on Λ. As Λ increases, the number of bound states increases. It is explicitly shown, in Ref. [9], that in the Λ regions where there are bound states, the phase shifts change very strongly. In the Λ range from 400 MeV to 4 GeV no bound states were found for higher partial waves, but they should appear once the value of Λ is increased. These results show that in these channels Weinberg's power counting is not consistent since there are not enough counterterms in LO available to absorb the Λ dependence.

The solution proposed in Ref. [9] consists in adding to each of the spin-triplet channels where the tensor force is attractive a counterterm that in Weinberg's power counting is present only at NLO for the ${}^3P_0$ and ${}^3P_2 - {}^3F_2$ and at N^{3}LO for the ${}^3D_2$ channel. Then fit each counterterm to its corresponding low-energy phase shift. The Λ independence is, then, confirmed for various laboratory energies. Higher partial waves were also analyzed with similar results. In addition to these results, Ref. [9]

found that after the Λ dependence was removed, there were still spurious bound states in some channels, but with different Λ dependence of the binding energies. For instance, a Λ-independent shallow bound state was found for the ${}^3S_1 - {}^3D_1$ coupled channels, the deuteron. In other channels, the spurious bound states were deeper. Other spurious bound states with very large binding energies appear, but only outside the regime of validity of the EFT.

In Chapter 3, we explore the idea of replacing the several counterterms, found in Ref. [9], with auxiliary fields. Such idea might be a good candidate to eliminate the $1/r^3$ singularity in the isovector tensor force from the one-pion-exchange potential. We build the lowest-order non-relativistic effective Lagrangian that includes not only pions and nucleons, but also auxiliary isovector vector and pseudovector fields and isoscalar scalar and vector fields. Once the two-nucleon potentials in momentum space for various spin and isospin are obtained we cancel the singularity by imposing a relation among the coupling constants that determine the strength of the NN potential. A Gaussian cutoff function is, then, used to obtain the same potentials in coordinate space. Some limiting cases like very large cutoff and decoupling of pseudovector/vector fields are compared to the two-nucleon potentials existing in the literature. Further, we present arguments, based on the large-N_c limit of QCD (with N_c the number of colors), to support our potential. The potential corresponding to the deuteron, i. e. the coupled ${}^3S_1 - {}^3D_1$ channels, is used to calculate the binding energy of the deuteron by perturbatively solving the Schrödinger equation. However, other cutoff functions besides the Gaussian one are considered in such solution. The work presented in Chapter 3 has not been published yet, and is the fruit of the collaboration with P. H. S. de Bruin, R. G. E. Timmermans and U. van Kolck.

1.4 Soft Collinear Effective Theory

Up until now, I have invoked ChPT to describe systems with a momentum scale $Q < M_{\rm QCD} \sim 1$ GeV, and HQET and NRQCD to describe systems with heavy quarks with $M \gg M_{\rm QCD} \sim Q$. Now, when light quarks have momenta Q much larger

than $M_{\rm QCD}$, $Q \gg M_{\rm QCD}$, the ratio $M_{\rm QCD}/Q$ provides an extra expansion parameter. Differently from HQET, energetic light quarks emit not only soft gluons but also collinear gluons, highly energetic gluons emitted in the direction of the quark, which cannot be integrated out. The effective theory that describes interactions among collinear quarks and soft and collinear gluons is the SCET [28, 29, 30, 31]. In order to build the SCET Lagrangian, the hard momentum $p_n \sim Q$ of the collinear (or hard) quark, whose mass m_q is much smaller than Q, is written in lightcone coordinates,

$$n^\mu = (1,0,0,-1)\,, \qquad \bar{n}^\mu = (1,0,0,1)\,, \tag{1.70}$$

where the 3-momentum is chosen to be in the z-direction. The coordinates n^μ and $\bar{n}^\mu$ obey the properties

$$\not{n} = \not{n}^\dagger, \qquad \not{\bar{n}} = \not{\bar{n}}^\dagger, \qquad \not{n}\not{\bar{n}}\not{n} = \not{\bar{n}}\not{n}\not{\bar{n}} = 0, \tag{1.71}$$

so that

$$p_n^\mu \;=\; \frac{n^\mu}{2}\bar{n}\cdot p_n + \frac{\bar{n}^\mu}{2} n\cdot p_n + p_n^{\perp\mu}, \tag{1.72}$$

which can be written as

$$\left(p_n^+, p_n^-, p_n^\perp\right) = \left(n\cdot p_n, \bar{n}\cdot p_n, p_n^\perp\right) \sim Q\left(\lambda^2, 1, \lambda\right), \tag{1.73}$$

where $\lambda \ll 1$ is the small expansion parameter of SCET, $n\cdot p_n^\perp = \bar{n}\cdot p_n^\perp = 0$, and $p_n^2 = m_q^2 = p_n^+ p_n^- + p_n^\perp \sim Q^2\lambda^2$. Similarly, one could find that the momentum scale of soft and ultrasoft particles are $p_s \sim Q\lambda$ and $p_{us} \sim Q\lambda^2$, respectively.

There are two different SCETs, SCET$_{\rm I}$ and SCET$_{\rm II}$, that define the explicit values of λ. In SCET$_{\rm I}$,

$$\lambda \;=\; \sqrt{\frac{M_{\rm QCD}}{Q}}, \tag{1.74}$$

which leads to $p_n^2 \sim QM_{\rm QCD}$ and $p_{us}^2 \sim M_{\rm QCD}^2$, while in SCET$_{\rm II}$,

$$\lambda = \frac{M_{\rm QCD}}{Q}, \tag{1.75}$$

Field 1	momentum 1	field 2	momentum 2	System momentum
collinear quark	$Q\,(\lambda^2, 1, \lambda)$	collinear gluon	$Q\,(\lambda^2, 1, \lambda)$	$Q\,(\lambda^2, 1, \lambda)$
ultrasoft quark	$Q\,(\lambda^2, \lambda^2, \lambda^2)$	collinear gluon	$Q\,(\lambda^2, 1, \lambda)$	$Q\,(\lambda^2, 1, \lambda)$
collinear quark	$Q\,(\lambda^2, 1, \lambda)$	ultrasoft gluon	$Q\,(\lambda^2, \lambda^2, \lambda^2)$	$Q\,(\lambda^2, 1, \lambda)$
ultrasoft quark	$Q\,(\lambda^2, \lambda^2, \lambda^2)$	ultrasoft gluon	$Q\,(\lambda^2, \lambda^2, \lambda^2)$	$Q\,(\lambda^2, \lambda^2, \lambda^2)$
soft quark	$(\lambda, \lambda, \lambda)$	collinear gluon	$Q\,(\lambda^2, 1, \lambda)$	$Q\,(\lambda, 1, \lambda)$

Table 1.1: Degrees of freedom in SCET and their respective momentum, scaling with λ. A similar analysis can bound in Ref. [32].

and therefore $p_n^2 \sim p_{us}^2 \sim M_{\rm QCD}^2$.

The power counting for the interactions has to be identified for various momentum regions, and is summarized in Tab. 1.1. A similar analysis can be found in Ref. [32]. The example given in the first line of Tab. 1.1 describes a collinear quark with momentum $Q\,(\lambda^2, 1, \lambda)$ interacting with a collinear gluon with momentum $Q\,(\lambda^2, 1, \lambda)$. The system momentum is $Q\,(\lambda^2, 1, \lambda)$ and the collinear quark is kept on-shell. In the third (or the fifth) line of Tab. 1.1, when an ultrasoft (or a soft) quark, such as N_v from HQET, interacts with a collinear gluon, the quark absorbs the momentum of the gluon and becomes off-shell. In this situation, the quark cannot be described by HQET and it is integrated out. The same analysis can be done for the other interactions.

To construct the SCET Lagrangian, one starts, again, from the QCD Lagrangian given by Eq. (1.1), which describes interactions among quarks and gluons in any momentum region. Because the masses of collinear quarks are much smaller than their momentum, the mass term in Eq. (1.1) can be neglected. The fermion field can be projected into the n direction

$$q(x) = (P_n + P_{\bar n})\, q(x) = \frac{\not{n}\bar{\not{n}}}{4} q(x) + \frac{\bar{\not{n}}\not{n}}{4} q(x) \equiv \xi_n(x) + \xi_{\bar n}(x), \tag{1.76}$$

where $\xi_n(x)$ and $\xi_{\bar n}(x)$ are the two large and two small components of $q(x)$, and P_n and $P_{\bar n}$ are projection operators that satisfy $P_n + P_{\bar n} = 1$, and have properties

$$P_n^\dagger = P_n, \qquad P_{\bar n}^\dagger = P_{\bar n}, \qquad P_n P_n = P_n, \qquad P_{\bar n} P_{\bar n} = P_{\bar n}, \qquad P_n P_{\bar n} = P_{\bar n} P_n = 0. \tag{1.77}$$

With the properties shown in Eq. (1.77), the quark-kinetic term in Eq. (1.1) can

be rewritten as

$$\begin{aligned}\mathcal{L}_{\rm SCET}(x) &= \bar{\xi}_n(x)\frac{\bar{n}\!\!\!/}{2} in\cdot D\xi_n(x) + \bar{\xi}_{\bar{n}}(x) i\bar{n}\cdot D\xi_{\bar{n}}(x) \\ &\quad + \bar{\xi}_n(x) iD\!\!\!/_\perp \xi_{\bar{n}}(x) + \bar{\xi}_{\bar{n}}(x) iD\!\!\!/_\perp \xi_n(x). \end{aligned} \tag{1.78}$$

The component $\xi_{\bar{n}}$ can be eliminated by a field redefinition, or through the equations of motion, which leads to the Lagrangian

$$\mathcal{L}_{\rm SCET}(x) = \bar{\xi}_n(x)\left(in\cdot D + iD\!\!\!/_\perp \frac{1}{i\bar{n}\cdot D} iD\!\!\!/_\perp\right)\frac{\bar{n}\!\!\!/}{2}\xi_n(x), \tag{1.79}$$

where the covariant derivative contains only collinear and ultrasoft gluons since the hard scale fields were integrated out.

However, in order to find the lowest-order SCET Lagrangian, it is necessary to separate the small (residual) momenta, $k^\mu = p^\mu - \tilde{p}^\mu$, from the large momenta $\tilde{p}^\mu$. The latter is removed by a field redefinition, which consists in introducing a label operator, $\mathcal{P}_\mu$, and defining a new collinear field, $\xi_{n,p}(x)$, such as

$$\xi_n(x) = \mathcal{P}_\mu \xi_{n,p}(x) = \sum_{\tilde{p}} e^{-i\tilde{p}\cdot x}\xi_{n,p}(x), \tag{1.80}$$

where $\xi_{n,p}(x)$ depends only on the label p. At the same time, the covariant derivative is shifted by a phase, through the same label operator $\mathcal{P}_\mu$, leading to

$$in\cdot D = in\cdot\partial + g_s n\cdot G_{n,\,q} + g_s n\cdot G_{us,\,q} \sim \lambda^2, \tag{1.81}$$

$$i\bar{n}\cdot D^c = \bar{\mathcal{P}} + g_s\bar{n}\cdot G_{n,\,q} + \mathcal{O}(\lambda) \sim 1, \tag{1.82}$$

$$iD\!\!\!/^c_\perp = \mathcal{P}_\perp + g_s G_{n,\,q_\perp} + \mathcal{O}(\lambda^2) \sim \lambda, \tag{1.83}$$

where $G_{n,\,q}$ and $G_{us,\,q}$ are the collinear and ultrasoft gluons with dependence on the momentum q, respectively, and $p_\perp$ is the perpendicular component of the momentum of the gluon. Thus the lowest-order SCET Lagrangian is

$$\mathcal{L}_{\rm SCET}(x) = \sum_{\tilde{p}} e^{-i\tilde{p}\cdot x}\bar{\xi}_{n,p}(x)\left(in\cdot D + iD\!\!\!/^c_\perp \frac{1}{i\bar{n}\cdot D^c} iD\!\!\!/^c_\perp\right)\frac{\bar{n}\!\!\!/}{2}\xi_{n,p}(x), \tag{1.84}$$

where the label momentum $\tilde{p}^\mu$ is removed due to the exponent. More details can be found in Refs. [33, 34, 35]. A similar analysis may be done to derive the LO interactions among gluons. Unfortunately, SCET has only residual gauge symmetries,

for example, in $\mathrm{SCET_I}$,

$$(\bar{n}\cdot\partial, n\cdot\partial, \partial_\perp)\, U_n(x) \sim Q\left(\lambda^2, 1, \lambda\right) U_n(x), \tag{1.85}$$

$$(\bar{n}\cdot\partial, n\cdot\partial, \partial_\perp)\, U_{us}(x) \sim Q\left(\lambda^2, \lambda^2, \lambda^2\right) U_{us}(x), \tag{1.86}$$

where $U_n(x)$ and $U_{us}(x)$ are the collinear and ultrasoft gauge transformations, respectively. Collinear fields are non-linearly transformed under both local $U_n(x)$ and $U_{us}(x)$ gauge transformations, while ultrasoft fields are non-linearly transformed only under $U_{us}(x)$. The latter is the usual QCD transformation that can be neglected due to Eq. (1.86). More details on the SCET gauge symmetries can be found in Ref. [28].

The LO SCET Lagrangian, given by Eq. (1.84), is not invariant under collinear gauge transformations. To build operators that contain collinear fields and at the same time are gauge invariant, one defines an unitary operator called a collinear Wilson line [29] by

$$W_n(x) \;=\; P\exp\left(ig_s\int_{-\infty}^{x} ds\bar{n}\cdot G_n(\bar{n}\cdot s)\right), \tag{1.87}$$

where $W_n^\dagger W_n = W_n W_n^\dagger = 1$ and P denotes path ordering. The Wilson line transforms under collinear gauge transformation as

$$W_n(y) \to U_n(y) W_n(y), \tag{1.88}$$

which multiplied by the collinear fields produces operators that are gauge invariant such as

$$\chi^c_{n,n\cdot p} \equiv \left(W_n^\dagger \xi_n^c\right)_{n\cdot p}, \tag{1.89}$$

and others, see Chapter 4. This kind of operator, used to build SCET, describes a collinear quark and many collinear gluons moving in the same n direction. The SCET Lagrangian, in Eq. (1.84), still contains interactions among collinear quarks and ultrasoft gluons. The fields can be decoupled, though, by the ultrasoft Wilson line Y_n, given by

$$Y_n(x) \;=\; P\exp\left(ig_s\int_{-\infty}^{x} dsn\cdot G^a_{us}(n\cdot s)t^a\right), \tag{1.90}$$

then, ultrasoft gluons can be integrated out by the collinear Wilson line transformation

$$W_n(x) \to Y_n(x) W_n^{(0)} Y_n(x). \tag{1.91}$$

In the same way, soft gluons can be decoupled by the soft Wilson line

$$S_n(x) \;=\; P \exp\left(i g_s \int_{-\infty}^{x} ds n \cdot G_s^a(n \cdot s) t^a \right), \tag{1.92}$$

and integrated out from the HQET or the NRQCD Lagrangian by the collinear Wilson line transformation, as in Eq. (1.91), with $Y_n(x)$ substituted by $S_n(x)$. The new $\mathrm{SCET_I}$ fields are now written as

$$\xi_{n,p}(x) = Y_n(x) \xi_{n,p}^{(0)}(x), \qquad G_{n,p}(x) = Y_n(x) G_{n,p}^{(0)}(x) Y_n^\dagger(x), \tag{1.93}$$

where $\xi_{n,p}^{(0)}(x)$ and $G_{n,p}^{(0)}(x)$ are the bare collinear quarks and gluons, while the new $\mathrm{SCET_{II}}$ fields are written as

$$\xi_{n,p}(x) = S_n(x) \xi_{n,p}^{(0)}(x), \qquad G_{n,p}(x) = S_n(x) G_{n,p}^{(0)}(x) S_n^\dagger(x). \tag{1.94}$$

The next step in solving a problem in the SCET framework is the factorization of operators. But before that, it is necessary to start the study by matching, order by order, SCET operators, $\mathcal{O}_{\mathrm{SCET}}$, onto the QCD operators, $\mathcal{O}_{\mathrm{QCD}}$,

$$\mathcal{O}_{\mathrm{QCD}} \;=\; C(\mu) \mathcal{O}_{\mathrm{SCET}}(\mu), \tag{1.95}$$

where $C(\mu)$ is a matching coefficient that depends on the renormalization scale μ. In Chapter 4, this is done by comparing the LO SCET diagrams to the QCD diagrams that represent the same processes. The $\mathcal{O}_{\mathrm{SCET}}(\mu)$ contains usoft Wilson lines that factorize the usoft degrees of freedom. Additionally, Soft Wilson lines may be introduced to match $\mathrm{SCET_I}$ onto $\mathrm{SCET_{II}}$. The matrix elements containing SCET operators have all the different momentum scales in different operators, naturally factorizing the matrix elements. Unfortunately, SCET operators are affected by low-energy scales and, as a consequence, logarithms appears in perturbative calculations. Further, matching coefficients are also affected by high-energy physics, leading to

a large logarithm content, ruining perturbation theory. The large logarithms need, then, to be resummed, which can be accomplished through renormalization-group equations (RGEs),

$$\frac{d}{d\ln\mu}C(\mu) \;=\; \gamma(\mu)C(\mu), \qquad \frac{d}{d\ln\mu}\mathcal{O}_{\rm SCET}(\mu) = \gamma(\mu)\mathcal{O}_{\rm SCET}, \tag{1.96}$$

where $\gamma(\mu) = \gamma(\alpha_s) + C_{\mathcal{O}}\Gamma_{\rm cusp}(\alpha_s)\ln(Q/\mu)$ is the anomalous dimension. The parameters $\gamma(\alpha_s)$ and $C_{\mathcal{O}}$ are an anomalous dimension and a coefficient that depend on the process studied, and $\Gamma_{\rm cusp}$ is the cusp anomalous dimension. From the RGEs, given by Eq. (1.96), the general solution for $C(\mu)$ is

$$C(\mu) = U(\mu_0,\mu)C(\mu_0), \tag{1.97}$$

where $U(\mu_0,\mu)$ embodies a sum of $\ln(\mu/\mu_0)$ with the leading-log term being $U(\mu_0,\mu) = \alpha_s^2\ln^2\mu/\mu_0$. At $\mu_0 \sim Q$, the large logarithms vanish in the perturbative function $C(\mu)$. Calculations of $\gamma(\mu)$ in higher order lead to resummation of more logarithms, and the solution of the RGEs includes convolutions of the momentum involved. Such solution can be found in Chapter 4.

In Chapter 4, we use HQET, NRQCD and SCET to investigate the exclusive decays of the non-relativistic bound states of b quarks and $\bar{b}$ antiquarks, χ_b and η_b, into two highly energetic D mesons, bound states of c or $\bar{c}$ quarks with light quarks u and d. To integrate out the scale m_b (mass of the b quark), b and $\bar{b}$ are described by NRQCD in the initial state, while c and $\bar{c}$ are described by SCET in the final state. Then, the scale m_c (mass of the c quark) is integrated out by applying potential NRQCD, a low-energy effective theory, and boosted HQET in the initial and final states, respectively. The factorized expressions for the decay rate that resummed logarithms of the ratio m_c/m_b and $M_{\rm QCD}/m_c$ are also found. Lastly, we perform perturbative and non-perturbative corrections to the decay rate. Note that gluon fields represented by G_μ here are represented by A_μ in Chapter 4. The work presented in Chapter 4 has been done in collaboration with E. Mereghetti and B. Long, and published in Ref. [36].

CHAPTER 2

PION-PION SCATTERING AND ELECTRON-POSITRON ANNIHILATION IN THE RHO REGION WITH VECTOR SYMMETRY

2.1 Introduction

Chiral perturbation theory (ChPT) [18, 38] is the effective field theory (EFT) of QCD for processes involving momenta Q comparable to the pion mass, m_π, but much smaller than the characteristic QCD scale, $M_{QCD} \sim 1$ GeV. An EFT derives its strength from the fact that it includes all interactions among the relevant low-energy degrees of freedom which are allowed by the symmetries of the underlying theory. In order to have any predictive power, however, it requires an expansion in terms of small ratios of scales. In ChPT, Q/M_{QCD} and m_π/M_{QCD} provide the basis for a successful description of processes involving pions and nucleons [39, 4, 40] using (approximate) chiral symmetry, $SU(2)_L \times SU(2)_R$.

A longstanding problem has been how to extend ChPT to energies comparable to the masses of heavier mesons. Among them, the rho meson stands out [41], showing up as a bump in scattering cross sections at the center-of-mass energy of about 770 MeV in reactions like elastic pion-pion scattering ($\pi\pi \to \pi\pi$) and electron-positron annihilation into two pions ($e^+e^- \to \pi\pi$). The T-matrix poles associated with resonances like the rho cannot be produced in ChPT.

One possibility is to perform a selective resummation of ChPT. To the extent that the ChPT parameters subsume information about the resonances, it is plausible that an iteration in the direct (s) channel will generate T-matrix poles near the observed locations. However, which interactions are to be resummed is not clear *a priori*, and various alternatives exist, see, for example, Refs. [42, 43, 44, 45, 46]. This ambiguity is not resolved by the mere inclusion in ChPT of explicit degrees of freedom for the resonances, even if this is done consistently with chiral symmetry

[47, 48, 49, 50, 38, 41, 51, 52, 53]. As long as all interactions are included, the choice of fields should not matter for the calculation of observables, as it has been shown explicitly for the rho in Ref. [52]. The difficulty is that the resonance positions are not, in the complex plane relative to thresholds of pion reactions, obviously within a circle of radius M_{QCD}. As a consequence, interactions with an arbitrary number of derivatives are not necessarily suppressed, nor are diagrams with an arbitrary number of loops, although one can invoke a large number of colors to justify an expansion on the latter [54].

One of the few ideas that allow the controlled inclusion in EFT of vector mesons is vector symmetry [55]. The assumption is that there is a limit, the "vector limit", in which QCD has a larger symmetry than chiral symmetry, where the rho mesons are massless: their transverse components decouple and the longitudinal components form with the pions an $SU(2) \times SU(2)$ multiplet. Although it is not obvious that such a limit exists, it is a possible scenario [56] for chiral restoration as the temperature increases towards the phase transition, where some other degree(s) of freedom should become massless (neglecting quark masses) to form a chiral multiplet with the pions [57]. The expansion around the vector limit might also yield lessons for the construction of alternative mechanisms for electroweak-symmetry breaking in the Standard Model [58].

Away from the vector limit, the vector mesons become massive, with mass m_ρ proportional to the pion decay constant. This gives a tree-level relation, which unfortunately differs from the corresponding, phenomenologically successful KSFR-II relation [59]. More generally, the proposed limit provides a symmetry basis for relations among properties of the rho meson, which however are of limited usefulness at tree level. Still, the main virtue of this assumption is that it allows a systematic expansion *beyond* tree level, because pions and rhos have, parametrically, masses that are small compared to M_{QCD}. In fact, one-loop corrections have been considered in the leading-log approximation in Ref. [60], and significant improvement was found for pion and rho parameters extracted from data.

Here we take the formulation and phenomenology of the proposed "Vector EFT"

a couple of steps further.

First, we enlarge the usual formulation [55, 60] to accommodate electromagnetic gauge invariance. In unitary gauge, the massless scalar fields become, through the Higgs mechanism, the longitudinal components of gauge bosons. The resulting Lagrangian has elements of both common versions [49, 61, 53, 62] of vector-meson-dominance dynamics, VMD-1 and VMD-2. The gauge-boson mass matrix is not diagonal (a VMD-2 feature), and its diagonalization leads to the standard massive rho and massless photon. However, the mass-eigenstates still mix via their field strengths (as in VMD-1), with a parameter $a_{\gamma\rho}$ that is not determined by vector symmetry. This gives rise to a second tree-level relation, now between the photon-rho mixing and the pion decay constant, which for a certain value of $a_{\gamma\rho}$ can reproduce another successful relation (KSFR-I) [59].

Second, we compare the EFT directly with data near the rho region. We consider explicitly not only the quintessential $\pi\pi \to \pi\pi$, but also $e^+e^- \to \pi\pi$, from which rho parameters are typically extracted, and the associated (time-like) pion form factor. In processes where all momenta are much below the rho mass, the rho can be integrated out and we recover ChPT, with its low-energy constants (LECs) determined by the LECs of the Vector EFT. As momenta grow and we enter the rho region, Vector EFT comes on its own, but one needs to resum certain diagrams. We do so by extending the generic power counting of Vector EFT [55, 60] to a kinematic region around the peak of the cross sections, exactly as done in other EFTs with P-wave resonances: halo/cluster EFT for nucleon-alpha scattering near the ^{5}He ground state [6] and ChPT for pion-nucleon scattering near the $\Delta(1232)$ [7] (or [8] for a slightly different, earlier version). We show that the rho width, a formally subleading effect in general, is enhanced due to the "kinematic" fine-tuning to the rho peak. For $e^+e^- \to \pi\pi$, a similar effect takes place also for the photon-rho mixing.

Third, we include all contributions that appear to a given order in the power counting, including finite terms from loops and the short-range interactions needed for renormalization-group invariance. In addition to renormalization of the rho mass

and the photon-rho mixing parameter, one-loop pion diagrams provide imaginary pieces, which can be identified with the partial amplitude for rho decay into two pions and with an imaginary component of photon-rho mixing.

The chapter is organized as follows. In Sect. 2.2 we construct the most general effective Lagrangian that has interactions between pions, rhos, and photons, consistent with gauge invariance and the assumed vector symmetry of QCD. We compare this Lagrangian to the one of ChPT in App. A. The power counting needed to describe reactions around the rho peak is presented in Sect. 2.3. The rho width and the photon-rho mixing are then calculated in Sect. 2.4 to one loop, from the two-point functions for the vector mesons. Vector symmetry is shown to be preserved at this level. A similar discussion of chiral symmetry is relegated to App. B, where a calculation of the pion self-energy to one loop, not needed in the text, is presented. The rho width is rederived from decay of an on-shell rho in App. C. With these basic ingredients, in Sect. 2.5 we calculate the scattering amplitudes for $\pi\pi \to \pi\pi$ and $e^+e^- \to \pi\pi$ in the region around the rho peak, to lowest order. These amplitudes depend on only two rho parameters, m_ρ and $a_{\gamma\rho}$, and have the characteristic resonance forms in terms of the partial decay widths of the rho to two pions and to electron-positron pairs. From the scattering amplitudes we extract the $\pi\pi \to \pi\pi$ phase shift and $e^+e^- \to \pi\pi$ cross section, which are compared in Sect. 2.6 to the corresponding data. We use the $e^+e^- \to \pi^+\pi^-$ data to determine m_ρ and $a_{\gamma\rho}$, and then compare the prediction for the $\pi\pi \to \pi\pi$ phase shift with values extracted from data. We show that discrepancies can be attributed to the small value of the width at the one-loop level. We conclude in Sect. 2.7.

2.2 Construction of the Lagrangian

In this section we review vector symmetry and the construction of the most general effective Lagrangian that incorporates it and its breaking [55, 60]. We include the effects of electromagnetic gauge invariance. For definiteness we work with $N_f = 2$ quark flavors, up and down, but the formalism can be extended straightforwardly

to arbitrary N_f.

The smallness of pion masses compared to the typical QCD scale M_{QCD} can be understood if, in the limit of vanishing quark masses, the pions are Goldstone bosons of the spontaneous breakdown of chiral symmetry. Other degrees of freedom are naturally light if they, too, are Goldstone bosons, which requires a larger symmetry to start with. Georgi's idea [55] was to postulate a limit of QCD where the invariance group is a product of four $SU(2)$ groups,

$$G \;=\; SU(2)_L \times SU(2)_{G_L} \times SU(2)_R \times SU(2)_{G_R}, \tag{2.1}$$

which is spontaneously broken by the non-perturbative dynamics to its subgroup

$$H \;=\; SU(2)_{L+G_L} \times SU(2)_{R+G_R}, \tag{2.2}$$

where $SU(2)_{A+B}$ denotes the diagonal subgroup of $SU(2)_A \times SU(2)_B$.

As a consequence of this breaking, there are six Goldstone bosons, which, following the standard theory of non-linear realizations [17], can be assembled into two matrices $\Sigma_{L,R}$ that transform as

$$\Sigma_L \to L\Sigma_L G_L^\dagger, \qquad \Sigma_R \to R\Sigma_R G_R^\dagger, \tag{2.3}$$

under elements L, G_L, R, and G_R of $SU(2)_L$, $SU(2)_{G_L}$, $SU(2)_R$, and $SU(2)_{G_R}$, respectively. It is convenient to write

$$\Sigma_L = \xi\zeta, \qquad \Sigma_R = \xi^\dagger\zeta, \tag{2.4}$$

with

$$\xi = e^{i\pi/f_\pi} = e^{i\pi^a t^a/f_\pi}, \qquad \zeta = e^{is/f_\pi} = e^{is^a t^a/f_\pi}, \tag{2.5}$$

where $t^a = \tau^a/2$ are the three generators of $SU(2)$; $\pi^a(x)$ are isovector pseudoscalar fields identified with the usual Goldstone bosons; $s^a(x)$ are isovector scalar fields associated with a new set of Goldstone bosons; and f_π is a constant, which for canonically normalized fields has dimension of mass —the pion decay constant $f_\pi \simeq 92$ MeV. The Goldstone bosons themselves have more complicated, non-linear transformation properties.

In the vector limit, an effective low-energy Lagrangian with these fields would describe interactions among three massless pseudoscalar mesons and three massless scalar mesons. In contrast with the standard scenario where the unbroken group is just $SU(2)$, here a chiral symmetry remains unbroken and manifest in the spectrum. Away from this limit there are no light isovector scalars, but there is a not very heavy isovector vector, the rho, the longitudinal components of which could be related to the isovector scalars. In order to account for the rho, we introduce spurion vector fields $\rho^a_{L\mu}$ and $\rho^a_{R\mu}$, which we choose to transform as gauge fields under the two identical local groups $SU(2)_{G_L}$ and $SU(2)_{G_R}$ [60],

$$\rho_{L\mu} = \rho^a_{L\mu} t^a \to G_L \left(\rho_{L\mu} - i\partial_\mu\right) G_L^\dagger, \qquad \rho_{R\mu} = \rho^a_{R\mu} t^a \to G_R \left(\rho_{R\mu} - i\partial_\mu\right) G_R^\dagger, \quad (2.6)$$

where $G_L = G_L(x)$ and $G_R = G_R(x)$.

The EFT will also contain a field for the massless photon, and an associated local $U(1)$ symmetry that remains unbroken:

$$U = \exp\left(i\theta(x) t^3\right), \quad (2.7)$$

with parameter $\theta(x)$. We take the Goldstone boson and vector fields to transform, respectively, as

$$\Sigma_{L(R)} \to U \Sigma_{L(R)} U^\dagger, \quad (2.8)$$

and

$$\rho_{L(R)\mu} \to U \left(\rho_{L(R)\mu} - i\partial_\mu\right) U^\dagger. \quad (2.9)$$

These transformations mean that $U(1)$ is in the diagonal part of H, and they guarantee that the components of π and $\rho_{L(R)\mu}$ change according to their usual electromagnetic charge, except that $\rho^3_{L(R)\mu}$ also changes. In order to account for the photon, we introduce further spurion vector fields, $B^3_{L\mu}$ and $B^3_{R\mu}$, transforming as

$$B_{L(R)\mu} = B^3_{L(R)\mu} t^3 \to U \left(B_{L(R)\mu} - i\partial_\mu\right) U^\dagger \quad (2.10)$$

under $U(1)$, and as

$$B_{L\mu} \to L B_{L\mu} L^\dagger, \qquad B_{R\mu} \to R B_{R\mu} R^\dagger \quad (2.11)$$

under the rest of G. In the vector limit the gauge boson of $U(1)$ is a combination of $B^3_{L\mu}$, $B^3_{R\mu}$, $\rho^3_{L\mu}$, and $\rho^3_{R\mu}$.

In order to construct interactions that are invariant under G and, specifically, $U(1)$, we define derivatives that transform covariantly. For the Goldstone bosons,

$$D_\mu \Sigma_L = \partial_\mu \Sigma_L - i\Sigma_L \rho_{L\mu} + iB_{L\mu}\Sigma_L, \qquad D_\mu \Sigma_R = \partial_\mu \Sigma_R - i\Sigma_R \rho_{R\mu} + iB_{R\mu}\Sigma_R \quad (2.12)$$

transform as Eq. (2.3) under G and as Eq. (2.8) under $U(1)$. Analogously, the field strengths

$$\rho_{L\mu\nu} = \partial_\mu \rho_{L\nu} - \partial_\nu \rho_{L\mu} + i[\rho_{L\mu}, \rho_{L\nu}], \qquad \rho_{R\mu\nu} = \partial_\mu \rho_{R\nu} - \partial_\nu \rho_{R\mu} + i[\rho_{R\mu}, \rho_{R\nu}] \quad (2.13)$$

for the rho-like spurions, and

$$B_{L\mu\nu} = \partial_\mu B_{L\nu} - \partial_\nu B_{L\mu}, \qquad B_{R\mu\nu} = \partial_\mu B_{R\nu} - \partial_\nu B_{R\mu} \quad (2.14)$$

for the photon-like spurions, transform linearly under G,

$$\rho_{L\mu\nu} \to G_L \rho_{L\mu\nu} G_L^\dagger, \qquad \rho_{R\mu\nu} \to G_R \rho_{R\mu\nu} G_R^\dagger, \quad (2.15)$$

$$B_{L\mu\nu} \to L B_{L\mu\nu} L^\dagger, \qquad B_{R\mu\nu} \to R B_{R\mu\nu} R^\dagger, \quad (2.16)$$

and under $U(1)$, in particular, as

$$\rho_{L(R)\mu\nu} \to U \rho_{L(R)\mu\nu} U^\dagger, \quad (2.17)$$

$$B_{L(R)\mu\nu} \to U B_{L(R)\mu\nu} U^\dagger. \quad (2.18)$$

The gauge structure ensures that the vector fields couple only to conserved currents.

In addition to the rho mass and electromagnetic interactions, vector symmetry is broken explicitly by the quark masses. As with just chiral symmetry, explicit breaking can be incorporated treating the quark mass matrix M as a spurion field,

$$M \to R M L^\dagger. \quad (2.19)$$

M generates the square of the Goldstone boson mass through an associated constant μ. The extra gauge symmetries can be accommodated by elevating μ to another spurion field [55],

$$\mu \to G_L \mu G_R^\dagger. \quad (2.20)$$

With these elements we can construct the most general Lagrangian incorporating vector symmetry,

$$\begin{aligned}\mathcal{L} &= \frac{f_\pi^2}{2}\mathrm{Tr}\left[(D^\mu\Sigma_L)^\dagger D_\mu\Sigma_L + (D^\mu\Sigma_R)^\dagger D_\mu\Sigma_R\right] + \frac{f_\pi^2}{2}\mathrm{Tr}\left(\mu\Sigma_R^\dagger M\Sigma_L + \mu^\dagger\Sigma_L^\dagger M^\dagger\Sigma_R\right) \\ &\quad -\frac{1}{4g^2}\mathrm{Tr}\left(\rho_{L\mu\nu}\rho_L^{\mu\nu} + \rho_{R\mu\nu}\rho_R^{\mu\nu}\right) - \frac{1}{4g'^2}\mathrm{Tr}\left(B_{L\mu\nu}B_L^{\mu\nu} + B_{R\mu\nu}B_R^{\mu\nu}\right) \\ &\quad -\frac{a_{\gamma\rho}}{(4\pi)^2}\mathrm{Tr}\left(B_{L\mu\nu}\Sigma_L\rho_L^{\mu\nu}\Sigma_L^\dagger + B_{R\mu\nu}\Sigma_R\rho_R^{\mu\nu}\Sigma_R^\dagger\right) + \ldots, \end{aligned} \tag{2.21}$$

where g, g', and $a_{\gamma\rho}$ are undetermined parameters characterizing the interactions with smallest number of derivatives, and "..." denote terms with more derivatives and powers of the quark mass matrix.

The degrees of freedom associated with the scalars, encoded in ζ, can be moved to the rho-like spurion fields $\rho_{L(R)\mu}$ by a field redefinition. We define fields in the "unitary gauge", labeled by a superscript ^{u}, by doing a transformation $G_L(x) = G_R(x) = \zeta(x)$:

$$\xi = \Sigma_L^u = \Sigma_L\zeta^\dagger = \Sigma_R^{u\dagger} = \zeta\Sigma_R^\dagger, \tag{2.22}$$

$$\rho_{L(R)\mu}^u = \zeta\rho_{L(R)\mu}\zeta^\dagger - i\zeta\partial_\mu\zeta^\dagger, \tag{2.23}$$

$$B_{L(R)\mu}^u = B_{L(R)\mu}, \tag{2.24}$$

$$M^u = M, \tag{2.25}$$

$$\mu^u = \zeta\mu\zeta^\dagger. \tag{2.26}$$

Such a field redefinition does not change the form of the vector-symmetric Lagrangian.

We are now ready to break G down to H by restricting the spurion fields to their actual values. While μ^u is a real constant and M^u is the quark-mass matrix,

$$\mu^u = \mu^{u\dagger}, \tag{2.27}$$

$$M^u = M^{u\dagger} = \begin{pmatrix} m_u & 0 \\ 0 & m_d \end{pmatrix} \equiv \bar{m}\left(1 - 2\varepsilon\, t^3\right), \tag{2.28}$$

$\rho_{L(R)\mu}^u$ and $B_{L(R)\mu}^u$ reduce to two vector-meson fields:

$$\rho_{L\mu}^u = \rho_{R\mu}^u \equiv g\tilde{\rho}_\mu, \tag{2.29}$$

$$B_{L\mu}^u = B_{R\mu}^u \equiv g'B_\mu. \tag{2.30}$$

The Lagrangian in unitary gauge becomes

$$\begin{aligned}\mathcal{L} &= f_\pi^2 \mathrm{Tr}\left[\left(\partial_\mu \xi^\dagger\right)\partial^\mu \xi\right] + \frac{f_\pi^2 m_\pi^2}{4}\mathrm{Tr}\left(\xi^2 + \xi^{\dagger 2}\right) \\ &+ i f_\pi^2 \mathrm{Tr}\left[\left(g\tilde{\rho}_\mu + g' B_\mu\right)\left(\xi^\dagger \partial^\mu \xi + \xi \partial^\mu \xi^\dagger\right)\right] - \frac{1}{2}\mathrm{Tr}\left(\tilde{\rho}_{\mu\nu}\tilde{\rho}^{\mu\nu}\right) - \frac{1}{2}\mathrm{Tr}\left(B_{\mu\nu}B^{\mu\nu}\right) \\ &+ f_\pi^2 \mathrm{Tr}\left(g^2 \tilde{\rho}_\mu \tilde{\rho}^\mu + g'^2 B_\mu B^\mu\right) - f_\pi^2 g g' \mathrm{Tr}\left[\tilde{\rho}^\mu\left(\xi^\dagger B_\mu \xi + \xi B_\mu \xi^\dagger\right)\right] \\ &- \frac{g g' a_{\gamma\rho}}{(4\pi)^2}\mathrm{Tr}\left[\tilde{\rho}^{\mu\nu}\left(\xi^\dagger B_{\mu\nu}\xi + \xi B_{\mu\nu}\xi^\dagger\right)\right] + \ldots, \end{aligned} \tag{2.31}$$

where we introduced the field strengths

$$\tilde{\rho}_{\mu\nu} = \partial_\mu \tilde{\rho}_\nu - \partial_\nu \tilde{\rho}_\mu + ig\left[\tilde{\rho}_\mu, \tilde{\rho}_\nu\right], \tag{2.32}$$

$$B_{\mu\nu} = \partial_\mu B_\nu - \partial_\nu B_\mu, \tag{2.33}$$

and the pion mass

$$m_\pi^2 = 2\mu^u \bar{m}. \tag{2.34}$$

The first two terms in Eq. (2.31) describe the kinetic energy, mass, and self-interactions of pions, and the third their interactions with the vector mesons. The fourth, fifth and sixth represent the kinetic energy, mass, and self-interactions of vector mesons. The last two terms displayed explicitly contain mixing of the vector mesons and more of their interactions with pions.

We see that the scalars have been "eaten" to become the longitudinal components of massive vector mesons —the Higgs mechanism. However, the fields $\tilde{\rho}_\mu^3$ and B_μ^3 do not have well defined masses, as in many models such as VMD-2 [49]. In addition, there is mixing via field strengths (parametrized by $a_{\gamma\rho}$), as in VMD-1 [61]. As in the hidden-gauge formulation [50], these gauge fields are a combination of the mass eigenstates

$$\rho_\mu^3 \equiv \left(1 - \frac{g^2 g'^2}{g^2 + g'^2}\frac{a_{\gamma\rho}}{4\pi^2}\right)^{1/2} \frac{1}{\left(g^2 + g'^2\right)^{1/2}}\left(g\tilde{\rho}_\mu^3 - g' B_\mu^3\right), \tag{2.35}$$

$$A_\mu \equiv \left(1 + \frac{g^2 g'^2}{g^2 + g'^2}\frac{a_{\gamma\rho}}{4\pi^2}\right)^{1/2} \frac{1}{\left(g^2 + g'^2\right)^{1/2}}\left(g'\tilde{\rho}_\mu^3 + g B_\mu^3\right). \tag{2.36}$$

In terms of the new fields,

$$
\begin{aligned}
\mathcal{L} \;=\;& f_\pi^2 \mathrm{Tr}\left[\left(\partial_\mu \xi^\dagger\right)\partial^\mu \xi\right] + \frac{f_\pi^2 m_\pi^2}{4}\mathrm{Tr}\left(\xi^2+\xi^{\dagger 2}\right) \\
& -\frac{1}{2}\mathrm{Tr}\left[(\partial_\mu\rho_\nu - \partial_\nu\rho_\mu)(\partial^\mu\rho^\nu - \partial^\nu\rho^\mu)\right] + m_\rho^2 \mathrm{Tr}\left(\rho_\mu\rho^\mu\right) + \frac{\delta m_\rho^2}{2}\rho_\mu^3\rho^{3\mu} - \frac{1}{4}F_{\mu\nu}F^{\mu\nu} \\
& + i f_\pi^2 \mathrm{Tr}\left[\left(g\rho_\mu + \delta g\,\rho_\mu^3 t^3 + 2eA_\mu t^3\right)\left(\xi^\dagger\partial^\mu\xi + \xi\partial^\mu\xi^\dagger\right)\right] \\
& + f_\pi^2\left[\left(\bar{\delta}g - \delta g\right)\rho_\mu^3 - eA_\mu\right] \\
& \quad \left\{\mathrm{Tr}\left[\left(g\rho^\mu + \bar{\delta}g\rho^{3\mu}t^3 + eA^\mu t^3\right)\left(\xi^\dagger t^3\xi + \xi t^3\xi^\dagger\right)\right] - \left(g+\bar{\delta}g\right)\rho^{3\mu} - eA^\mu\right\} \\
& -\frac{i}{g^2}\mathrm{Tr}\left\{\left[g\rho^\mu + \bar{\delta}g\rho^{3\mu}t^3 + eA^\mu t^3, g\rho^\nu + \bar{\delta}g\rho^{3\nu}t^3 + eA^\nu t^3\right]\right. \\
& \qquad \left[g\left(\partial_\mu\rho_\nu - \partial_\nu\rho_\mu\right) + \bar{\delta}g\left(\partial_\mu\rho_\nu^3 - \partial_\nu\rho_\mu^3\right)t^3 + eF_{\mu\nu}t^3\right. \\
& \qquad \left.\left. + \frac{i}{2}\left[g\rho_\mu + \bar{\delta}g\rho_\mu^3 t^3 + eA_\mu t^3, g\rho_\nu + \bar{\delta}g\rho_\nu^3 t^3 + eA_\nu t^3\right]\right]\right\} \\
& -\frac{a_{\gamma\rho}e(g+\delta g)}{(4\pi)^2}F_{\mu\nu}(\partial^\mu\rho^{3\nu} - \partial^\nu\rho^{3\mu}) \\
& + \frac{a_{\gamma\rho}}{(4\pi)^2}\left[\left(\bar{\delta}g - \delta g\right)\left(\partial_\mu\rho_\nu^3 - \partial_\nu\rho_\mu^3\right) - eF_{\mu\nu}\right] \\
& \quad \left\{\mathrm{Tr}\left[\left(g\left(\partial^\mu\rho^\nu - \partial^\nu\rho^\mu\right) + \bar{\delta}g(\partial^\mu\rho^{3\nu} - \partial^\nu\rho^{3\mu})t^3 + eF^{\mu\nu}t^3\right.\right.\right. \\
& \qquad \left.\left.\left. + i\left[g\rho^\mu + \bar{\delta}g\rho^{3\mu}t^3 + eA^\mu t^3, g\rho^\nu + \bar{\delta}g\rho^{3\nu}t^3 + eA^\nu t^3\right]\right)\left(\xi^\dagger t^3\xi + \xi t^3\xi^\dagger\right)\right] \\
& \quad - \left(g+\bar{\delta}g\right)(\partial^\mu\rho^{3\nu} - \partial^\nu\rho^{3\mu}) - eF^{\mu\nu}\Big\} \\
& + \ldots,
\end{aligned}
\tag{2.37}
$$

where we introduced the electromagnetic field strength

$$
F_{\mu\nu} = \partial_\mu A_\nu - \partial_\nu A_\mu, \tag{2.38}
$$

the new parameters

$$
e = \frac{g'}{(1+g'^2/g^2)^{1/2}}\left(1 + \frac{g'^2}{1+g'^2/g^2}\frac{a_{\gamma\rho}}{4\pi^2}\right)^{-1/2}, \tag{2.39}
$$

$$
\frac{\delta g}{g} = \frac{1-g'^2/g^2}{(1+g'^2/g^2)^{1/2}}\left(1 - \frac{g'^2}{1+g'^2/g^2}\frac{a_{\gamma\rho}}{4\pi^2}\right)^{-1/2} - 1, \tag{2.40}
$$

$$
\frac{\bar{\delta}g}{g} = \frac{1}{(1+g'^2/g^2)^{1/2}}\left(1 - \frac{g'^2}{1+g'^2/g^2}\frac{a_{\gamma\rho}}{4\pi^2}\right)^{-1/2} - 1, \tag{2.41}
$$

and the mass

$$
m_\rho = g f_\pi \tag{2.42}
$$

for the charged rhos, with the neutral-charged rho mass splitting

$$\frac{\delta m_\rho^2}{m_\rho^2} = \frac{g'^2}{g^2}\frac{1 + g'^2/g^2 + g^2 a_{\gamma\rho}/4\pi^2}{1 + g'^2/g^2 - g'^2 a_{\gamma\rho}/4\pi^2}. \tag{2.43}$$

When $g' = 0$, the Lagrangian (2.37) reduces to the one in Ref. [60].

As it is apparent in Eq. (2.37) there is no mass term for A_μ. One can easily show that the new rho field ρ_μ^3 is invariant under the transformation (2.7), while A_μ changes as a $U(1)$ gauge field,

$$A_\mu t^3 \to U\left(A_\mu t^3 - i\partial_\mu\right) U^\dagger. \tag{2.44}$$

We can thus identify A_μ with the photon field. From the transformation properties of π and ρ_μ, we see that e defined in Eq. (2.39) is the proton charge $e = \sqrt{4\pi\alpha}$. Note that the photon couples directly to the pions.

On the other hand, ρ_μ represents the three states of the rho meson. The charged rhos couple to themselves and to two pions with a "universal" strength g. It is conventional to define the $\rho\pi\pi$ coupling constant $g_{\rho\pi\pi} \equiv -g/2$ [52]. The charged rho mass m_ρ, Eq. (2.42), is related via g to the pion decay constant f_π [55] and

$$\frac{m_\rho^2}{2g_{\rho\pi\pi}^2 f_\pi^2} = 2, \tag{2.45}$$

which is larger by a factor of 2 than the so-called KSFR-II relation [59]. The mass mixing between B_μ and $\tilde{\rho}_\mu^3$ led to isospin breaking in the properties of the rho mesons, since ρ_μ^3 has slightly different couplings $g + \delta g$ and $g + \bar{\delta} g$, Eqs. (2.40) and (2.41), and mass $(m_\rho^2 + \delta m_\rho^2)^{1/2}$, Eq. (2.43).

Still, mixing between the neutral rho and the photon remains in the "kinetic" form represented by the parameter $a_{\gamma\rho}$. Again, it is standard [52] to define the coefficient of the mixing term in the Lagrangian as $e g_{\rho\gamma}/m_\rho^2$ in terms of a $\rho\gamma$ mixing parameter

$$\frac{g_{\rho\gamma}}{2g_{\rho\pi\pi}f_\pi^2} = \frac{g^2 a_{\gamma\rho}}{(4\pi)^2}\left(1 + \frac{\delta g}{g}\right). \tag{2.46}$$

The KSFR-I relation [59] can be reproduced if $a_{\gamma\rho} = (4\pi)^2/g^2(1 + \delta g/g)$, but the value of $a_{\gamma\rho}$ is not determined by symmetries.

The size of the independent parameters in the effective Lagrangian can be estimated using naive dimensional analysis (NDA) [37, 63]. To keep track of factors of 4π and the mass scale $M_{QCD} \sim 4\pi f_\pi$ below which QCD non-perturbative effects are dominant, a simple rule [63] is to associate to each coupling constant c a "reduced" coupling $c_R = (4\pi)^{2-N} M_{QCD}^{D-4} c$, where N and D are respectively the number of fields and dimension of the corresponding operator. The reduced coupling appearing in a low-energy effective Lagrangian is expected to be of the order of magnitude of the product of reduced parameters of the underlying Lagrangian that generate the corresponding operator. The reduced couplings in the QCD Lagrangian are $g_{sR} = g_s/4\pi$ for the strong-interaction strength g_s, $\bar{m}_R = \bar{m}/M_{QCD}$ for the average quark mass $\bar{m}$, and $e_R = e/4\pi$ for the electromagnetic charge e. Terms in the effective Lagrangian that are chiral invariant stem from g_s; since non-perturbative effects imply all powers of g_s, for consistency we need to take $g_{sR} \sim 1$. One can then verify that pion self-interactions stemming from the first term in Eq. (2.37) come out correctly. For example, for the term of form $(\partial_\mu \pi)^2 \pi^2 / f_\pi^2$, the reduced coupling is $(1/f_\pi^2)_R = M_{QCD}^2/(4\pi f_\pi)^2 \sim 1$, implying $f_\pi \sim M_{QCD}/4\pi$ as it should. Terms that break chiral symmetry explicitly come from powers of $\bar{m}$. The simplest example is the pion mass, whose reduced coupling $m_{\pi R}^2 = m_\pi^2/M_{QCD}^2 \sim \bar{m}_R$; this amounts to $m_\pi^2 \sim M_{QCD}\bar{m}$, which is the correct order of magnitude.

NDA is usually assumed in ChPT, where it works well. A straightforward application of NDA would lead to the well-known implication that $m_\rho \sim M_{QCD}$. For example, from the isospin-conserving rho self-interactions, $g\mathrm{Tr}(\partial_\mu \rho_\nu [\rho^\mu, \rho^\nu])$, the reduced coupling $g_R = g/4\pi \sim 1$ would lead to $g \sim 4\pi$ and to $m_\rho = g f_\pi \sim 4\pi f_\pi$. Instead, vector symmetry is an assumed dynamical symmetry that supplies a rationale to consider m_ρ a lighter scale. One has to incorporate it by hand, requiring that its breaking, parametrized by g in Eq. (2.29), be relatively small: $g \sim 1$. In this case $m_\rho \sim f_\pi$ counts as a light scale. Of course, numerically $g \simeq 8$, which means the vector-EFT expansion in $(m_\rho/4\pi f_\pi)^2 = (g/4\pi)^2 \sim 1/2$ will converge slowly, at best.

The mixing parameter $a_{\gamma\rho}$ stems from both vector-symmetry breaking and elec-

tromagnetic effects. Thus we expect $(a_{\gamma\rho}eg/(4\pi)^2)_R = a_{\gamma\rho}eg/(4\pi)^2 \sim e_R g_R = eg/(4\pi)^2$, implying $a_{\gamma\rho} = \mathcal{O}(1)$. The mixing terms in Eq. (2.37) are then subleading. The leading-order Lagrangian has only four independent parameters, which we can take as f_π, m_π, g, and e. The common rho mass m_ρ, the rho mass splitting δm_ρ, and the coupling corrections δg and $\bar{\delta} g$ are determined by f_π, g, and e (and, in subleading order, $a_{\gamma\rho}$). Alternatively, we can trade g for m_ρ using Eq. (2.42), as we do below.

Since $e \sim 1/3$, an expansion in powers of e^2 converges quickly, and from Eq. (2.39) we see that $g' = e[1 + \mathcal{O}(e^2)]$, leading to

$$\frac{\delta g}{g} = -\frac{3e^2}{2g^2}\left(1 - \frac{g^2 a_{\gamma\rho}}{12\pi^2}\right)\left[1 + \mathcal{O}(e^2)\right], \tag{2.47}$$

$$\frac{\bar{\delta} g}{g} = -\frac{e^2}{2g^2}\left(1 - \frac{g^2 a_{\gamma\rho}}{4\pi^2}\right)\left[1 + \mathcal{O}(e^2)\right], \tag{2.48}$$

and

$$\delta m_\rho^2 = 4\pi\alpha f_\pi^2 \left[1 + 4a_{\gamma\rho}\left(\frac{m_\rho}{4\pi f_\pi}\right)^2\right]\left[1 + \mathcal{O}(e^2)\right]. \tag{2.49}$$

When $a_{\gamma\rho} = 0$, $\delta m_\rho^2/m_\rho^2$ reduces to the expression obtained in the hidden-gauge approach [50], which gives a relatively large value $\delta m_\rho \simeq 30$ MeV. However, the $a_{\gamma\rho}$ correction is not small, and if $a_{\gamma\rho} < 0$ there could be a large cancellation between the two terms. This shows the limitations of the expansion considered here. Moreover, there are other contributions at the same order, such as radiative corrections. Since we limit ourselves in this chapter to $SU(2)$ and have no isoscalar vector field that can mix with the rho, we refrain from an analysis of isospin-violation effects. (For some of the related issues regarding the ω meson, see Ref. [53].)

We study here processes involving rho mesons, pions, and photons to lowest order in e and, accordingly, neglect $\mathcal{O}(\alpha)$ corrections in all hadronic quantities. In

the following we will need explicitly

$$\begin{aligned}
\mathcal{L} \;=\; & \frac{1}{2}\left(\partial_\mu \boldsymbol{\pi}\cdot\partial^\mu\boldsymbol{\pi} - m_\pi^2\boldsymbol{\pi}^2\right) + \frac{1}{24f_\pi^2}\left[\boldsymbol{\pi}\cdot\partial_\mu\boldsymbol{\pi}\;\boldsymbol{\pi}\cdot\partial^\mu\boldsymbol{\pi} - \boldsymbol{\pi}^2\left(\partial_\mu\boldsymbol{\pi}\cdot\partial^\mu\boldsymbol{\pi} - m_\pi^2\boldsymbol{\pi}^2\right)\right] \\
& -\frac{1}{2}\left[\partial_\mu\boldsymbol{\rho}_\nu\cdot(\partial^\mu\boldsymbol{\rho}^\nu - \partial^\nu\boldsymbol{\rho}^\mu) - m_\rho^2\boldsymbol{\rho}_\mu\cdot\boldsymbol{\rho}^\mu\right] - \frac{1}{4}F_{\mu\nu}F^{\mu\nu} \\
& +\frac{m_\rho}{2f_\pi}\boldsymbol{\rho}_\mu\cdot(2\boldsymbol{\rho}_\nu\times\partial^\mu\boldsymbol{\rho}^\nu - \boldsymbol{\pi}\times\partial^\mu\boldsymbol{\pi}) + \frac{m_\rho^2}{4f_\pi^2}\left[\boldsymbol{\rho}_\mu\cdot\boldsymbol{\rho}_\nu\,\boldsymbol{\rho}^\mu\cdot\boldsymbol{\rho}^\nu - (\boldsymbol{\rho}_\mu\cdot\boldsymbol{\rho}^\mu)^2\right] \\
& +\frac{e}{2}F_{\mu\nu}\left(\boldsymbol{\rho}^\mu\times\boldsymbol{\rho}^\nu\right)_3 + eA_\mu\left[\boldsymbol{\rho}_\nu\times(\partial^\mu\boldsymbol{\rho}^\nu - \partial^\nu\boldsymbol{\rho}^\mu) - \boldsymbol{\pi}\times\partial^\mu\boldsymbol{\pi}\right]_3 \\
& -\frac{em_\rho}{2f_\pi}A_\mu\left[2\left(\boldsymbol{\rho}_\nu\cdot\boldsymbol{\rho}^\nu\boldsymbol{\rho}^\mu - \boldsymbol{\rho}^\mu\cdot\boldsymbol{\rho}^\nu\boldsymbol{\rho}_\nu\right) + \boldsymbol{\pi}\boldsymbol{\pi}\cdot\boldsymbol{\rho}^\mu - \boldsymbol{\pi}^2\boldsymbol{\rho}^\mu\right]_3 \\
& -\frac{em_\rho a_{\gamma\rho}}{(4\pi)^2 f_\pi}F_{\mu\nu}(\partial^\mu\boldsymbol{\rho}^\nu - \partial^\nu\boldsymbol{\rho}^\mu)_3 + \ldots,
\end{aligned} \tag{2.50}$$

where $\boldsymbol{\pi}$ ($\boldsymbol{\rho}$) denotes the pion (rho) isospin triplet.

Since $m_\pi \simeq 140$ MeV, $f_\pi \simeq 92$ MeV, and $e \simeq 4\pi/137$ are well known from low-energy processes, we want to determine the other parameters, m_ρ and $a_{\gamma\rho}$, from data in the rho region. The idea is to fit $a_{\gamma\rho}$ and m_ρ to $e^+e^- \to \pi\pi$ data, then predict the $\pi\pi \to \pi\pi$ phase shift. To address a process involving a lepton field l of charge $-e$ and mass m_l, we consider, in accordance with $U(1)$ electromagnetic invariance,

$$\mathcal{L}_l = \bar{l}\left(i\gamma^\mu\partial_\mu - e\gamma^\mu A_\mu - m_l\right)l + \ldots \tag{2.51}$$

Direct interactions between strong-interacting particles (pions, rhos) and the lepton, such as considered in Ref. [62], arise from hard photons (*i.e.* those of momenta $Q \gtrsim M_{QCD}$) and are of higher order. Indeed, they involve at least one loop, or equivalently two photons, and are thus, by NDA, suppressed by at least $\alpha/4\pi$ compared to effects we keep.

2.3 Power Counting Near the Rho Peak

The predictive power of an EFT rests on the existence of a power counting that justifies a systematic truncation of observables at an order determined by the desired accuracy. In Vector EFT, we can construct an expansion in powers of Q/M_{QCD} just like in ChPT, but now Q denotes not only external momenta and the pion mass, but

also the rho mass [55]. This expansion is not only in derivatives in the Lagrangian, but also in the number of loops at the quantum level. Formally, it applies to a generic $Q < M_{QCD}$. In practice, m_ρ is not very small compared to M_{QCD}, so the expansion is slow. Still, agreement with data improves in the leading-log approximation to NLO [60].

If we consider a process where the initial state has the quantum numbers of the rho in the s channel, however, one needs to refine the power counting. Being an NLO loop effect, for generic $Q < M_{QCD}$ the rho width is treated in perturbation theory. However, a purely perturbative expansion in Q/M_{QCD} cannot apply in the whole region $Q < M_{QCD}$. The very existence of the rho resonance, which produces large cross sections for energies near m_ρ, is a sign of non-perturbative effects. The need to account for the width is of course recognized in any description of a resonance. In this section we merely incorporate width effects in a power counting that accounts for a "kinematic" fine-tuning to the resonance peak. Analogous arguments hold for other resonances in EFT, for example the delta isobar in ChPT [8, 7] and nuclear resonances in Halo EFT [6].

If the rho can appear alone in the s channel, there are contributions to the amplitude proportional to $1/(s - m_\rho^2)$ from the "bare" rho propagator obtained from the LO Lagrangian. For generic Q, $s - m_\rho^2 = \mathcal{O}(Q^2)$, while the self-energy, illustrated in Fig. 2.1, is $\Pi = \mathcal{O}(Q^4/M_{QCD}^2)$, and can thus be treated as small. However, within a window

$$\frac{\delta s}{m_\rho^2} = \frac{s - m_\rho^2}{m_\rho^2} = \mathcal{O}\left(\frac{Q^2}{M_{QCD}^2}\right) \tag{2.52}$$

around the peak of the resonance, the self-energy can no longer be treated perturbatively. Within this window, an nth-order insertion of Π in the rho propagator brings in an additional factor $(\Pi/\delta s)^n \sim \mathcal{O}(1)$, and a resummation is necessary, leading to a "dressed" propagator $D \propto 1/(s - m_\rho^2 - \Pi)$. This resummation is shown in Fig. 2.2.

Thus, within the window, the $\mathcal{O}(Q^4/M_{QCD}^2)$ contributions to the rho self-energy need to be accounted for already at LO. In addition, the dressed propagator now is

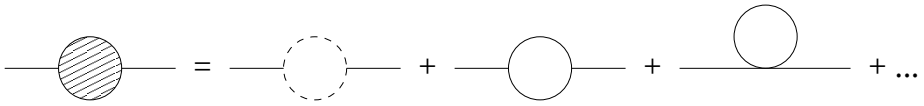

Figure 2.1: Self-energy $i\Pi^{\mu\nu}$ of the rho meson. A solid (dashed) line represents a rho (pion). Vertices are from the LO Lagrangian.

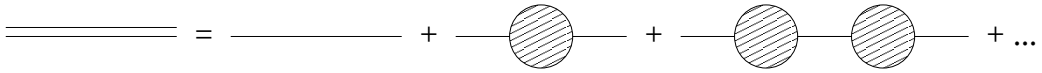

Figure 2.2: Dressed rho propagator $iD^{\mu\nu}$, where the self-energy is resummed.

enhanced, being of $\mathcal{O}(M_{QCD}^2/Q^4)$, instead of $\mathcal{O}(1/Q^2)$ as outside the window. That, of course, is just the power-counting implementation of the large contribution of the resonance to the cross section. Corrections to the rho self-energy of $\mathcal{O}(Q^6/M_{QCD}^4)$ can still be treated in perturbation theory together with other NLO corrections of size $\mathcal{O}(Q^2/M_{QCD}^2)$ relative to LO.

We now consider two specific reactions where this power counting applies.

2.3.1 $\pi\pi \to \pi\pi$

ChPT has been extensively used in the study of $\pi\pi$ scattering [18, 38, 39], and even though it can describe experimental results very well at low energies, it cannot account for the rho peak. Here we focus on this region, the connection with ChPT being discussed in App. A.

At a generic momentum $Q \ll M_{QCD}$, in LO pions interact at a single spacetime point due to the four-pion vertex in Eq. (2.37), which contributes $\mathcal{O}(Q^2/f_\pi^2)$ to the scattering amplitude. In addition, there are three $\mathcal{O}(g^2Q^2/m_\rho^2) = \mathcal{O}(Q^2/f_\pi^2)$ contributions from rho exchange in the s, t, and u channels. At NLO, as usual we have one-loop diagrams and their associated counterterms from the NLO Lagrangian.

Around the rho peak, the contributions from the rho in the s channel is enhanced by two powers and becomes $\mathcal{O}(g^2Q^2/\delta s) = \mathcal{O}(M_{QCD}^2/f_\pi^2)$. The LO $\pi\pi$ scattering amplitude is depicted in Fig. 2.3. Below we show that, as one would expect, the

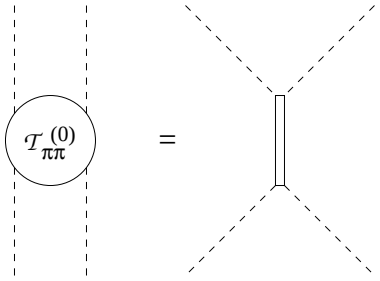

Figure 2.3: LO pion-pion scattering amplitude $i\mathcal{T}^{(0)}_{\pi\pi}$ around the rho peak.

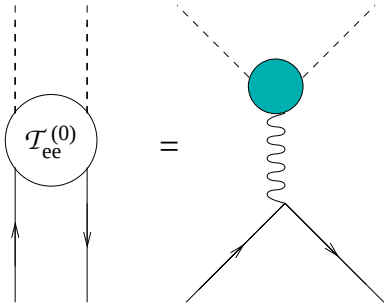

Figure 2.4: LO amplitude $i\mathcal{T}^{(0)}_{ee}$ for annihilation of a lepton-antilepton pair into two pions around the rho peak. A wavy line (solid line with arrow) represents a photon (fermion), and the shaded blob denotes the time-like pion form factor $F_\pi(s)$.

dressed rho propagator gives rise to a resonance at a complex energy, and we confront the corresponding $\pi\pi$ amplitude with empirical phase shifts. Again, the extension to NLO includes not only the mechanisms that are LO outside the rho window, but also one-loop vertex corrections to the dressed s-channel rho exchange and two-loop rho self-energy diagrams.

2.3.2 $e^+e^- \to \pi\pi$

In lowest orders, electron-positron annihilation proceeds through a virtual photon, thanks to Eq. (2.51), but the final two-pion state can be formed in a variety of ways. It is convenient to introduce the pion form factor F_π that groups all such mechanisms, see Fig. 2.4. In the lowest orders the $e^+e^- \to \pi\pi$ cross section is determined by the (time-like) form factor $F_\pi(s)$. In this subsection we organize the contributions to $F_\pi(s)$ near the rho resonance.

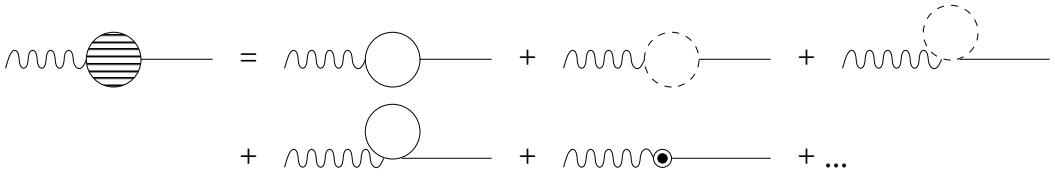

Figure 2.5: Photon-rho mixing $i\Xi^{\mu\nu}$. The circled circle denotes a vertex from the NLO Lagrangian.

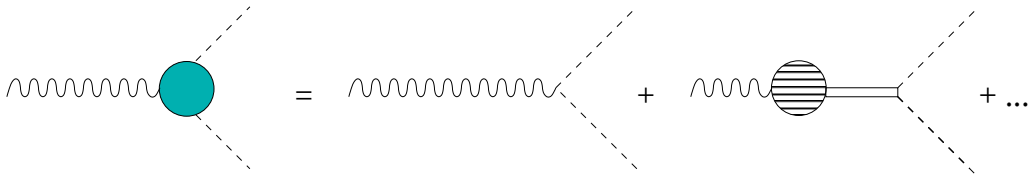

Figure 2.6: Pion form factor $F_\pi(s)$ in Vector EFT.

Away from the window (2.52), we can expand the pion form factor in Vector EFT in a straightforward perturbative fashion. Its behavior at low energies is discussed in App. A. The LO contribution is just the direct photon-pion charge coupling from the LO Lagrangian, which gives a trivial "point-pion" form factor. At NLO more derivatives and loops at the photon-pion vertex give NLO corrections.

In addition, the photon can mix with the neutral rho, followed by rho propagation and coupling to the pions. These contributions will be enhanced by a factor $\mathcal{O}(M_{QCD}^2/Q^2)$ within the window. Thus, $\mathcal{O}(Q^2/M_{QCD}^2)$ effects that generate photon-rho mixing will contribute $\mathcal{O}(1)$ relative to the point-pion coupling, that is, at LO. The dominant contributions to photon-rho mixing are shown in Fig. 2.5: in addition to one-loop diagrams, there is the $a_{\gamma\rho}$ term in the Lagrangian (2.37). Thus the LO form factor is given by the diagrams shown explicitly in Fig. 2.6. In forthcoming sections we calculate the corresponding cross section and compare it with data. The calculation can be extended to higher orders, although the appearance of two-loop diagrams at NLO requires significantly more effort.

2.4 Main Ingredients

In this section we calculate the main ingredients used in the calculation of the $\pi\pi \to \pi\pi$ and $e^+e^- \to \pi\pi$ cross sections around the rho peak: the dressed rho propagator and the photon-rho mixing, both at one-loop level. In App. B we discuss the pion self-energy at the same level.

When dealing with vector mesons, it is convenient to introduce the transverse and longitudinal projectors

$$P_T^{\mu\nu} = \eta^{\mu\nu} - \frac{p^\mu p^\nu}{p^2}, \qquad P_L^{\mu\nu} = \frac{p^\mu p^\nu}{p^2}, \tag{2.53}$$

respectively, with the properties

$$P_{T,L}^{\alpha\beta} P_{T,L}^{\beta\gamma} = P_{T,L}^{\alpha\gamma}, \qquad P_{T,L}^{\alpha\beta} P_{L,T}^{\beta\gamma} = 0. \tag{2.54}$$

For the loops, we use regularization in d spacetime dimensions and introduce the renormalization scale μ. We encode terms that diverge in four dimensions and the μ dependence in

$$L_\rho = \frac{2}{4-d} - \gamma + \ln\frac{4\pi\mu^2}{m_\rho^2}, \tag{2.55}$$

where $\gamma = 0.577...$ is the Euler-Mascheroni constant. We express our results in terms of the standard (see, *e.g.*, Ref. [64]) integral over two propagators,

$$J(x) = \begin{cases} 2\sqrt{\frac{1}{x}-1}\,\cot^{-1}\sqrt{\frac{1}{x}-1} & \text{if } 0 \le x \le 1, \\ \sqrt{1-\frac{1}{x}}\left[\ln\frac{\sqrt{1-\frac{1}{x}}+1}{\left|\sqrt{1-\frac{1}{x}}-1\right|} - i\pi\,\Theta(x)\right] & \text{if } x < 0 \text{ or } x \ge 1 \text{ and } x \ne \infty. \end{cases} \tag{2.56}$$

2.4.1 Rho Self-Energy

The bare rho propagator $iK_{\mu\nu}$ can be read from the Lagrangian (2.50),

$$K^{\mu\nu}(p^2) = -\frac{P_T^{\mu\nu}}{p^2 - m_\rho^2 + i\epsilon} + \frac{P_L^{\mu\nu}}{m_\rho^2}. \tag{2.57}$$

The rho self-energy, shown in Fig. 2.1, can also be written in terms of transverse and longitudinal components,

$$\Pi^{\mu\nu}(p^2) = \Pi_T(p^2) P_T^{\mu\nu} + \Pi_L(p^2) P_L^{\mu\nu}. \tag{2.58}$$

The Dyson-Schwinger matrix equation for the dressed rho propagator, displayed in Fig. 2.2, is

$$D^{\mu\nu}(p^2) = K^{\mu\nu}(p^2) - K^{\mu\alpha}(p^2)\Pi^{\alpha\beta}(p^2)K^{\beta\nu}(p^2) + \dots \tag{2.59}$$

Around $p^2 = m_\rho^2$, we can Taylor expand

$$\Pi_{T,L}(p^2) = \Pi_{T,L}(m_\rho^2) + (p^2 - m_\rho^2)\frac{d\Pi_{T,L}(p^2)}{dp^2}\Big|_{p^2=m_\rho^2} + \dots \tag{2.60}$$

As discussed in the previous section, when the rho is alone in the s channel, in the window (2.52) the leading term is $\Pi_T^{(0)}(m_\rho^2)$ as given by one-loop diagrams, which we can decompose the self-energy into real and imaginary parts,

$$\Pi_T^{(0)}(m_\rho^2) = \Pi_{Tr}^{(0)}(m_\rho^2) + i\Pi_{Ti}^{(0)}(m_\rho^2). \tag{2.61}$$

We have to resum the transverse components in LO,

$$D^{(0)\mu\nu}(p^2) = -\frac{P_T^{\mu\nu}}{p^2 - m_\rho^2 - \Pi_{Tr}^{(0)}(m_\rho^2) - i\Pi_{Ti}^{(0)}(m_\rho^2)} + \frac{P_L^{\mu\nu}}{m_\rho^2}. \tag{2.62}$$

In the interaction of the rho with conserved currents, only the transverse component contributes.

The observable mass of the rho is defined as the real part of the pole in the dressed propagator:

$$m_\rho^{(R)2} = m_\rho^2 + \Pi_{Tr}^{(0)}(m_\rho^2) + \dots \tag{2.63}$$

Vector symmetry at this order demands that $\Pi_{Tr}^{(0)}(0) = 0$. From the imaginary part of the pole we define

$$\Gamma_{\pi\pi}^{(0)}(m_\rho^2) = -\frac{1}{m_\rho}\Pi_{Ti}^{(0)}(m_\rho^2), \tag{2.64}$$

which, as we show later, can be thought of as the leading piece of the partial decay width of the rho into two pions.

The one-loop diagrams we consider are shown explicitly in Fig. 2.1. We neglect here photon contributions, which are down by at least a factor e^2/g^2, and other isospin-violating contributions that originate in vector-boson mixing and the quark-mass difference, which appear in the subleading Lagrangians. We obtain

$$\Pi_L^{(0)}(p^2) \;=\; \frac{m_\rho^2}{2}\left(\frac{m_\rho}{4\pi f_\pi}\right)^2\left[\frac{m_\pi^2}{m_\rho^2}\left(L_\rho + 1 + \ln\frac{m_\rho^2}{m_\pi^2}\right) - 1 - \frac{2p^2}{m_\rho^2} + \frac{p^4}{3m_\rho^4}\right] \tag{2.65}$$

and

$$\begin{aligned}\Pi_T^{(0)}(p^2) &= \frac{m_\rho^2}{12}\left(\frac{m_\rho}{4\pi f_\pi}\right)^2\left\{\frac{6p^2}{m_\rho^2}\left(\frac{83}{6}-\frac{7p^2}{3m_\rho^2}-\frac{p^4}{6m_\rho^4}+\frac{m_\pi^2}{p^2}\right)L_\rho\right.\\ &+96+\frac{2p^2}{3m_\rho^2}\left(200-\frac{35p^2}{m_\rho^2}-\frac{4p^4}{m_\rho^4}\right)+\frac{14m_\pi^2}{m_\rho^2}\\ &-12\left(4+\frac{17p^2}{3m_\rho^2}-\frac{4p^4}{3m_\rho^4}-\frac{p^6}{12m_\rho^6}\right)J\left(\frac{p^2}{4m_\rho^2}\right)\\ &\left.+\frac{p^2}{m_\rho^2}\left[\left(1-\frac{6m_\pi^2}{p^2}\right)\ln\frac{m_\pi^2}{m_\rho^2}+\left(1-\frac{4m_\pi^2}{p^2}\right)J\left(\frac{p^2}{4m_\pi^2}\right)\right]\right\}. \quad (2.66)\end{aligned}$$

The terms in L_ρ agree with Ref. [60]. The terms proportional to p^4/m_ρ^2 and p^6/m_ρ^4 come exclusively from the longitudinal component of the rho propagator, given by Eq. (2.57), and appear to be non renormalizable. This happens as a consequence of the field redefinitions in unitary gauge, which has the advantage of making the particle spectrum transparent. The disadvantage is that the spin-1 propagator, in Eq. (2.57), does not converge to zero at large momenta, rather it behaves like a constant. Thus, it could be inappropriate for calculations beyond tree level in perturbation expansion. A non-rigorous, but intuitive, argument for keeping such terms is given in Ref. [65]. It is based on the fact that although the Green's functions for the theory are gauge dependent, the S-matrix must be independent, and therefore the theory is both unitary and renormalizable. In Ref. [66], 't Hooft prove that even after symmetry breaking, the theory remains renormalizable. Since at tree level the longitudinal component of the rho propagator does not contribute, as in the $\pi\pi \to \pi\pi$ and $e^+e^- \to \pi\pi$ cross sections analyzed in this chapter, the non renormalizability appearance is not a problem, as long as the observables are renormalizable, which is the case in this chapter, as one can see next.

Now

$$\begin{aligned}\Pi_T^{(0)}(m_\rho^2) &= \frac{m_\rho^2}{12}\left(\frac{m_\rho}{4\pi f_\pi}\right)^2\left[6\left(\frac{34}{3}+\frac{m_\pi^2}{m_\rho^2}\right)L_\rho+\frac{610}{3}-33\sqrt{3}\pi+\frac{14m_\pi^2}{m_\rho^2}\right.\\ &\left.+\left(1-\frac{6m_\pi^2}{m_\rho^2}\right)\ln\frac{m_\pi^2}{m_\rho^2}+\left(1-\frac{4m_\pi^2}{m_\rho^2}\right)J\left(\frac{m_\rho^2}{4m_\pi^2}\right)\right]. \quad (2.67)\end{aligned}$$

From this expression we can see that $\Pi_T^{(0)}(0) = 0$. For $m_\rho > 2m_\pi$, the real part gives

$$\begin{aligned}\frac{m_\rho^{(R)2}}{m_\rho^2} &= 1 + \frac{1}{12}\left(\frac{m_\rho}{4\pi f_\pi}\right)^2 \left[6\left(\frac{34}{3} + \frac{m_\pi^2}{m_\rho^2}\right) L_\rho + \frac{610}{3} - 33\sqrt{3}\pi + \frac{14m_\pi^2}{m_\rho^2}\right. \\ &\quad \left. + \left(1 - \frac{6m_\pi^2}{m_\rho^2}\right)\ln\frac{m_\pi^2}{m_\rho^2} + \left(1 - \frac{4m_\pi^2}{m_\rho^2}\right)^{3/2}\ln\left(\frac{1 + \left(1 - 4m_\pi^2/m_\rho^2\right)^{1/2}}{1 - \left(1 - 4m_\pi^2/m_\rho^2\right)^{1/2}}\right)\right] \\ &\quad + \ldots \end{aligned} \tag{2.68}$$

The regulator-dependent terms are absorbed in m_ρ itself. On the other hand, the imaginary part comes from the one-loop diagram with a pion bubble and is finite,

$$\Gamma_{\pi\pi}^{(0)}(m_\rho^2) = \frac{\pi m_\rho}{12}\left(\frac{m_\rho}{4\pi f_\pi}\right)^2 \left(1 - \frac{4m_\pi^2}{m_\rho^2}\right)^{3/2}, \tag{2.69}$$

which agrees with Ref. [60].

Since $\Pi_T^{(0)}(m_\rho^2)/m_\rho^2 = \mathcal{O}(Q^2/M_{QCD}^2)$, we can substitute $m_\rho^{(R)2}$ for m_ρ^2 everywhere in Eq. (2.62) and neglect the higher-order terms. From here on we drop the superscript $^{(R)}$. Then

$$D^{(0)\mu\nu}(p^2) = -\frac{P_T^{\mu\nu}}{p^2 - m_\rho^2 + i m_\rho \Gamma_{\pi\pi}^{(0)}(m_\rho^2)} + \frac{P_L^{\mu\nu}}{m_\rho^2}. \tag{2.70}$$

2.4.2 Photon-Rho Mixing

We denote photon-rho mixing as

$$\Xi^{\mu\nu}(p^2) = \Xi_T(p^2) P_T^{\mu\nu} + \Xi_L(p^2) P_L^{\mu\nu}. \tag{2.71}$$

It first enters Vector EFT in the subleading Lagrangian through the parameter $a_{\gamma\rho}$, and receives contributions also from the one-loop diagrams shown explicitly in Fig. 2.5.

Again, around $p^2 = m_\rho^2$, we can Taylor expand

$$\Xi_{T,L}(p^2) = \Xi_{T,L}(m_\rho^2) + (p^2 - m_\rho^2)\frac{d\Xi_{T,L}(p^2)}{dp^2}\Big|_{p^2=m_\rho^2} + \ldots \tag{2.72}$$

As discussed in the Sect. 2.3.2, when the rho appears alone in the direct channel of electron-positron annihilation its contributions are enhanced, and we need to

include the one-loop $\Xi^{(0)}_{T,L}(m_\rho^2)$. Interaction with conserved currents guarantee that only $\Xi^{(0)}_{T}(m_\rho^2)$ is needed.

The loops are very similar to the ones in the rho self-energy, except that there is an extra diagram with a pion loop. Neglecting corrections of relative size e^2/g^2, explicit calculation gives

$$\begin{aligned}\Xi^{(0)}_T(p^2) &= \frac{ef_\pi m_\rho}{6}\left(\frac{m_\rho}{4\pi f_\pi}\right)^2\left\{\frac{6p^2}{m_\rho^2}\left(\frac{41}{3}-\frac{7p^2}{3m_\rho^2}-\frac{p^4}{6m_\rho^4}\right)L_\rho\right.\\ &+96+\frac{2p^2}{3m_\rho^2}\left(196-\frac{35p^2}{m_\rho^2}-\frac{4p^4}{m_\rho^4}\right)+\frac{16m_\pi^2}{m_\rho^2}+12a_{\gamma\rho}\\ &-12\left(4+\frac{17p^2}{3m_\rho^2}-\frac{4p^4}{3m_\rho^4}-\frac{p^6}{12m_\rho^6}\right)J\left(\frac{p^2}{4m_\rho^2}\right)\\ &\left.+2\frac{p^2}{m_\rho^2}\left[\ln\frac{m_\pi^2}{m_\rho^2}+\left(1-\frac{4m_\pi^2}{p^2}\right)J\left(\frac{p^2}{4m_\pi^2}\right)\right]\right\}. \qquad (2.73)\end{aligned}$$

The terms in L_ρ are the same as Eq. (2.66), except for the missing m_π^2 term that cancels due to the extra pion loop diagram in the rho-photon mixing, shown in Fig. 2.5, compared to rho selfenergy, Fig. 2.1. For the same reason, the terms proportional to m_π^2/m_ρ^2, $\ln\left(m_\pi^2/m_\rho^2\right)$ and $392p^2/3m_\rho^2$ differ from Eq. (2.66). The term proportional to $J\left(p^2/4m_\pi^2\right)$ has a factor 2 relative to the same term in Eq. (2.66), since the vertex $A_\mu\pi\pi$ is proportional to $2eQ$ and the vertex $\rho_\mu\pi\pi$ is only proportional to gQ.

Thus the mixing at the peak is finite, as the regulator dependence that appears in the real part can be absorbed in

$$\begin{aligned}a^{(R)}_{\gamma\rho} &= a_{\gamma\rho}-\frac{67}{12}L_\rho+\frac{11\sqrt{3}\pi}{3}-\frac{301}{18}-\frac{4m_\pi^2}{3m_\rho^2}-\frac{1}{6}\ln\frac{m_\pi^2}{m_\rho^2}\\ &-\frac{1}{6}\left(1-\frac{4m_\pi^2}{m_\rho^2}\right)^{3/2}\ln\left(\frac{1+\left(1-4m_\pi^2/m_\rho^2\right)^{1/2}}{1-\left(1-4m_\pi^2/m_\rho^2\right)^{1/2}}\right). \qquad (2.74)\end{aligned}$$

The imaginary part is again given by the pion loop, and it is related to the rho width.

From now on we drop the superscript $^{(R)}$ in $a_{\gamma\rho}$ as well, so we write

$$\Xi^{(0)\mu\nu}(m_\rho^2) = -2ef_\pi m_\rho \left(\frac{m_\rho}{4\pi f_\pi}\right)^2 \left[\left(a_{\gamma\rho} + \frac{2i}{m_\rho}\left(\frac{4\pi f_\pi}{m_\rho}\right)^2 \Gamma^{(0)}_{\pi\pi}\left(m_\rho^2\right)\right) P_T^{\mu\nu} + \frac{4}{3}P_L^{\mu\nu}\right]. \tag{2.75}$$

2.5 Cross Sections

In this section we calculate in LO in Vector EFT the scattering cross sections for the processes $\pi\pi \to \pi\pi$ and $e^+e^- \to \pi\pi$ near the rho peak, using the ingredients derived in Sect. 2.4. The cross sections much below the rho peak are well described by ChPT.

We denote the momenta of the incoming (outgoing) particles by p_1 and p_2 (p_3 and p_4). We use the standard Mandelstam variables given by

$$s = (p_1 + p_2)^2, \qquad t = (p_1 - p_3)^2, \qquad u = (p_1 - p_4)^2. \tag{2.76}$$

These variables are not independent; in the isospin-symmetric limit,

$$s + t + u = 2\left(m_i^2 + m_\pi^2\right), \tag{2.77}$$

where m_i denotes the incoming particle mass. We can then write amplitudes as a function of only two variables. We work in the center-of-mass (CM) frame and choose the independent variables to be the total energy $\sqrt{s}$ and the scattering angle θ. For the reactions to occur, $s \geq 4m_\pi^2$. We are interested in the cross sections in the window (2.52) around $s = m_\rho^2$, where they follow the power counting of Sect. 2.3.

The two outgoing pions can be in any of three total isospin states $I = 1, 2, 3$. For both reactions we denote the isospin of the outgoing pions with momenta p_3 and p_4 by a_3 and a_4, respectively.

2.5.1 $\pi\pi \to \pi\pi$

If we denote the isospin of the incoming pions with momenta p_1 and p_2 by a_1 and a_2, respectively, we can write the general Lorentz-invariant scattering amplitude for

this process as

$$\mathcal{T}_{\pi\pi}^{a_1a_2a_3a_4}(s,t,u) = A(s,t,u)\delta^{a_1a_2}\delta^{a_3a_4} + B(s,t,u)\delta^{a_1a_3}\delta^{a_2a_4} + C(s,t,u)\delta^{a_1a_4}\delta^{a_2a_3}, \tag{2.78}$$

in terms of three functions $A(s,t,u)$, $B(s,t,u)$ and $C(s,t,u)$. We can decompose the amplitude into its three total-isospin components [67], $\mathcal{T}^I(s,t,u)$,

$$\begin{aligned}\mathcal{T}_{\pi\pi}^{a_1a_2a_3a_4}(s,t,u) &= \frac{1}{3}\delta^{a_1a_2}\delta^{a_3a_4}\mathcal{T}_{\pi\pi}^0(s,t,u) + \frac{1}{2}\left(\delta^{a_1a_3}\delta^{a_2a_4} - \delta^{a_1a_4}\delta^{a_2a_3}\right)\mathcal{T}_{\pi\pi}^1(s,t,u) \\ &\quad + \frac{1}{2}\left(\delta^{a_1a_3}\delta^{a_2a_4} + \delta^{a_1a_4}\delta^{a_2a_3} - \frac{2}{3}\delta^{a_1a_2}\delta^{a_3a_4}\right)\mathcal{T}_{\pi\pi}^2(s,t,u), \end{aligned} \tag{2.79}$$

where

$$\mathcal{T}_{\pi\pi}^0(s,t,u) = 3A(s,t,u) + B(s,t,u) + C(s,t,u), \tag{2.80}$$

$$\mathcal{T}_{\pi\pi}^1(s,t,u) = B(s,t,u) - C(s,t,u), \tag{2.81}$$

$$\mathcal{T}_{\pi\pi}^2(s,t,u) = B(s,t,u) + C(s,t,u). \tag{2.82}$$

In the CM frame, we can expand $\mathcal{T}^I(s,\theta)$ in partial-wave amplitudes $\mathcal{T}^{I,l}(s)$ [67],

$$\mathcal{T}_{\pi\pi}^I(s,\theta) = 16\pi\sum_{l=0}^{\infty}(2l+1)\,\mathrm{P}_l(\cos\theta)\,\mathcal{T}_{\pi\pi}^{I,l}(s), \tag{2.83}$$

where $\mathrm{P}_l(\cos\theta)$ is the Legendre polynomial corresponding to orbital angular momentum l. The phase shift $\delta_l^I(s)$ for each I and l is defined through

$$\mathcal{T}_{\pi\pi}^{I,l}(s) = -i\left(1 - \frac{4m_\pi^2}{s}\right)^{-1/2}\left(e^{2i\delta_l^I(s)} - 1\right). \tag{2.84}$$

Using the dressed rho propagator (2.70), the invariant scattering amplitude corresponding to Fig. 2.3 is found to be

$$A^{(0)}(s,t,u) = 0, \tag{2.85}$$

$$B^{(0)}(s,t,u) = -C^{(0)}(s,t,u) = \frac{m_\rho^2}{4f_\pi^2}\frac{u-t}{s - m_\rho^2 + i\sqrt{s}\Gamma_{\pi\pi}^{(0)}(s)}. \tag{2.86}$$

The longitudinal component Π_L of the rho self-energy does not contribute. Not surprisingly, the only non-vanishing isospin component of the amplitude is

$$\mathcal{T}_{\pi\pi}^{(0)1}(s,\theta) = -\frac{m_\rho^2}{2f_\pi^2}\frac{(s-4m_\pi^2)\cos\theta}{s - m_\rho^2 + i\sqrt{s}\Gamma_{\pi\pi}^{(0)}(s)}, \tag{2.87}$$

which contributes only to the P wave,

$$\mathcal{T}^{(0)1,1}_{\pi\pi}(s) = -\frac{\pi}{6}\left(\frac{m_\rho}{4\pi f_\pi}\right)^2 \frac{(s-4m_\pi^2)}{s-m_\rho^2+i\sqrt{s}\Gamma^{(0)}_{\pi\pi}(s)} \tag{2.88}$$

The final equation for the $\pi\pi$ phase shift is

$$e^{2i\delta_1^{(0)1}(s)} = 1 - 2i\frac{(\sqrt{s}\Gamma^{(0)}_{\pi\pi}(s))|_{s=m_\rho^2}}{s-m_\rho^2+i(\sqrt{s}\Gamma^{(0)}_{\pi\pi}(s))|_{s=m_\rho^2}}. \tag{2.89}$$

This is the standard relativistic Breit-Wigner form for a resonance of mass m_ρ and width $\Gamma_{\pi\pi}(m_\rho^2)$. Indeed, at $s = m_\rho^2$ the phase shift goes through 90^o,

$$\delta_1^{(0)1}(m_\rho^2) = \frac{\pi}{2}, \tag{2.90}$$

at a rate

$$\frac{d\delta_1^{(0)1}(s)}{d\sqrt{s}}\Big|_{s=m_\rho^2} = \frac{2}{\Gamma^{(0)}_{\pi\pi}(m_\rho^2)}. \tag{2.91}$$

which shows that $\Gamma^{(0)}_{\pi\pi}(m_\rho^2)$ can be indeed interpreted as the partial decay width of the rho into two pions. What is characteristic of vector symmetry at LO is the specific form of $\Gamma^{(0)}_{\pi\pi}(m_\rho^2)$, Eq. (2.69): the partial width is entirely determined by m_ρ itself, and has no further parameter.

2.5.2 $e^+e^- \to \pi^+\pi^-$

To lowest order in e, $e^+e^- \to \pi\pi$ proceeds by one annihilation of the fermion-antifermion pair into one photon, followed by photon propagation and the time-like pion form factor, see Fig. 2.4. The polarized differential cross section in terms of the invariant amplitude is given by [68]

$$\begin{aligned} d\sigma_{\rm pol} &= \frac{(2\pi)^4}{4\sqrt{(p_1\cdot p_2)^2-m_e^4}}\left|\mathcal{T}_{ee}\left(p_1,p_2,p_3,p_4\right)\right|^2 \\ &\quad \delta^4\left(p_1+p_2-p_3-p_4\right)\frac{d^3p_3 d^3p_4}{(2\pi)^3 2p_3^0 (2\pi)^3 2p_4^0}. \end{aligned} \tag{2.92}$$

In the CM frame, Eq. (2.92) reduces to

$$\frac{d\sigma_{\rm pol}(s,\theta)}{d\Omega} = \frac{\left|\mathcal{T}_{ee}\left(s,\theta\right)\right|^2}{64\pi^2 s}\left(\frac{s-4m_\pi^2}{s-4m_e^2}\right)^{1/2}. \tag{2.93}$$

If we denote the spins of the electron and positron by s_1 and s_2, the Lorentz-invariant scattering amplitude can then be written as

$$\mathcal{T}_{ee}^{a_3a_4}\left(p_1,p_2,p_3,p_4\right)=e^2\varepsilon^{3a_3a_4}\frac{F_\pi(s)}{s}\,\bar{v}_e(p_2,s_2)(\not{p}_4-\not{p}_3)u_e(p_1,s_1), \tag{2.94}$$

where $\not{p}=p_\mu\gamma^\mu$ and the spinors $u_e(p_1,s_1)$ and $\bar{v}_e(p_2,s_2)=v_e^\dagger(p_2,s_2)\gamma^0$ are the positive- and negative-frequency solutions of the Dirac equation, respectively. Since the lepton beams are unpolarized, the experimental cross section is actually an average over the spins s_1 and s_2. Thus the square of the invariant amplitude can be written as

$$\begin{aligned}\frac{1}{4}\sum_{a_3a_4}\sum_{s_1,s_2}|\mathcal{T}_{ee}^{a_3a_4}\left(p_1,p_2,p_3,p_4,s_1,s_2\right)|^2=e^4\varepsilon^{3a_3a_4}\varepsilon^{3a_3a_4}\frac{|F_\pi(s)|^2}{s^2}\left(p_4-p_3\right)_\mu(p_4-p_3)_\nu\\ \frac{1}{4}\sum_{s_1,s_2}\bar{u}_e(p_1,s_1)\gamma^\mu v_e(p_2,s_2)\bar{v}_e(p_2,s_2)\gamma^\nu u_e(p_1,s_1).\end{aligned} \tag{2.95}$$

From the properties [68],

$$\sum_{s_1}u_e(p_1,s_1)\bar{u}_e(p_1,s_1)=\not{p}_1+m_e \tag{2.96}$$

$$\sum_{s_2}v_e(p_2,s_2)\bar{v}_e(p_2,s_2)=\not{p}_2-m_e, \tag{2.97}$$

we have

$$\sum_{s_1,s_2}\bar{u}_e(p_1,s_1)\gamma^\mu v_e(p_2,s_2)\bar{v}_e(p_2,s_2)\gamma^\nu u_e(p_1,s_1)=\mathrm{Tr}\left[\left(\not{p}_1+m_e\right)\gamma^\mu\left(\not{p}_1-m_e\right)\gamma^\nu\right]. \tag{2.98}$$

Using trace technology and Levi-Civita property like

$$\gamma^\alpha\gamma^\mu\gamma^\beta\gamma^\nu=4\left(\eta^{\alpha\mu}\eta^{\beta\nu}-\eta^{\alpha\beta}\eta^{\mu\nu}+\eta^{\alpha\nu}\eta^{\nu\beta}\right), \tag{2.99}$$

$$\varepsilon^{3a_3a_4}\varepsilon^{3a_3a_4}=2, \tag{2.100}$$

and neglecting the electron mass m_e ($m_e\ll m_\pi$) the unpolarized cross section is

$$\sigma(s)_{\text{unpol.}}=\frac{\pi\alpha^2}{3s}\left(1-\frac{4m_\pi^2}{s}\right)^{3/2}|F_\pi(s)|^2. \tag{2.101}$$

The contributions to the pion form factor in Vector EFT are sketched in Fig. 2.6. When we specialize in the window region, given by Eq. (2.52), i. e. around $s = m_\rho^2$, the power counting of Sect. 2.3.2 shows that in LO we need to include both diagrams shown explicitly in Fig. 2.6. Using the photon-rho mixing, Eq. (2.75), and the dressed rho propagator, Eq. (2.70), we find

$$F_\pi^{(0)}(s) = \frac{s - m_\rho^2 - i m_\rho \Gamma_{\pi\pi}^{(0)}(m_\rho^2)}{s - m_\rho^2 + i m_\rho \Gamma_{\pi\pi}^{(0)}(m_\rho^2)} - \left(\frac{m_\rho}{4\pi f_\pi}\right)^2 \frac{a^{(0)} m_\rho^2}{s - m_\rho^2 + i m_\rho \Gamma_{\pi\pi}^{(0)}(m_\rho^2)}. \qquad (2.102)$$

Neglecting subleading terms, Eq. (2.101) reduces to

$$\begin{aligned} \sigma(s)_{\text{unpol.}} &= \frac{\pi\alpha^2}{3m_\rho^2}\left(1 - \frac{4m_\pi^2}{m_\rho^2}\right)^{3/2} \left| \frac{s - m_\rho^2 - i m_\rho \Gamma_{\pi\pi}^{(0)}(m_\rho^2)}{s - m_\rho^2 + i m_\rho \Gamma_{\pi\pi}^{(0)}(m_\rho^2)} \right. \\ &\quad \left. - \left(\frac{m_\rho}{4\pi f_\pi}\right)^2 \frac{a^{(0)} m_\rho^2}{s - m_\rho^2 + i m_\rho \Gamma_{\pi\pi}^{(0)}(m_\rho^2)} \right|^2 . \qquad (2.103) \end{aligned}$$

Around the window, Eq. (2.52), Eq. (2.103) can be simplified to

$$\begin{aligned} \sigma(s)_{\text{unpol.}} &= \frac{\pi\alpha^2}{3m_\rho^2}\left(1 - \frac{4m_\pi^2}{m_\rho^2}\right)^{3/2} \\ &\quad \left(1 - \left(\frac{m_\rho}{4\pi f_\pi}\right)^2 \frac{2a^{(0)} m_\rho^2 \left(s - m_\rho^2\right) - \left(\frac{m_\rho}{4\pi f_\pi}\right)^2 a^{(0)2} m_\rho^4}{\left(s - m_\rho^2\right)^2 + m_\rho^2 \Gamma_{\pi\pi}^{(0)2}(m_\rho^2)}\right) . \qquad (2.104) \end{aligned}$$

For completeness, if we define a general coupling constant,

$$g_{\rho ee} \equiv -\frac{2e^2 f_\pi}{m_\rho}\left(\frac{m_\rho}{4\pi f_\pi}\right)^2 \left(a_{\gamma\rho} + \frac{2i}{m_\rho}\Gamma_{\pi\pi}^{(0)}\left(m_\rho^2\right)\left(\frac{4\pi f_\pi}{m_\rho}\right)^2\right), \qquad (2.105)$$

and the rho decay into an electron and a positron,

$$\Gamma_{ee}^{(0)}(m_\rho^2) = \frac{m_\rho g_{\rho ee}^2}{12\pi}, \qquad (2.106)$$

see details in App. C, we can write the cross section, given by Eq. (2.104), as a

function of the rho decay widths, $\Gamma^{(0)}_{\pi\pi}(m_\rho^2)$ and $\Gamma^{(0)}_{ee}(m_\rho^2)$,

$$\begin{aligned}\sigma_{\text{unpol.}}(s) &= \frac{4\alpha^2\Gamma^{(0)}_{\pi\pi}(m_\rho^2)}{m_\rho^3}\left(\frac{4\pi f_\pi}{m_\rho}\right)^2\{1 \\ &+\frac{1}{\left(s-m_\rho^2\right)^2+m_\rho^2\Gamma^{(0)2}_{\pi\pi}(m_\rho^2)}\left[\frac{3\pi m_\pi^3\Gamma^{(0)}_{ee}(m_\rho^2)}{\alpha^2}\left(\frac{m_\rho}{4\pi f_\pi}\right)^2+\left(2\Gamma^{(0)\ 2}_{\pi\pi}(m_\rho^2)\right.\right. \\ &\left.\left.+\left(\frac{12\pi\Gamma^{(0)}_{ee}(m_\rho^2)}{m_\rho}-\frac{4\Gamma^{(0)\ 2}_{\pi\pi}(m_\rho^2)}{m_\rho^2}\right)^{\frac{1}{2}}\left(s-m_\rho^2\right)\right)\frac{m_\rho^3}{8\pi\alpha f_\pi}\right]\Bigg\}. \qquad (2.107)\end{aligned}$$

Eq. (2.104), or Eq. (2.107), will be fit to the $e^+e^-\to\pi^+\pi^-$ cross section, where the parameters $a_{\gamma\rho}$ and m_ρ can be found. With these parameters, we will be able to predict the $\pi\pi\to\pi\pi$ phase shifts.

2.6 Comparison to Data

We are now in position to compare the vector EFT results of the previous section with data. We first determine the parameters m_ρ and $a_{\gamma\rho}$ from a fit of the $e^+e^-\to\pi^+\pi^-$ cross section using the expression given by Eq. (2.104) and then use Eq. (2.89) to predict the $\pi\pi\to\pi\pi$ phase shifts.

2.6.1 $e^+e^-\to\pi^+\pi^-$

The experimental values for the rho mass, found in Ref. [14], is, usually, extracted from the pion form factor or $e^+e^-\to\pi^+\pi^-$ cross section as a function of the center-of-mass energy. In the most recent measurements, the center-of-mass energy range is about $\sqrt{s}<1.4$ GeV [72, 73, 74]. In Ref. [72] the cross section is measured in the CMD-2 detector, with systematic uncertainty of 0.8%, while in Ref. [73], the cross section is measured in the SND detector at the VEPP-2M e^+e^- collider, with systematic error estimated to be 1.3% and in REf. [74] the detectors used are OLYA or CMD at the VEPP-2M collider. Particle data group [14] gives the rho-mass average from the recent experiments, $m_\rho=(774.49\pm0.34)$ MeV, and the averages of the partial decay widths of the rho into two pions and into electron-

positron, $\Gamma(\rho \to \pi\pi) = (146.2 \pm 0.7)$ MeV and $\Gamma(\rho \to e^+e^-) = (7.04 \pm 0.11)$ keV, respectively.

We fit the parameters m_ρ and $a_{\gamma\rho}$ in the $e^+e^- \to \pi^+\pi^-$ cross section as a function of the center-of-mass energy, given by Eq. (2.7), in vector EFT, to the experimental data cited above, AKMETSHIN 07 (Experiment NOVOSIBIRKSK - CMD - 2) [72], ACHASOV 06 (Experiment NOVOSIBIRSK - SND) [73], and BARKOV 85 (Experiment OLYA Part I and Part II) [74]. The fit is done by using χ^2 method in two regions of energy, around rho mass and all energies up to 900 MeV. With the values for m_ρ and $a_{\gamma\rho}$, the partial decay widths $\Gamma^{(0)}_{\pi\pi}(m_\rho^2)$ and $\Gamma^{(0)}_{ee}(m_\rho^2)$ are obtained using Eqs. (2.69) and (C.10), respectively.

The values obtained for the LO parameters are $m_\rho \simeq 769$ MeV, whose error compared to the Particle data group [14] is about 0.7%, and $a_{\gamma\rho} = 1.48$, while the LO partial decay widths of the rho into two pions and into electron-positron were found to be, in vector EFT, $\Gamma^{(0)}_{\pi\pi}(m_\rho^2) \simeq 71$ MeV and $\Gamma^{(0)}_{ee}(m_\rho^2) \simeq 4.5$ keV, whose errors are about 52% and 37%, when compared to Ref. [14]. The values, found for m_ρ, $a_{\gamma\rho}$, $\Gamma^{(0)}_{\pi\pi}(m_\rho^2)$, and $\Gamma^{(0)}_{ee}(m_\rho^2)$, from the fit with these two different energy regions differ by less than 0.1%, and the $e^+e^- \to \pi^+\pi^-$ cross section as a function of the center-of-mass energy graphs are the same, hence we only show one graph in Fig. 2.7. The data, CMD-2, SND, OLYA-I and OLYA-II are represented by bullets, squares, triangle, and diamond, respectively, while the $e^+e^- \to \pi^+\pi^-$ cross section, in vector EFT, as a function of the center-of-mass energy, and its "modifications" are represented by the dot-dashed line, and by the full and dotted lines, respectively. For comparison, we show the $e^+e^- \to \pi^+\pi^-$ cross section in ChPT, represented by Eq. (A.5) in App. A, represented by the thick-dashed line. Note that the sets of data are very close to each other, making almost impossible to distinguish them, in addition, because the error bars are very small it is very difficult to see them.

In order to verify how the results can be improved, we try two modifications to Eq. (2.104), seen below.

The first modification corresponds in considering higher orders only in the cross-section kinematics. In other words, the $e^+e^- \to \pi^+\pi^-$ cross section, in Eq. (2.104),

is modified to

$$\sigma(s)_{\text{unpol.}} = \frac{\pi\alpha^2}{3s}\left(1-\frac{4m_\pi^2}{s}\right)^{3/2}\left(1 - s\left(\frac{m_\rho}{4\pi f}\right)^2 \frac{2a^{(0)}\left(s-m_\rho^2\right) - s\left(\frac{m_\rho}{4\pi f}\right)^2 a^{(0)2}}{\left(s-m_\rho^2\right)^2 + s b_w^2 \Gamma_{\pi\pi}^{(0)2}(s)}\right), \tag{2.108}$$

where the constant $b_w = 1$ is an added parameter. With such modification, a large range in the values of $a_{\gamma\rho}$ is generated in the fit. Based on fits done by using Eq. (2.104), we chose the parameter results, $m_\rho \simeq 768$ MeV, whose error compared to Ref. [14] is now 0.8%, and $a_{\gamma\rho} \simeq 1.5$. The values for the partial decay widths do not change. The curve for the last equation, with the new parameters, is shown by the full line in Fig.2.7. Note that the full and dot-dashed lines are not very different from each other, except for center-of-mass energies below 400 MeV, as expected when higher orders only in the kinematics are taken into account.

The second modification consists in adding, to the first modification, a parameter that tell us what would happen if one consider $\Gamma_{\pi\pi}(s)$ at higher orders, i. e . we set, in Eq. (2.108), $b_w \neq 1$. The values found from the fit for m_ρ, $a_{\gamma\rho}$ and b_w are, now, approximately 768 MeV, 2.5 and 1.8, respectively. The error of the obtained m_ρ, compared to known value [14], is now 0.9%. And for the "new" partial widths, $b_w\Gamma_{\pi\pi}^{(0)}(m_\rho^2)$ and $b_w\Gamma_{ee}^{(0)}(m_\rho^2)$ the values found are 128 MeV and 12.3 keV, whose errors are about 13% and 75%,respectively. While the decay width of the rho into e^+e^- did not improve, the decay of the rho into two pions greatly improve, by approximately 45%, as well as the cross section graph as one can see in the dotted line, shown in Fig. 2.7, suggesting that higher-order calculations in the rho width could be attempted.

Note that both modified curves match the low-energy data as well as ChPT, and have better fit at higher energies. Although next-to-leading order calculations have to be attempted, one can see the improvement of the shape of the graphs compared to ChPT shape.

2.6.2 $\pi\pi \to \pi\pi$

With the values $m_\rho \simeq 769$ MeV and $\Gamma^{(0)}_{\pi\pi}(m^2_\rho) \simeq 71$ MeV found from the fit in the last subsection, we predict the $\pi\pi \to \pi\pi$ phase-shift as a function of the center-of-mass energy, obtained in Vector EFT, as one can see in Eq. (2.89). Such prediction can be found in the dot-dashed line in Fig. 2.8. The experimental data from Refs. [75] and [76] are represented by the bullets and squares, and, again, the error bars are very small, but still included. Because the value of the decay width of the rho is more than 50% off, the matching of the curve to experimental data is off by a factor of ~ 2.

From the modified values, corresponding to $m_\rho \simeq 768$ MeV and $\Gamma^{(0)}_{\pi\pi}(s) \to b_w \Gamma^{(0)}_{\pi\pi}(s) \simeq 128$ MeV, in addition to the higher-order-phase-shift kinematics, we predict the dotted line in Fig. 2.8. For comparison, we show the $\pi\pi \to \pi\pi$ phase-shift as a function of the center-of-mass energy obtained in ChPT, found in App. A and given by Eq. (A.3), in the thick-dashed line in Fig. 2.8.

Again, we show that higher-order calculations in the partial decay width of the rho, $\Gamma^{(0)}_{\pi\pi}(s)$, could lead to significant improvements in the results, in this case the phase shift, including at low-energies.

2.7 Conclusion

To explain the bump that appears in cross sections, such as those for $\pi\pi \to \pi\pi$ and $e^+e^- \to \pi^+\pi^-$ processes, at the center-of-mass energy around the rho resonance, whose mass $m_\rho \simeq 770$ MeV is just below $M_{\rm QCD} \sim 1$ GeV, we extended ChPT to allow the controlled inclusion in EFT of vector mesons — vector EFT. In such EFT, it is assumed that there exists a limit, the vector limit, where QCD contains a symmetry, vector symmetry, larger than chiral symmetry. In the vector limit, the transverse components of the rhos decouple and the longitudinal component is massless, as is the pion. Away from the vector limit, the rhos acquire mass. In this chapter, we constructed the most general effective Lagrangian that features vector symmetry and its breaking [55, 60], and enlarged the usual formulation to include

electromagnetic gauge invariance. After vector symmetry is spontaneously broken, chiral symmetry remains unbroken, which leads to the appearance of six Goldstone bosons, three pseudoscalars and three scalars. The three scalars are eaten by Higgs mechanism to become the longitudinal components of the rhos. To describe the transverse components of the rhos, we introduced spurion fields that transform as gauge fields under $SU(2)_{G_L} \times SU(2)_{G_R}$, while for the description of photons, spurion fields that transform under the local $U(1)$ symmetry were introduced. To account for the Goldstone bosons masses, we introduced the quark mass matrix, again, as a spurion field, explicitly breaking vector symmetry. Under the local $U(1)$ symmetry, the components of the pions and rhos transforms according to their electromagnetic charge, except the third component of the rho. We showed that, in unitary gauge, the effective Lagrangian has a non-diagonal gauge-boson mass matrix and has both VMD-1 and VMD-2 aspects. After diagonalizing the gauge-boson mass matrix the resulting LO Lagrangian describes, besides the interactions, a massive rho, with mass proportional to the pion decay constant, massless photons, a VMD-1 component, and has four independent parameters, where f_π, m_π and e are known from low-energy processes and m_ρ was determined in this chapter. Our LO Lagrangian was compared to the ChPT Lagrangian in App. A. Unfortunately, because of the strict relation among m_ρ, $g_{\rho\pi\pi}$ and f_π, the tree-level that relates them, in vector EFT, is twice as large as the phenomenologically successful KSFR-II relation. The tree-level relation that could be compared to KSFR-I relation depends on the photon- and rho-field-strengths-mixing parameter, $a_{\gamma\rho}$.

Since, in vector EFT, pions and rhos have, parametrically, small masses compared to $M_{\rm QCD}$, vector EFT allows for a systematic expansion in powers of $Q/M_{\rm QCD}$, where $Q \sim m_\pi \sim m_\rho$, although, realistically, when $Q \sim m_\rho$, the expansion can be rather slow. In the whole region where $Q < M_{\rm QCD}$, reactions, such as the ones mentioned above, $\pi\pi \to \pi\pi$ and $e^+e^- \to \pi^+\pi^-$, have a peak around the rho resonance, a non-perturbative phenomenon that spoils perturbation theory. To describe such peak, we accounted for the rho width, which was incorporated in a power counting that was extended to the "kinematic" region around the peak. We proved

that within a window, around the rho peak, the dressed propagator of the rho is enhanced compared to the rho propagator outside such window, and thus, the rho self-energy had to be taken into account at LO. Specifically, the contributions of the rho to both LO processes amplitudes, around the rho peak, was found to be of $\mathcal{O}(M_{\rm QCD}^2/Q^2)$.

For explicit calculations of the observables, we included all the contributions at LO, including loops with finite terms and also the short-range interactions that kept the theory renormalizable. For completeness, in App. B, we calculated and discussed the pion self-energy at LO. Because we defined our fields in unitary gauge, the rho self-energy had some terms, coming from the longitudinal component of the bare-rho propagator in loop calculations, that did not seem to be renormalizable. Ref. [65], based on Ref. [66], briefly explains how spontaneously broken gauge theories can be unitary and renormalizable at the same time. Thus, apparent non-renormalizability is not a problem with the condition that the observables are renormalizable. The dressed propagator of the rho had an imaginary piece, which comes, exclusively, from the pion loop and contributes to the rho decay width. The real piece defines the rho mass.

The experimental values for the rho mass and partial decay widths of the rho into two pions and into electron-positron pair are extracted from the $e^+e^- \to \pi^+\pi^-$ cross section as a function of the center-of-mass energy, measured in detectors at colliders, as examples given in the main text. The average of the values found in the most recent experiments can be found in the Particle Data Book [14], and was used to compare to the values found in this chapter. With the expression found for the $e^+e^- \to \pi^+\pi^-$ cross section as a function of the center-of-mass energy in vector EFT, we fitted $a_{\gamma\rho}$ and m_ρ to the corresponding experimental data, and found $a_{\gamma\rho} \simeq 1.5$ and $m_\rho \simeq 769$ MeV, with an error of 0.7% compared to the value found in [14]. Unfortunately, the values obtained for the decay widths, $\Gamma^{(0)}_{\pi\pi}(m_\rho^2) \simeq 71$ MeV and $\Gamma^{(0)}_{ee}(m_\rho^2) = 4.5$ keV, have errors of 52% and 37% compared to the values in Ref. [14], and the curve, although matched experimental data around the rho mass, as expected, fails to match the data at other energies. Another unfortunate is that

vector EFT could not reproduce KSFR-I relation. By making some modifications to our cross-section expression, we showed that the results, including the fit, greatly improve if higher-order calculations of the rho decay width are considered. With the values found for the rho mass and decay width, we predicted the P-wave $\pi\pi \to \pi\pi$ phase shifts. Again, we showed that the decay width of the rho at higher orders may improve the fit.

One possible prospect would be the calculation of observables at next-to-leading order and the check of our conjecture that the cross sections should improve. The power counting extended to the non-perturbative region was very efficient to describe processes, such as the ones studied in this chapter, that shows non-perturbative effects in a certain region of energy. We believe that many other non-perturbative phenomenon can be described with a systematic construction of a non-perturbative EFT.

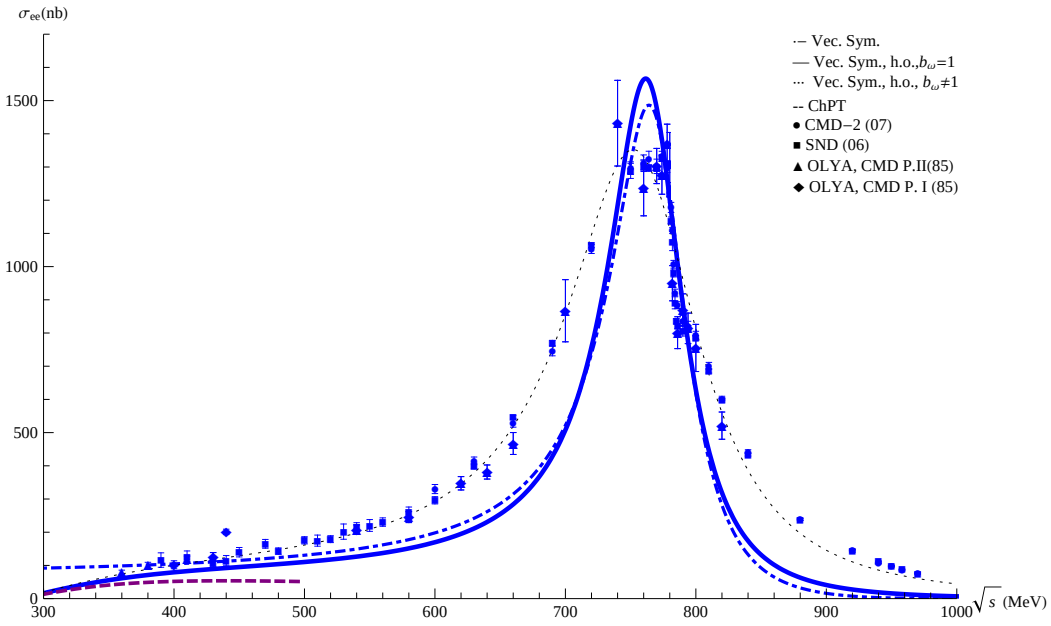

Figure 2.7: $e^+e^- \to \pi\pi$ cross section, $\sigma_{ee}(nb)$, as a function of the center-of-mass energy, $\sqrt{s}$. The dot-dashed, full, dotted and the thick-dashed lines represent the cross sections obtained in Vector EFT around rho meson, in Vector EFT using "higher-order calculations" in the cross-section kinematics, in Vector EFT using a "higher-order decay width", and in ChPT, respectively. The bullets, squares, triangle, and diamond represent the experimental data AKMETSHIN 07 (Experiment NOVOSIBIRKSK - CMD - 2) [72], ACHASOV 06 (Experiment NOVOSIBIRSK-SND) [73] and BARKOV 85 (Experiment OLYA Part I and Part II) [74], respectively. The error bars are included, but they are very small to be seen.

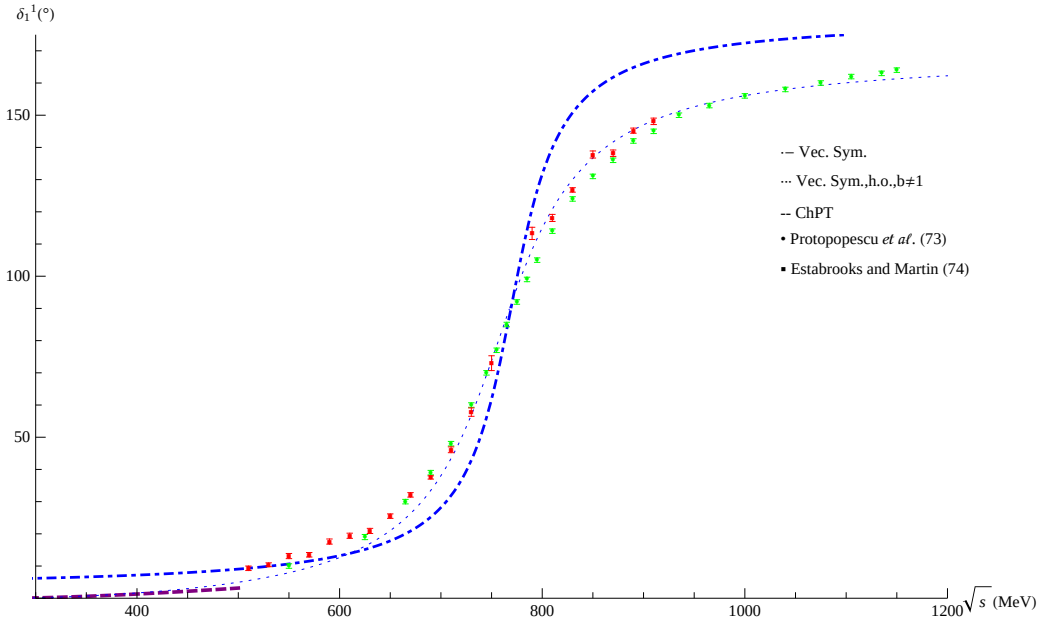

Figure 2.8: $\pi\pi \to \pi\pi$ phase-shift, $\delta_1^1(^o)$, as a function of the center-of-mass energy, $\sqrt{s}$. The dot-dashed, dotted and thick dashed-lines represent the phase-shifts in Vector EFT, using "higher-order-rho-decay width" in Vector EFT, and in ChPT, respectively. The bullets and squares represent the experimental data from Protopopescu [75] and Estabrooks [76], respectively. The error bars are small, but included.

CHAPTER 3

RENORMALIZATION OF PION EXCHANGE WITH AUXILIARY FIELDS AND A PERTURBATIVE SOLUTION FOR THE DEUTERON

3.1 Introduction

The foundation of the nucleon-nucleon (NN) potential remains one of the most important problems in nuclear physics. During the last two decades, considerable progress has been achieved in constructing an effective field theory (EFT) that describes many-nucleons problems [4, 78, 79]. Even though the development of an EFT NN potential is simpler than of an EFT many-nucleon potential, it is still a complex venture. The EFT that describes nuclear systems, with pions and nucleons as degrees of freedom, is Chiral Perturbation Theory, which makes use of the chiral symmetry of QCD and its breaking. The EFT framework allows a systematic organization of nuclear amplitudes due to power-counting techniques. Because of the non-perturbative nature of the NN interaction, manifested in the existence of a shallow bound state and in the large size of scattering lengths compared to $M_{\rm QCD}^{-1}$, such systematic organization can be rather difficult.

Weinberg [22] proposed to that the full amplitudes could be generated systematically by a truncation at the level of the irreducible diagrams that constitute the potential. Such truncation would be guided by ChPT power counting. The lowest-order potential in ChPT consists of one-pion-exchange (OPE) potential as the long-range term and of short-range terms given by chiral-invariant non-derivative contact interactions. In this scheme, the Schrödinger equation must be solved numerically and requires, as in any other approach, the introduction of an arbitrary regulator that separates low- from high-energy dynamics at a cutoff Λ. Regulator dependence of the low-energy observables must be eliminated by renormalization. Kaplan, Savage and Wise (KSW) [23] found some fundamental problems in Weinberg's power

counting: the first few diagrams resummed in the solution of the Schrödinger equation for one-pion exchange require more counterterms than present at the same order in Weinberg's power counting. To solve this problem, KSW suggested that pions should be treated as other subleading corrections in perturbation theory, instead of fully iterating OPE. In this case, power counting can be expressed directly at the level of the amplitude, so that observables are expanded in powers of $Q/M_{\rm QCD}$ or $m_\pi/M_{\rm QCD}$. The advantage of the KSW scheme is that the ultraviolet divergences are absorbed by the same- or lower-order operators in the expansion. Naive dimensional analysis show that the KSW expansion converges slowly, though. By calculating the NN phase shifts up to next-to-leading order in the KSW expansion [24], the slow convergence was confirmed. To verify if the convergence of the expansion persists, calculations to higher orders were done. Ref. [25] computed the ${}^1S_0$, ${}^3S_1$ and ${}^3D_1$ NN phase shifts at next-to-next-to-leading order ($\mathrm{N^2LO}$) using the KSW expansion scheme, and showed that the KSW expansion in the ${}^1S_0$ channel indeed converges slowly, while in the spin triplet ${}^3S_1 - {}^3D_1$ channels, however, no perturbative convergence was found for momenta of order 100 MeV. It was observed [25] that the failure of convergence comes from a singularity that appears to be more dramatic in spin-triplet channels than in spin-singlet channels. In Ref. [27], it was confirmed that the KSW expansion is consistent in the ${}^1S_0$ channel while Weinberg's expansion is not, and Weinberg's power counting is consistent in the ${}^3S_1 - {}^3D_1$ channels while KSW expansion is not. Ref. [27], thus, suggested that OPE should be treated perturbatively in ${}^1S_0$ channel, but not in ${}^3S_1 - {}^3D_1$ channels. The lack of convergence is related to the renormalization of singular potentials [26], in this specific case, the $1/r^3$ singularity in the isovector tensor force from one-pion exchange.

A non-perturbative calculation of the renormalization of the OPE in lower-order partial waves, ${}^1S_0$ and ${}^3S_1 - {}^3D_1$, is consistent with Weinberg's power counting [27, 80]. However, it is expected that higher-order partial waves from spin-triplet channels in the OPE , such as ${}^3P_0$, ${}^3P_2 - {}^3F_2$ and ${}^3D_2$, to be cutoff dependent, since there are no LO counterterms, for these waves, predicted by dimensional analysis, which means that Weinberg's power counting fails. It has been shown [9] that several

counterterms are needed to renormalize the two-nucleon problem in leading order in chiral EFT, where each counterterm for the LO spin-triplet channels corresponds to some higher-order operator in Weinberg's power counting. Here we investigate the possibility of essentially replacing such counterterms with auxiliary fields. That this might work is a consequence of the fact that the $1/r^3$ singularity can be eliminated by the exchange of either isovector vector [81, 82] or isovector pseudovector [83, 84, 85] mesons, and thus also an appropriate combination of both. Exchange of other auxiliary mesons —for example isoscalar scalar and isoscalar vector— can to some extent compensate the spurious r dependence introduced in some channels. Large-N_c arguments can be used to select the appropriate auxiliary fields. Note that there might be a connection with Weinberg's algebraic realization of chiral symmetry [86], as the argument for the introduction of these fields in both cases is based on taming the short-distance behavior of amplitudes.

In Sec. 3.2, we show the non-relativistic Lagrangian that accommodates nucleons, isovector pseudoscalars-pions, auxiliary isovector vectors and pseudovectors and auxiliary isoscalar scalars and vectors, which might be viewed as lowest order in an expansion in the large number of colors N_c. Sec. 3.3 describes the corresponding NN potentials in momentum coordinates for different spin and isospin channels. We identify the term problematic for renormalization and present a combination of coupling constants that cancels the strong singularity in the tensor force. Frequently, space coordinates are used to calculate observables from a two-nucleon potential. To perform the transformation from momentum to space coordinates, we apply in Sec. 3.4 the Fourier transform with a Gaussian regulator $e^{-\vec{q}^2/\Lambda^2}$, where $\vec{q}$ is the transferred momentum and Λ is the cutoff momentum that separates low- from high-energy dynamics. Sec. 3.5 is devoted to the analysis of limiting cases, such as the form of the potential in the limit of large cutoff, or when pseudovector or vector fields are decoupled. In addition, possible arguments supporting our potential with added extra auxiliary fields, besides vectors and pseudovectors, are given. In principle, from the potentials obtained and from the fit to low-energy experimental data, such as low-channel phase shifts, we could determine high-channel phase shifts and

deuteron parameters. In particular, the Hamiltonian for the potential obtained in the spin-triplet channel, shown in Sec. 3.6, is used to determine the deuteron binding energy. In Sec. 3.7, we solve the Schrödinger equation for the dominant short-range interaction of the deuteron potential exactly and treat the residual short-range and long-range interactions in perturbation theory. We consider different cutoff functions for the calculations of the first correction of the deuteron binding energy. Our conclusions and outlook are given in Sec. 3.8.

3.2 Lagrangian

We start with the Lagrangian involving, in addition to the nucleon field N, isospin-vector fields for the pion $\boldsymbol{\pi}$, auxiliary vector $\boldsymbol{V}_\mu$, and auxiliary pseudovector $\boldsymbol{A}_\mu$, and isoscalar fields for the auxiliary scalar s and vector v_μ,

$$\begin{aligned}
\mathcal{L} \;=\; & \frac{1}{2}\partial_\mu\boldsymbol{\pi}\cdot\partial^\mu\boldsymbol{\pi} - \frac{m_\pi^2}{2}\boldsymbol{\pi}^2 + \frac{m_v^2}{2}v_\mu v^\mu + \frac{1}{2}\partial_\mu s\partial^\mu s - \frac{m_s^2}{2}s^2 + \frac{1}{4}\boldsymbol{F}_V^{\mu\nu}\cdot\boldsymbol{F}_{V\,\mu\nu} \\
& + \frac{1}{4}F_v^{\mu\nu}F_{v\,\mu\nu} + \frac{m_V^2}{2}\boldsymbol{V}_\mu\cdot\boldsymbol{V}^\mu + \frac{1}{4}\boldsymbol{F}_A^{\mu\nu}\cdot\boldsymbol{F}_{A\,\mu\nu} + \frac{m_{PV}^2}{2}\boldsymbol{A}_\mu\cdot\boldsymbol{A}^\mu \\
& + N^\dagger\left(i\partial^0 + \frac{\nabla^2}{2m_N}\right)N \\
& - \frac{1}{2f_\pi}\left\{g_A\vec{\nabla}\boldsymbol{\pi} + g_T\vec{\nabla}\times\vec{\boldsymbol{V}} + g_{PT}\left(\vec{\nabla}\boldsymbol{A}^0 + \partial^0\vec{\boldsymbol{A}}\right) + g_{PV}m_{PV}\vec{\boldsymbol{A}}\right\}\cdot N^\dagger\vec{\sigma}\boldsymbol{\tau}N \\
& - \frac{1}{2f_\pi}\left\{\left[g_s m_s s + g_{sd}m_s\partial^0 s + g_v m_v v^0\right]N^\dagger N + g_t\vec{\nabla}\times\vec{v}\cdot N^\dagger\vec{\sigma}N\right. \\
& \left. + g_V m_V\boldsymbol{V}^0\cdot N^\dagger\boldsymbol{\tau}N\right\} \\
& - \frac{1}{(2f_\pi)^2}\left\{C_0^{(V)}N^\dagger\boldsymbol{\tau}N\cdot N^\dagger\boldsymbol{\tau}N + C_0^{(T)}N^\dagger\vec{\sigma}\boldsymbol{\tau}N\cdot N^\dagger\vec{\sigma}\boldsymbol{\tau}N\right\} + \ldots, \qquad (3.1)
\end{aligned}$$

where m_N, m_π, m_V, m_{PV}, m_v and m_s are the masses for N, $\boldsymbol{\pi}$, $\boldsymbol{V}_\mu$, $\boldsymbol{A}_\mu$, v_μ and s, respectively, $\vec{\sigma}$ and $\boldsymbol{\tau}$ are the spin and isospin Pauli matrices, $\boldsymbol{F}_{V\,\mu\nu} = \partial_\mu\boldsymbol{V}_\nu - \partial_\nu\boldsymbol{V}_\mu$, $\boldsymbol{F}_{A\,\mu\nu} = \partial_\mu\boldsymbol{A}_\nu - \partial_\nu\boldsymbol{A}_\mu$, $F_{v\,\mu\nu} = \partial_\mu v_\nu - \partial_\nu v_\mu$, and the "..." stand for interactions necessary to ensure chiral symmetry, which are not relevant to the two-nucleon potential in leading order. (This Lagrangian can be obtained from a non-relativistic reduction of a relativistic Lagrangian.)

Note that the Lagrangian has enough terms to encode the correct leading be-

havior at large number of colors N_c [87]. Indeed, the scalings are $f_\pi = \mathcal{O}(\sqrt{N_c})$, $m_N = \mathcal{O}(N_c)$, $m_i = \mathcal{O}(1)$ $(i = \pi, V, PV, v, s)$, $g_A = \mathcal{O}(N_c)$, $g_T = \mathcal{O}(N_c)$, $g_{PT} = \mathcal{O}(N_c)$, $g_{PV} = \mathcal{O}(N_c)$, $g_s = \mathcal{O}(N_c)$, $g_{sd} = \mathcal{O}(N_c)$, $g_v = \mathcal{O}(N_c)$, $g_t = \mathcal{O}(1)$, $g_V = \mathcal{O}(1)$, $C_0^{(V)} = \mathcal{O}(1)$, and $C_0^{(T)} = \mathcal{O}(N_c^2)$. Thus, in the large-$N_c$ limit the exchange of pion, isovector vector, isovector pseudovector, scalar, and isoscalar vector dominate together with the contact $C_0^{(T)}$ interaction, generating a potential of $\mathcal{O}(N_c)$. Note that the spatial components of the isoscalar vector, the temporal component of the isovector vector, and the contact $C_0^{(V)}$ interaction only contribute a potential of $\mathcal{O}(N_c^{-1})$ —if we work at leading order in N_c we can ignore these terms. One could introduce also isovector scalar, isoscalar pseudoscalar and isoscalar pseudovector fields, but up to interactions with one derivative they would, likewise, lead to a potential of $\mathcal{O}(N_c^{-1})$.

This large-N_c argument is heuristic for at least two reasons. First, it assumes that momenta scale as N_c^0. This is consistent with the non-relativistic expansion for the nucleon, but at the same time implies that the kinetic energy of nucleons is much smaller than the potential, so there is no scattering at $N_c \to \infty$. Instead, we will retain the nucleon kinetic term in the Lagrangian, as necessary to infrared regulate loop integrals. Second, in the $N_c \to \infty$ limit a tower of other fermions, starting with the delta isobar, becomes degenerate with the nucleon and the full problem needs to be treated as a coupled-channels system where the propagation of all fermions is included on the same footing, and subject to the same infrared enhancement, as pure-nucleon intermediate states. Instead, we will relegate delta propagation to higher-order loops in the potential and integrate out other baryons, as appropriate for $N_c = 3$, where the delta-nucleon mass splitting is comparable to the pion mass and other baryons lie high in the spectrum.

3.3 Two-Nucleon Potential in Momentum Space

The leading-order two-nucleon potentials $V^{(S,I)}$ for the various spin S and isospin I channels can be found from the tree-level diagrams. At leading order we can set

energies to zero because they are proportional to the small scale m_N^{-1}. This is consistent with the large-N_c expansion of the potential. As a consequence, the potential at this order is static and the terms involving $\partial^0 s$ and $\partial^0 \vec{\boldsymbol{A}}$ do not contribute.

If we denote by $\vec{q}$ the momentum transferred between the nucleons, the tree-level potential in momentum space is

$$\begin{aligned} V(\vec{q}) &= \frac{1}{(2f_\pi)^2}\left\{ \boldsymbol{\tau}_1\cdot\boldsymbol{\tau}_2\ \vec{\sigma}_1\cdot\vec{q}\,\vec{\sigma}_2\cdot\vec{q}\left[-\frac{g_A^2}{\vec{q}^{\,2}+m_\pi^2}+\frac{g_T^2}{\vec{q}^{\,2}+m_V^2}+\frac{g_{PT}^2-g_{PV}^2}{\vec{q}^{\,2}+m_{PV}^2}\right]\right. \\ &\quad +\boldsymbol{\tau}_1\cdot\boldsymbol{\tau}_2\ \vec{\sigma}_1\cdot\vec{\sigma}_2\left[C_0^{(T)}-g_T^2+\frac{g_T^2 m_V^2}{\vec{q}^{\,2}+m_V^2}-\frac{g_{PV}^2 m_{PV}^2}{\vec{q}^{\,2}+m_{PV}^2}\right] \\ &\quad +\boldsymbol{\tau}_1\cdot\boldsymbol{\tau}_2\left[C_0^{(V)}+\frac{g_V^2 m_V^2}{\vec{q}^{\,2}+m_V^2}\right]+\left(\vec{\sigma}_1\cdot\vec{q}\,\vec{\sigma}_2\cdot\vec{q}-\vec{q}^{\,2}\vec{\sigma}_1\cdot\vec{\sigma}_2\right)\frac{g_t^2}{\vec{q}^{\,2}+m_v^2} \\ &\quad \left.+\frac{g_v^2 m_v^2}{\vec{q}^{\,2}+m_v^2}-\frac{g_s^2 m_s^2}{\vec{q}^{\,2}+m_s^2}\right\}. \end{aligned} \tag{3.2}$$

The most singular terms when $|\vec{q}|\to\infty$ go as $|\vec{q}|^0$, or, in coordinate space, as $\delta^{(3)}(\vec{r})$ (central) and $1/r^3$ (tensor). The latter requires additional counterterms in all waves where it is strongly attractive. In order to cancel the $1/r^3$ singularity we impose

$$g_T^2+g_{PT}^2-g_{PV}^2=g_A^2 \tag{3.3}$$

and

$$g_t=0. \tag{3.4}$$

In this case, eliminating for example g_{PT},

$$\begin{aligned} V(\vec{q}) &= \frac{1}{(2f_\pi)^2}\left\{ \boldsymbol{\tau}_1\cdot\boldsymbol{\tau}_2\ \vec{\sigma}_1\cdot\hat{q}\,\vec{\sigma}_2\cdot\hat{q}\left[g_A^2\left(\frac{m_\pi^2}{\vec{q}^{\,2}+m_\pi^2}-\frac{m_{PV}^2}{\vec{q}^{\,2}+m_{PV}^2}\right)\right.\right. \\ &\quad \left.-g_T^2\left(\frac{m_V^2}{\vec{q}^{\,2}+m_V^2}-\frac{m_{PV}^2}{\vec{q}^{\,2}+m_{PV}^2}\right)\right] \\ &\quad +\boldsymbol{\tau}_1\cdot\boldsymbol{\tau}_2\ \vec{\sigma}_1\cdot\vec{\sigma}_2\left[C_0^{(T)}-g_T^2+(g_T^2-g_{PV}^2)\frac{m_{PV}^2}{\vec{q}^{\,2}+m_{PV}^2}\right. \\ &\quad \left.+g_T^2\left(\frac{m_V^2}{\vec{q}^{\,2}+m_V^2}-\frac{m_{PV}^2}{\vec{q}^{\,2}+m_{PV}^2}\right)\right] \\ &\quad \left.+\boldsymbol{\tau}_1\cdot\boldsymbol{\tau}_2\left[C_0^{(V)}+\frac{g_V^2 m_V^2}{\vec{q}^{\,2}+m_V^2}\right]+\frac{g_v^2 m_v^2}{\vec{q}^{\,2}+m_v^2}-\frac{g_s^2 m_s^2}{\vec{q}^{\,2}+m_s^2}\right\}. \end{aligned} \tag{3.5}$$

The $\boldsymbol{\tau}_1\cdot\boldsymbol{\tau}_2$ terms are subleading in large N_c. The only terms that do not vanish as $|\vec{q}|\to\infty$ are $\boldsymbol{\tau}_1\cdot\boldsymbol{\tau}_2\ \vec{\sigma}_1\cdot\vec{\sigma}_2$ and $\boldsymbol{\tau}_1\cdot\boldsymbol{\tau}_2$ momentum-independent terms. These are delta

functions in coordinate space, and by a suitable choice of the cutoff-dependence of $C_0^{(i)}$ the problem can be properly renormalized.

3.4 Two-Nucleon Potential in Coordinate Space

We obtain the coordinate-space potential by Fourier-transforming $V(\vec{q})$,

$$V(\vec{r}) = \int d^3q e^{i\vec{q}\cdot\vec{r}} V(\vec{q}) F\left(\vec{q}^{\,2}/\Lambda^2\right), \tag{3.6}$$

with a cutoff function $F(x)$ such that $F(0) = 1$ and $\lim_{x\to\infty} F(x) = 0$. Since $F(x)$ is arbitrary, observables should be independent of the form of $F(x)$ and, for a given form, of the value of the cutoff parameter Λ. Following earlier work [88], we here use a Gaussian cutoff,

$$F\left(\vec{q}^{\,2}/\Lambda^2\right) = e^{-\vec{q}^{\,2}/\Lambda^2}. \tag{3.7}$$

We employ the functions [88]

$$I_0(r) = \frac{\Lambda^3}{8\pi\sqrt{\pi}} e^{-(\Lambda r/2)^2}, \tag{3.8}$$

$$\begin{aligned}\phi_{\rm C}^0(mr) &= \frac{e^{m^2/\Lambda^2}}{2mr}\left[e^{-mr}{\rm erfc}\left(-\frac{\Lambda r}{2}+\frac{m}{\Lambda}\right) - e^{mr}{\rm erfc}\left(\frac{\Lambda r}{2}+\frac{m}{\Lambda}\right)\right] \\ &= \phi_{\rm C}^1(mr) + \frac{4\pi}{m^3} I_0(r),\end{aligned} \tag{3.9}$$

$$\begin{aligned}\phi_{\rm T}^{-1}(mr) &= \frac{e^{m^2/\Lambda^2}}{2(mr)^3}\left[\left(1+mr+\frac{1}{3}(mr)^2\right)e^{-mr}{\rm erfc}\left(-\frac{\Lambda r}{2}+\frac{m}{\Lambda}\right)\right. \\ &\qquad \left. -\left(1-mr+\frac{1}{3}(mr)^2\right)e^{mr}{\rm erfc}\left(\frac{\Lambda r}{2}+\frac{m}{\Lambda}\right)\right] \\ &= \phi_{\rm T}^0(mr) + \frac{4\pi}{3m^3}\left(1+\frac{6}{\Lambda^2 r^2}\right) I_0(r),\end{aligned} \tag{3.10}$$

$${\rm erfc}(x) = \frac{2}{\sqrt{\pi}}\int_x^\infty dt\; e^{-t^2}. \tag{3.11}$$

Eliminating through Eq. (3.3) for example g_{PT}, we further define

$$\begin{aligned} t(r) &= 3\Bigg\{\phi^0_{\rm T}(m_\pi r) - \left(\frac{m_{PV}}{m_\pi}\right)^3 \phi^0_{\rm T}(m_{PV} r) \\ &\quad -\frac{g_T^2}{g_A^2}\left[\left(\frac{m_V}{m_\pi}\right)^3 \phi^0_{\rm T}(m_V r) - \left(\frac{m_{PV}}{m_\pi}\right)^3 \phi^0_{\rm T}(m_{PV} r)\right]\Bigg\}, \qquad (3.12) \\ y(r) &= \phi^0_{\rm C}(m_\pi r) - \left(\frac{m_{PV}}{m_\pi}\right)^3 \phi^0_{\rm C}(m_{PV} r) \\ &\quad +2\frac{g_T^2}{g_A^2}\left[\left(\frac{m_V}{m_\pi}\right)^3 \phi^0_{\rm C}(m_V r) - \left(\frac{m_{PV}}{m_\pi}\right)^3 \phi^0_{\rm C}(m_{PV} r)\right] \\ &\quad +3\frac{g_T^2 - g_{PV}^2}{g_A^2}\left(\frac{m_{PV}}{m_\pi}\right)^3 \phi^0_{\rm C}(m_{PV} r), \qquad (3.13) \\ \tilde{y}(r) &= \frac{g_v^2}{g_A^2}\left(\frac{m_v}{m_\pi}\right)^3 \phi^0_{\rm C}(m_v r) - \frac{g_s^2}{g_A^2}\left(\frac{m_s}{m_\pi}\right)^3 \phi^0_{\rm C}(m_s r), \qquad (3.14) \\ \tilde{y}_V(r) &= \frac{g_V^2}{g_A^2}\left(\frac{m_V}{m_\pi}\right)^3 \phi^0_{\rm C}(m_V r), \qquad (3.15) \\ \Delta(r) &= \frac{12\pi}{m_\pi^3} I_0(r). \qquad (3.16) \end{aligned}$$

The potentials in spin-singlet ($S = 0$) channels are:

$$\begin{aligned} V^{(0,0)}(r) &= -\frac{m_\pi^3}{4\pi(2f_\pi)^2}\left\{-3g_A^2 F^{(0,0)}(r) + C_0^{(0)}\Delta(r)\right\}, \qquad (3.17) \\ V^{(0,1)}(r) &= \frac{m_\pi^3}{12\pi(2f_\pi)^2}\left\{-3g_A^2 F^{(0,1)}(r) + C_0^{(0)}\Delta(r)\right\}, \qquad (3.18) \end{aligned}$$

where

$$\begin{aligned} F^{(0,0)}(r) &= y(r) + \frac{\tilde{y}(r)}{3} - \tilde{y}_V(r), \qquad (3.19) \\ F^{(0,1)}(r) &= y(r) - \tilde{y}(r) - \tilde{y}_V(r), \qquad (3.20) \end{aligned}$$

and

$$C_0^{(0)} = C_0^{(V)} - 3\left(C_0^{(T)} - g_T^2\right). \qquad (3.21)$$

The potentials in spin-triplet ($S = 1$) channels of total angular momentum j are:

$$\begin{aligned} V_j^{(1,0)}(r) &= -\frac{m_\pi^3}{4\pi(2f_\pi)^2}\left\{g_A^2 F_j^{(1,0)}(r) + C_0^{(1)}\Delta(r)\right\}, \qquad (3.22) \\ V_j^{(1,1)}(r) &= \frac{m_\pi^3}{12\pi(2f_\pi)^2}\left\{g_A^2 F_j^{(1,1)}(r) + C_0^{(1)}\Delta(r)\right\}, \qquad (3.23) \end{aligned}$$

where

$$F_j^{(1,0)}(r) = y(r) - \tilde{y}(r) + 3\tilde{y}_V(r) + 2 \begin{pmatrix} -\frac{j-1}{2j+1} & 0 & 3\frac{\sqrt{j(j+1)}}{2j+1} \\ 0 & 1 & 0 \\ 3\frac{\sqrt{j(j+1)}}{2j+1} & 0 & -\frac{j+2}{2j+1} \end{pmatrix} t(r), \quad (3.24)$$

$$F_j^{(1,1)}(r) = y(r) + 3\tilde{y}(r) + 3\tilde{y}_V(r) + 2 \begin{pmatrix} -\frac{j-1}{2j+1} & 0 & 3\frac{\sqrt{j(j+1)}}{2j+1} \\ 0 & 1 & 0 \\ 3\frac{\sqrt{j(j+1)}}{2j+1} & 0 & -\frac{j+2}{2j+1} \end{pmatrix} t(r), \quad (3.25)$$

and

$$C_0^{(1)} = C_0^{(V)} + C_0^{(T)} - g_T^2. \quad (3.26)$$

3.5 Limiting Cases

These potentials reduce in certain limits to one-boson-exchange potentials found in the literature. When $\Lambda \to \infty$ the functions $\Delta(r)$ and $\tilde{y}_X(r)$, $X = V, v, s$, become, apart from constants, $\delta^{(3)}(\vec{r})$ and $e^{-m_X r}/r$. When we decouple the isoscalar fields ($g_s = g_v = 0$), the potentials simplify. If we further

(1) decouple the pseudovector field ($g_{PT} = g_{PV} = 0$), then in the $\Lambda \to \infty$ limit $t(r)$ and $y(r)$ become, apart from constants, the functions $K(mr)$ and $J(mr)$ defined in Ref. [81] ($K_S(mr)$ and $J_S(mr)$ defined in Ref. [85]). Equations (3.17), (3.18), (3.22), and (3.23) then reduce to the corresponding equations in the mixed pseudoscalar-vector theory [82, 85] when we make $C_0^{(T)} = g_T^2$ and $C_0^{(V)} = 0$. Note that in this case the magnetic (tensor) coupling of the vector field is fixed at a value $|g_T| = |g_A|$, which is within 10% of the value used for the rho meson in typical one-boson-exchange potentials (*e.g.* [89]). This suggests that the main role of the rho in such potentials is to remove sensitivity to very-short-range physics. A model that gives $|g_T| = |g_A|$ is found in Ref. [90].

(2) decouple the vector field ($g_T = g_V = 0$) instead of the pseudovector, then in the $\Lambda \to \infty$ limit $t(r)$ and $y(r)$ (for $g_{PV} = 0$) become, apart from constants, the functions $\chi(mr)$ and $\phi(mr)$ defined in Ref. [83] ($K_A(mr)$ and $J_A(mr)$ defined in Ref. [85]).

Note that in this case the $\delta^{(3)}(\vec{r})$ disappears [83] and the two-nucleon amplitude is well defined if we take $C_0^{(T)} = C_0^{(V)} = 0$. Equations (3.17), (3.18), (3.22), and (3.23) then reduce to the corresponding equations in the mixed pseudoscalar-pseudovector theory [83, 85].

Note that when $\Lambda \to \infty$ the most singular terms in the potential go as $\delta^{(3)}(\vec{r})$ and $1/r$. The latter is renormalizable by itself, but in the presence of the delta function it requires renormalization of the coefficients of $\delta^{(3)}(\vec{r})$ [27]. Therefore, only when $g_T = 0$ is the potential well defined with $C_0^{(T)} = C_0^{(V)} = 0$. Since the $1/r$ interaction has terms proportional to both m_π^2 and the square of other masses, which presumably are finite in the chiral limit, $C_0^{(0,1)}$ are to be understood as having two pieces, one that is finite and another that vanishes in the chiral limit.

As the cutoff is increased, the contributions from the $\Delta(r)$ terms decrease in waves higher than S, so as usual the waves sensitive to $C_0^{(0)}$ and $C_0^{(1)}$ are ${}^1S_0$ and ${}^3S_1$, respectively. Since the vector and pseudovector exchanges remove the singularity that affects mostly the ${}^3P_{0,2}$ and ${}^3D_2$ waves, one would expect these channels to depend sensitively on g_T^2, m_V, and m_{PV}: as m_V and m_{PV} increase the same aggregation of bound states should appear in these waves as observed in Ref. [9]. Since the previously required higher-wave counterterms had sizes set by $2f_\pi$, one would expect m_V and m_{PV} to be of similar size. In either pseudoscalar-vector or pseudoscalar-pseudovector theories, there is only one parameter (the corresponding auxiliary-field mass) to replace three counterterms. It is not obvious that either of these simplified scenarios would work, suggesting we might need both vector and pseudovector fields.

The vector coupling of the vector field (g_V), the pseudovector coupling of the pseudovector field (g_{PV}), and isoscalar scalar (g_s and m_s) and vector (g_v and m_v) interactions have no obvious renormalization role. Note, however, that vector and pseudovector exchanges (with $g_{PV} = 0$) not only cancel the tensor-force singularity, but also introduce six new independent contributions in $t(r)$ and $y(r)$, with dependencies on $m_V r$ and $m_{PV} r$. This goes beyond the role of the higher-wave counterterms, and could prevent a good description of channels without fitting pa-

rameters. We could therefore use the six parameters g_{PV}, g_s, m_s, g_v, m_v, and g_V to mitigate these extraneous dependencies. With only one vector or one pseudovector field, or even two such fields, this could not be fully achieved. That suggests the need for extra fields, here taken to be isoscalar scalar and vector for simplicity. In this case, the six parameters g_{PV}, g_s, m_s, g_v, m_v, and g_V should be seen as dependent quantities, the number of independent non-pion parameters being five ($C_0^{(T)}$, $C_0^{(V)}$, g_T, m_V, and m_{PV}) just as in the original potential [9].

Could there be a more fundamental argument supporting this potential? It has been argued that the pion, isovector vector and axial-vector and isoscalar scalar fields (π, $\boldsymbol{V}$, $\boldsymbol{A}$, and s) form an algebraic realization of $SU(2) \times SU(2)$ [86], with a relation among their masses in the chiral limit. A model that gives the appropriate relation between the vector and axial-vector ($m_{PV} = \sqrt{2} m_V$) masses can be found in Ref. [91] (but in this model $|g_{PV}| = |g_A|$, $g_{PT} = 0$, and $g_T = 0$ so that Eq. (3.3) is not satisfied.)

Another possibility is the large-N_c limit of QCD. The above potential has all the structures present in this limit [87], where in leading order we can set

$$g_V = 0, \qquad C_0^{(V)} = 0. \tag{3.27}$$

It has been remarked [87] that there is a relation between this limit and Wigner's $SU(4)_W$ symmetry [92]. The even-angular-momentum waves have $I = 1, S = 0$ and $I = 0, S = 0$, and they form the **6** representation, while odd-angular-momentum waves have $I = 0, S = 0$ and $I = 1, S = 1$, and they form the **10** representation. The difference between our $I = 1, S = 0$ and $I = 0, S = 0$ potentials is made of isovector-vector terms and a tensor force. The former vanish in the large-N_c limit (3.27), while the latter is leading in $1/N_c$ but, because of Eq. (3.3), it vanishes as $|\vec{q}|^2 \to \infty$, and at any $|\vec{q}|^2$ if the meson masses are degenerate. The differences between our $I = 0, S = 0$ and $I = 1, S = 1$ potentials have additional contributions from $y(r)$ and $C_0^{(T)}\Delta(r)$ that do not vanish at large N_c either. However, the $C_0^{(T)}\Delta(r)$ contribution vanishes in these channels as $\Lambda \to \infty$, and thus is a renormalization artifact of the leading order. The $y(r)$ term also vanishes as $|\vec{q}|^2 \to \infty$. So for our potential

$SU(4)_W$ is an accidental "short-range" symmetry in the large-N_c limit. (For the suggestion that $SU(4)_W$ should be seen as a "long-range" symmetry, see Ref. [93].) Note that the entire large-N_c potential is $SU(4)_W$ symmetric if $m_\pi = m_V = m_{PV}$ and $g_{PV}^2 = g_T^2 = C_0^{(T)}$.

A possible initial strategy is to start with the simplest theory, taking $g_{PT} = g_{PV} = g_s = g_v = g_V = 0$, fitting $C_0^{(1)}$ and m_V to the low-energy ${}^3S_1$ and ${}^3P_0$ phase shifts, and, with this m_V, fit $C_0^{(0)}$ to the low-energy ${}^1S_0$ phase shifts. One could then calculate other phase shifts and deuteron parameters. If a good description is obtained, maybe a global fit should be attempted.

A promising scenario is the large-N_c theory, where Eq. (3.27) holds. The loss of one delta-function parameter compared to EFT is compensated by the presence of the isoscalar fields. It is not obvious whether the absence of g_V will lead to any fitting problems.

The potentials (3.17), (3.18), (3.22), and (3.23) now need to be included non-perturbatively in the Schrödinger equation, with parameters fitted to scattering data. At low energies, where KSW power counting applies, OPE and the associated auxiliary fields could be treated in perturbation theory. This, in particular, is the case of the shallow deuteron, to which I turn next. Note that here, contrary to KSW, the potential is to be fitted to data at energies where OPE is not necessarily perturbative.

3.6 Deuteron Binding Energy

In this section, we will use the potential in spin-triplet channels $V_j^{(1,0)}(r)$ to construct a Hamiltonian in the ${}^3S_1 - {}^3D_1$ coupled channels, and solve the Schrödinger equation exactly for the short-range piece of the potential. The long-range piece will be treated in perturbation theory in order to find first corrections. In the long-range part of the potential, we include only OPE since in these channels Weinberg's power counting is correct [27] and there is no proliferation of contact interactions.

We are interested, at first, in calculating the binding energy B of the deuteron

for the Hamiltonian in the coupled ${}^3S_1$-${}^3D_1$ channels

$$H = -\frac{\vec{\nabla}^2}{m_N} - \frac{m_\pi^3}{16\pi f_\pi^2}\left[g_A^2 F_1^{(1,0)}(r) + C_0^{(1)}\Delta(r)\right], \tag{3.28}$$

where

$$F_1^{(1,0)}(r) = y(r) - \tilde{y}(r) + 3\tilde{y}_V(r) + 2\begin{pmatrix} 0 & 0 & \sqrt{2} \\ 0 & 1 & 0 \\ \sqrt{2} & 0 & -1 \end{pmatrix} t(r). \tag{3.29}$$

To simplify the notation, we define

$$\alpha \equiv \frac{g_A^2 m_\pi^3 m_N}{16\pi f_\pi^2}, \tag{3.30}$$

$$J(r) \equiv y(r) - \tilde{y}(r) + 3\tilde{y}_V(r), \tag{3.31}$$

$$K(r) \equiv 2t(r), \tag{3.32}$$

$$\frac{\alpha}{g_A^2} C_0^{(1)}\Delta(r) \equiv \tilde{C}_0(\Lambda) I_0(r,\Lambda), \tag{3.33}$$

$$M(\hat{r}) \equiv \begin{pmatrix} 0 & 0 & \sqrt{2} \\ 0 & 1 & 0 \\ \sqrt{2} & 0 & -1 \end{pmatrix}. \tag{3.34}$$

Then, the (dimensionless) long-range potential, which includes one-pion exchange, is defined by

$$X(\vec{r}) \equiv J(r) + K(r)M(\hat{r}). \tag{3.35}$$

With the new variables, the Hamiltonian is

$$H = -\frac{\vec{\nabla}^2}{m_N} - \frac{1}{m_N}\left[\alpha X(\vec{r}) + \tilde{C}_0(\Lambda) I_0(r,\Lambda)\right]. \tag{3.36}$$

Note that the short-range potential with a strength $\tilde{C}_0(\Lambda)/m_N$ is a delta function regulated by a cutoff Λ, given by Eq. (3.8), which can be written as

$$I_0(r,\Lambda) = \int \frac{d^3q}{(2\pi)^3} e^{i\vec{q}\cdot\vec{r}} F(\vec{q}^{\,2}/\Lambda^2). \tag{3.37}$$

Since the cutoff function $F(x)$ satisfies $F(x \ll 1) = 1 + \mathcal{O}(x)$, then

$$\lim_{\Lambda\to\infty} I_0(r,\Lambda) = \int \frac{d^3q}{(2\pi)^3} e^{i\vec{q}\cdot\vec{r}} = \delta^{(3)}(\vec{r}). \tag{3.38}$$

However, we demand $\lim_{x\to\infty} F(x) = 0$ in order to dampen modes with momentum $|\vec{q}| \gg \Lambda$. Low-energy observables should be independent of the form of $F(x)$ and of the value of Λ. Specific examples will be considered below.

We present a solution where the long-range potential is treated in perturbation theory.

3.7 Perturbative Solution

The deuteron corresponds to a pole at a positive imaginary momentum of magnitude $\kappa \sim 45$ MeV. Since this is small compared to the mass of the pion $m_\pi \simeq 140$ MeV, one expects the long-range potential to be weak. Indeed, one can describe [94] the deuteron and its low-energy reactions in an EFT where all meson fields are integrated out. In this section we treat the long-range potential in perturbation theory, which, as we are going to see, is an expansion in κ^2/m_π^2.

We want to calculate the deuteron binding energy in an expansion

$$B = B^{(0)} + B^{(1)} + \ldots = \frac{\kappa^{(0)2}}{m_N} + \frac{\kappa^{(1)2}}{m_N} + \ldots \tag{3.39}$$

The idea is to first isolate in the dominant short-range interaction a piece for which an exact solution of the Lippmann-Schwinger or the Schrödinger equations gives a good first approximation to the deuteron binding energy. This can be done provided its parameter is suitably renormalized [95]. The contributions from both the remaining parts of the short-range interaction and the long-range interactions will be suppressed by powers of κ^2/m_π^2, and thus are treated in conventional perturbation theory. First corrections of $\mathcal{O}(\kappa^2/m_\pi^2)$ come from the long-range potential treated in first order. This, however, will introduce arbitrary dependence on the cutoff, unless another piece of the short-range interaction is included at this order. Second corrections come from the long-range potential in second-order perturbation theory, together with the appropriate piece of the short-range interaction, and so on. Here we present explicit results up to first order.

We write the short-range parameter as

$$\tilde{C}_0(\Lambda) \;=\; \tilde{C}_0^{(0)}(\Lambda) + \tilde{C}_0^{(1)}(\Lambda) + \ldots \tag{3.40}$$

where $\tilde{C}_0^{(i)}$ is the piece that appears in i-th order in perturbation theory. The Hamiltonian is

$$H = H^{(0)} + H^{(1)} + \ldots, \tag{3.41}$$

where the leading Hamiltonian is written as

$$H^{(0)} = -\frac{1}{m_N}\left[\vec{\nabla}^2 + \tilde{C}_0^{(0)} I_0(r)\right], \tag{3.42}$$

and the sub-leading Hamiltonian,

$$H^{(1)} = -\frac{1}{m_N}\left[\alpha X(\vec{r}) + \tilde{C}_0^{(1)} I_0(r)\right]. \tag{3.43}$$

Decomposing the wavefunction in a similar way,

$$\psi(\vec{r}) = \psi^{(0)}(\vec{r}) + \psi^{(1)}(\vec{r}) + \ldots \tag{3.44}$$

with

$$\int d^3r \left|\psi^{(0)}(\vec{r})\right|^2 = 1, \tag{3.45}$$

the zeroth-order binding energy comes from the Schrödinger equation,

$$H^{(0)}\psi^{(0)}(\vec{r}) = -B^{(0)}\psi^{(0)}(\vec{r}), \tag{3.46}$$

the first-order correction from

$$B^{(1)} = -\int d^3r\ \psi^{(0)*}(\vec{r})\ H^{(1)}\ \psi^{(0)}(\vec{r}), \tag{3.47}$$

and so on.

It is convenient to solve Eq. (3.46) in momentum space, where we introduce the Fourier-transformed wavefunction $\tilde{\psi}^{(0)}(\vec{q})$:

$$\psi^{(0)}(\vec{r}) = \int \frac{d^3q}{(2\pi)^3} e^{i\vec{q}\cdot\vec{r}} F(\vec{q}^2/\Lambda^2)\ \tilde{\psi}^{(0)}(\vec{q}). \tag{3.48}$$

Substituting this into Eq. (3.46), we find

$$\tilde{\psi}^{(0)}(\vec{q}) = \tilde{C}_0^{(0)} \frac{\psi^{(0)}(0)}{\vec{q}^2 + \kappa^{(0)2}}. \tag{3.49}$$

Going back to coordinate space,

$$\psi^{(0)}(\vec{r}) = \tilde{C}_0^{(0)}(\Lambda)\ \psi^{(0)}(0)\ I_1(r, \kappa^{(0)}, \Lambda), \tag{3.50}$$

where

$$I_1(r, \kappa^{(0)}, \Lambda) = \int \frac{d^3q}{(2\pi)^3} e^{i\vec{q}\cdot\vec{r}} \frac{F(\vec{q}^2/\Lambda^2)}{\vec{q}^2 + \kappa^{(0)2}}. \tag{3.51}$$

Consistency of Eq. (3.50) requires that the coupling constant be given as function of the cutoff as

$$\tilde{C}_0^{(0)}(\Lambda) = \lim_{r\to 0} \frac{1}{I_1(r, \kappa^{(0)}, \Lambda)}. \tag{3.52}$$

Finally, $\psi^{(0)}(0)$ can be determined from the normalization condition (3.45):

$$\left|\psi^{(0)}(0)\right|^2 = \left[\tilde{C}_0^{(0)}(\Lambda)\right]^{-2} I_2^{-1}(\kappa^{(0)}, \Lambda), \tag{3.53}$$

where

$$I_2(\kappa^{(0)}, \Lambda) \;=\; \int d^3r \left|I_1(r, \kappa^{(0)}, \Lambda)\right|^2 = \int \frac{d^3q}{(2\pi)^3} \left[\frac{F(\vec{q}^2/\Lambda^2)}{\vec{q}^2 + \kappa^{(0)2}}\right]^2. \tag{3.54}$$

We can project the wavefunction in the ${}^3S_1$ and ${}^3D_1$ partial waves,

$$\psi^{(0)}(\vec{r}) \;=\; \psi_0^{(0)}(r) Y_{00}(\theta, \phi) + \psi_{2\mathrm{m}}^{(0)}(r) Y_{2\mathrm{m}}(\theta, \phi). \tag{3.55}$$

Here the ${}^3S_1$ component is

$$\psi_0^{(0)}(r) = \int d\Omega\ Y_{00}^*(\theta, \phi)\ \psi^{(0)}(\vec{r}) = \sqrt{4\pi}\ \tilde{C}_0^{(0)}(\Lambda)\ \psi^{(0)}(0)\ I_1(r, \kappa^{(0)}, \Lambda), \tag{3.56}$$

and the ${}^3D_1$ component,

$$\psi_{2\mathrm{m}}^{(0)}(r) = \int d\Omega\ Y_{2m}^*(\theta, \phi)\ \psi^{(0)}(\vec{r}) = 0, \tag{3.57}$$

since the wavefunction (3.50) is a function of r only.

Note that the one physical scale that appears above is $\kappa^{(0)}$. Thus, as we take the cutoff to be large, $\Lambda \gg \kappa^{(0)}$, the largest piece of a convergent integral will come

from $F \to 1$, while corrections will be suppressed by powers of $\kappa^{(0)}/\Lambda$. In the limit of large cutoff, Eqs. (3.51) and (3.54) become

$$\begin{aligned} I_1(r \neq 0, \kappa^{(0)}, \Lambda \gg \kappa^{(0)}) &= \int \frac{d^3q}{(2\pi)^3} \frac{e^{i\vec{q}\cdot\vec{r}}}{\vec{q}^2 + \kappa^{(0)2}} F(\vec{q}^2/\Lambda^2) \\ &= \frac{e^{-\kappa^{(0)}r}}{4\pi r}\left[1 + \mathcal{O}\left(\frac{\kappa^{(0)}}{\Lambda}\right)\right], \qquad (3.58) \\ I_2(\kappa^{(0)}, \Lambda \gg \kappa^{(0)}) &= \int \frac{d^3q}{(2\pi)^3} \left[\frac{F(\vec{q}^2/\Lambda^2)}{\vec{q}^2 + \kappa^{(0)2}}\right]^2 \\ &= \frac{1}{8\pi\kappa^{(0)}}\left[1 + \mathcal{O}\left(\frac{\kappa^{(0)}}{\Lambda}\right)\right], \qquad (3.59) \end{aligned}$$

while Eq. (3.51), for $r = 0$, becomes

$$\begin{aligned} I_1(r = 0, \kappa^{(0)}, \Lambda \gg \kappa^{(0)}) &= \int \frac{d^3q}{(2\pi)^3} \frac{1}{\vec{q}^2 + \kappa^{(0)2}} F(\vec{q}^2/\Lambda^2) \\ &= \frac{\Lambda a}{2\pi^2}\left[1 - \frac{\kappa^{(0)}}{\Lambda}\frac{\pi}{2a} + \mathcal{O}\left(\frac{\kappa^{(0)2}}{\Lambda^2}\right)\right], \qquad (3.60) \end{aligned}$$

where a is a constant that depends on the choice of the cutoff. As we will see later, $a = 1$ and $a = \sqrt{\pi}/2$ for the sharp-cutoff and for the Gaussian-cutoff functions, respectively.

From Eqs. (3.58) and (3.59), Eq. (3.50) for the wavefunction, with the normalization given by Eq. (3.53), is

$$\psi^{(0)}(\vec{r}) = \sqrt{\frac{\kappa^{(0)}}{2\pi}}\frac{e^{-\kappa^{(0)}r}}{r}\left[1 + \mathcal{O}\left(\frac{\kappa^{(0)}}{\Lambda}\right)\right], \qquad (3.61)$$

matching the wavefunction found in Ref. [95], and whose projection on the ${}^3S_1$ wave from Eq. (3.56) is

$$\psi_0^{(0)}(r) = \sqrt{2\kappa^{(0)}}\frac{e^{-\kappa^{(0)}r}}{r}\left[1 + \mathcal{O}\left(\frac{\kappa^{(0)}}{\Lambda}\right)\right]. \qquad (3.62)$$

The coupling constant, given by Eq. (3.52), can be found, in the limit of large cutoff, through Eq. (3.60):

$$\tilde{C}_0^{(0)}(\Lambda \gg \kappa^{(0)}) = \frac{2\pi^2}{\Lambda a}\left[1 + \frac{\kappa^{(0)}}{\Lambda}\frac{\pi}{2a} + \mathcal{O}\left(\frac{\kappa^{(0)2}}{\Lambda^2}\right)\right], \qquad (3.63)$$

while its inversion leads in the limit of large cutoff to the deuteron binding momentum

$$\kappa^{(0)} = \frac{2\Lambda a}{\pi}\left[\frac{\Lambda\tilde{C}_0^{(0)}(\Lambda)a}{2\pi^2}-1\right]+\mathcal{O}\left(\Lambda^2\tilde{C}_0^{(0)2}(\Lambda)\right), \tag{3.64}$$

and to the deuteron binding energy

$$B^{(0)} = \frac{4\Lambda^2 a^2}{\pi^2 m_N}\left[\frac{\Lambda\tilde{C}_0^{(0)}(\Lambda)a}{2\pi^2}-1\right]^2+\mathcal{O}\left(\Lambda^2\tilde{C}_0^{(0)2}(\Lambda)\right). \tag{3.65}$$

The next step is to calculate the first-order correction to the deuteron binding energy, Eq. (3.47), stemming from the subleading-order Hamiltonian, Eq. (3.43). The first-order correction in the coupling constant, $\tilde{C}_0^{(1)}$, is related to $B^{(1)}$ via $\kappa^{(1)}$:

$$\tilde{C}_0^{(1)}(\Lambda)=\frac{\kappa^{(1)2}-\alpha I_3(\kappa^{(0)},\Lambda)}{I_4(\kappa^{(0)},\Lambda)}, \tag{3.66}$$

where

$$\begin{aligned} I_3(\kappa^{(0)},\Lambda) &= \int_0^\infty dr r^2\left\{J(r)\left[\left|\psi_0^{(0)}(r)\right|^2+\left|\psi_{2m}^{(0)}(r)\right|^2\right]\right. \\ &\quad +K(r)\left[\sqrt{2}\psi_0^{(0)*}(r)\psi_{2m}^{(0)}(r)+\sqrt{2}\psi_{2m}^{(0)*}(r)\psi_0^{(0)}(r)\right. \\ &\quad \left.\left.-\left|\psi_{2m}^{(0)}(r)\right|^2\right]\right\} \\ &= 4\pi I_2^{-1}(\kappa^{(0)},\Lambda)\int_0^\infty dr r^2 J(r) I_1^2(r,\kappa^{(0)},\Lambda) \end{aligned} \tag{3.67}$$

and

$$\begin{aligned} I_4(\kappa^{(0)},\Lambda) &= \int_0^\infty dr r^2 I_0(r)\left(\left|\psi_0^{(0)}(r)\right|^2+\left|\psi_{2m}^{(0)}(r)\right|^2\right) \\ &= 4\pi I_2^{-1}(\kappa^{(0)},\Lambda)\int_0^\infty dr r^2 I_0(r) I_1^2(r,\kappa^{(0)},\Lambda). \end{aligned} \tag{3.68}$$

In the limit of large cutoff, Eqs. (3.67) and (3.68) are

$$I_3(\kappa^{(0)},\Lambda) = 2\kappa^{(0)}\int_0^\infty dr J(r) e^{-2\kappa^{(0)}r}\left[1+\mathcal{O}\left(\frac{\kappa^{(0)}}{\Lambda}\right)\right], \tag{3.69}$$

and

$$\begin{aligned} I_4(\kappa^{(0)},\Lambda) &= \int d^3r\left|\psi^{(0)}(\vec{r})\right|^2=\left[\tilde{C}_0^{(0)}(\Lambda)\right]^{-2} I_2^{-1}(\kappa^{(0)},\Lambda) \\ &= \frac{2\kappa^{(0)}\Lambda^2}{\pi}\left[1+\mathcal{O}\left(\frac{\kappa^{(0)}}{\Lambda}\right)\right]. \end{aligned} \tag{3.70}$$

The final result does not have any dependence on the tensor force term, $K(r)$, which is expected since the tensor force takes a ${}^3S_1$ state into a ${}^3D_1$ state, absent at leading order.

Parameters of both the long-range and short-range potentials are fitted to nucleon-nucleon scattering data (or to phase shifts extracted from data) for various values of the cutoff with a given cutoff function. In particular, $\tilde{C}_0(\Lambda)$ can be obtained this way. For this cutoff function, the integrals I_i can be calculated. The zeroth-order approximation to the binding energy, $B^{(0)}$, is extracted by fitting $\tilde{C}_0(\Lambda)$ with $\tilde{C}_0^{(0)}(\Lambda)$ given in Eq. (3.52). In first-order, we fit $\tilde{C}_0(\Lambda) - \tilde{C}_0^{(0)}(\Lambda)$ with the $\tilde{C}_0^{(1)}(\Lambda)$ given in Eq. (3.66), thus extracting $B^{(1)}$. The procedure can be repeated at arbitrary order, yielding the deuteron binding energy through Eq. (3.39).

We now turn to specific choices for the cutoff function F.

3.7.1 Sharp cutoff

We now specialize for a particular choice of the cutoff function,

$$F(\vec{q}^2/\Lambda^2) = \theta(1 - \vec{q}^2/\Lambda^2), \tag{3.71}$$

in which case the short-range potential, Eq. (3.37), becomes

$$\begin{aligned} I_0(r,\Lambda) &= \int \frac{d^3q}{(2\pi)^3} e^{i\vec{q}\cdot\vec{r}} \theta\left(1 - \vec{q}^2/\Lambda^2\right) \\ &= \frac{1}{2\pi^2 r^3}\left(\sin\Lambda r - \Lambda r \cos\Lambda r\right). \end{aligned} \tag{3.72}$$

This regularization of the delta function generates wiggles that complicate numerical calculations in coordinate space. However, some of the formulas become particularly simple.

In this case, from Eq. (3.51) and the sharp cutoff function, Eq. (3.71), we obtain

$$\begin{aligned} I_1(r\neq 0,\kappa^{(0)},\Lambda) &= \int \frac{d^3q}{(2\pi)^3}\frac{e^{i\vec{q}\cdot\vec{r}}\theta\left(1-\vec{q}^{\,2}/\Lambda^2\right)}{\vec{q}^{\,2}+\kappa^{(0)2}} \\ &= \frac{1}{4\pi^2 r}\left\{\cosh(\kappa^{(0)}r)\left[\mathrm{Si}\left(r\Lambda\left(1-i\frac{\kappa^{(0)}}{\Lambda}\right)\right)\right.\right. \\ &\qquad \left.+\mathrm{Si}\left(r\Lambda\left(1+i\frac{\kappa^{(0)}}{\Lambda}\right)\right)\right] \\ &\quad -\sinh(\kappa^{(0)}r)\left[-i\mathrm{Ci}\left(r\Lambda\left(1-i\frac{\kappa^{(0)}}{\Lambda}\right)\right)+\pi\right. \\ &\qquad \left.\left.+i\mathrm{Ci}\left(r\Lambda\left(1+i\frac{\kappa^{(0)}}{\Lambda}\right)\right)\right]\right\}, \end{aligned} \tag{3.73}$$

where $Si[z]$ and $Ci[z]$ stand for sinintegral of z and cosintegral of z,

$$\mathrm{Si}[z] = \int_0^z dt\frac{\sin(t)}{t}, \qquad \mathrm{Ci}[z]=\int_z^\infty dt\frac{\cos(t)}{t}, \tag{3.74}$$

with

$$\mathrm{Si}(\infty)=\frac{\pi}{2}, \qquad \mathrm{Ci}(\infty)=0. \tag{3.75}$$

To find the equation for the deuteron binding energy, using the sharp cutoff function, one needs Eq. (3.51) for $r=0$,

$$I_1(0,\kappa^{(0)},\Lambda)=\int\frac{d^3q}{(2\pi)^3}\frac{\theta\left(1-\vec{q}^{\,2}/\Lambda^2\right)}{\vec{q}^{\,2}+\kappa^{(0)2}}=\frac{\Lambda}{2\pi^2}\left[1-\frac{\kappa^{(0)}}{\Lambda}\tan^{-1}\left(\frac{\Lambda}{\kappa^{(0)}}\right)\right], \tag{3.76}$$

which can be matched to Eq. (3.60) to find $a=1$, and leads, from Eq. (3.52), to the coupling constant

$$\tilde{C}_0^{(0)}(\Lambda) = \frac{1}{I_1(0,\kappa^{(0)},\Lambda)}=\frac{2\pi^2}{\Lambda}\left[1-\frac{\kappa^{(0)}}{\Lambda}\tan^{-1}\left(\frac{\Lambda}{\kappa^{(0)}}\right)\right]^{-1}. \tag{3.77}$$

Equation (3.77) cannot be solved in an algebraic way. One possibility is to solve the equation for $\Lambda\gg\kappa^{(0)}$, which is reduced exactly to Eq. (3.64). The other possibility is to use renormalization-group invariance, i. e. that observables are independent of the Λ. The LO deuteron binding momentum, $\kappa^{(0)}$, can be obtained by applying the derivative with respect to Λ on of both sides of Eq. (3.77), and then setting

$$\frac{d\kappa^{(0)}}{d\Lambda}=0. \tag{3.78}$$

From Eqs. (3.77) and (3.78), the LO deuteron binding momentum is

$$\kappa^{(0)} = \Lambda \left[-1 - \frac{\tilde{C}_0^{(0)2}(\Lambda)}{2\pi^2} \left(\frac{d\tilde{C}_0^{(0)}(\Lambda)}{d\Lambda} \right)^{-1} \right]^{1/2} , \tag{3.79}$$

which leads to the leading-order binding energy of the deuteron,

$$B^{(0)} = \frac{\Lambda^2}{m_N} \left[-1 - \frac{\tilde{C}_0^{(0)\ 2}(\Lambda)}{2\pi^2} \left(\frac{d\tilde{C}_0^{(0)}(\Lambda)}{d\Lambda} \right)^{-1} \right] . \tag{3.80}$$

From the reduction of Eq. (3.54), in the sharp-cutoff limit, to

$$I_2(\kappa^{(0)}, \Lambda) \ = \ = \frac{1}{4\pi^2 \kappa^{(0)}} \left[\tan^{-1}\left(\frac{\Lambda}{\kappa^{(0)}} \right) - \frac{\kappa^{(0)}}{\Lambda} \left(1 + \frac{\kappa^{(0)2}}{\Lambda^2} \right)^{-1} \right] \tag{3.81}$$

the wavefunction, given by Eq. (3.50), becomes

$$\begin{aligned} \psi^{(0)}(\vec{r}) \ = \ & \frac{1}{2\pi r} \left[\tan^{-1}\left(\frac{\Lambda}{\kappa^{(0)}} \right) - \frac{\kappa^{(0)}}{\Lambda} \left(1 + \frac{\kappa^{(0)2}}{\Lambda^2} \right)^{-1} \right]^{-1} \times \\ & \left\{ \cosh(\kappa^{(0)} r) \left[\mathrm{Si}\left(r\Lambda \left(1 - i\frac{\kappa^{(0)}}{\Lambda} \right) \right) + \mathrm{Si}\left(r\Lambda \left(1 + i\frac{\kappa^{(0)}}{\Lambda} \right) \right) \right] \right. \\ & - \sinh(\kappa^{(0)} r) \left[-i\mathrm{Ci}\left(r\Lambda \left(1 - i\frac{\kappa^{(0)}}{\Lambda} \right) \right) + i\mathrm{Ci}\left(r\Lambda \left(1 + i\frac{\kappa^{(0)}}{\Lambda} \right) \right) \right. \\ & \left. \left. + \pi \right] \right\} . \end{aligned} \tag{3.82}$$

The first-order correction of the binding energy of deuteron is given by Eq. (3.66), with

$$\begin{aligned} I_3(\kappa^{(0)}, \Lambda) \ = \ & \frac{\kappa^{(0)}}{8\pi^4} \int_0^\infty dr J(r) \left\{ \cosh(\kappa^{(0)} r) \left[\mathrm{Si}\left(r\Lambda \left(1 - i\frac{\kappa^{(0)}}{\Lambda} \right) \right) \right. \right. \\ & \left. + \mathrm{Si}\left(r\Lambda \left(1 + i\frac{\kappa^{(0)}}{\Lambda} \right) \right) \right] \\ & - \sinh(\kappa^{(0)} r) \left[-i\mathrm{Ci}\left(r\Lambda \left(1 - i\frac{\kappa^{(0)}}{\Lambda} \right) \right) + \pi \right. \\ & \left. \left. \left. + i\mathrm{Ci}\left(r\Lambda \left(1 + i\frac{\kappa^{(0)}}{\Lambda} \right) \right) \right] \right\}^2 \end{aligned} \tag{3.83}$$

and

$$I_4(\kappa^{(0)},\Lambda) = \frac{\kappa^{(0)}}{8\pi^4}\int_0^\infty dr I_0(r)\left\{\cosh(\kappa^{(0)}r)\left[\mathrm{Si}\left(r\Lambda\left(1-i\frac{\kappa^{(0)}}{\Lambda}\right)\right)\right.\right.$$
$$\left.+\mathrm{Si}\left(r\Lambda\left(1+i\frac{\kappa^{(0)}}{\Lambda}\right)\right)\right]$$
$$-\sinh(\kappa^{(0)}r)\left[-i\mathrm{Ci}\left(r\Lambda\left(1-i\frac{\kappa^{(0)}}{\Lambda}\right)\right)+\pi\right.$$
$$\left.\left.+i\mathrm{Ci}\left(r\Lambda\left(1+i\frac{\kappa^{(0)}}{\Lambda}\right)\right)\right]\right\}^2. \quad (3.84)$$

To extract the first-order approximation to the binding energy, $B^{(1)}$, we can fit $\tilde{C}_0(\Lambda)-\tilde{C}_0^{(0)}(\Lambda)$ with the function $\tilde{C}_0^{(1)}(\Lambda)$, given by Eq. (3.66), where the integrals $I_3(\kappa^{(0)},\Lambda)$ and $I_4(\kappa^{(0)},\Lambda)$ are, now, given by Eqs. (3.83) and (3.84), respectively, for the sharp-cutoff function.

When the cutoff is much larger than leading-order binding momentum of the deuteron, $\Lambda \gg \kappa^{(0)}$, the expressions $I_1(r\neq 0,\kappa^{(0)},\Lambda)$, $I_1(r=0,\kappa^{(0)},\Lambda)$, $I_2(\kappa^{(0)},\Lambda)$, $\tilde{C}_0^{(0)}(\Lambda)$, $\psi^{(0)}(\vec{r})$, $I_3(\kappa^{(0)},\Lambda)$ and $I_4(\kappa^{(0)},\Lambda)$, presented in Eqs (3.73), (3.76), (3.81), (3.77), (3.82), (3.83) and (3.84), respectively, reduce to Eqs. (3.58), (3.60), (3.59), (3.63), (3.61), (3.67), and (3.70), respectively. Next, a new cutoff function will be used to solve for the deuteron binding energy and wavefunction.

3.7.2 Gaussian cutoff

Here we consider a second example of regulator function,

$$F(\vec{q}^{\,2}/\Lambda^2) = e^{-\vec{q}^{\,2}/\Lambda^2}, \quad (3.85)$$

which is well-suited for numerical calculations in coordinate space. Using this regulator, the short-range potential, Eq. (3.37), is a Gaussian,

$$I_0(r,\Lambda) = \int \frac{d^3q}{(2\pi)^3} e^{i\vec{q}\cdot\vec{r}} e^{-\vec{q}^{\,2}/\Lambda^2} = \frac{\Lambda^3}{8\pi\sqrt{\pi}} e^{-\left(\frac{\Lambda r}{2}\right)^2}. \quad (3.86)$$

For this specific regulator, Eq. (3.51), for $r \neq 0$ and $r = 0$, become

$$\begin{aligned} I_1(r,\kappa^{(0)},\Lambda) &= \int \frac{d^3q}{(2\pi)^3} e^{i\vec{q}\cdot\vec{r}} \frac{e^{-\vec{q}^{\,2}/\Lambda^2}}{\vec{q}^{\,2}+\kappa^{(0)2}} \\ &= \frac{e^{\kappa^{(0)2}/\Lambda^2}}{8\pi r}\left[e^{-\kappa^{(0)}r}\mathrm{erfc}\left(-\frac{\Lambda r}{2}+\frac{\kappa^{(0)}}{\Lambda}\right) - e^{\kappa^{(0)}r}\mathrm{erfc}\left(\frac{\Lambda r}{2}+\frac{\kappa^{(0)}}{\Lambda}\right)\right] \\ &\equiv \frac{\kappa^{(0)}}{4\pi}\phi_C^0(\kappa^{(0)}r), \end{aligned} \tag{3.87}$$

and

$$I_1(r=0,\kappa^{(0)},\Lambda) = \frac{\Lambda}{4\pi\sqrt{\pi}}\left[1-\sqrt{\pi}\frac{\kappa^{(0)}}{\Lambda}e^{\kappa^{(0)2}/\Lambda^2}\mathrm{erfc}\left(\frac{\kappa^{(0)}}{\Lambda}\right)\right], \tag{3.88}$$

respectively. In the limit of large cutoff, we obtain Eq. (3.60) with $a = \sqrt{\pi}/2$. The leading-order coupling constant necessary to obtain the deuteron binding energy is constructed from Eqs. (3.52) and (3.87),

$$\tilde{C}^{(0)}(\Lambda) = \frac{4\pi\sqrt{\pi}}{\Lambda}\left[1-\sqrt{\pi}\frac{\kappa^{(0)}}{\Lambda}e^{\kappa^{(0)2}/\Lambda^2}\mathrm{erfc}\left(\frac{\kappa^{(0)}}{\Lambda}\right)\right]^{-1}. \tag{3.89}$$

In order to obtain the normalized wavefunction, one needs to solve Eq.(3.54) for this cutoff function,

$$\begin{aligned} I_2(r,\kappa^{(0)},\Lambda) = \frac{1}{16\pi}e^{2\kappa^{(0)2}/\Lambda^2}\int_0^\infty dr\left[e^{-\kappa^{(0)}r}\mathrm{erfc}\left(-\frac{\Lambda r}{2}+\frac{\kappa^{(0)}}{\Lambda}\right)\right. \\ \left. -e^{\kappa^{(0)}r}\mathrm{erfc}\left(\frac{\Lambda r}{2}+\frac{\kappa^{(0)}}{\Lambda}\right)\right]^2, \end{aligned} \tag{3.90}$$

which can be solved numerically, and, together with Eqs. (3.50) and (3.87), leads to

$$\begin{aligned} \psi^{(0)}(\vec{r}) = \frac{I_2^{-1/2}}{8\pi r}e^{\kappa^{(0)2}/\Lambda^2}\left[e^{-\kappa^{(0)}r}\mathrm{erfc}\left(-\frac{\Lambda r}{2}+\frac{\kappa^{(0)}}{\Lambda}\right)\right. \\ \left. -e^{\kappa^{(0)}r}\mathrm{erfc}\left(\frac{\Lambda r}{2}+\frac{\kappa^{(0)}}{\Lambda}\right)\right]. \end{aligned} \tag{3.91}$$

Again, the first-order correction of the binding energy of the deuteron is given by Eqs. (3.66), with

$$\begin{aligned} I_3(\kappa^{(0)},\Lambda) = \frac{I_2^{-1}}{16\pi}e^{\kappa^{(0)2}/\Lambda^2}\int_0^\infty dr J(r)\left[e^{-\kappa^{(0)}r}\mathrm{erfc}\left(-\frac{\Lambda r}{2}+\frac{\kappa^{(0)}}{\Lambda}\right)\right. \\ \left. -e^{\kappa^{(0)}r}\mathrm{erfc}\left(\frac{\Lambda r}{2}+\frac{\kappa^{(0)}}{\Lambda}\right)\right]^2 \end{aligned} \tag{3.92}$$

and

$$I_4(\kappa^{(0)},\Lambda) = \frac{I_2^{-1}}{16\pi}e^{\kappa^{(0)2}/\Lambda^2}\int_0^\infty dr I_0(r)\left[e^{-\kappa^{(0)}r}\mathrm{erfc}\left(-\frac{\Lambda r}{2}+\frac{\kappa^{(0)}}{\Lambda}\right)\right. \\ \left. -e^{\kappa^{(0)}r}\mathrm{erfc}\left(\frac{\Lambda r}{2}+\frac{\kappa^{(0)}}{\Lambda}\right)\right]^2, \quad (3.93)$$

both of which are to be computed numerically.

In the limit of large cutoff, $\Lambda \gg \kappa^{(0)}$, Eqs. (3.87), (3.88), and (3.89) is reduced to Eqs. (3.58), (3.51), and (3.63), respectively. Again, to solve the deuteron binding energy up to first correction, it is necessary to fit $\tilde{C}_0^{(1)}$ to experimental data.

3.8 Conclusions and Outlook

To construct the nucleon-nucleon potential in leading order we used a non-relativistic reduction of a Lagrangian that contains the relevant interactions among nucleons, isovector pseudoscalar fields, auxiliary isovector vectors and pseudovectors and auxiliary isoscalar scalars and vectors. Such Lagrangian contains sufficient terms to produce the leading-order potential in the limit of large N_c. The nucleon kinetic term is a subleading term in the $N_c \to \infty$ limit because of its smallness compared to the potential, nonetheless it is kept in the Lagrangian to regulate the infrared limit of loop integrals. Additionally, even though other fermions are degenerate with nucleons in the $N_c \to \infty$ limit, we entrust the delta isobar to higher-order loops, where the mass splitting between the delta and nucleon is of the order of the mass of the pion, and other fermions were integrated out for being heavier than the nucleon, as seen in the spectrum. From the leading-order two-nucleon potentials for various combinations of spin and isospin, we identified the most singular terms and imposed a combination among the coupling constants that, when substituted in the potential, cancels the singularity corresponding to $1/r^3$ in coordinate space. We, then, Fourier transformed the potential from momentum to coordinate space, since the latter is oftentimes used to calculate observables. To separate low- from high-energy physics at a cutoff momenta Λ, we regulate the integral with a gaussian cutoff function $e^{-\vec{q}^2/\Lambda^2}$, with $\vec{q}$ being the momentum transferred.

To check our potentials against the ones presented in literature, we considered the large-cutoff limit and the decoupling of the pseudovector or vector fields. Moreover, we analyzed the potentials for certain values of coupling constants and masses to find that the short-range coupling constants $C_0^{(0,1)}$ have a finite term and a term that vanishes in the chiral limit. Further, we expected that both isovector vector and isovector pseudovector fields are needed to replace the counterterms found in literature. The validity of our potential was discussed in an algebraic realization of chiral symmetry and in the large-N_c limit of QCD contexts.

With the spin-triplet NN potential corresponding to the ${}^3S_1 - {}^3D_1$ coupled channels, we constructed a Hamiltonian that describes the deuteron features. We presented an exact solution of the Schrödinger equation for the dominant short-range interaction. Since the deuteron binding momentum, corresponding to a pole at positive imaginary momentum, is small compared to the pion mass, the long-range as well as the remaining short-range interactions are treated in perturbation theory. The solution of the Schrödinger equation involves a cutoff function that satisfies delta-like conditions. In particular, two types of cutoff function were used, a sharp and a Gaussian cutoffs, to obtain the leading-order coupling constant of the short-range interaction, the LO deuteron binding energy, and their first corrections.

Unfortunately, there are no conclusive results, since this work needs to be complemented by a numerical solution of the Schrödinger equation in an energy region where OPE is not perturbative. The next step consists in fitting $C_0^{(1)}$ and m_V parameters to the low-energy experimental data, such as ${}^3S_1$ and ${}^3P_0$ phase shifts, and fitting $C_0^{(0)}$ to the low-energy ${}^1S_0$ phase shift. From these parameters, it is possible to determine higher-channels phase shifts. The parameter $\tilde{C}_0$ can be then constructed from $C_0^{(0)}$ and $C_0^{(1)}$ and the zeroth-order binding energy of the deuteron can be found by fitting $\tilde{C}_0^{(0)}$ to $\tilde{C}_0$. The first-order correction to the deuteron binding energy $B^{(1)}$ can be extracted from the fit $\tilde{C}_0^{(1)}$ to $\tilde{C}_0 - \tilde{C}_0^{(0)}$. This can be done order by order to the desired accuracy.

CHAPTER 4

EXCLUSIVE DECAYS OF χ_{bJ} AND η_b INTO TWO CHARMED MESONS

4.1 Introduction

The exclusive two-body decays of heavy quarkonium into light hadrons have been studied in the framework of perturbative QCD by many authors (for reviews, see [96, 97]). These processes exhibit a large hierarchy between the heavy quark mass, which sets the scale for annihilation processes, and the scales that determine the dynamical structure of the particles in the initial and final states. The large energy released in the annihilation of the heavy quark-antiquark pair and the kinematics of the decay — with the products flying away from the decay point in two back-to-back, almost light-like directions— allow for rigorously deriving a factorization formula for the decay rate at leading twist (for an up-to-date review of the theoretical and experimental status of the exclusive decays into light hadrons, see [98]).

For the bottomonium system, a particularly interesting class of two-body final states is the ones containing two charmed mesons. In these cases the picture is complicated by the appearance of an additional intermediate scale, the charm mass m_c, which is much smaller than the bottom mass m_b but is large enough to be perturbative. These decays differ significantly from those involving only light quarks. The creation of mesons that are made up of purely light quarks involves creating two quark-antiquark pairs, with the energy shared between the quark and antiquark in each pair. In the production of two D mesons, however, almost all the energy of the bottomonium is carried away by the heavy c and $\bar{c}$, while the light quark and antiquark, which bind to the $\bar{c}$ and c respectively, carry away (boosted) residual energies.

The existence of well-separated scales in the system and the intuitive picture of the decay process suggest to tackle the problem using a sequence of effective field

theories (EFTs) that are obtained by subsequently integrating out the dynamics relevant to the perturbative scales m_b and m_c.

In the first step, we integrate out the scale m_b by describing the b and $\bar{b}$ with Non-Relativistic QCD (NRQCD) [99], and the highly energetic c and $\bar{c}$ with two copies of Soft-Collinear Effective Theory (SCET) [100, 28, 31, 101, 102] in opposite light-cone directions. In the second step, we integrate out the dynamics manifested at scales of order m_c by treating the quarkonium with potential NRQCD (pNRQCD) [103, 104, 105], and the D mesons with a boosted version of Heavy-Quark Effective Theory (HQET) [106, 107, 12, 108, 109, 110, 111]. The detailed explanation of why the aforementioned EFTs are employed is offered in Sec. 4.2. We will prove that, at leading order in the EFT expansion, the decay rate factors into a convolution of two perturbative matching coefficients and three (one for each hadron) non-perturbative matrix elements. The non-perturbative matrix elements are process-independent and encode information on both the initial and final states.

For simplicity, in this chapter we focus on the decays of the C-even quarkonia χ_{bJ} and η_b that, at leading order in the strong coupling α_s, proceed via the emission of two virtual gluons. The same method can be generalized to the decays of C-odd states Υ and h_b, which require an additional virtual gluon. We also refrain from processes that have vanishing contributions at leading order in the EFT power counting. So the specific processes studied in this chapter are $\chi_{b0,2} \to DD$, $\chi_{b0,\,2} \to D^*D^*$, and $\eta_b \to DD^* + \text{c.c.}$ However, the EFT approach developed in this chapter enables one to systematically include power-suppressed effects, making it possible to go beyond the leading-twist approximation.

The study of the inclusive and exclusive charm production in bottomonium decays and of the role played by the charm mass m_c in such processes have recently drawn renewed attention [112, 113, 114, 115], in connection with the experimental advances spurred in the past few years by the abundance of bottomonium data produced at facilities like BABAR, BELLE, and CLEO. The most notable result was the observation of the bottomonium ground state η_b, recently reported by the BABAR collaboration [116]. Furthermore, the CLEO collaboration published the

first results for several exclusive decays of χ_b into light hadrons [117] and for the inclusive decay of χ_b into open charm [118]. In particular, they measured the branching ratio $\mathcal{B}(\chi_{bJ} \to D^0 X)$, where J is the total angular momentum of the χ_b state, and conclusively showed that for $J = 1$ the production of open charm is substantial: $\mathcal{B}(\chi_{b1}(1P) \to D^0 X) = 12.59 \pm 1.94\%$. For the $J = 0, 2$ states the data are weaker, but the production of open charm still appears to be relevant. The measurements of the CLEO collaboration are in good agreement with the prediction of Bodwin *et al.* [112], where EFT techniques (in particular NRQCD) were for the first time applied to study the production of charm in bottomonium decays.

The double-charm decay channels analyzed here have not yet been observed, so one of our aims is to see if they may be observable given the current data. Unfortunately, the poor knowledge of the D-meson matrix elements prevents us from providing definitive predictions for the decay rates $\Gamma(\chi_{bJ} \to DD)$, $\Gamma(\chi_{bJ} \to D^*D^*)$, and $\Gamma(\eta_b \to DD^* + \text{c.c.})$. As we will show, these rates are indeed strongly dependent on the parameters of the D- and D^*-meson distribution amplitudes, in particular on their first inverse moments λ_D and λ_{D^*}: the rates vary by an order of magnitude in the accepted ranges for λ_D and λ_{D^*}. On the other hand, the factorization formula implies that these channels, if measured with sufficient accuracy, could constrain the form of the D-meson distribution amplitude and the value of its first inverse moment. In turn, the details of the D-meson structure are relevant to other D-meson observables, which are crucial for a model-independent determination of the CKM matrix elements $|V_{cd}|$ and $|V_{cs}|$ [119].

This chapter is organized as follows. In Sec. 4.2 we discuss the degrees of freedom and the EFTs we use. In Sec. 4.3.1 we match QCD onto NRQCD and SCET at the scale $2m_b$. The renormalization-group equation (RGE) for the matching coefficient is derived and solved in Sec. 4.3.2. In Sec. 4.4.1 the scale m_c is integrated out by matching NRQCD and SCET onto pNRQCD and bHQET. The renormalization of the low-energy EFT operators is performed in Sec. 4.4.2, with some technical details left to App. D. The decay rates are calculated in Sec. 4.5 using two model distribution amplitudes. The derivations of the distribution amplitude in the D-

meson and in the bottomonium rest frames are shown in App. E. In Sec. 4.6 we draw our conclusions.

4.2 Degrees of freedom and the Effective Field Theories

Several well-separated scales are involved in the decays of the C-even bottomonia η_b and χ_{bJ} into two D mesons, making them ideal processes for the application of EFT techniques. The distinctive structures of the bottomonium (a heavy quark-antiquark pair) and the D meson (a bound state of a heavy quark and a light quark) suggest that one needs different EFTs to describe the initial and final states.

We first look at the initial state. The η_b is the ground state of the bottomonium system. It is a pseudoscalar particle, with spin $S = 0$, orbital angular momentum $L = 0$, and total angular momentum $J = 0$. In what follows we will often use the spectroscopic notation $^{2S+1}L_J$, in which the η_b is denoted by $^1S_0$. The χ_{bJ} is a triplet of states with quantum numbers ^3P_J. The η_b and χ_{bJ} are non-relativistic bound states of a b quark and a $\bar{b}$ antiquark. The scales in the system are the b quark mass m_b, the relative momentum of the $b\bar{b}$ pair $m_b w$, the binding energy $m_b w^2$, and $\Lambda_{\rm QCD}$, the scale where QCD becomes strongly coupled. w is the relative velocity of the quark-antiquark pair in the meson, and from the bottomonium spectrum it can be inferred that $w^2 \sim 0.1$. Since $m_b \gg \Lambda_{\rm QCD}$, m_b can be integrated out in perturbation theory and the bottomonium can be described in NRQCD. The degrees of freedom of NRQCD are non-relativistic heavy quarks and antiquarks, with energy and momentum $(E, |\vec{p}\,|)$ of order $(m_b w^2, m_b w)$, light quarks and gluons. In NRQCD, the gluons can be soft $(m_b w, m_b w)$, potential $(m_b w^2, m_b w)$, and ultrasoft (usoft) $(m_b w^2, m_b w^2)$. The NRQCD Lagrangian is constructed as a systematic expansion in $1/m_b$ whose first few terms are

$$\mathcal{L}_{\rm NRQCD} = \psi^\dagger \left(iD_0 + \frac{\vec{D}^2}{2m_b} + \frac{\vec{\sigma}\cdot g\vec{B}}{2m_b} + \dots \right) \psi + \chi^\dagger \left(iD_0 - \frac{\vec{D}^2}{2m_b} - \frac{\vec{\sigma}\cdot g\vec{B}}{2m_b} + \dots \right) \chi \,,$$

where ψ and $\chi^\dagger$ annihilate a b quark and a $\bar{b}$ antiquark respectively, and $\cdots$ denotes higher-order contributions in $1/m_b$. In NRQCD several mass scales are still dynam-

ical and different assumptions on the hierarchy of these scales may lead to different power countings for operators of higher dimensionality. However, as long as $w \ll 1$, higher-dimension operators are suppressed by powers of w (for a critical discussion on the different power countings we refer to [105]).

NRQCD still contains interactions that can excite the heavy quarkonium far from its mass shell, for example, through the interaction of a non-relativistic quark with a soft gluon. In the case $m_b w \gg \Lambda_{\rm QCD}$, we can integrate out these fluctuations, matching perturbatively NRQCD onto a low-energy effective theory, pNRQCD. We are then left with a theory of non-relativistic quarks and ultrasoft gluons, with non-local potentials induced by the integration over soft- and potential-gluon modes. The interactions of the heavy quark with ultrasoft gluons are still described by the NRQCD Lagrangian, with the constraint that all the gluons are ultrasoft. In the weak coupling regime $m_b w \gg \Lambda_{\rm QCD}$, the potentials are organized by an expansion in $\alpha_s(m_b w)$, $1/m_b$, and r, where r is the distance between the quark and antiquark in the quarkonium, $r \sim 1/m_b w$. If we assume $m_b w^2 \sim \Lambda_{\rm QCD}$, each term in the expansion has a definite power counting in w and the leading potential is Coulombic $V \sim \alpha_s(m_b w)/r$.

An alternative approach, which does not require a two-step matching, has been developed in the effective theory vNRQCD [120, 121, 122, 123]. In the vNRQCD approach there is only one EFT below m_b, which is obtained by integrating out all the off-shell fluctuations at the hard scale m_b and introducing different fields for various propagating degrees of freedom (non-relativistic quarks and soft and ultrasoft gluons). In spite of the differences between the two formalisms, pNRQCD and vNRQCD give equivalent final answers in all the known examples in which both theories can be applied.

We now turn to the structure of the D meson. The most relevant features of the D meson are captured by a description in HQET. In HQET, in order to integrate out the inert scale m_c, the momentum of the heavy quark is generically written as [12]

$$p = m_c v + k \ , \tag{4.1}$$

where v is the four-velocity label, satisfying $v^2 = 1$, and k is the residual momentum. If one chooses v to be the center-of-mass velocity of the D meson, k scales as $k \sim v\Lambda_{\rm QCD}$. Introducing the light-cone vectors $n^\mu = (1, 0, 0, 1)$ and $\bar{n}^\mu = (1, 0, 0, -1)$, one can express the residual momentum in light-cone coordinates, $k^\mu = \bar{n} \cdot k \, n^\mu/2 + n \cdot k \, \bar{n}^\mu/2 + k_\perp^\mu$ or simply $k = (n \cdot k, \bar{n} \cdot k, \vec{k}_\perp)$. There are two relevant frames. One is the D-meson rest frame, in which v is conveniently chosen as $v_0 = (1, 0, 0, 0)$, and the other is the bottomonium rest frame, in which the D mesons are highly boosted in opposite directions, with v chosen as $v = v_D$, the four-velocity of one of the D mesons. By a simple consideration of kinematics and the scaling $k \sim v\Lambda_{\rm QCD}$, one can work out the scalings for k in the two frames. In the D-meson rest frame, $k \sim \Lambda_{\rm QCD}(1, 1, 1)$, and in the bottomonium rest frame (supposing the D meson moving in the positive z-direction),

$$k \sim \Lambda_{\rm QCD} \left(n \cdot v_D, \bar{n} \cdot v_D, 1\right) \sim \Lambda_{\rm QCD} \bar{n} \cdot v_D \left(\lambda^2, 1, \lambda\right) \ , \tag{4.2}$$

where $\bar{n} \cdot v_D \sim 2m_b/m_c$ and $\lambda = m_c/2m_b \ll 1$. It is convenient for the calculation in this chapter to use the bottomonium rest frame, so we drop the subscript in v_D and we assume $v = v_D$ in the rest of this chapter. The momentum scaling in Eq. (4.2) is called ultracollinear (ucollinear), and boosted HQET (bHQET) is the theory that describes heavy quarks with ultracollinear residual momenta and light degrees of freedom (including gluons and light quarks) with the same momentum scaling.

The bHQET Lagrangian is organized as a series in powers of $\Lambda_{\rm QCD}/m_c$ and, for residual momentum ultracollinear in the n-direction, the leading term is [110]

$$\mathcal{L}_{\rm bHQET} = \bar{h}_n i v \cdot D h_n \ , \tag{4.3}$$

where the field h_n annihilates a heavy quark and the covariant derivative D contains ultracollinear and ultrasoft gluons,

$$iD^\mu = \frac{n^\mu}{2} \left(i\bar{n} \cdot \partial + g\bar{n} \cdot A_n\right) + \frac{\bar{n}^\mu}{2} \left(in \cdot \partial + gn \cdot A_n + gn \cdot A_{us}\right) + \left(i\partial_\perp^\mu + gA_{n,\perp}^\mu\right) \ . \tag{4.4}$$

The ultrasoft gluons only enter in the small component of the covariant derivative. This fact can be exploited to decouple ultrasoft and ultracollinear modes in the

	NRQCD	field	momentum	SCET	field	momentum
quark	b, b	$\psi_b,\ \chi_{\bar{b}}$	$(m_b w^2, m_b w)$	c,	$\xi^c_{\bar{n}}$	$2m_b(1,\lambda^2,\lambda)$
				$\bar{c}$	$\xi^{\bar{c}}_n$	$2m_b(\lambda^2,1,\lambda)$
gluon	potential	A^μ	$(m_b w^2, m_b w)$	collinear	$A^\mu_{\bar{n}}$	$2m_b(1,\lambda^2,\lambda)$
					A^μ_n	$2m_b(\lambda^2,1,\lambda)$
	soft	A^μ	$(m_b w, m_b w)$	soft	A^μ_s	$2m_b(\lambda,\lambda,\lambda)$
	usoft	A^μ	$(m_b w^2, m_b w^2)$	usoft	A^μ_{us}	$2m_b(\lambda^2,\lambda^2,\lambda^2)$

Table 4.1: Degrees of freedom in $\mathrm{EFT_I}$(NRQCD + SCET). w is the $b\bar{b}$ relative velocity in the bottomonium rest frame, while $\lambda \sim m_c/2m_b$ is the SCET expansion parameter. We assume $m_b w \sim m_c$ (or, equivalently, $w \sim \lambda$) and $m_b w^2 \sim m_b\lambda^2 \sim \Lambda_{\mathrm{QCD}}$.

leading-order Lagrangian through a field redefinition reminiscent of the collinear-ultrasoft decoupling in SCET [31, 110]. The ultracollinear-ultrasoft decoupling is an essential ingredient for the factorization of the decay rate.

Therefore, the appropriate EFT to calculate the decay rate is a combination of pNRQCD, for the bottomonium, and two copies of bHQET, with fields collinear to the n and $\bar{n}$ directions, for the D and $\bar{D}$ mesons, symbolically written as $\mathrm{EFT_{II}} \equiv$ pNRQCD + bHQET.

As we mentioned earlier, we plan to describe the bottomonium structure with a two-step scheme QCD $\to$ NRQCD $\to$ pNRQCD. However, at the intermediate stage, where we first integrate out the hard scale $2m_b$ and arrive at the scale $m_b w$, the D meson cannot yet be described in bHQET. This is because the interactions relevant at the intermediate scale $m_b w$ can change the c-quark velocity and leave the D meson off-shell of order $\sim (m_b w)^2 \sim m_c^2 \gg \Lambda^2_{\mathrm{QCD}}$. Highly energetic c and $\bar{c}$ travelling in opposite directions can be described properly by SCET with mass. Thus, at the scale $\mu = 2m_b$, we match QCD onto an intermediate EFT, $\mathrm{EFT_I} \equiv$ NRQCD+SCET, in which the EFT expansion is organized by λ and w. The degrees of freedom of $\mathrm{EFT_I}$ are tabulated in Tab. 4.1.

Then, we integrate out m_c and $m_b w$ at the same time, matching $\mathrm{EFT_I}$ onto $\mathrm{EFT_{II}}$ at the scale $\mu' = m_c$. In $\mathrm{EFT_{II}}$, the low-energy approximation is organized by $\Lambda_{\mathrm{QCD}}/m_c$ and w. The degrees of freedom of $\mathrm{EFT_{II}}$ are summarized in Tab.

	pNRQCD	field	momentum	bHQET	field	momentum
quark	b, b	ψ_b, $\chi_{\bar{b}}$	$(m_b w^2, m_b w)$	c	$h^c_{\bar{n}}$	$Q\,(1, \lambda^2, \lambda)$
				u, d	$\xi_{\bar{n}}$	$Q\,(1, \lambda^2, \lambda)$
gluon	usoft	A^μ	$(m_b w^2, m_b w^2)$	usoft	A^μ_{us}	$Q(\lambda, \lambda, \lambda)$
				ucollinear	$A^\mu_{\bar{n}}$	$Q\,(1, \lambda^2, \lambda)$

Table 4.2: Degrees of freedom in $\mathrm{EFT_{II}}$(pNRQCD + bHQET). The scale Q in bHQET is $Q = n \cdot v' \Lambda_{\mathrm{QCD}}$ for the $\bar{n}$-collinear sector and $Q = \bar{n} \cdot v \Lambda_{\mathrm{QCD}}$ for the n-collinear sector. $n \cdot v'$ and $\bar{n} \cdot v$ are the large light-cone components of the D-meson velocities in the bottomonium rest frame, $n \cdot v' \sim \bar{n} \cdot v \sim 2m_b/m_c$. λ and w are defined as in Tab. 4.1. The scaling of quark and gluon fields collinear in the n direction is obtained by exchanging the p^+ and p^- components of $\bar{n}$-collinear fields

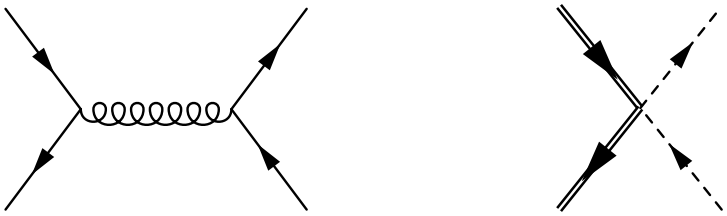

Figure 4.1: Matching QCD onto $\mathrm{EFT_I}$. On the r.h.s., the double lines represent the non-relativistic b ($\bar{b}$) (anti)quark, while the dashed lines represent the collinear c ($\bar{c}$) (anti)quark.

4.2. When no subscript is specified in the rest of this chapter, any reference to EFT applies to both $\mathrm{EFT_I}$ and $\mathrm{EFT_{II}}$. To facilitate the power counting, we adopt $w \sim \lambda \sim \Lambda_{\mathrm{QCD}}/m_c$. As a first study, we will perform in this chapter the leading-order calculation of the bottomonium decay rates.

4.3 NRQCD + SCET

4.3.1 Matching

In the first step, we integrate out the dynamics related to the hard scale $2m_b$ by matching the QCD diagrams for the production of a $c\,\bar{c}$ pair in the annihilation of a $b\,\bar{b}$ pair onto their $\mathrm{EFT_I}$ counterparts. The tree-level diagrams for the process are shown in Fig. 4.1. The gluon propagator in the QCD diagram has off-shellness of order $q^2 = (2m_b)^2$ and it is not resolved in $\mathrm{EFT_I}$, giving rise to a point-like interaction.

We calculate the diagrams on shell, finding

$$J_{\rm QCD} = C(\mu) J_{\rm EFT_I}(\mu) \,, \tag{4.5}$$

with, at tree level,

$$J_{\rm EFT_I} = \chi_b^\dagger \sigma_\perp^\mu t^a \psi_b \; \bar\chi_{\bar n}^c \, S_{\bar n}^\dagger \, \gamma_{\mu\perp} t^a \, S_n \, \chi_n^{\bar c} \quad \text{and} \quad C(\mu = 2m_b) = \frac{\alpha_s(2m_b)\pi}{m_b^2} \,, \tag{4.6}$$

where t^a are color matrices and the symbol σ^μ denotes the four matrices $\sigma^\mu = (1, \vec\sigma)$, with $\vec\sigma$ the Pauli matrices. The subscript $\perp$ refers to the components orthogonal to the light-cone vectors n^μ and $\bar n^\mu$. The fields ψ_b and $\chi_b^\dagger$ are two-component spinors that annihilate respectively a b quark and a $\bar b$ antiquark. $\chi^{\bar c}_{n,\,\bar n\cdot p}$ and $\chi^c_{\bar n,\,n\cdot p}$ are collinear gauge-invariant fermion fields:

$$\chi^{\bar c}_{n,\,\bar n\cdot p} \equiv (W_n^\dagger \xi_n^{\bar c})_{\bar n\cdot p} \,, \qquad \chi^c_{\bar n,\,n\cdot p} \equiv (W_{\bar n}^\dagger \xi_{\bar n}^c)_{n\cdot p} \,, \tag{4.7}$$

where W_n is defined as

$$W_n \equiv \sum_{\rm perms} \exp\left(-\frac{g}{\bar n\cdot\mathcal{P}} \bar n \cdot A_n\right) \,. \tag{4.8}$$

$W_{\bar n}$ has an analogous definition with $n \to \bar n$. Collinear fields are labeled by the large component of their momentum. Note, however, we omit in Eq. (4.6) the subscripts $n\cdot p$ and $\bar n\cdot p$ of the collinear fermion fields, in order to simplify the notation. The operator $\bar n\cdot\mathcal{P}$ in the definition (4.8) is a label operator that extracts the large component of the momentum of a collinear field, $\bar n\cdot\mathcal{P}\,\phi_{n,\,\bar n\cdot p} = \bar n\cdot p\,\phi_{n,\,\bar n\cdot p}$, where $\phi_{n,\,\bar n\cdot p}$ is a generic collinear field. $S_{n(\bar n)}$ is a soft Wilson line,

$$S_n \equiv \sum_{\rm perms} \left[\exp\left(-\frac{g}{n\cdot\mathcal{P}} n\cdot A_s\right)\right] , \tag{4.9}$$

where the operator $n\cdot\mathcal{P}$ acts on soft fields, $n\cdot\mathcal{P}\,\phi_s = n\cdot k\,\phi_s$.

Since in SCET different gluon modes are represented by different fields, we have to guarantee the gauge invariance of the operator $J_{\rm EFT_I}$ under separate soft and collinear gauge transformations. A soft transformation is defined by $V_s(x) = \exp\left(i\beta_s^a t^a\right)$, with $\partial_\mu V \sim 2m_b(\lambda,\lambda,\lambda)$, while a gauge transformation $U(x)$

is n-collinear if $U(x) = \exp\left(i\alpha^a(x)t^a\right)$ and $\partial_\mu U(x) \sim 2m_b(\lambda^2, 1, \lambda)$. It has been shown in Ref. [31] that collinear fields do not transform under a soft transformation and that the combination $W_n^\dagger \xi_n$ is gauge invariant under a collinear transformation. Soft fields do not transform under collinear transformations but they do under soft transformations. For example, the NRQCD quark and antiquark fields transform as $\psi_b \to V_s(x)\psi_b$. The soft Wilson line has the same transformation, $S_n \to V_s(x)S_n$. Therefore, $\chi_{\bar{b}}^\dagger \sigma_\perp^\mu t^a \psi_b$ transforms as an octet under soft gauge transformations. Since $\bar{\chi}_{\bar{n}}^c \, S_{\bar{n}}^\dagger \, \gamma_{\mu\perp} t^a \, S_n \, \chi_n^{\bar{c}}$ behaves like an octet as well, $J_{\mathrm{EFT_I}}$ is invariant. It is worth noting that the soft Wilson lines are necessary to guarantee the gauge invariance of $J_{\mathrm{EFT_I}}$. We have explicitly checked their appearance at one gluon by matching QCD diagrams like the one in Fig. 4.1, with all the possible attachments of an extra soft or collinear gluon, onto four-fermion operators in $\mathrm{EFT_I}$.

4.3.2 Running

The matching coefficient C and the effective operator $J_{\mathrm{EFT_I}}$ depend on the renormalization scale μ. Since the effective operator is sensitive to the low-energy scales in $\mathrm{EFT_I}$, logarithms that would appear in the evaluation of $J_{\mathrm{EFT_I}}$ are minimized by the choice $\mu \sim m_c$. On the other hand, since the coefficient encodes the high-energy dynamics of the scale $2m_b$, such a choice would induce large logarithms of $m_c/2m_b$ in the matching coefficient. These logarithms can be resummed using RGEs in NRQCD + SCET.

The μ dependence of $J_{\mathrm{EFT_I}}$ is governed by an equation of the following form [124],

$$\frac{d}{d\ln\mu} J_{\mathrm{EFT_I}}(\mu) = -\gamma_{\mathrm{EFT_I}}(\mu) J_{\mathrm{EFT_I}}(\mu) \,, \tag{4.10}$$

where the anomalous dimension $\gamma_{\mathrm{EFT_I}}$ is given by

$$\gamma_{\mathrm{EFT_I}} = Z_{\mathrm{EFT_I}}^{-1} \frac{d}{d\ln\mu} Z_{\mathrm{EFT_I}} \tag{4.11}$$

and $Z_{\mathrm{EFT_I}}$ is the counterterm that relates the bare operator $J_{\mathrm{EFT_I}}^{(0)}$ to the renormalized one, $J_{\mathrm{EFT_I}}^{(0)} = Z_{\mathrm{EFT_I}}(\mu) J_{\mathrm{EFT_I}}(\mu)$. Since the l.h.s. of Eq. (4.5) is independent of the

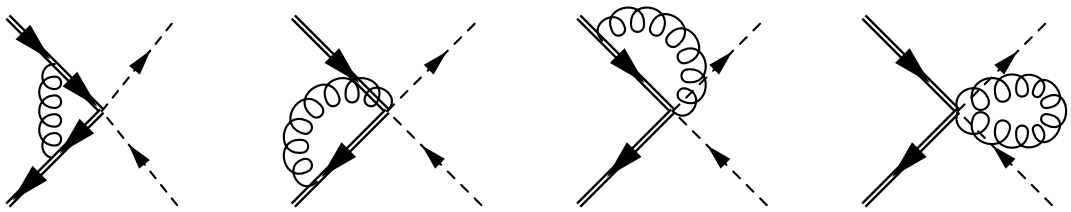

Figure 4.2: Soft diagrams at one loop.

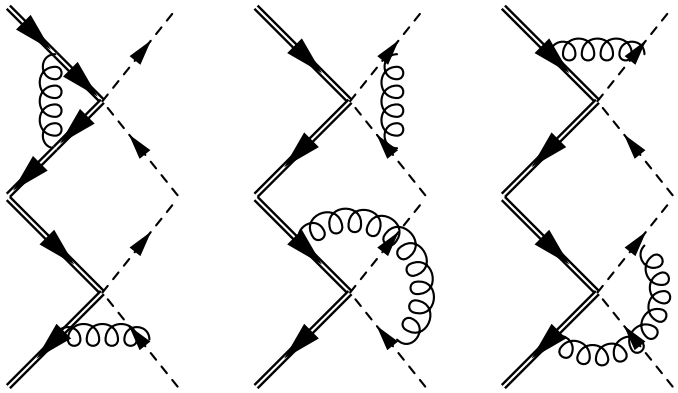

Figure 4.3: Ultrasoft diagrams at one loop.

scale μ, the RGE (4.10) can be recast as an equation for the matching coefficient $C(\mu)$,

$$\frac{d}{d\ln\mu}C(\mu) = \gamma_{\mathrm{EFT_I}}(\mu)C(\mu)\ . \tag{4.12}$$

The counterterm $Z_{\mathrm{EFT_I}}$ cancels the divergences that appear in Green functions with the insertion of the operator $J_{\mathrm{EFT_I}}$. We calculate $Z_{\mathrm{EFT_I}}$ in the $\overline{\mathrm{MS}}$ scheme by evaluating the divergent part of the four-point Green function at one loop, given by the diagrams in Figs. 4.2 - 4.4.

Since in NRQCD we do not introduce different gluon fields for different momentum modes, "soft" and "ultrasoft" in Fig. 4.2 and Fig. 4.3 refer to the convention that we impose soft or ultrasoft scaling to the corresponding loop momentum. The potential region, which should be considered in the diagrams of Fig. 4.2, does not give any divergent contribution.

The integrals are evaluated in dimensional regularization, with $d = 4 - 2\varepsilon$. We regulate the infrared divergences by keeping the non-relativistic b and $\bar{b}$ and the

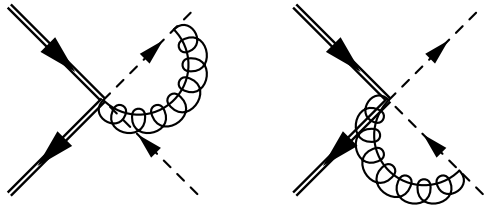

Figure 4.4: Collinear diagrams at one loop.

collinear c and $\bar{c}$ off-shell: $E_{b,\bar{b}} - \vec{p}^{\,2}_{b,\bar{b}}/2m_b = \Delta_b$, $p_c^2 - m_c^2 = \Delta^2$ and $p_{\bar{c}}^2 - m_c^2 = \bar{\Delta}^2$. We power count the c-quark off-shellness as $\Delta^2 \sim \bar{\Delta}^2 \sim m_b^2\lambda^2$ and the b-quark off-shellness as $\Delta_b \sim m_b w^2$. We also assume Δ^2, $\bar{\Delta}^2 > 0$. To avoid double counting, we define the one-loop integrals with the 0-bin subtraction [125].

Even with an off-shellness, the soft diagrams in Fig. 4.2 do not contain any scale and they are completely canceled by their 0-bin.

The divergent part of the ultrasoft diagrams in Fig. 4.3 is

$$\begin{aligned}\mathcal{M}_{usoft} = -\frac{\alpha_s}{4\pi}\Bigg\{2C_F\left[\frac{1}{\varepsilon^2} - \frac{1}{\varepsilon}\ln\left(\frac{\Delta^2\,\bar{\Delta}^2}{n\cdot p_c \bar{n}\cdot p_{\bar{c}}\,\mu^2}\right)\right] \\ + \frac{1}{N_c}\frac{1}{\varepsilon}\ln(-1-i0) - \frac{1}{N_c}\frac{1}{\varepsilon}\Bigg\} J_{\mathrm{EFT_I}}\,,\end{aligned} \tag{4.13}$$

where $C_F = (N_c^2 - 1)/2N_c$ and μ is the $\overline{\mathrm{MS}}$ unit mass, $\mu^2 = 4\pi\mu_{\mathrm{MS}}^2 \exp(-\gamma_E)$. The first term in the curly brackets of Eq. (4.13) corresponds to the sum of the divergences in the second diagram in Fig. 4.3, where an ultrasoft gluon is exchanged between the c and $\bar{c}$ quarks collinear in back-to-back directions, and those in the last four diagrams of the same figure, which contain ultrasoft interactions between the initial and final states. The second term is an extra imaginary piece generated by the second diagram in Fig. 4.3. The $-i0$ prescription in the argument of the logarithm, where 0 is a positive infinitesimal quantity, follows from the prescriptions in the quark propagators and from the choice $\Delta^2, \bar{\Delta}^2 > 0$. The divergences arising from the ultrasoft exchanges between the $b\bar{b}$ pair in the first diagram in Fig. 4.3 are encoded in the last term in Eq. (4.13).

The initial and final states cannot interact by exchanging collinear gluons because the emission or absorption of a collinear gluon would give the b quark an off-shellness of order m_b^2, which cannot appear in the effective theory. For the same reason, the

c and $\bar{c}$ cannot exchange n or $\bar{n}$-collinear gluons. The only collinear loop diagrams consist of the emission of a $n(\bar{n})$-collinear gluon from the Wilson line $W_{n\,(\bar{n})}$ in $J_{\mathrm{EFT_I}}$ and its absorption by the $\bar{c}(c)$ quark, as shown in Fig. 4.4. The divergent part of the sum of the two collinear diagrams is

$$\mathcal{M}_{\mathrm{coll}} = \frac{\alpha_s}{4\pi} 2C_F \left[\frac{2}{\varepsilon^2} + \frac{1}{\varepsilon} \left(2 - \ln \left(\frac{\Delta^2 \bar{\Delta}^2}{\mu^2 \mu^2} \right) \right) \right] J_{\mathrm{EFT_I}} \,. \tag{4.14}$$

The collinear diagrams are calculated with a 0-bin subtraction [125], that is, we subtract from the naive collinear integrals the same integrals in the limit in which the loop momentum is ultrasoft. In this way we avoid double counting between the diagrams in Figs. 4.3 and 4.4.

Summing Eqs. (4.13) and (4.14) and adding factors of $Z_\psi^{1/2}$ for each field,

$$Z_{\psi_b} = Z_{\chi_b} = 1 + \frac{1}{\varepsilon} \frac{\alpha_s}{2\pi} C_F \,, \qquad Z_{\xi_n} = Z_{\xi_{\bar{n}}} = 1 - \frac{1}{\varepsilon} \frac{\alpha_s}{4\pi} C_F \,,$$

the divergent piece becomes

$$\mathcal{M}_{\mathrm{div}} = \frac{\alpha_s}{4\pi} \left\{ C_F \left[\frac{2}{\varepsilon^2} + \frac{2}{\varepsilon} \left(\frac{3}{2} - \ln \left(\frac{n \cdot p_c \bar{n} \cdot p_{\bar{c}}}{\mu^2} \right) \right) \right] + \frac{1}{\varepsilon} N_c + \frac{i\pi}{\varepsilon} \frac{1}{N_c} \right\} J_{\mathrm{EFT_I}} \,. \tag{4.15}$$

The counterterm $Z_{\mathrm{EFT_I}}$ is chosen so as to cancel the divergence in Eq. (4.15),

$$Z_{\mathrm{EFT_I}} = \frac{\alpha_s}{4\pi} \left\{ C_F \left[\frac{2}{\varepsilon^2} + \frac{2}{\varepsilon} \left(\frac{3}{2} - \ln \left(\frac{n \cdot p_c \bar{n} \cdot p_{\bar{c}}}{\mu^2} \right) \right) \right] + \frac{1}{\varepsilon} N_c + \frac{i\pi}{\varepsilon} \frac{1}{N_c} \right\} \,. \tag{4.16}$$

From the definition (4.11), Eq. (4.16), and recalling that $d\alpha_s / d\ln\mu = -2\varepsilon\alpha_s + \mathcal{O}(\alpha_s^2)$, the anomalous dimension at one loop is

$$\gamma_{\mathrm{EFT_I}} = -2 \frac{\alpha_s(\mu)}{4\pi} \left\{ 3C_F + N_c + 4C_F \ln \left(\frac{\mu}{\sqrt{n \cdot p_c \bar{n} \cdot p_{\bar{c}}}} \right) + i\pi \frac{1}{N_c} \right\} \,. \tag{4.17}$$

An important feature of the anomalous dimension (4.17) is the presence of a term proportional to $\ln\mu$. Because of this term, the RGE (4.12) can be used to resum Sudakov double logarithms. As we will show shortly, the general solution of Eq. (4.12) can be written in the following form:

$$C(\mu) = C(\mu_0) \left(\frac{\mu_0}{\sqrt{n \cdot p_c \bar{n} \cdot p_{\bar{c}}}} \right)^{g(\mu_0, \mu)} \exp U(\mu_0, \mu) \,, \tag{4.18}$$

where g and U depend on the initial scale μ_0 and the final scale μ that we run down to. For an anomalous dimension of the form (4.17), U can be expanded as a series,

$$U(\mu_0,\mu)=\sum_{n=1}^{\infty}\alpha_s^n(\mu_0)\sum_{L=0}^{n+1}u_{n,L}\ln^{n-L+1}\frac{\mu}{\mu_0}\ . \tag{4.19}$$

If $\mu/\mu_0\ll 1$, the most relevant terms in the expansion (4.19) are those with $L=0$, which we call "leading logs" (LL). Terms with higher L are subleading; we call the terms with $L=1$ "next-to-leading logs" (NLL), those with $L=2$ "next-to-next-leading logs" (NNLL), and, if $L=m$, we denote them with N^{m}LL. The RGE (4.12) determines the coefficients in the expansion (4.19). With the anomalous dimensions written as

$$\gamma_{\mathrm{EFT_I}}=-2\left\{\gamma(\alpha_s)+\Gamma(\alpha_s)\ln\left(\frac{\mu}{\sqrt{n\cdot p_c\bar{n}\cdot p_{\bar{c}}}}\right)\right\}\ , \tag{4.20}$$

where $\gamma(\alpha_s)$ and $\Gamma(\alpha_s)$ are series in powers of α_s,

$$\gamma(\alpha_s)=\frac{\alpha_s}{4\pi}\gamma^{(0)}+\left(\frac{\alpha_s}{4\pi}\right)^2\gamma^{(1)}+\dots\ ,\qquad \Gamma(\alpha_s)=\frac{\alpha_s}{4\pi}\Gamma^{(0)}+\left(\frac{\alpha_s}{4\pi}\right)^2\Gamma^{(1)}+\dots\ ,$$

it can be proved that the coefficients of the LL, u_{n0}, are determined by the knowledge of $\Gamma^{(0)}$ and of the QCD β function at one loop. The NLL coefficients u_{n1} are instead completely determined if Γ and β are known at two loops and $\gamma(\alpha_s)$ at one loop.

In the case we are studying, the ratio of the scales $\mu/\mu_0\sim m_c/2m_b$ is not extremely small. Indeed, as to be seen shortly, the numerical contributions of the LL and NLL terms in the series (4.19) are of the same size. It is therefore important to work at NLL accuracy, which requires the calculation of the coefficient of $\ln\mu$ to two loops. The factors of $\ln\mu$ are induced by cusp angles involving light-like Wilson lines and their coefficients are universal $\Gamma(\alpha_s)\propto\Gamma_{\mathrm{cusp}}(\alpha_s)$ [126]. The cusp anomalous dimension $\Gamma_{\mathrm{cusp}}(\alpha_s)$ is known at two loops [126],

$$\Gamma_{\mathrm{cusp}}(\alpha_s)=\frac{\alpha_s}{4\pi}\Gamma^{(0)}_{\mathrm{cusp}}+\left(\frac{\alpha_s}{4\pi}\right)^2\Gamma^{(1)}_{\mathrm{cusp}}\ , \tag{4.21}$$

with

$$\Gamma^{(0)}_{\mathrm{cusp}}=4C_F\ ,\qquad \Gamma^{(1)}_{\mathrm{cusp}}=4C_F\left[\left(\frac{67}{9}-\frac{\pi^2}{3}\right)N_c-\frac{10}{9}n_f\right]\ , \tag{4.22}$$

while the constant of proportionality between $\Gamma(\alpha_s)$ and $\Gamma_{\rm cusp}(\alpha_s)$ is fixed by the one-loop calculation. Since we have determined $\gamma^{(0)}$,

$$\gamma^{(0)} = 3C_F + N_c + i\frac{\pi}{N_c}\,, \tag{4.23}$$

and the β function is known, we have all the ingredients to provide the NLL approximation for $U(\mu_0,\mu)$ and $g(\mu_0,\mu)$. Taking into account the tree-level initial condition in Eq. (4.6), Eq. (4.18) determines the leading-order matching coefficient, with NLL resummation.

The solution (4.18) can be derived by writing Eq. (4.12) as

$$d\ln C = -2\frac{d\alpha}{\beta(\alpha)}\left\{\gamma(\alpha) + \Gamma_{\rm cusp}(\alpha)\left[\ln\left(\frac{\mu_0}{\sqrt{n\cdot p_c \bar{n}\cdot p_{\bar{c}}}}\right) + \int_{\alpha(\mu_0)}^{\alpha}\frac{d\alpha'}{\beta(\alpha')}\right]\right\}\,, \tag{4.24}$$

where we have used the definition of the β function, $\beta(\alpha) = d\alpha/d\ln\mu$, to write $\ln\mu$ and $d\ln\mu$ in terms of α. Integrating both sides from μ_0 to μ and exponentiating the result we find the form given in Eq. (4.18), with

$$\begin{aligned} U(\mu_0,\mu) &= -2\int_{\alpha_s(\mu_0)}^{\alpha_s(\mu)}\frac{d\alpha}{\beta(\alpha)}\left\{\gamma(\alpha) + \Gamma_{\rm cusp}(\alpha)\int_{\alpha(\mu_0)}^{\alpha}\frac{d\alpha'}{\beta(\alpha')}\right\}\,, \\ g(\mu_0,\mu) &= -2\int_{\alpha_s(\mu_0)}^{\alpha_s(\mu)}\frac{d\alpha}{\beta(\alpha)}\Gamma_{\rm cusp}(\alpha)\,. \end{aligned} \tag{4.25}$$

At NLL, we find

$$\begin{aligned} U(\mu_b,\mu) = \frac{2\pi\Gamma^{(0)}_{\rm cusp}}{\beta_0^2}\Bigg[&\frac{r-1-r\ln r}{\alpha_s(\mu)} + \frac{\beta_0\gamma^{(0)}_{\rm Re}}{2\pi\Gamma^{(0)}_{\rm cusp}}\ln r + \left(\frac{\Gamma^{(1)}_{\rm cusp}}{\Gamma^{(0)}_{\rm cusp}} - \frac{\beta_1}{\beta_0}\right)\frac{1-r+\ln r}{4\pi} \\ &+ \frac{\beta_1}{8\pi\beta_0}\ln^2 r\Bigg] + \frac{\gamma^{(0)}_{\rm Im}}{\beta_0}\ln r\,, \end{aligned} \tag{4.26}$$

and

$$g(\mu_b,\mu) = \frac{\Gamma^{(0)}_{\rm cusp}}{\beta_0}\left[\ln r + \left(\frac{\Gamma^{(1)}_{\rm cusp}}{\Gamma^{(0)}_{\rm cusp}} - \frac{\beta_1}{\beta_0}\right)\frac{\alpha_{\rm s}(\mu_b)}{4\pi}(r-1)\right]\,, \tag{4.27}$$

where $r = \alpha_s(\mu)/\alpha_s(\mu_b)$ and we have renamed the initial scale μ_b, to denote its connection to the scale $2m_b$. In Eqs. (4.26) and (4.27) we have used the two-loop beta function,

$$\beta(\alpha_s) = -2\alpha_s\left(\frac{\alpha_s}{4\pi}\beta_0 + \left(\frac{\alpha_s}{4\pi}\right)^2\beta_1\right)\,, \tag{4.28}$$

with

$$\beta_0 = 11 - \frac{2}{3} n_f \,, \qquad \beta_1 = \frac{34}{3} N_c^2 - \frac{10}{3} N_c n_f - 2 C_F n_f \,. \tag{4.29}$$

In Eq. (4.26) we have kept the contributions of the real and imaginary part of $\gamma^{(0)}$ separated. The imaginary part of $\gamma^{(0)}$ changes the phase of the matching coefficient $C(\mu)$, but this phase is irrelevant for the calculation of physical observables like the decay rate, which depend on the square modulus of $C(\mu)$. In Sec. 4.5 the factor $U(\mu_b, \mu)$ will be evaluated between the scales $\mu_b = 2m_b$ and $\mu = m_c$, with $n_f = 4$ active quark flavors. The numerical evaluation shows that the LL term, represented by the first term in the brackets in Eq. (4.26), is slightly smaller than and have the opposite sign of the term proportional to $\gamma^{(0)}_{\rm Re}$, which dominates the NLL contribution. This observation confirms, *a posteriori*, the necessity to work at NLL accuracy in the resummation of logarithms of $m_c/2m_b$.

The RGE (4.12) and its solution (4.18) thus allow us to rewrite Eq. (4.5) as

$$J_{\rm QCD} = C(\mu) J_{\rm EFT_I}(\mu) = C(\mu_b = 2m_b) \exp U(2m_b, m_c) J_{\rm EFT_I}(\mu = m_c) \,,$$

which avoids the occurrence of any large logarithm in the matching coefficient or in the matrix element of the effective operator.

4.4 pNRQCD + bHQET

4.4.1 Matching

In the second step, we integrate out the soft modes by matching $\rm EFT_I$ onto $\rm EFT_{II}$. In NRQCD + SCET, contributions to the exclusive decay processes are obtained by considering time-ordered products of $J_{\rm EFT_I}$ and the terms in the $\rm EFT_I$ Lagrangian that contain soft-gluon emissions. The soft gluons have enough virtuality to produce a pair of light quarks travelling in opposite directions with ultracollinear momentum scaling. These light quarks bind to the charm quarks to form back-to-back D mesons. The total momentum of two back-to-back ultracollinear quarks is $2m_b\Lambda_{\rm QCD}/m_c\,(1, 1, \lambda)$ and the invariant mass of the pair is

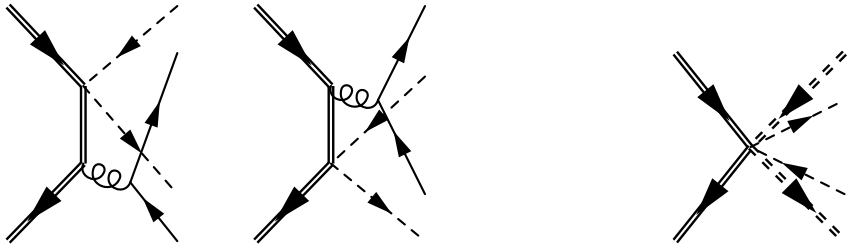

Figure 4.5: Matching NRQCD + SCET onto pNRQCD + bHQET. On the r.h.s. the double solid lines represent heavy b ($\bar{b}$) (anti)quarks, the double dashed lines bHQET c ($\bar{c}$) (anti)quarks, and the single dashed lines collinear light quarks.

$q^2 \sim (2m_b\Lambda_{\rm QCD}/m_c)^2 \sim m_c^2$: in NRQCD + SCET, only soft gluons have enough energy to produce them. The time-ordered products in NRQCD + SCET are matched onto six-fermion operators in pNRQCD + bHQET, where fluctuations of order m_c^2 cannot be resolved.

We consider the scale $\mu' = m_c$ to be much bigger than $\Lambda_{\rm QCD}$, so the matching can be done in perturbation theory. The Feynman diagrams contributing to the matching are shown in Fig. 4.5. The gluon and the b-quark propagators have off-shellness of order m_c^2, so the two diagrams on the l.h.s. match onto six-fermion operators on the r.h.s.

The amplitude for the decay of a bottomonium with quantum numbers ${}^{2S+1}L_J$ into two D mesons has the following form:

$$\mathcal{M} = C(\mu) \int \frac{d\omega}{\omega}\frac{d\bar{\omega}}{\bar{\omega}} T(\omega, \bar{\omega}, \mu, \mu'; {}^{2S+1}L_J) F^2(\mu') \\ \langle DA,\, DB | \mathcal{O}_{AB}^{{}^{2S+1}L_J}(\omega, \bar{\omega}, \mu') | \bar{b}b({}^{2S+1}L_J)\rangle. \tag{4.30}$$

A and B, which label the final states and the $\mathrm{EFT_{II}}$ operators $\mathcal{O}_{AB}^{{}^{2S+1}L_J}$, denote the possible parity, spin, and polarization of the D mesons, $A, B = \{P, V_L, V_T\}$, indicating respectively a pseudoscalar D meson, a longitudinally-polarized vector meson D^*, and a transversely-polarized vector meson D^*. Unlike $J_{\mathrm{EFT_I}}$, we have dropped the subscript $\mathrm{EFT_{II}}$ in $\mathcal{O}_{AB}^{{}^{2S+1}L_J}$ in order to simplify the notation.

The $\mathrm{EFT_{II}}$ operators that contribute to the decay of the P-wave states are

$$\begin{aligned}
F^2(\mu')\,\mathcal{O}^{^3P_J}_{PP}(\omega,\bar\omega,\mu') &= \chi^\dagger_{\bar b}\,\vec p_b\cdot\vec\sigma_\perp\psi_b\;\bar{\mathcal{H}}^c_{\bar n}\,\frac{\bar{n}\!\!\!/}{2}\gamma^5\,\delta\left(-\bar\omega - n\cdot\mathcal{P}\right)\chi^{\bar l}_{\bar n} \\
&\quad\times\bar\chi^l_n\delta\left(\omega-\bar n\cdot\mathcal{P}^\dagger\right)\,\frac{\bar{\vec n}\!\!\!/}{2}\gamma^5\,\mathcal{H}^{\bar c}_n\,, \\
F^2(\mu')\,\mathcal{O}^{^3P_J}_{V_LV_L}(\omega,\bar\omega,\mu') &= \chi^\dagger_{\bar b}\,\vec p_b\cdot\vec\sigma_\perp\psi_b\;\bar{\mathcal{H}}^c_{\bar n}\,\frac{\bar{n}\!\!\!/}{2}\,\delta\left(-\bar\omega - n\cdot\mathcal{P}\right)\chi^{\bar l}_{\bar n} \\
&\quad\times\bar\chi^l_n\delta\left(\omega-\bar n\cdot\mathcal{P}^\dagger\right)\,\frac{\bar{\vec n}\!\!\!/}{2}\,\mathcal{H}^{\bar c}_n\,, \\
F^2(\mu')\,\mathcal{O}^{^3P_J}_{V_TV_T}(\omega,\bar\omega,\mu') &= \chi^\dagger_{\bar b}\,p_{b\perp}^{(\mu}\sigma_\perp^{\nu)}\psi_b\;\bar{\mathcal{H}}^c_{\bar n}\,\frac{\bar{n}\!\!\!/}{2}\gamma_{\mu\perp}\,\delta\left(-\bar\omega - n\cdot\mathcal{P}\right)\chi^{\bar l}_{\bar n} \\
&\quad\times\bar\chi^l_n\delta\left(\omega-\bar n\cdot\mathcal{P}^\dagger\right)\,\frac{\bar{\vec n}\!\!\!/}{2}\gamma_{\nu\perp}\,\mathcal{H}^{\bar c}_n,
\end{aligned} \tag{4.31}$$

where $p_{b\perp}^{(\mu}\sigma_\perp^{\nu)}$ is a symmetric, traceless tensor,

$$p_{b\perp}^{(\mu}\sigma_\perp^{\nu)} = \frac{1}{2}\left(p^\mu_{b\perp}\sigma^\nu_\perp + p^\nu_{b\perp}\sigma^\mu_\perp - g^{\mu\nu}_\perp\,\vec p_b\cdot\vec\sigma_\perp\right)\,.$$

At leading order in the $\mathrm{EFT_{II}}$ expansion, the η_b can only decay into a pseudoscalar and a vector meson, with an operator given by

$$\begin{aligned}
F^2(\mu')\,\mathcal{O}^{^1S_0}_{PV_L}(\omega,\bar\omega,\mu') = \chi^\dagger_{\bar b}\,\psi_b\;\Bigg[&\bar{\mathcal{H}}^c_{\bar n}\,\frac{\bar{n}\!\!\!/}{2}\gamma^5\,\delta\left(-\bar\omega - n\cdot\mathcal{P}\right)\chi^{\bar l}_{\bar n}\;\bar\chi^l_n\delta\left(\omega-\bar n\cdot\mathcal{P}^\dagger\right)\,\frac{\bar{\vec n}\!\!\!/}{2}\,\mathcal{H}^{\bar c}_n \\
&+\bar{\mathcal{H}}^c_{\bar n}\,\frac{\bar{n}\!\!\!/}{2}\,\delta\left(-\bar\omega - n\cdot\mathcal{P}\right)\chi^{\bar l}_{\bar n}\;\bar\chi^l_n\delta\left(\omega-\bar n\cdot\mathcal{P}^\dagger\right)\,\frac{\bar{\vec n}\!\!\!/}{2}\gamma^5\,\mathcal{H}^{\bar c}_n\Bigg]\,.
\end{aligned} \tag{4.32}$$

For later convenience, in the definition of the effective operators (4.31) and (4.32) we have factored out the term $F^2(\mu')$, which is related to the D-meson decay constant. The definition of $F^2(\mu')$ will become clear when we introduce the D-meson distribution amplitudes. The fields χ^l_n and $\chi^{\bar l}_{\bar n}$ are ultracollinear gauge-invariant light-quark fields, while $\mathcal{H}^c_{\bar n} = W^\dagger_{\bar n}h^c_{\bar n}$ and $\mathcal{H}^{\bar c}_n = W^\dagger_n h^{\bar c}_n$ are bHQET heavy-quark fields, which are invariant under an ultracollinear gauge transformation. The Wilson lines W_n and $W_{\bar n}$ have the same definition as in Eq. (4.8), with the restriction to ultracollinear gluons. Eqs. (4.31) and (4.32) allow us to interpret ω as the component of the light-quark momentum along the direction n. Similarly, $\bar\omega$ represents the component of the light-antiquark momentum along $\bar n$. The minus sign in the delta function $\delta(-\bar\omega - n\cdot\mathcal{P})$ is chosen so that $\bar\omega$ is positive.

The tree-level matching coefficients are

$$\begin{aligned} T(\omega,\bar\omega,\mu,\mu'=m_c;\,{}^3P_J) &= \frac{C_F}{N_c^2}\frac{4\pi\alpha_s(m_c)}{m_b}\frac{1}{\omega+\bar\omega}\,, \\ T(\omega,\bar\omega,\mu,\mu'=m_c;\,{}^1S_0) &= \frac{C_F}{N_c^2}\frac{4\pi\alpha_s(m_c)}{m_b}\frac{1}{2}\frac{\omega-\bar\omega}{\omega+\bar\omega}\,. \end{aligned} \tag{4.33}$$

Note that, at leading order in the $\mathrm{EFT_{II}}$ expansion, the matching coefficient $T(\omega,\bar\omega,\mu,\mu';\,{}^3P_J)$ is independent of the spin and polarization of the final states, or of the total angular momentum J of the χ_b.

An important feature of bHQET is that the ultracollinear and ultrasoft sectors can be decoupled at leading order in the power counting by a field redefinition reminiscent of the collinear-usoft decoupling in SCET [31, 110]. For bHQET in the n direction, the decoupling is achieved by defining $h_n^{\bar c}\to Y_n h_n^{\bar c}$ and $\bar\xi_n^l\to\bar\xi_n^l Y_n^\dagger$, where Y_n is an ultrasoft Wilson line,

$$Y_n=\sum_{\text{perms}}\left[\exp\left(-\frac{g}{n\cdot\mathcal{P}}n\cdot A_{us}\right)\right]\,. \tag{4.34}$$

An analogous redefinition with $n\to\bar n$ decouples ultrasoft from $\bar n$-ultracollinear quarks and gluons. These redefinitions do not affect the operators in Eqs. (4.31) and (4.32) because all the induced Wilson lines cancel out. As a consequence, at leading order in the $\mathrm{EFT_{II}}$ power counting, there is no interaction between the initial and the final states, since the former can only emit and absorb ultrasoft gluons that do not couple to ultracollinear degrees of freedom. Furthermore, fields in the two copies of bHQET, boosted in opposite directions, cannot interact with each other because the interaction with a $\bar n$-ultracollinear gluon would give a n-ultracollinear quark or gluon a virtuality of order m_c^2, which, however, cannot appear in $\mathrm{EFT_{II}}$. The matrix elements of the operators $\mathcal{O}_{AB}^{{}^{2S+1}L_J}(\omega,\bar\omega,\mu)$, therefore, factorize as

$$\begin{aligned} &F^2(\mu')\langle AB|\mathcal{O}_{A\,B}^{{}^{2S+1}L_J}(\omega,\bar\omega,\mu')|\bar b b\rangle = \\ &\langle 0|\chi_b^\dagger T_{AB}^{{}^{2S+1}L_J}\psi_b|\bar b b\rangle\,\langle A|\bar{\mathcal{H}}_{\bar n}^c\,\frac{\bar{n}\!\!\!/}{2}\Gamma_A\,\delta\left(-\bar\omega-n\cdot\mathcal{P}\right)\chi_{\bar n}^{\bar l}|0\rangle\,\langle B|\bar\chi_n^l\delta\left(\omega-\bar n\cdot\mathcal{P}^\dagger\right)\,\frac{n\!\!\!/}{2}\Gamma_B\,\mathcal{H}_n^{\bar c}|0\rangle\,, \end{aligned} \tag{4.35}$$

where $\Gamma_A=\{\gamma_5,1,\gamma_\perp^\mu\}$ and $T_{AB}^{{}^{2S+1}L_J}=\{1,\,\vec p_b\cdot\vec\sigma_\perp,\,p_{b\perp}^{(\mu}\sigma_\perp^{\nu)}\}$. The charge-conjugated contribution is understood in the η_b case.

The quarkonium state and the D mesons in Eq. (4.35) have respectively non-relativistic and HQET normalization:

$$\langle \chi_{bJ}(E',\vec{p}')|\chi_{bJ}(E,\vec{p})\rangle = (2\pi)^3\delta^{(3)}(\vec{p}-\vec{p}') \ ,$$
$$\langle D(v',k')|D(v,k)\rangle = 2v^0\delta_{v,v'}(2\pi)^3\delta^{(3)}(\vec{k}-\vec{k}') \ ,$$

where v^0 is the 0th component of the 4-velocity v^μ.

The D-meson matrix elements can be expressed in terms of the D-meson light-cone distribution amplitudes:

$$\langle P|\bar{\chi}_n^l \frac{\bar{n}\!\!\!/}{2}\gamma^5\,\delta\left(\omega-\bar{n}\cdot\mathcal{P}^\dagger\right)\mathcal{H}_n^{\bar{c}}|0\rangle = iF_P(\mu')\frac{\bar{n}\cdot v}{2}\phi_P(\omega,\mu') \ , \tag{4.36}$$

$$\langle V_L|\bar{\chi}_n^l \frac{\bar{n}\!\!\!/}{2}\,\delta\left(\omega-\bar{n}\cdot\mathcal{P}^\dagger\right)\mathcal{H}_n^{\bar{c}}|0\rangle = F_{V_L}(\mu')\frac{\bar{n}\cdot v}{2}\phi_{V_L}(\omega,\mu') \ , \tag{4.37}$$

$$\langle V_T|\bar{\chi}_n^l \frac{\bar{n}\!\!\!/}{2}\gamma_\perp^\mu\,\delta\left(\omega-\bar{n}\cdot\mathcal{P}^\dagger\right)\mathcal{H}_n^{\bar{c}}|0\rangle = F_{V_T}(\mu')\frac{\bar{n}\cdot v}{2}\varepsilon_\perp^\mu\phi_{V_T}(\omega,\mu') \ , \tag{4.38}$$

where $\varepsilon_\perp^\mu$ is the transverse polarization of the vector meson. The constants $F_A(\mu')$, with $A=\{P,V_L,V_T\}$, are related to the matrix elements of the local heavy-light currents in coordinate space. In the heavy-quark limit, where D and D^* are degenerate, F_A is the same for all the three states: $F\equiv F_P=F_{V_L}=F_{V_T}$. In this limit,

$$\langle 0|\bar{\xi}_n^{\bar{l}}\frac{\bar{n}\!\!\!/}{2}\gamma^5 h_n^c(0)|P\rangle = -iF(\mu')\frac{\bar{n}\cdot v'}{2} \ . \tag{4.39}$$

At tree level, the matrix element is proportional to the D-meson decay constant $f_D = 205.8\pm8.5\pm2.5$ MeV [127]. More precisely, $F(\mu')=f_D\sqrt{m_D}$, where the factor $\sqrt{m_D}$ is due to HQET normalization. The scale dependence of F is determined by the renormalization of heavy-light HQET currents. At one loop, Ref. [124] showed that

$$\frac{d}{d\ln\mu'}F(\mu') = -\gamma_F F(\mu') = 3C_F\frac{\alpha_s}{4\pi}F(\mu') \ . \tag{4.40}$$

The pNRQCD matrix elements can be expressed in terms of the heavy quarkonium wavefunctions. The operator $\chi_{\bar{b}}^\dagger\vec{p}_b\cdot\vec{\sigma}_\perp\psi_b$ contains a component with $J=0$ and a component with $J=2$ and $J_z=0$, so its matrix element has non-vanishing overlap with both χ_{b0} and χ_{b2}. The operator $\chi_{\bar{b}}^\dagger p_b^{(\mu}\sigma_\perp^{\nu)}\psi_b$ instead has only contributions with $J=2$ and $J_z=\pm2$ and therefore it only overlaps with χ_{b2}. In terms of

the bottomonium wavefunctions, the pNRQCD matrix elements are expressed as

$$\langle 0|\chi_{\bar{b}}^{\dagger}\vec{p}_b\cdot\vec{\sigma}_{\perp}\psi_b|\chi_{b0}\rangle = \frac{2}{\sqrt{3}}\sqrt{\frac{3N_c}{2\pi}}R'_{\chi_{b0}}(0,\mu')\ , \tag{4.41}$$

$$\langle 0|\chi_{\bar{b}}^{\dagger}\vec{p}_b\cdot\vec{\sigma}_{\perp}\psi_b|\chi_{b2}\rangle = -\sqrt{\frac{2}{15}}\sqrt{\frac{3N_c}{2\pi}}R'_{\chi_{b2}}(0,\mu')\ , \tag{4.42}$$

$$\langle 0|\chi_{\bar{b}}^{\dagger}p_b^{(\mu}\sigma_{\perp}^{\nu)}\psi_b|\chi_{b2}\rangle = (\varepsilon^{(2)}_{\mu\nu}+\varepsilon^{(-2)}_{\mu\nu})\sqrt{\frac{3N_c}{2\pi}}R'_{\chi_{b2}}(0,\mu')\ , \tag{4.43}$$

where $R'_{\chi_{bJ}}(0)$ is the derivative of the radial wavefunction of the χ_{bJ} evaluated at the origin. At leading order, the pNRQCD Hamiltonian does not depend on J, so, up to corrections of order w^2, $R'_{\chi_{b2}}(0)=R'_{\chi_{b0}}(0)$. The numerical pre-factors in Eqs. (4.41) and (4.42) follow from decomposing $\vec{p}_b\cdot\vec{\sigma}_{\perp}$ into components with definite J_z. $\varepsilon^{(j)}_{\mu\nu}$ is the polarization tensor of the χ_{b2} state, and Eq. (4.43) states that, at leading order in the w^2 expansion, only the particles with polarization $J_z=\pm 2$ contribute to χ_{b2} decay into two transversely-polarized vector mesons. Similarly, one finds

$$\langle 0|\chi_{\bar{b}}^{\dagger}\psi_b|\eta_b\rangle = \sqrt{\frac{N_c}{2\pi}}R_{\eta_b}(0,\mu')\ . \tag{4.44}$$

The factorization of the matrix elements (4.35) implies that the decay rate also factorizes. For the decays of χ_{b0} and χ_{b2} into two pseudoscalar mesons or two longitudinally-polarized vector mesons, we find

$$\begin{aligned}\Gamma(\chi_{b0}\to AA) =& \frac{4}{3}\frac{m_D^2\sqrt{m_{\chi_{b0}}^2-4m_D^2}}{8\pi m_{\chi_{b0}}}\frac{3N_c}{2\pi}\,|C(\mu)|^2\,|R'_{\chi_{b0}}(0,\mu')|^2 \\ & \left[F^2(\mu')\frac{n\cdot v'}{2}\frac{\bar{n}\cdot v}{2}\int\frac{d\omega}{\omega}\frac{d\bar{\omega}}{\bar{\omega}}T\left(\omega,\bar{\omega},\mu,\mu';\,{}^3P_J\right)\phi_A(\bar{\omega},\mu')\phi_A(\omega,\mu')\right]^2\end{aligned} \tag{4.45}$$

and

$$\begin{aligned}\Gamma(\chi_{b2}\to AA) =& \frac{2}{15}\frac{m_D^2\sqrt{m_{\chi_{b2}}^2-4m_D^2}}{8\pi m_{\chi_{b2}}}\frac{3N_c}{2\pi}|C(\mu)|^2\,|R'_{\chi_{b2}}(0,\mu')|^2 \\ & \left[F^2(\mu')\frac{n\cdot v'}{2}\frac{\bar{n}\cdot v}{2}\int\frac{d\omega}{\omega}\frac{d\bar{\omega}}{\bar{\omega}}T\left(\omega,\bar{\omega},\mu,\mu';\,{}^3P_J\right)\phi_A(\bar{\omega},\mu')\phi_A(\omega,\mu')\right]^2\ ,\end{aligned} \tag{4.46}$$

where $A = P, V_L$. For the decay of χ_{b2} into two transversely-polarized vector mesons, one finds the decay rate by summing over the possible transverse polarizations:

$$\Gamma\left(\chi_{b2} \to V_T V_T\right) = \frac{2}{5}\frac{m_D^2\sqrt{m_{\chi_{b2}}^2 - 4m_D^2}}{8\pi m_{\chi_{b2}}}\frac{3N_c}{2\pi}|C\left(\mu\right)|^2\ |R'_{\chi_{b2}}(0,\mu')|^2 \left[F^2(\mu')\frac{n\cdot v'}{2}\frac{\bar{n}\cdot v}{2}\int\frac{d\omega}{\omega}\frac{d\bar{\omega}}{\bar{\omega}}T\left(\omega,\bar{\omega},\mu,\mu';{}^3P_J\right)\phi_{V_T}(\bar{\omega},\mu')\phi_{V_T}(\omega,\mu')\right]^2 . \tag{4.47}$$

In the case of η_b decay into a pseudoscalar and a longitudinally-polarized vector meson, we find

$$\Gamma\left(\eta_b \to PV_L + \text{c.c.}\right) = \frac{m_D^2\sqrt{m_{\eta_b}^2 - 4m_D^2}}{8\pi m_{\eta_b}}\frac{N_c}{2\pi}|C\left(\mu\right)|^2\ |R_{\eta_b}(0,\mu')|^2\,\frac{1}{2}\left[F^2(\mu')\frac{n\cdot v'}{2}\frac{\bar{n}\cdot v}{2}\int\frac{d\omega}{\omega}\frac{d\bar{\omega}}{\bar{\omega}}T\left(\omega,\bar{\omega},\mu,\mu';\,{}^1S_0\right)\left(\phi_{V_L}(\bar{\omega},\mu')\phi_P(\omega,\mu') - \phi_{V_L}(\omega,\mu')\phi_P(\bar{\omega},\mu')\right)\right]^2 . \tag{4.48}$$

Note that we are working in the limit $m_c \to \infty$, where the $m_{D^*} - m_D$ mass splitting vanishes.

The factorized formulas Eqs. (4.35) and (4.45) - (4.48) are the main results of this chapter. Each decay rate of (4.45) - (4.48) depends on two calculable matching coefficients, C and T, and three non-perturbative, process-independent matrix elements, namely, two D-meson distribution amplitudes and the bottomonium wavefunction. In Sec. 4.5 we will provide a model-dependent estimate of the decay rates (4.45) - (4.48) and will discuss the phenomenological implications. We conclude this section by observing that all the non-perturbative matrix elements cancel out in the ratios $\Gamma(\chi_{b0} \to PP)/\Gamma(\chi_{b2} \to PP)$ and $\Gamma(\chi_{b0} \to V_L V_L)/\Gamma(\chi_{b2} \to V_L V_L)$, since the spin symmetry of pNRQCD guarantees $R'_{\chi_{b0}}(0) = R'_{\chi_{b2}}(0)$, at leading order in EFT_{II}. Neglecting the χ_{b0} - χ_{b2} mass difference, we find, up to corrections of order w^2,

$$\Gamma(\chi_{b0} \to AA)/\Gamma(\chi_{b2} \to AA) = \frac{4}{3}\frac{15}{2} = 10\ , \tag{4.49}$$

with $A = P, V_L$.

4.4.2 Running

The dependence of the matching coefficient $T(\omega, \bar{\omega}, \mu, \mu';\, ^{2S+1}L_J)$ and of the operators in Eqs. (4.45) - (4.48) on the scale μ' is driven by a RGE that can be obtained by renormalizing the $\mathrm{EFT_{II}}$ operators. The RGE for the $\mathrm{EFT_{II}}$ operators, which also defines the anomalous dimension $\gamma_{\mathrm{EFT_{II}}}$, is similar to Eq. (4.10),

$$\frac{d}{d\ln\mu'}\left[F^2(\mu')\mathcal{O}_{AB}^{^{2S+1}L_J}(\omega,\bar{\omega},\mu')\right] = \\ -\int d\omega' \int d\bar{\omega}' \gamma_{\mathrm{EFT_{II}}}(\omega,\omega';\bar{\omega},\bar{\omega}';\mu') F^2(\mu') \mathcal{O}_{AB}^{^{2S+1}L_J}(\omega',\bar{\omega}',\mu') \ . \tag{4.50}$$

To calculate the anomalous dimension at one loop, we compute the divergent part of the diagrams in Figs. 4.6 and 4.7. As mentioned in Sec. 4.2, the pNRQCD Lagrangian has the following structure,

$$L_{\mathrm{pNRQCD}} = \int d^3x\, \mathcal{L}_{\mathrm{NRQCD}}^{usoft} + L_{\mathrm{pot}} \ ,$$

where the superscript $usoft$ indicates that the gluons in the NRQCD Lagrangian are purely ultrasoft $(m_b w^2, m_b w^2)$, while L_{pot} contains four-fermions operators, which are non-local in space,

$$L_{\mathrm{pot}} = \int d^3x_1 d^3x_2 \psi^\dagger_\alpha(t,\vec{x}_1)\chi_\beta(t,\vec{x}_2) V_{\alpha\beta,\gamma\delta}(\vec{r}) \chi^\dagger_\gamma(t,\vec{x}_2)\psi_\delta(t,\vec{x}_1) \ .$$

At leading order in $\alpha_s(m_b w)$ and r, V is the Coulomb potential

$$V_{\alpha\beta,\gamma\delta} = \frac{\alpha_s(m_b w)}{r} t^a_{\alpha\delta} t^a_{\gamma\beta} \ .$$

For the explicit form of higher-order potentials, see, for example, Refs. [105, 123]. Vertices from L_{pot} generate one-loop diagrams as the first diagram in Fig. 4.6. However, these diagrams do not give any contribution to the anomalous dimension at one loop. Indeed, the insertion of the Coulomb potential $1/r$ in Fig. 4.6 does not produce UV divergences. Insertions of the $1/m_b$ potentials yield divergences but the coefficient of the $1/m_b$ potential is proportional to $\alpha_s^2(m_b w)$, so it is not relevant if we are content with a NLL resummation. Insertions of $1/m_b^2$ potentials

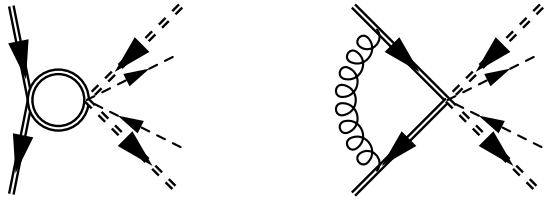

Figure 4.6: One-loop diagrams in pNRQCD. The first diagram contains insertions of quark-antiquark potentials. In the second diagram the gluon is ultrasoft.

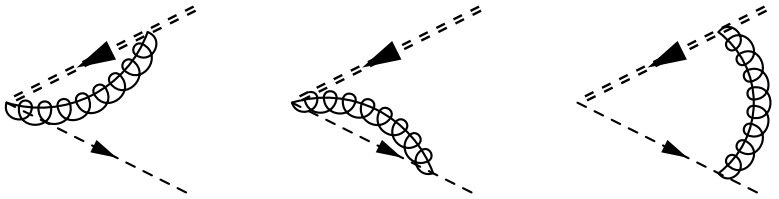

Figure 4.7: One-loop diagrams in bHQET. There are three analogous diagrams for the other copy of bHQET.

give divergences proportional to subleading operators, which can be neglected. The second diagram in Fig. 4.6 yields a result completely analogous to the last term in Eq. (4.13), with the only difference of a color pre-factor,

$$\mathcal{M}_{\rm pNRQCD} = -\frac{\alpha_s}{2\pi}\,\frac{C_F}{\varepsilon}\mathcal{O}_{AB}^{^{2S+1}L_J}(\omega,\bar\omega,\mu)\;. \tag{4.51}$$

This divergence is completely canceled by the b-quark field renormalization constant Z_b, and hence the pNRQCD diagrams in Fig. 4.6 do not contribute to the anomalous dimension at one loop.

On the bHQET side, the third diagram in Fig. 4.7 is convergent, and hence it does not contribute to the anomalous dimension. The first two diagrams give

$$\mathcal{M}_{\rm bHQET,\bar n} = \int d\omega' d\bar\omega' \Delta(\omega,\omega',\,\bar\omega,\bar\omega')\mathcal{O}_{AB}^{^{2S+1}L_J}(\omega',\bar\omega',\mu)\;, \tag{4.52}$$

with

$$\begin{aligned}\Delta(\omega,\omega',\,\bar\omega,\bar\omega') =& \frac{\alpha_s}{2\pi}C_F\delta(\omega-\omega')\left\{\delta\left(\bar\omega-\bar\omega'\right)\left[-\frac{1}{2\varepsilon^2}-\frac{1}{\varepsilon}\ln\left(\frac{\mu' n\cdot v'}{\bar\omega'}\right)+\frac{1}{\varepsilon}\right]\right.\\ &\left.+\,\frac{1}{\varepsilon}\left[\theta\left(\bar\omega-\bar\omega'\right)\left(\frac{1}{\bar\omega-\bar\omega'}\right)_+ + \theta\left(\bar\omega'-\bar\omega\right)\theta\left(\bar\omega\right)\frac{\bar\omega}{\bar\omega'}\left(\frac{1}{\bar\omega'-\bar\omega}\right)_+\right]\right\}\;.\end{aligned} \tag{4.53}$$

The diagrams for the bHQET copy in the n-direction give a result analogous to Eqs. (4.52) and (4.53), with $\bar{\omega} \to \omega$, $\bar{\omega}' \to \omega'$, and $n \cdot v' \to \bar{n} \cdot v$. Extracting $\gamma_{\mathrm{EFT_{II}}}$ from the divergence is again standard, just as we did in the case of $\gamma_{\mathrm{EFT_I}}$. After adding to Eq. (4.53) the bHQET field renormalization constants Z_h and Z_ξ for heavy and light quarks

$$Z_h = 1 + \frac{1}{\varepsilon}\frac{\alpha_s}{2\pi}C_F \ , \qquad Z_\xi = 1 - \frac{1}{\varepsilon}\frac{\alpha_s}{4\pi}C_F \ ,$$

we find

$$\gamma_{\mathrm{EFT_{II}}}(\omega, \omega'; \bar{\omega}, \bar{\omega}'; \mu') = 2\gamma_F \, \delta(\omega - \omega') \, \delta(\bar{\omega} - \bar{\omega}') + \gamma_{\mathcal{O}}(\omega, \omega'; \bar{\omega}, \bar{\omega}'; \mu') \ , \tag{4.54}$$

with

$$\begin{aligned}
&\gamma_{\mathcal{O}}(\omega, \omega'; \bar{\omega}, \bar{\omega}'; \mu') \\
&= \frac{\alpha_s}{4\pi} 4C_F \delta(\omega - \omega') \, \delta(\bar{\omega} - \bar{\omega}') \left[-1 + \ln\left(\frac{\mu' n \cdot v'}{\bar{\omega}'}\right) + \ln\left(\frac{\mu' \bar{n} \cdot v}{\omega'}\right) \right] \\
&- \frac{\alpha_s}{4\pi} 4C_F \delta(\omega - \omega') \left[\theta(\bar{\omega} - \bar{\omega}') \left(\frac{1}{\bar{\omega} - \bar{\omega}'}\right)_+ + \theta(\bar{\omega}' - \bar{\omega}) \, \theta(\bar{\omega}) \, \frac{\bar{\omega}}{\bar{\omega}'} \left(\frac{1}{\bar{\omega}' - \bar{\omega}}\right)_+ \right] \\
&- \frac{\alpha_s}{4\pi} 4C_F \delta(\bar{\omega} - \bar{\omega}') \left[\theta(\omega - \omega') \left(\frac{1}{\omega - \omega'}\right)_+ + \theta(\omega' - \omega) \, \theta(\omega) \, \frac{\omega}{\omega'} \left(\frac{1}{\omega' - \omega}\right)_+ \right] \ .
\end{aligned} \tag{4.55}$$

The term proportional to γ_F in Eq. (4.54) reproduces the running of $F^2(\mu')$ (4.40). $\gamma_{\mathcal{O}}$ is responsible for the running of the D-meson distribution amplitudes and it agrees with the result found in Ref. [128]. Also, in Eq. (4.55) the coefficient of $\ln \mu'$ is proportional to $\Gamma_{\mathrm{cusp}}(\alpha_s)$. Note that, since the bHQET Lagrangian is spin-independent, the anomalous dimension does not depend on the spin or on the polarization of the D meson in the final state, at leading order in the power counting.

Using Eqs. (4.50) and (4.54) we find the following integro-differential RGE for the operator $\mathcal{O}(\omega, \bar{\omega}, \mu')$:

$$\frac{d}{d \ln \mu'} \mathcal{O}(\omega, \bar{\omega}, \mu') = - \int d\omega' \int d\bar{\omega}' \gamma_{\mathcal{O}}(\omega, \omega'; \bar{\omega}, \bar{\omega}'; \mu') \mathcal{O}(\omega', \bar{\omega}', \mu') \ , \tag{4.56}$$

where we have dropped both the subscripts A, B, and the superscript ${}^{2S+1}L_J$, since $\gamma_{\mathcal{O}}$ does not depend on the quantum numbers of the initial or final state.

Using the fact that the convolution of $F^2(\mu')\,T(\omega,\bar\omega,\mu,\mu';\,{}^{2S+1}L_J)$ and the operator $\mathcal{O}_{AB}^{{}^{2S+1}L_J}(\omega,\bar\omega,\mu')$ is μ'-independent, we can write an equation for the coefficient,

$$\begin{aligned}\frac{d}{d\ln\mu'}&[F^2(\mu')\,T(\omega,\bar\omega,\mu,\mu')]\\ &= \int d\omega' \int d\bar\omega' \frac{\omega}{\omega'}\frac{\bar\omega}{\bar\omega'} F^2(\mu')\,T(\omega',\bar\omega',\mu,\mu')\gamma_{\mathcal{O}}(\omega',\omega;\bar\omega',\bar\omega;\mu') \\ &= \int d\omega' \int d\bar\omega' F^2(\mu')\,T(\omega',\bar\omega',\mu,\mu')\gamma_{\mathcal{O}}(\omega,\omega';\bar\omega,\bar\omega';\mu')\ ,\end{aligned} \tag{4.57}$$

where the last line follows from the property of $\gamma_{\mathcal{O}}$ at one loop,

$$\frac{\omega}{\omega'}\frac{\bar\omega}{\bar\omega'}\gamma_{\mathcal{O}}(\omega',\omega;\bar\omega',\bar\omega;\mu') = \gamma_{\mathcal{O}}(\omega,\omega';\bar\omega,\bar\omega';\mu')\ ,$$

as can be explicitly verified from the expression in Eq. (4.55).

Eq. (4.57) can be solved following the methods described in Ref. [128]. We discuss the details of the solution in App. D, where we derive the analytic expressions for $T(\omega,\bar\omega,\mu,\mu';\,{}^3P_J)$ and $T(\omega,\bar\omega,\mu,\mu';\,{}^1S_0)$, with the initial conditions at the scale $\mu_c' = m_c$ expressed in Eq. (4.33).

4.5 Decay Rates and Phenomenology

In Sec. 4.4.1 we gave the factorized expressions for the decay rates (4.45) - (4.48): $\Gamma(\chi_{b0,\,2}\to PP)$, $\Gamma(\chi_{b0,\,2}\to V_LV_L)$, $\Gamma(\chi_{b2}\to V_TV_T)$, and $\Gamma(\eta_b\to PV_L+\text{c.c.})$. In Secs. 4.3.2 and 4.4.2 we exploited the RGEs (4.12) and (4.57) to run the scales μ and μ', respectively, from the matching scales $\mu = 2m_b$ and $\mu' = m_c$ to the natural scales that contribute to the matrix elements, $\mu = m_c$ and $\mu'\sim 1$ GeV, resumming in this way Sudakov logarithms of the ratios $m_c/2m_b$ and $m_c/1$ GeV.

We proceed now to estimate the decay rates (4.45) - (4.48). In order to do so, we need to evaluate the following ingredients: the light-cone distribution amplitudes of the D meson and of the longitudinally- and transversely-polarized D^* mesons, and the wavefunctions of the states η_b and χ_{bJ}. In principle, these non-perturbative objects could be extracted from other η_b, χ_b, and D-meson observables. In the case of the η_b, the value of the wavefunction at the origin can be obtained from a

measurement of the inclusive hadronic width or of the decay rate for the electromagnetic process $\eta_b \to \gamma\gamma$, since they are both proportional to $|R_{\eta_b}(0)|^2$. Unfortunately, at the moment there are not sufficient data on η_b decays. Another way to proceed is to use the spin symmetry of the leading-order pNRQCD Hamiltonian, which implies $R_{\eta_b}(0) = R_\Upsilon(0)$, and to extract the Upsilon wavefunction from $\Gamma(\Upsilon \to e^+e^-) = 1.28 \pm 0.07$ KeV [129]. Using the leading-order expression for $\Gamma(\Upsilon \to e^+e^-)$ [130], one finds $|R_\Upsilon(0)|^2 = 6.92 \pm 0.38\,\mathrm{GeV}^3$, where the error only includes the experimental uncertainty. The above value is in good agreement with the lattice evaluation by Bodwin, Sinclair, and Kim [131] and it falls within the range of values obtained with four different potential models, as listed in Ref. [132].

$|R'_{\chi_{b0,\,2}}(0)|^2$ can be obtained from the electromagnetic decay $\chi_{b0,2} \to \gamma\gamma$. Unfortunately, such decay rates have not been measured yet. The values listed in Ref. [132] range from a minimum of $|R'_{\chi_{bJ}}(0)|^2 = 1.417$ GeV^5, obtained with the Buchmuller-Tye potential [133], to a maximum of $|R'_{\chi_{bJ}}(0)|^2 = 2.067$ GeV^5, obtained with a Coulomb-plus-linear potential. The lattice value is roughly of the same size, $|R'_{\chi_{bJ}}(0)|^2 = 2.3$ GeV^5, with an uncertainty of about 15% [131]. We use this value in our estimate.

For the pseudoscalar D-meson distribution amplitude we use two model functions widely adopted in the study of B physics. A first possible choice, suggested for example in Ref. [128], is a simple exponential decay:

$$\phi_{P,0}^{\mathrm{Exp}}(\omega, \mu' = 1\mathrm{GeV}) = \theta(\omega)\frac{\omega}{\lambda_\mathrm{D}^2}\exp\left(-\frac{\omega}{\lambda_\mathrm{D}}\right) . \tag{4.58}$$

Another form, suggested in Ref. [134], is

$$\phi_{P,0}^{\mathrm{Braun}}(\omega, \mu' = 1\,\mathrm{GeV}) = \theta(\tilde{\omega})\frac{4}{\lambda_D \pi}\frac{\tilde{\omega}}{1+\tilde{\omega}^2}\left[\frac{1}{1+\tilde{\omega}^2} - \frac{2(\sigma_D - 1)}{\pi^2}\ln\tilde{\omega}\right] , \tag{4.59}$$

where $\tilde{\omega} = \omega/\mu'$. The theta function in Eqs. (4.58) and (4.59) reflects the fact that the distribution amplitudes $\phi_A(\omega, \mu')$, with $A = \{P, V_L, V_T\}$, have support on $\omega > 0$ [135].

The subscript 0 indicates that these functional forms are valid in the D-meson rest frame, with a HQET velocity-label $v_0 = (1, 0, 0, 0)$. With the definition we

adopt in Eq. (4.36), the distribution amplitude is not boost-invariant and in the bottomonium rest frame, in which the D meson has a velocity $(n\cdot v, \bar{n}\cdot v, 0) \sim (m_c/2m_b, 2m_b/m_c, 0)$, it becomes

$$\phi_P(\omega,\mu') = \frac{1}{\bar{n}\cdot v}\phi_{P,0}\left(\frac{\omega}{\bar{n}\cdot v},\mu'\right) \ , \tag{4.60}$$

as shown in App. E. λ_D and σ_D in Eqs. (4.58) and (4.59) are, respectively, the first inverse moment and the first logarithmic moment of the D-meson distribution amplitude in the D-meson rest frame,

$$\lambda_D^{-1}(\mu') = \int_0^\infty \frac{d\omega}{\omega}\phi_{P,0}(\omega,\mu') \ ,$$

$$\sigma_D(\mu')\lambda_D^{-1}(\mu') = -\int_0^\infty \frac{d\omega}{\omega}\ln\left(\frac{\omega}{\mu'}\right)\phi_{P,0}(\omega,\mu') \ .$$

Furthermore we assume that the vector-meson distribution amplitudes $\phi_{V_L}(\omega)$ and $\phi_{V_T}(\omega)$ have the same functional form as $\phi_P(\omega)$, but with different parameters $\lambda_{D_L^*}$, $\sigma_{D_L^*}$ and $\lambda_{D_T^*}$, $\sigma_{D_T^*}$.

The D-meson distribution amplitude and its moments have not been intensively studied unlike, for example, the B-meson distribution amplitude. Therefore, we invoke heavy-quark symmetry and use the moments of the B-meson distribution amplitude in order to estimate the decay rate. However, the value of λ_B is affected by a noticeable uncertainty. Using QCD sum rules, Braun *et al.* estimated [134] $\lambda_B(\mu' = 1\,\text{GeV}) = 0.460 \pm 0.110$ GeV, where the uncertainty is about 25%. Other authors [136, 137, 138] give slightly different central values and comparable uncertainties, so that λ_B falls in the range $0.350\ \text{GeV} < \lambda_B < 0.600$ GeV. The first logarithmic moment σ_D is given in Ref. [134], $\sigma_D = \sigma_B(\mu' = 1\,\text{GeV}) = 1.4 \pm 0.4$. We assume that the moments of the D^*-meson distribution amplitudes fall in the same range as the moments of $\phi_P(\omega)$.

We evaluate numerically the convolution integrals in Eqs. (4.45) - (4.48). We choose the matching scales μ_b and μ_c' to be $2m_b$ and m_c respectively. Using the RGEs we run the matching coefficients down to the scales $\mu = m_c$ and $\mu' = 1$ GeV.

For the b and c quark masses we adopt the 1S mass definition [139],

$$\begin{aligned} m_b(1S) &= \frac{m_\Upsilon}{2} = 4730.15 \pm 0.13 \text{ MeV} , \\ m_c(1S) &= \frac{m_{J/\psi}}{2} = 1548.46 \pm 0.01 \text{ MeV} . \end{aligned} \tag{4.61}$$

The values of α_s at the relevant scales are [129] $\alpha_s(2m_b) = 0.178 \pm 0.005$, $\alpha_s(m_c) = 0.340 \pm 0.020$, and $\alpha_s(1\,\text{GeV}) \sim 0.5$. With these choices, the value of g in Eq. (D.5) is $g(m_c, 1\,\text{GeV}) = -0.12 \pm 0.02$.

The decay rates $\Gamma(\chi_{bJ} \to AA)$ with $A = \{P, V_L, V_T\}$, (4.45) - (4.47), depend on the masses of the χ_{bJ} and of the D mesons, whose most recent values are reported in Ref. [129]. Since the effects due to the mass splitting of the χ_{bJ} and D multiplets are subleading in the EFT power counting, we use in the evaluation the average mass of the χ_{bJ} multiplet and the average mass of D and D^* mesons: $m_{\chi_{bJ}} = 9898.87 \pm 0.28 \pm 0.31$ MeV and $m_D = 1973.27 \pm 0.18$ MeV. Therefore, the velocity of the D mesons in χ_{bJ} decay is $\bar{n} \cdot v = n \cdot v' = m_{\chi_{bJ}}/m_D = 5.02$, with negligible error. The decay rate $\Gamma(\eta_b \to PV_L + \text{c.c.})$ (4.48) depends on the mass of the η_b, which has been recently measured: $m_{\eta_b} = 9388.9^{+3.1}_{-2.3} \pm 2.7$ MeV [116]. The velocity of the D meson in the η_b decay is $\bar{n} \cdot v = n \cdot v' = m_{\eta_b}/m_D = 4.76$, again with negligible error.

The decay rate $\Gamma(\chi_{b0} \to PP)$ (4.45), obtained with ϕ^{Exp} and ϕ^{Braun} separately, is shown in Fig. 4.8. In order to see the impact of resumming Sudakov logarithms, we show for both distribution amplitudes the results with (i) the LL and NLL resummations and (ii) without any resummation at all. In the plots, we call the resummed results NLL-resummed, indicating that Sudakov logarithms are resummed up to NLL. For both distribution amplitudes the resummation does have a relevant effect on the decay rate. In the case of ϕ^{Exp} the resummation decreases the decay rate by a factor of $2 - 1.5$ as λ_D goes from the lowest to the highest value under consideration. In the case of ϕ^{Braun} the decay rate decreases too, for example, by a factor 1.5 when $\sigma_D = 1.4$. In Fig. 4.9 we compare the decay rates obtained with the two distribution amplitudes. Over the range of λ_D we are considering the two decay rates are in rough agreement with each other.

Figs. 4.8 - 4.9 also describe the relation between the decay rate $\Gamma(\chi_{b0} \to V_L V_L)$

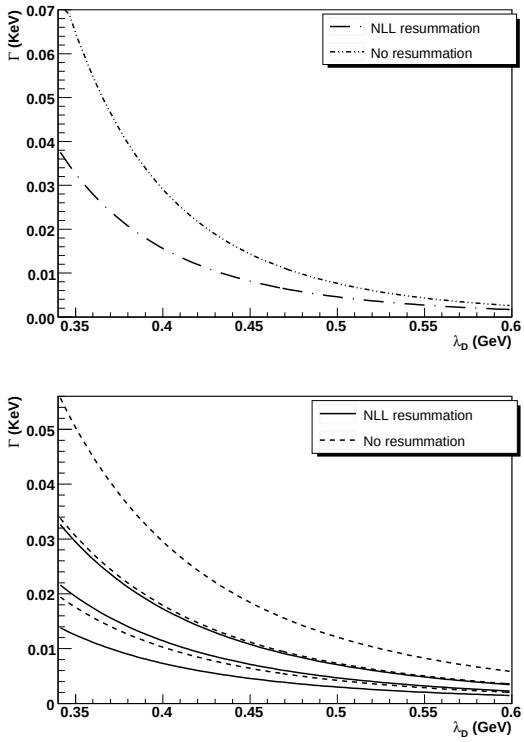

Figure 4.8: $\Gamma(\chi_{b0} \to PP)$ as a function of λ_D, calculated with the distribution amplitudes $\phi^{\rm Exp}$ (*top*) and $\phi^{\rm Braun}$ (*bottom*). The dash dotted and solid lines denote the NLL-resummed decay rate. For comparison, the decay rate without resummation is also shown, denoted by dash double-dotted (*top*) and dashed (*bottom*) lines. For $\phi^{\rm Braun}$ we vary the parameter σ_D from $\sigma_D = 1$ (lower curve) to $\sigma_D = 1.4$ (middle curve) to $\sigma_D = 1.8$ (upper curve).

and $\lambda_{D_L^*}$. According to Eqs. (4.46) and (4.47), the processes $\chi_{b2} \to PP$, $\chi_{b2} \to V_L V_L$, and $\chi_{b2} \to V_T V_T$ show an analogous dependence on the first inverse moments of the light-cone distribution amplitudes, and they differ from Figs. 4.8 - 4.9 by constant pre-factors. Therefore, we do not show explicitly their plots.

Qualitatively, Figs. 4.8 - 4.9 show a dramatic dependence of the decay rate on the inverse moment λ_D. Using Eqs. (4.45), (4.60) and (D.16), one can show that when $\phi^{\rm Braun}$ is used, the decay rate is proportional to λ_D^{-4}, while it scales as λ_D^{-6-4g} when we adopt $\phi^{\rm Exp}$, with g defined in Eq. (D.5). As a consequence, the decay rate drops by an order of magnitude when λ_D goes from 0.350 GeV to 0.600 GeV. The particular sensitivity of exclusive bottomonium decays into two charmed mesons to

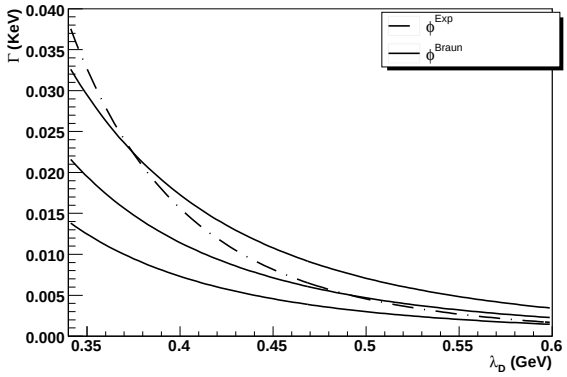

Figure 4.9: $\Gamma(\chi_{b0} \to PP)$ as a function λ_D. The dash dotted line denotes the decay rate calculated with $\phi^{\rm Exp}$, while the three solid lines with $\phi^{\rm Braun}$. For $\phi^{\rm Braun}$ we vary the value of the parameter σ_D from $\sigma_D = 1$ (lower curve) to $\sigma_D = 1.4$ (middle curve) to $\sigma_D = 1.8$ (upper curve).

the light-cone structure of the D meson —much stronger than usually observed in D- and B-decay observables— is due to the dependence of the amplitude on the product of two distributions (one for each meson) and to the non-trivial dependence of the matching coefficient T on the light-quark momentum labels ω and $\bar{\omega}$ at tree level. On one hand, the strong dependence on a relatively poorly known quantity prevents us from predicting the decay rate $\Gamma(\chi_{b0} \to DD)$. On the other hand, however, it suggests that, if the decay rate is measured, this channel could be used to better determine interesting properties of the D-meson distribution amplitude, such as λ_D and σ_D. The viability of this suggestion relies on the control over the theoretical error attached to the curves in Fig. 4.8 and on the actual chances to observe the process $\chi_b \to DD$ at current experiments.

The uncertainty of the decay rate stems mainly from three sources. First, there are corrections coming from subleading EFT operators. In matching NRQCD + SCET onto pNRQCD + bHQET (Sec. 4.4.1), we neglected the subleading $\mathrm{EFT_{II}}$ operators that are suppressed by powers of $\Lambda_{\rm QCD}/m_c$ and w^2, relative to the leading $\mathrm{EFT_{II}}$ operators in Eqs. (4.31) and (4.32). In matching QCD onto NRQCD+SCET (Sec. 4.3.1), we kept only $J_{\mathrm{EFT_I}}$ (4.6) and neglected subleading $\mathrm{EFT_I}$ operators, suppressed by powers of λ and w^2. These subleading $\mathrm{EFT_I}$ operators would match

onto subleading $\mathrm{EFT_{II}}$ operators, suppressed by powers of $\Lambda_{\mathrm{QCD}}/m_c$ and w^2. Using $w^2 \sim 0.1$ and $\Lambda_{\mathrm{QCD}}/m_c \sim 0.3$, we find a conservative estimate for the non-perturbative corrections to be about 30%.

Second, there are perturbative corrections to the matching coefficients C and T. Since $\alpha_s(2m_b) = 0.178$, we expect a 20% correction from the one-loop contributions in matching QCD onto NRQCD + SCET. In the second matching step, similarly, the one-loop corrections to $T(\omega, \bar{\omega}, \mu, \mu';\, ^{2S+1}L_J)$ would be proportional to $\alpha_s(m_c) \sim 30\%$. We can get an idea of their relevance by estimating the dependence of the decay rate (4.45) on the matching scales μ_b and μ_c'. If the matching coefficients C and T and the anomalous dimensions $\gamma_{\mathrm{EFT_I}}$ and $\gamma_{\mathcal{O}}(\omega, \omega', \bar{\omega}, \bar{\omega}'; \mu')$ were known at all orders, the decay rate would be independent of the matching scales μ_b and μ_c'. However, since we only know the first terms in the perturbative expansions, the decay rate bears a residual renormalization-scale dependence, whose size is determined by the first neglected terms.

In Fig. 4.10 we show the effect of varying μ_b between $4m_b \sim 20$ GeV and $m_b \sim 5$ GeV on the decay rate, using ϕ^{Braun}. The solid line represents the choice $\mu_b = 2m_b$, while the dashed and dotted lines, which overlap almost perfectly, correspond respectively to $\mu_b = 20$ GeV and $\mu_b = 5$ GeV. The dependence on μ_b is mild, its effect being a variation of about 5%. We obtain analogous results for the decay rate computed with ϕ^{Exp}, which are not shown here in order to avoid redundancy.

On the other hand, even after the resummation, the decay rate strongly depends on μ_c'. We vary this scale between 1.2 GeV and 2.5 GeV and we observe an overall variation of about 50%. We expect the scale dependence to be compensated by the one-loop corrections to the matching coefficient $T(\omega, \bar{\omega}, \mu, \mu';\, ^3P_J)$. This observation is reinforced by the fact that the numerical values of the running factors $U(\mu_b, \mu)$ and $V(\mu_c', \mu')$ (defined respectively in Eqs. (4.26) and (D.6)) at NLL accuracy are smaller than expected on the basis of naive counting of the logarithms. As a consequence, the next-to-leading-order corrections to the matching coefficient could be as large as the effect of the NLL resummation. In the light of Fig. 4.10, the one-loop correction to $T(\omega, \bar{\omega}, \mu, \mu';\, ^3P_J)$ seems to be an important ingredient for a reliable estimate of

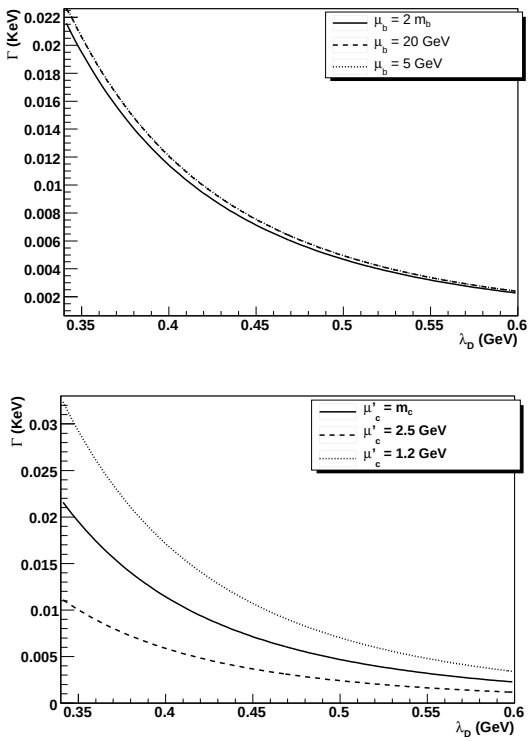

Figure 4.10: *Top*: Scale dependence of $\Gamma(\chi_{b0} \to PP)$ on the matching scale μ_b. We vary μ_b from a central value $\mu_b = 2m_b$ (solid line) to a maximum of $\mu_b = 20$ GeV (dashed line) and a minimum of $\mu_b = 5$ GeV (dotted line). The dashed and dotted lines overlap almost perfectly. *Bottom*: Scale dependence of $\Gamma(\chi_{b0} \to PP)$ on the matching scale μ_c'. We varied μ_c' from a central value of $\mu_c' = m_c$ (solid line) to a maximum of $\mu_c' = 2.5$ GeV (dashed line) and a minimum of $\mu_c' = 1.2$ GeV (dotted line).

the decay rate.

A third source of error comes from the unknown functional form of the D-meson distribution amplitude. For the study of the B-meson shape function, an expansion in a complete set of orthonormal functions has recently been proposed and it has provided a systematic procedure to control the uncertainties due to the unknown functional form [140]. The same method should be generalized to the B- and D-meson distribution amplitudes, in order to reduce the model dependence of the decay rate. We leave such an analysis to future work.

To summarize, the calculation of the one-loop matching coefficients and the

inclusion of power corrections of order $\Lambda_{\rm QCD}/m_c$ appear to be necessary to provide a decay rate with an accuracy of 10%, that would make the decays $\chi_{bJ} \to D^+D^-$, $\chi_{bJ} \to D^0\bar{D}^0$ competitive processes to improve the determination of λ_D and σ_D, if the experimental decay rate is observed with comparable accuracy.

We estimate the decay rate $\Gamma(\eta_b \to PV_L + \text{c.c.})$ (4.48) using $\phi^{\rm Exp}$ and $\phi^{\rm Braun}$ for both ϕ_P and ϕ_{V_L}. In the limit $m_c \to \infty$, spin symmetry of the bHQET Lagrangian would imply the equality of the pseudoscalar and vector distribution amplitudes, $\phi_P = \phi_{V_L}$, and hence the vanishing of the decay rate $\Gamma(\eta_b \to PV_L + \text{c.c.})$. Assuming spin-symmetry violations, the decay rate depends on (i) the two parameters $\bar{\lambda}_D = (\lambda_D + \lambda_{D_L^*})/2$ and $\delta = (\lambda_{D_L^*} - \lambda_D)/(\lambda_D + \lambda_{D_L^*})$, if $\phi^{\rm Exp}$ is used, and on (ii) three parameters $\bar{\lambda}_D$, δ, and $|\sigma_{D_L^*} - \sigma_D|$, if $\phi^{\rm Braun}$ is used.

The two plots in the left column of Fig. 4.11 show the decay rate, computed with $\phi^{\rm Exp}$, as a function of $\bar{\lambda}_D$ with δ adopting various values, and as a function of δ with $\bar{\lambda}_D$ now being the parameter. In the right column, the decay rate computed with $\phi^{\rm Braun}$ is shown. Since in this case the decay rate does not strongly depend on δ, we fix it at $\delta = 0$ and we show the dependence of the decay rate on $\bar{\lambda}_D$ and $|\sigma_{D_L^*} - \sigma_D|$. We "normalize" the difference between the first logarithmic moments by dividing them by $\sigma = 2\sigma_D$.

The most striking feature of Fig. 4.11 is the huge sensitivity to the chosen functional form. Though a precise comparison is difficult, due to the dependence on different parameters, the decay rate increases by two orders of magnitude when we switch from $\phi^{\rm Exp}$ to $\phi^{\rm Braun}$. Once again, this effect hinders our ability to predict $\Gamma(\eta_b \to PV_L + \text{c.c.})$ but it opens up the interesting possibility to discriminate between different model distribution amplitudes.

Using Eqs. (4.48) and (D.17), we know that $\Gamma(\eta_b \to PV_L + \text{c.c.})$ goes like $\bar{\lambda}_D^{-4-4g}$ when $\phi^{\rm Exp}$ used or $\bar{\lambda}_D^{-4}$ when $\phi^{\rm Braun}$ used. Fig. 4.11 appears to confirm this strong dependence on $\bar{\lambda}_D$. The plots in the lower half of Fig. 4.11 reflect the fact that the decay rate vanishes if one assumes $\phi_P(\omega) = \phi_{V_L}(\omega)$.

We conclude this section with the determination of the branching ratios $\mathcal{B}(\chi_{b0} \to PP) = \Gamma(\chi_{b0} \to PP)/\Gamma(\chi_{b0} \to \text{light hadrons})$ and $\mathcal{B}(\eta_b \to PV_L + \text{c.c.}) = \Gamma(\eta_b \to$

$PV_L + \text{c.c.})/\Gamma(\eta_b \to \text{light hadrons})$. At leading order in pNRQCD, the only non-perturbative parameter involved in the inclusive decay width of the η_b is $|R_{\eta_b}(0)|^2$ [99],

$$\Gamma(\eta_b \to \text{light hadrons}) = \frac{2\text{Im}f_1(^1S_0)}{m_b^2}\frac{N_c}{2\pi}|R_{\eta_b}(0)|^2 \,. \tag{4.62}$$

Therefore, $\mathcal{B}(\eta_b \to PV_L + \text{c.c.})$ does not depend on the quarkonium wavefunction and the only non-perturbative parameters in $\mathcal{B}(\eta_b \to PV_L + \text{c.c.})$ are those describing the D-meson distribution amplitudes.

For P-wave states, the inclusive decay rate was obtained in Refs. [99, 141], where the contributions of the configurations in which the quark-antiquark pair is in a color-octet S-wave state were first recognized. In pNRQCD the inclusive decay rate is written as [142, 143]

$$\Gamma(\chi_{b0} \to \text{light hadrons}) = \frac{1}{m_b^4}\frac{3N_c}{\pi}|R'_{\chi_b}(0)|^2\left[\text{Im}f_1(^3P_0) + \frac{1}{9N_c^2}\text{Im}f_8(^3S_1)\mathcal{E}\right] \,, \tag{4.63}$$

where the color-octet matrix element has been expressed in terms of the heavy quarkonium wavefunction and of the gluonic correlator $\mathcal{E}$, whose precise definition is given in Ref. [142]. $\mathcal{E}$ is a universal parameter and is completely independent of any particular heavy quarkonium state under consideration. Its value has been obtained by fitting to existing charmonium data and, thanks to the universality, the same value can be used to predict properties of bottomonium decays. It is found in Ref. [142] $\mathcal{E} = 5.3\,^{+3.5}_{-2.2}$. The matching coefficients in Eqs. (4.62) and (4.63) are known to one loop. For the updated value we refer to Ref. [144] and references therein. For reference, the tree-level values of the coefficients are as follows [99]:

$$\begin{aligned} &\text{Im}f_1(^1S_0) = \alpha_s^2(2m_b)\pi\frac{C_F}{2N_c} \,, \quad \text{Im}f_1(^3P_0) = 3\alpha_s^2(2m_b)\pi\frac{C_F}{2N_c} \,, \\ &\text{Im}f_8(^3S_1) = \frac{n_f}{6}\alpha_s^2(2m_b)\pi \,. \end{aligned} \tag{4.64}$$

With the above parameters, we plot $\mathcal{B}(\chi_{b0} \to PP)$ and $\mathcal{B}(\eta_b \to PV_L + \text{c.c.})$ as a function of λ_D and $\bar{\lambda}_D$, respectively, in Fig. 4.12. Over the range of λ_D we are considering, $\mathcal{B}(\chi_{b0} \to PP)$ varies between $4 \cdot 10^{-5}$ and $4 \cdot 10^{-6}$; it is approximately one or two orders of magnitude smaller than the branching ratios observed in Ref.

[117] for χ_{bJ} decays into light hadrons. $\mathcal{B}(\eta_b \to PV_L + \text{c.c.})$ depends on the choice of the distribution amplitude. Choosing the parameterization ϕ^{Braun} (4.59), it appears that, despite the suppression at $|\sigma_{D_L^*} - \sigma_D| = 0$, $\mathcal{B}(\eta_b \to PV_L + \text{c.c.})$ assumes values comparable to $\mathcal{B}(\chi_{b0} \to PP)$ even for a small deviation from the spin-symmetry limit. If ϕ^{Exp} is chosen, the branching ratio is suppressed over a wide range of $|\sigma_{D_L^*} - \sigma_D|$. The branching ratio $\mathcal{B}(\eta_b \to PV_L + \text{c.c.})$ was first estimated in [145]. The authors of [145] assumed that the exclusive decays into DD^* dominate the inclusive decay into charm, $\Gamma(\eta_b \to PV_L + \text{c.c.}) \sim \Gamma(\eta_b \to c\bar{c} + X)$. With this assumption, they estimated the branching ratio to be in the range $10^{-3} < \mathcal{B}(\eta_b \to PV_L + \text{c.c.}) < 10^{-2}$. Our analysis shows that such an assumption does not appear to be justified in the range of $\bar{\lambda}_D$ considered in Fig. 4.12, while it would be appropriate for smaller values of the first inverse moments, for example for $\bar{\lambda}_D \sim 0.200$ GeV if the distribution amplitudes are described by ϕ^{Braun}.

Our estimates indicate that observing the exclusive processes $\eta_b \to DD^* + \text{c.c.}$ and $\chi_b \to DD$ would be extremely challenging. A preliminary analysis for $\chi_b \to D^0\bar{D}^0$ [146] suggests that the number of $\Upsilon(2S)$ produced at BABAR allows for the measurement of a branching ratio $\mathcal{B}(\chi_{b0} \to D^0\bar{D}^0) \sim 10^{-3}$, which is two or three orders of magnitude bigger than the values in Fig. 4.12. An even bigger branching ratio would be required for the smaller $\Upsilon(2S)$ sample of CLEO. However, we stress once again the strong dependence of the decay rates on the values of the first inverse moments. In particular, our estimates rely on the relation $\lambda_D = \lambda_B$, which is valid in the limit of $m_b, m_c \to \infty$; even small corrections to the heavy flavor symmetry, if they had the effect of shifting the value of λ_D towards the range $0.250 - 0.350$ GeV, could considerably increase the branching ratios.

4.6 Conclusions

In this chapter we have analyzed the exclusive decays of the C-even bottomonia into a pair of charmed mesons. We approached the problem using a series of EFTs that lead to the factorization formulas for the decay rates (Eqs. (4.45) - (4.48)),

valid at leading order in the EFT power counting and at all orders in α_s. We improved the perturbative results by resumming Sudakov logarithms of the ratios of the characteristic scales that are germane to the dynamics of the processes.

The decay rates (4.45) - (4.48) receive both perturbative and non-perturbative corrections. Perturbative corrections come from loop corrections to the matching coefficients C and T, which are respectively of order $\alpha_s(2m_b) \sim 0.2$ and $\alpha_s(m_c) \sim 0.3$. The largest non-perturbative contribution could be as big as $\Lambda_{\rm QCD}/m_c$, which would amount approximately to a 30% correction. Therefore, corrections to the leading-order decay rates could be noticeable, as the strong dependence of the decay rates on the renormalization-scale μ_c' suggests. However, the EFT approach shown in this chapter allows for a systematic treatment of both perturbative corrections and power-suppressed operators, so that, if the experimental data require, it is possible to extend the present analysis beyond the leading order.

For simplicity, we have focused in this chapter on the decays of C-even bottomonia, in which cases the decays proceed via two intermediate gluons and both the matching coefficients C and T are non-trivial at tree level. The same EFT approach can be applied to the decays of C-odd states, in particular, to the decays $\Upsilon \to DD$ and $\Upsilon \to D^*D^*$, with the complication that the matching coefficient T arises only at one-loop level. Moreover, the same EFT formalism developed in this chapter can be applied to the study of the channels that have vanishing decay rates at leading order in the power counting, such as $\eta_b \to D^*D^*$, $\Upsilon \to DD^* + \text{c.c.}$, and $\chi_{b2} \to DD^* + \text{c.c.}$. Experimental data for the charmonium system show that, for the decays of charmonium into light hadrons, the expected suppression of the subleading twist processes is not seen. It is interesting to see whether such an effect appears in bottomonium decays into two charmed mesons, using the EFT approach of this chapter to evaluate the power-suppressed decay rates.

Finally, in Sec. 4.5 we used model distribution amplitudes to estimate the decay rates. The most evident, qualitative feature of the decay rates is the strong dependence on the parameters of the D-meson distribution amplitude. Even though this feature may prevent us from giving reliable estimates of the decay rates or of

the branching ratios, it makes the channels analyzed here ideal candidates for the extraction of important D-meson parameters, when the branching ratios can be observed with sufficient accuracy.

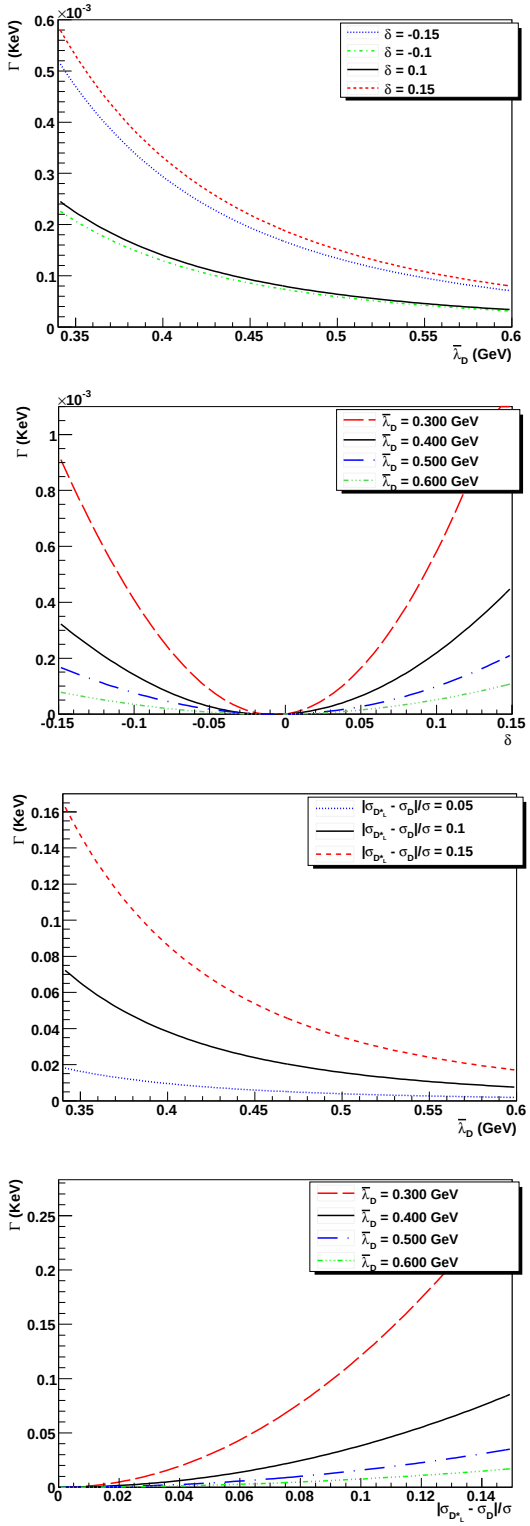

Figure 4.11: *First two*: $\Gamma(\eta_b \to PV_L + \text{c.c.})$ as a function of λ_D and δ, computed using exponential distribution amplitudes ϕ_P^{Exp} and $\phi_{V_L}^{\text{Exp}}$. *Last two*: $\Gamma(\eta_b \to PV_L + \text{c.c.})$ as a function of λ_D and $|\sigma_{D_L^*} - \sigma_D|/\sigma$, computed with the Braun distribution amplitudes ϕ_P^{Braun} and $\phi_{V_L}^{\text{Braun}}$.

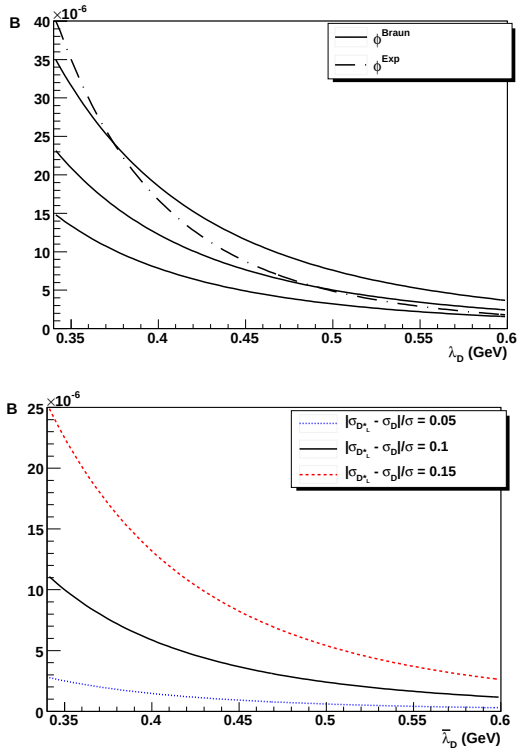

Figure 4.12: Branching ratios $\mathcal{B}(\chi_{b0} \to PP)$ (*top*) and $\mathcal{B}(\eta_b \to PV_L + \text{c.c.})$ (*bottom*). The latter is computed using the distribution amplitude ϕ^{Braun}.

CHAPTER 5

CONCLUSION

In this dissertation, Effective Field Theory was applied to the study of problems at the intersection of nuclear and particle physics, which span many different energy scales.

In Chapter 1, we introduced ChPT, an EFT that successfully describes strong interactions of mesons at low energies. The chiral Lagrangian was constructed based on a non-linear realization of chiral symmetry of QCD and its breaking. We described the power counting for general processes including pions and photons that allows for a systematic truncation of the Lagrangian and of the observables. Nonetheless, in some problems, perturbation theory is spoiled by the appearance of non-perturbative effects, as in Chapter 2 and as in Chapter 3, or by the appearance of large logarithms, as in Chapter 4. We analyzed the three EFT frameworks corresponding to each of the three different cases.

In the first application, Chapter 2, we presented an attempt to broaden ChPT to momenta of the order of the masses of vector mesons, such as the rho. We included vector mesons in a low-energy EFT that has an assumed symmetry of QCD, vector symmetry, larger than chiral symmetry. Such symmetry has a limit, called vector limit, where the rhos are massless, as are the pions. We built the most general effective Lagrangian, associated with local $U(1)$ symmetry plus vector symmetry and its breaking, to accommodate pions, rhos and photons, where the last two were introduced as spurious fields. The interesting observation here is that the photon-rho mixed only via their field strenghts, as in VMD-1. We investigated $\pi\pi$ elastic scattering and e^+e^- annihilation into $\pi^+\pi^-$ in the window around the rho resonance. The rho resonance is a non-perturbative effect that gives rise to large cross sections, in the processes considered, when momenta are of the order of m_ρ. We treated the rho mass as a scale of the same order of the pion mass, and performed a power

counting within the window, which allows the research on hadronic physics in the kinematic region around the rho peak. We showed that the rho propagator had to be resummed, accounting for the width incorporation.

Unfortunately, after we compared the results from vector EFT to experimental data, the LO partial decay width of the rho into two pions is rather small, about 52% off from the experimental result found in Ref. [14], even though the rho mass had only 0.7% error compared to value found in the same reference. An analysis with respect to modifications on the decay width proved the sensitivity of the cross sections with the rho width. We believe that NLO calculations will greatly improve the rho widths as well as the comparison of the vector EFT results to data.

Experimental data of $e^+e^- \to \pi^+\pi^-$ cross section show an extra little peak around the ω meson, whose mass is very close to the rho mass. It would be interesting to extend vector EFT to include $SU(3)_L \times SU(3)_{G_L} \times SU(3)_R \times SU(3)_{G_R}$ symmetry and see if improvements in the results can be extracted from data.

In Chapter 3, we examined another aspect of non-perturbative dynamics in EFT. Several derivative counterterms are needed to renormalize the nucleon-nucleon amplitude already at leading order. We studied the possibility of substituting such counterterms by the potential generated by auxiliary fields, mainly those with quantum numbers of isovector vector and isovector pseudovector mesons. The needed of several derivative counterterms arised, in the first place, because of the inconsistency of the ChPT power counting with RGI, related to the non-perturbative singularity, $1/r^3$, from the one-pion exchange. The non-relativistic Lagrangian involving nucleons, pions and auxiliary fields has enough terms to produce a leading-order NN potential in the $N_c \to \infty$ limit. We proved that a combination of the coupling constants of pions and auxiliary fields to nucleons cancels the singularity. Even though we did not show explicitly the power counting for the non-perturbative singular potential, it is important to check its correctness by running an RG analysis, as will be attempted in the future.

The resultant potential should be fitted to NN scattering data. In the shallow deuteron, the long-range components of the potential could be treated per-

turbatively. Only part of the short-range interactions need to be included non-perturbatively in the Schrödinger equation. We thus solved exactly for the short-range interaction to find the zeroth-order binding energy of the deuteron. The long-range interaction from OPE was treated in perturbation theory to find first corrections. Once the fit to NN scattering data is performed, the deuteron binding energy can be predicted.

In our third example, illustrated in Chapter 4, we used a combination of various EFTs, such as HQET, NRQCD and SCET, to investigate the exclusive decays of a non-relativistic bound state, χ_b or η_b, into a pair of highly energetic massive D mesons. The combination of two non-relativistic EFTs, NRQCD and potential NRQCD, was used to describe the initial state, while two EFTs applied for fast moving massive fields, SCET and boosted HQET, described the final state. Thanks to the EFT approach, the decay rates can be written, in a factorized way, as a function of two perturbative matching coefficients and three non-perturbative matrix elements, two for the D mesons and one for the bottomonium. To improve perturbation theory, we resummed large logarithms of the ratio of the scales in the problem, $2m_b$ and m_c, by evolving the matching coefficients, through renormalization group equation, from these scales to the non-perturbative matrix element (low) scale.

Our results for the branching ratios were very small, but did strongly depend on the D-meson distribution amplitude, whose perturbative and non-perturbative corrections still need to be included. Studying this process lead us to familiarize with various EFT techniques, such as those of the most important, again HQET, NRQCD and SCET, and apply to study processes containing fast-moving, but massive, particles.

The main lesson we draw from this dissertation is that EFTs can be developed to tackle non-perturbative phenomena. Sometimes an adaptation of the power counting to non-perturbative region is enough to describe the processes of interest, as is the case around a resonance. It is very important to check renormalization-group invariance, since a simple power counting based on naive dimensional analysis can

fail, as for singular potentials. With a consistent power counting, even quite complex processes such as the decays of heavy hadrons can be accounted for by EFT. One can apply EFT to systematically solve non-perturbative systems.

APPENDIX A

CONNECTION BETWEEN VECTOR EFT AND CHIRAL PERTURBATION THEORY

Here we show that, for processes where the typical momentum is small, $Q \ll m_\rho$, one can recover ChPT [18, 38, 39] from Vector EFT. We do this explicitly only for interactions in the LO Lagrangian, since those are sufficient for the analysis carried out in the main text. The procedure here can, of course, be pursued to any order.

As one can see in Sect. 1.2, low-energy observables that involve pions and photons can be calculated in LO from tree-level diagrams stemming from $\mathcal{L}^{(0)}_{\rm ChPT}$. In Vector EFT, the same is true for the $\mathcal{L}^{(0)}$ of Sect. 2.2, as no resummations of the type discussed in Sects. 2.3 and 2.4 are needed away from the rho peak. The rho contributions account for the difference in structure between Eqs. (1.57) and (2.37).

Let us first consider $\pi\pi \to \pi\pi$, in the notation of Sect. 2.5.1. The relevant LO tree-level diagrams in ChPT and Vector EFT are shown in Fig. A.1. While in ChPT there is just a four-pion vertex, in Vector EFT there is not only a different four-pion vertex, but also contributions from the rho is s, t, and u channels. In Vector EFT, the LO amplitude is given by Eq. (2.78) with

$$A^{(0)}(s,t,u) = B^{(0)}(t,u,s) = C^{(0)}(u,s,t) = \frac{1}{4f_\pi^2}\left(s + \frac{s-u}{1-t/m_\rho^2} + \frac{s-t}{1-u/m_\rho^2}\right). \tag{A.1}$$

When $s \sim t \sim u \ll m_\rho^2$, the amplitude reduces to

$$A^{(0)}_{\rm ChPT}(s,t,u) = B^{(0)}_{\rm ChPT}(t,u,s) = C^{(0)}_{\rm ChPT}(u,s,t) = \frac{s-m_\pi^2}{f_\pi^2}, \tag{A.2}$$

using Eq. (2.77). This is the well-known result of ChPT in LO [18, 38]. From this the $I = 1$, $l = 1$ phase shift is found to be

$$e^{2i\delta^1_{1,\rm ChPT}(s)} = 1 + i\frac{s}{48\pi f_\pi^2}\left(1 - \frac{4m_\pi^2}{s}\right)^{3/2}, \tag{A.3}$$

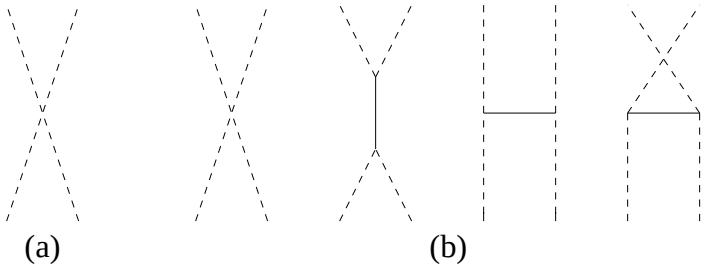

Figure A.1: LO contributions to pion-pion scattering at low energies in (a) ChPT and (b) Vector EFT.

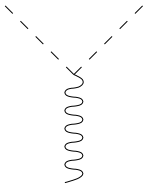

Figure A.2: LO pion form factor at low energies.

which is indicated by the thick dashed line in Fig. 2.8.

We now turn to the pion form factor, defined in Sect. 2.5.2, which appears in electromagnetic processes such as $e^+e^- \to \pi\pi$ and $e^-\pi \to e^-\pi$. At LO the pion is point-like in both ChPT and Vector EFT (away from the rho peak), and only the vertex in Fig. A.2 contributes with the pion charge. At NLO there is a tree-level contribution from photon-rho mixing given by the parameter $a_{\gamma\rho}$, and many one-loop diagrams built from the LO Lagrangian $\mathcal{L}^{(0)}$ together with other necessary counterterms from the NLO Lagrangian $\mathcal{L}^{(2)}$. As discussed in Sect. 2.3, $a_{\gamma\rho}$ itself is necessary for renormalization. With the definition in Eq. (2.102),

$$F_\pi(q^2) = 1 - \frac{q^2}{(4\pi f_\pi)^2}\left[\frac{a_{\gamma\rho} m_\rho^2}{q^2 - m_\rho^2} + L\left(\frac{q^2}{m_\rho^2}, \frac{m_\pi^2}{m_\rho^2}\right)\right] + \ldots, \tag{A.4}$$

where L is a complicated function and "..." are higher-order terms. The tree-level form is characteristic of the VMD-1 model with $g_{\rho\pi\pi}/g_\rho = a_{\gamma\rho} m_\rho^2/(4\pi f_\pi)^2 = a_{\gamma\rho}(g/4\pi)^2$. Complete vector-meson dominance [49] would follow from $a_{\gamma\rho} = (4\pi/g)^2 \simeq 2.6$ and $L(0, m_\pi^2/m_\rho^2) = 0$.

For $|q^2| \ll m_\rho^2$, one regains the trivial ChPT LO result, which in terms of the $e^+e^- \to \pi\pi$ cross section is just

$$\sigma^{(0)}_{\rm chpt} = \frac{\pi\alpha^2}{3s}\left(1 - \frac{4m_\pi^2}{s}\right)^{3/2}, \tag{A.5}$$

as shown by the thick dashed line in Fig. 2.7. While accounting for NLO and NNLO corrections improves the ChPT description of the low-energy data [69], it cannot generate the "bump" around the rho mass, which is incorporated in Vector EFT.

At NLO $a_{\gamma\rho}$ gives a contribution to the pion charge radius,

$$\langle r^2\rangle_\pi = \frac{6a_{\gamma\rho}}{(4\pi f_\pi)^2} + \dots \tag{A.6}$$

If $a_{\gamma\rho} = (4\pi/g)^2$, the tree-level rho contribution would acquire the complete vector-meson dominance form $\langle r^2\rangle_\pi = 6/m_\rho^2$ [49]. Using instead the value $a_{\gamma\rho} = 1.484$ found in the main text, we obtain for this contribution $\langle r^2\rangle_\pi = 0.25$ fm^2, which is almost a half compared to the extraction $\langle r^2\rangle_\pi = 0.437 \pm 0.016$ fm^2 [69] from low-energy data. This lack of agreement is seen in Fig. 2.7, where Vector EFT does a decent job in describing the cross section at low energies. This is a manifestation of the well-known vector-meson dominance of the form factor. The difference can be accounted for a relatively small vertex counterterm.

APPENDIX B

PION SELF-ENERGY

Chiral symmetry demands that the pion mass vanishes when the quark mass is set to zero. While that is evident in Vector EFT at the Lagrangian level (Sect. 2.2), we would like to check that it is preserved quantum-mechanically. Here we do this by calculating the pion self-energy at one-loop level. We continue to use dimensional regularization, now defining

$$L_\pi = \frac{2}{4-d} - \gamma + \ln \frac{4\pi\mu^2}{m_\pi^2}. \tag{B.1}$$

We denote the bare pion propagator by iK, with

$$K(p^2) = \frac{1}{p^2 - m_\pi^2 + i\epsilon}, \tag{B.2}$$

and the pion self-energy by $-i\Sigma$. Diagrams contributing to the pion self-energy in Vector EFT are shown in Fig. B.1. The dressed pion propagator is

$$\begin{aligned} D(p^2) &= K(p^2) + K(p^2)\Sigma(p^2)K(p^2) + K(p^2)\Sigma(p^2)K(p^2)\Sigma(p^2)K(p^2) + \ldots \\ &= \frac{1}{p^2 - m_\pi^2 - \Sigma(p^2)}, \end{aligned} \tag{B.3}$$

as represented in Fig. B.2. The pole of the pion propagator defines the physical (observable) mass of the pion,

$$m_\pi^{(R)2} = m_\pi^2 + \Sigma(m_\pi^2). \tag{B.4}$$

Chiral symmetry requires $\Sigma(0) = 0$.

Calculating the one-loop diagrams shown explicitly in Fig. B.1,

$$\begin{aligned} \Sigma(p^2) &= \left(\frac{m_\rho}{4\pi f_\pi}\right)^2 \left[-\frac{m_\pi^2 p^2}{6m_\rho^2}\left(1 - \frac{4m_\pi^2}{p^2}\right)(L_\pi + 1) + \frac{1}{2}\left(3p^2 - \frac{(p^2 - m_\pi^2)^2}{m_\rho^2}\right) L_\rho \right. \\ &\quad + \left(2m_\pi^2 + 2p^2 - m_\rho^2 - \frac{(p^2 - m_\pi^2)^2}{m_\rho^2}\right) \tilde{J}(p^2) - m_\pi^2 \ln \frac{m_\rho^2}{m_\pi^2} \\ &\quad \left. + 5p^2 + 2m_\pi^2 - m_\rho^2 - 2\frac{(p^2 - m_\pi^2)^2}{m_\rho^2} \right], \end{aligned} \tag{B.5}$$

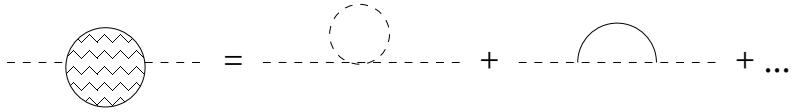

Figure B.1: Pion self-energy $-i\Sigma$ in Vector EFT.

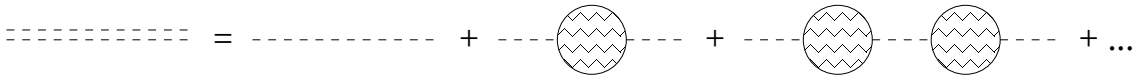

Figure B.2: Dressed pion propagator iD in terms of multiple insertions of the pion self-energy.

where

$$\tilde{J}(p^2) = \begin{cases} -\frac{1}{p^2}\left[(m_\rho^2 - m_\pi^2 - p^2)\ln\frac{m_\rho}{m_\pi}\right. \\ +m_\rho^2\sqrt{-\tilde{\lambda}}\left(\tan^{-1}\left(\frac{\sqrt{-\tilde{\lambda}}}{1+\frac{m_\pi^2}{m_\rho^2}-\frac{p^2}{m_\rho^2}}\right)\right. \\ \left.\left.+\pi\Theta(p^2 - m_\rho^2 - m_\pi^2)\right)\right] \\ \qquad \text{if } (m_\rho - m_\pi)^2 < p^2 < (m_\rho + m_\pi)^2, \\ \\ -\frac{1}{p^2}\left[(m_\rho^2 - m_\pi^2 - p^2)\ln\frac{m_\rho}{m_\pi}\right. \\ -\frac{m_\rho^2\sqrt{\tilde{\lambda}}}{2}\ln\left(\frac{1+\frac{m_\pi^2}{m_\rho^2}-\frac{p^2}{m_\rho^2}+\sqrt{\tilde{\lambda}}}{1+\frac{m_\pi^2}{m_\rho^2}-\frac{p^2}{m_\rho^2}-\sqrt{\tilde{\lambda}}}\right) \\ \left.-i\pi m_\rho^2\sqrt{\tilde{\lambda}}\Theta\left(p^2 - (m_\rho + m_\pi)^2\right)\right] \\ \qquad \text{if } p^2 \le (m_\rho - m_\pi)^2 \text{ and } p^2 \ge (m_\rho + m_\pi)^2, \end{cases} \tag{B.6}$$

with

$$\tilde{\lambda} = 1 + \frac{m_\pi^4}{m_\rho^4} + \frac{p^4}{m_\rho^4} - 2\frac{m_\pi^2 p^2}{m_\rho^4} - 2\frac{m_\pi^2}{m_\rho^2} - 2\frac{p^2}{m_\rho^2}. \tag{B.7}$$

Chiral symmetry can be verified by integrating the rho meson out of Vector EFT, *i.e.* $m_\rho \gg m_\pi^2$. In this limit $\tilde{J}(p^2)$ can be written as

$$\tilde{J}(p^2) \;=\; -\left(1 + \frac{m_\pi^2}{2m_\rho^2}\right)\left(1 - \frac{p^2 + m_\pi^2 + 2p^2 m_\pi^2/m_\rho^2}{m_\rho^2}\right) - \frac{m_\pi^2}{m_\rho^2}\ln\frac{m_\rho^2}{m_\pi^2}, \tag{B.8}$$

then

$$\Sigma(p^2) = \Sigma_{\rm ChPT}(p^2) + \left(\frac{m_\rho}{4\pi f_\pi}\right)^2 \frac{1}{2}\left(3p^2 - \frac{\left(p^2-m_\pi^2\right)^2}{m_\rho^2}\right)(L_\rho+1)$$
$$-[\left(\frac{m_\pi}{4\pi f_\pi}\right)^2 \left[\left(p^2+m_\pi^2\right)\ln\frac{m_\rho^2}{m_\pi^2} + \mathcal{O}\left(\frac{m_\rho^2}{m_\pi^2}\right) \times \text{finite polynomials}\right] \quad \text{(B.9)}$$

where

$$\Sigma_{\rm ChPT}(p^2) = -\left(\frac{m_\pi}{4\pi f_\pi}\right)^2 \frac{4p^2}{6}\left(1-\frac{m_\pi^2}{4p^2}\right)(L_\pi+1)\,, \quad \text{(B.10)}$$

see Ref. [64] for details. It is clear that when the bare mass of the pion goes to zero, $m_\pi^2 = 0$, the pion self-energy in ChPT and in Vector EFT, $\Sigma_{\rm ChPT}(m_\pi^2)$ and $\Sigma(m_\pi^2)$, also go to zero preserving chiral symmetry. Again Eqs. (B.5) and (B.9) are not manifestly renormalizable due to the fact that fields are redefined in unitary gauge, but this is not a problem since the observable, pion mass, is renormalizable.

APPENDIX C

DECAYS OF THE RHO

In this appendix, we confirm the expressions associated with the partial widths of the rho into two pions, $\Gamma_{\pi\pi}$ (2.69), and into an electron-positron pair, Γ_{ee} (2.106), which can be obtained from the decay of an on-shell rho.

We denote the four-momentum, isospin, and polarization of the decaying rho by p, a and ε^μ, respectively. The four-momenta of the decay products are denoted by $p_3^\mu = (E_3, \boldsymbol{p}_3)$ and $p_4^\mu = (E_4, \boldsymbol{p}_4)$. The differential decay width, like the cross section, can be written in terms of an amplitude $\mathcal{T}$ [68],

$$d\Gamma_{\text{pol.}} = \frac{(2\pi)^4}{2m_\rho \mathcal{S}!} |\mathcal{T}\left(p, p_3, p_4\right)|^2 \frac{d^3p_3 d^3p_4}{(2\pi)^3 2E_3 (2\pi)^3 2E_4} \delta^4(p - p_3 - p_4), \tag{C.1}$$

where $\mathcal{S} = 2$ is the number of identical particles in the final state, and which in the rest frame of the rho is

$$d\Gamma_{\text{unpol.}} = \frac{|\boldsymbol{p_3}|}{64\pi^2 m_\rho^2} |\mathcal{T}\left(p, p_3, p_4\right)|^2 d\Omega. \tag{C.2}$$

C.1 $\rho \to \pi\pi$

In the case of $\rho \to \pi\pi$, the pions are characterized by isospin indices a_3 and a_4 and momentum p_3 and p_4. In LO, the only contribution comes from Fig. C.1(a). The invariant amplitude is

$$\mathcal{T}^{(0)\mu a a_3 a_4}_{\pi\pi\,\text{pol.}}(p_3, p_4) = \frac{g}{2f_\pi} \epsilon^{a a_4 a_4} (p_4 - p_3)^\mu, \tag{C.3}$$

where a is the isospin of the rho. Since $p_4 - p_3$ does not depend on the scattering angle

$$\Gamma^{(0)}_{\pi\pi\,\text{unpol.}}(p_3, p_4) = \frac{|\boldsymbol{p_3}|}{16\pi m_\rho^2} \frac{1}{3} \sum_{i=1}^{3} \left| \mathcal{T}_\mu^{a a_3 a_4}\left(p_3, p_4\right) \epsilon^{\mu * i} \right|^2, \tag{C.4}$$

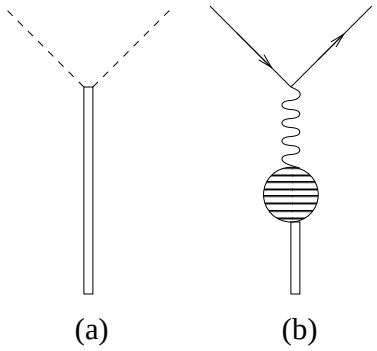

Figure C.1: Decays (a) $\rho \to \pi\pi$ and (b) $\rho \to e^+e^-$ at LO.

where a is fixed and a_3 and a_4 are summed, see Eq. (2.100). In the CM frame the rho is at rest and its polarizations simply are

$$\epsilon^{\mu 1} = (0,1,0,0)\,, \qquad \epsilon^{\mu 2} = (0,0,1,0)\,, \qquad \epsilon^{\mu 3} = (0,0,0,1)\,. \tag{C.5}$$

The partial width of the rho into two pions becomes

$$\Gamma^{(0)}_{\pi\pi}(s) = \frac{\pi}{12}\frac{s\sqrt{s}}{m_\rho^2}\left(\frac{m_\rho}{4\pi f_\pi}\right)^2\left(1-\frac{4m_\pi^2}{s}\right)^{3/2}, \tag{C.6}$$

which for $s = m_\rho^2$ reduces to Eq. (2.69). Equations (C.6) and (2.69) match the ones in Refs. [60, 71].

C.2 $\rho \to e^+e^-$

In the case of $\rho \to e^+e^-$, the electron and positron are characterized by spins s_3 and s_4 and momentum p_3 and p_4. In LO, the only contribution comes from Fig. C.1(b). The invariant amplitude is

$$\begin{aligned}\mathcal{T}^{(0)}_{\nu ee}(p_3,s_3,p_4,s_4) &= -\frac{2e^2 f_\pi}{s}\left(a^{(R)} m_\rho\left(\frac{m_\rho}{4\pi f_\pi}\right)^2 + i2\Gamma^{(0)}_{\pi\pi}\left(m_\rho^2\right)\right)\bar{v}_e(p_3,s_3)\gamma^\lambda u_e(p_4,s_4)\\ &\quad\left(\eta_{\nu\lambda} - \frac{(p_3+p_4)_\nu (p_3+p_4)_\lambda}{(p_3+p_4)^2}\right),\end{aligned} \tag{C.7}$$

since the longitudinal component does not contribute. The width decay of the rho into an electron and a positron can be written, as a function of the invariant

amplitude,

$$\frac{d\Gamma_{ee\,\mathrm{unpol}}(p_3,p_4)}{d\Omega} = \frac{|\boldsymbol{p_3}|}{32\pi^2 m_\rho}\frac{1}{3}\sum_{i=1}^{3}\sum_{s_3,s_4}\left|\mathcal{T}_\nu^{(0)}(p_3,p_4)\epsilon^{*\nu i}\right|^2. \tag{C.8}$$

From Eqs. (C.5), (2.97), (2.98), (2.99), we find the partial width decay

$$\Gamma^{(0)}_{ee\,\mathrm{unpol}}(s) = \frac{\alpha^2 m_\rho^3}{3\pi s}\left(\frac{m_\rho}{4\pi f_\pi}\right)^2\left(a^{(R)2} + \frac{4\Gamma^{(0)2}_{\pi\pi}}{m_\rho^2}\left(\frac{4\pi f_\pi}{m_\rho}\right)^4\right). \tag{C.9}$$

For $s = m_\rho^2$, Eq. (C.9) becomes

$$\Gamma^{(0)}_{ee\,\mathrm{unpol}}(m_\rho^2) = \frac{\alpha^2 m_\rho}{3\pi}\left(\frac{m_\rho}{4\pi f_\pi}\right)^2\left(a^{(R)2} + \frac{4\Gamma^{(0)2}_{\pi\pi}}{m_\rho^2}\left(\frac{4\pi f_\pi}{m_\rho}\right)^4\right). \tag{C.10}$$

Equation (C.10) matches the one in Ref. [71] for

$$g_{\rho ee} = -\frac{2e^2 f_\pi}{m_\rho^2}\left(a^{(R)} m_\rho\left(\frac{m_\rho}{4\pi f_\pi}\right)^2 + i2\Gamma^{(0)}_{\pi\pi}\left(m_\rho^2\right)\right), \tag{C.11}$$

where $g_{\rho ee}$ is the coupling constant between the rho, electron and positron in Ref. [71], confirming Eq. (2.105). In the main text, the cross section was written as a function of Eq. (C.10). Again the subscript $_{\mathrm{unpol.}}$ is dropped everywhere else.

APPENDIX D

SOLUTION OF THE RUNNING EQUATION IN pNRQCD AND bHQET

The RGE in Eq. (4.57) can be solved by applying the methods discussed in Ref. [128] to find the evolution of the B-meson distribution amplitude. We generalize this approach to the specific case discussed here, where two distribution amplitudes are present. Following Ref. [128], we define

$$\omega\Gamma(\omega,\omega',\alpha_s) = -\frac{\alpha_s C_F}{\pi}\left[\theta\left(\omega-\omega'\right)\left(\frac{1}{\omega-\omega'}\right)_+ + \theta\left(\omega'-\omega\right)\theta\left(\omega\right)\frac{\omega}{\omega'}\left(\frac{1}{\omega'-\omega}\right)_+\right] .$$

Lange and Neubert [128] prove that

$$\int d\omega'\omega\Gamma(\omega,\omega',\alpha_s)(\omega')^a = \omega^a\mathcal{F}(a,\alpha_s) , \tag{D.1}$$

with

$$\mathcal{F}(a,\alpha_s) = \frac{\alpha_s C_F}{\pi}\left[\psi(1+a)+\psi(1-a)+2\gamma_E\right] .$$

ψ is the digamma function and γ_E the Euler constant. Eq. (D.1) is valid if $-1 < \mathrm{Re}\, a < 1$. Exploiting (D.1), a solution of the running equation Eq. (4.57) with initial condition $T(\omega,\bar\omega,\mu_0') = (\omega/\mu_0')^\eta\,(\bar\omega/\mu_0')^\xi$ at a certain scale μ_0' is

$$F^2(\mu')T(\omega,\bar\omega,\mu') = F^2(\mu_0')f(\omega,\mu',\mu_0',\eta)f(\bar\omega,\mu',\mu_0',\xi) , \tag{D.2}$$

with

$$\begin{aligned}
f(\omega,\mu',\mu_0',\eta) &= \left(\frac{\omega}{\mu_0'}\right)^{\eta-g}(\bar n\cdot v)^g \exp U(\mu_0',\mu',\eta) ,\\
g \equiv g(\mu_0',\mu') &= \int_{\alpha_s(\mu_0')}^{\alpha_s(\mu')}\frac{d\alpha}{\beta(\alpha)}\Gamma_{\mathrm{cusp}}(\alpha) ,\\
U(\mu_0',\mu',\eta) &= \int_{\alpha_s(\mu_0')}^{\alpha_s(\mu')}\frac{d\alpha}{\beta(\alpha)}\left[\Gamma_{\mathrm{cusp}}(\alpha)\int_{\alpha_s(\mu_0')}^{\alpha}\frac{d\alpha'}{\beta(\alpha')}+\gamma_1(\alpha)+\mathcal{F}(\eta-g,\alpha)\right] ,\\
\gamma_1(\alpha_s) &= -2\frac{\alpha_s C_F}{4\pi} .
\end{aligned} \tag{D.3}$$

The function $f(\bar\omega,\mu',\mu_0',\xi)$ has the same form as $f(\omega,\mu',\mu_0',\eta)$ and is obtained by replacing $\omega\to\bar\omega$, $\eta\to\xi$, and $\bar n\cdot v\to n\cdot v'$ in Eq. (D.3). The integrals over α can be performed explicitly using the beta function in Eq. (4.28). The result is

$$\begin{aligned} f(\omega,\mu',\mu_0',\eta)f(\bar\omega,\mu',\mu_0',\xi) = &\left(\frac{\omega}{\mu_0'}\right)^{\eta-g}\left(\frac{\bar\omega}{\mu_0'}\right)^{\xi-g}(\bar n\cdot v\, n\cdot v')^g \exp\left[V(\mu_0',\mu')\right] \\ &\frac{\Gamma(1-\eta+g)\Gamma(1+\eta)}{\Gamma(1+\eta-g)\Gamma(1-\eta)}\frac{\Gamma(1-\xi+g)\Gamma(1+\xi)}{\Gamma(1+\xi-g)\Gamma(1-\xi)}\,, \end{aligned} \tag{D.4}$$

Where, at NLL,

$$g(\mu_0',\mu') = -\frac{\Gamma^{(0)}_{\rm cusp}}{2\beta_0}\left\{\ln r + \left(\frac{\Gamma^{(1)}_{\rm cusp}}{\Gamma^{(0)}_{\rm cusp}}-\frac{\beta_1}{\beta_0}\right)\frac{\alpha_{\rm s}(\mu_0')}{4\pi}(r-1)\right\}\,, \tag{D.5}$$

and

$$\begin{aligned} V(\mu_0',\mu') = &-\Gamma^{(0)}_{\rm cusp}\frac{2\pi}{\beta_0^2}\left\{\frac{r-1-r\ln r}{\alpha_s(\mu')}+\left(\frac{\Gamma^{(1)}_{\rm cusp}}{\Gamma^{(0)}_{\rm cusp}}-\frac{\beta_1}{\beta_0}\right)\frac{1-r+\ln r}{4\pi}+\frac{\beta_1}{8\pi\beta_0}\ln^2 r\right\} \\ &+\frac{C_F}{\beta_0}(2-8\gamma_E)\ln r\,, \end{aligned} \tag{D.6}$$

with $r=\alpha_s(\mu')/\alpha_s(\mu_0')$. Notice that in the running from $\mu_0'=m_c$ to $\mu'=1$ GeV only three flavors are active, so in the expressions for β_0, β_1, and $\Gamma^{(1)}_{\rm cusp}$ we use $n_f=3$.

Eq. (D.4) is the solution for the initial condition $T(\omega,\bar\omega,\mu_0')=(\omega/\mu_0')^\eta\,(\bar\omega/\mu_0')^\xi$. To solve the RGE for a generic initial condition, we express T as the Fourier transform with respect to $\ln\omega/\mu_0'$,

$$\begin{aligned} T(\omega,\bar\omega,\mu_0') &= \frac{1}{(2\pi)^2}\int_{-\infty}^{+\infty} drds\exp\left(-ir\ln\frac{\omega}{\mu_0'}\right)\exp\left(-is\ln\frac{\bar\omega}{\mu_0'}\right)F[T](r,s,\mu_0') \\ &= \frac{1}{(2\pi)^2}\int_{-\infty}^{+\infty} drds\left(\frac{\omega}{\mu_0'}\right)^{-ir}\left(\frac{\bar\omega}{\mu_0'}\right)^{-is}F[T](r,s,\mu_0')\,, \end{aligned}$$

where $F[T]$ denotes the Fourier transform of T. From the solution (D.2)-(D.4) it follows that

$$\begin{aligned} F^2(\mu')T(\omega,\bar\omega,\mu') = &\frac{F^2(\mu_0')}{(2\pi)^2}\int_{-\infty}^{+\infty} drds\left(\frac{\omega}{\mu_0'}\right)^{-ir-g}\left(\frac{\bar\omega}{\mu_0'}\right)^{-is-g}(\bar n\cdot v\, n\cdot v')^g \\ &F[T](r,s,\mu_0')\exp\left[V(\mu_0',\mu')\right]\frac{\Gamma(1+ir+g)\Gamma(1-ir)}{\Gamma(1-ir-g)\Gamma(1+ir)}\frac{\Gamma(1+is+g)\Gamma(1-is)}{\Gamma(1-is-g)\Gamma(1+is)}\,. \end{aligned} \tag{D.7}$$

The Fourier transform of the matching coefficient in Eq. (D.7) has to be understood in the sense of distributions [147]. That is, we define the Fourier transform of T as the function of r and s that satisfies

$$\frac{1}{(2\pi)^2}\int dr ds\, F[T](r,s,\mu')\varphi_A(r,\mu')\varphi_B(s,\mu') = \int_0^{+\infty}\frac{d\omega}{\omega}\frac{d\bar{\omega}}{\bar{\omega}}T(\omega,\bar{\omega},\mu')\phi_A(\omega,\mu')\phi_B(\bar{\omega},\mu')\ , \tag{D.8}$$

or, more precisely, $F[T](r,s,\mu')$ is the linear functional that acts on the test functions $\varphi_A(r)$ and $\varphi_B(s)$ according to

$$\frac{1}{(2\pi)^2}(F[T](r,s,\mu'),\, \varphi_A(r,\mu')\varphi_B(s,\mu')) = \int_0^{+\infty}\frac{d\omega}{\omega}\frac{d\bar{\omega}}{\bar{\omega}}T(\omega,\bar{\omega},\mu')\phi_A(\omega,\mu')\phi_B(\bar{\omega},\mu')\ . \tag{D.9}$$

The function φ_A is the Fourier transform of the D-meson distribution amplitude,

$$\varphi_A(r,\mu') = \int_0^{\infty}\frac{d\omega}{\omega}\left(\frac{\omega}{\mu'}\right)^{ir}\phi_A(\omega,\mu')\ , \tag{D.10}$$

where the integral on the r.h.s. should converge in the ordinary sense because of the regularity properties of the D-meson distribution amplitude. As in Sec. 4.4, the subscript A denotes the spin and polarization of the D meson.

In the distribution sense, the Fourier transform of the coefficient $1/(\omega+\bar{\omega})$ is

$$\begin{aligned} F\left[\frac{1}{\omega+\bar{\omega}}\right](r,s,\mu_0') &= (2\pi)^2\frac{1}{2\mu_0'}\delta(r+s+i)\,\mathrm{sech}\left[\frac{\pi}{2}(r-s)\right] \\ &= \frac{1}{2}(2\pi)^2\frac{1}{2\mu_0'}\delta(R+i)\,\mathrm{sech}\left[\frac{\pi}{2}S\right]\ , \end{aligned} \tag{D.11}$$

where $R=r+s$, $S=r-s$, and the factor $\frac{1}{2}$ comes from the Jacobian of the change of variables. The hyperbolic secant is defined as $\mathrm{sech}=1/\cosh$. Similarly, we find

$$F\left[\frac{\omega-\bar{\omega}}{\omega+\bar{\omega}}\right](R,S,\mu_0') = \frac{i}{2}(2\pi)^2\delta(R)\left(\mathrm{cosech}\left[\frac{\pi}{2}S+i\varepsilon\right]+\mathrm{cosech}\left[\frac{\pi}{2}S-i\varepsilon\right]\right)\ . \tag{D.12}$$

The δ function in Eq. (D.11) has complex argument. The definition is analogous to the one in real space [147],

$$(\delta(R+i),\varphi(R)) = \varphi(-i)\ . \tag{D.13}$$

Using Eqs. (D.11) and (D.12), we can perform the integral in Eq. (D.7), obtaining respectively $T(\omega,\bar{\omega},\mu,\mu';\,^3P_J)$ and $T(\omega,\bar{\omega},\mu,\mu';\,^1S_0)$. In order to give an explicit example, we proceed using Eq. (D.11). Integrating the δ function we are left with

$$\begin{aligned} F^2(\mu')T(\omega,\bar{\omega};\mu') &= F^2(\mu'_0)\exp\left[V(\mu'_0,\mu')\right]\frac{1}{\mu'_0}\left(\frac{\mu'^2_0}{\omega\bar{\omega}}\right)^{1/2+g}(\bar{n}\cdot v\,n\cdot v')^g \\ &\int_{-\infty}^{\infty}dS\exp\left[-i\frac{S}{2}\ln\frac{\omega}{\bar{\omega}}\right]\mathrm{sech}\left[\frac{\pi}{2}S\right]\frac{1}{1+S^2}\frac{\Gamma\left(\frac{3}{2}+g+\frac{i}{2}S\right)}{\Gamma\left(\frac{1}{2}-g-\frac{i}{2}S\right)}\frac{\Gamma\left(\frac{3}{2}+g-\frac{i}{2}S\right)}{\Gamma\left(\frac{1}{2}-g+\frac{i}{2}S\right)}\,. \end{aligned} \tag{D.14}$$

The integral (D.14) can be done by contour. The integrand has poles along the imaginary axis. In $S=\pm i$ there is a double pole, coming from the coincidence of one pole of the hyperbolic secant and the singularities in $1/(1+S^2)$. The Γ functions in the numerator have poles respectively in $S=\pm i\,(2n+3+2g)$ with $n>0$, while the other poles of sech are in $S=\pm i(2n+1)$, with $n\geq 1$. We close the contour in the upper half plane for $\bar{\omega}>\omega$ and in the lower half plan for $\omega>\bar{\omega}$, obtaining

$$\begin{aligned} F^2(\mu')T(\omega,\bar{\omega},\mu') &= F^2(\mu'_0)\exp\left[V(\mu'_0,\mu')\right]\,\theta(\bar{\omega}-\omega)\frac{1}{\bar{\omega}}\left(\frac{\mu'^2_0\bar{n}\cdot v\,n\cdot v'}{\omega\bar{\omega}}\right)^g \\ &\left\{\frac{\Gamma(1+g)\Gamma(2+g)}{\Gamma(1-g)\Gamma(-g)}\left[1-\ln\frac{\omega}{\bar{\omega}}+\psi(1-g)-\psi(-g)+\psi(1+g)-\psi(2+g)\right]\right. \\ &+\sum_{n=1}^{\infty}(-)^{n+1}\left(\frac{\omega}{\bar{\omega}}\right)^n\frac{1}{n(n+1)}\frac{\Gamma(1-n+g)\Gamma(2+n+g)}{\Gamma(-n-g)\Gamma(1-g+n)} \\ &\left.-\sum_{n=1}^{\infty}\left(\frac{\omega}{\bar{\omega}}\right)^{n+g}\frac{\pi}{(n-1)!}\csc(g\pi)\frac{1}{(n+g)(1+n+g)}\frac{\Gamma(2+n+2g)}{\Gamma(1+n)\Gamma(-n-2g)}\right\} \\ &+(\omega\to\bar{\omega})\ , \end{aligned} \tag{D.15}$$

with $\csc(g\pi)=1/\sin(g\pi)$ and ψ is the digamma function. More compactly, we can

express Eq. (D.15) using the hypergeometric functions ${}_4F_3$ and ${}_3F_2$,

$$
\begin{aligned}
&F^2(\mu')\,T(\omega,\bar\omega,\mu,\mu';\,{}^3P_J) = F^2(\mu'_c)\frac{C_F}{N_c^2}\frac{4\pi\alpha_s(\mu'_c)}{m_b}\exp\left[V(\mu'_c,\mu')\right]\,\left(\frac{\mu_c'^2\bar n\cdot v n\cdot v'}{\omega\,\bar\omega}\right)^g\\
&\frac{\theta(\bar\omega-\omega)}{\bar\omega}\left\{\frac{\Gamma(1+g)\Gamma(2+g)}{\Gamma(1-g)\Gamma(-g)}\left[1-\ln\frac{\omega}{\bar\omega}+\psi(1-g)-\psi(-g)+\psi(1+g)-\psi(2+g)\right]\right.\\
&+\frac{1}{2}\frac{\omega}{\bar\omega}\,\frac{\Gamma(g+2)\Gamma(g+3)}{\Gamma(1-g)\Gamma(2-g)}\,{}_4F_3\left(1,1,g+2,g+3;3,1-g,2-g;-\frac{\omega}{\bar\omega}\right)\\
&\left.-\left(\frac{\omega}{\bar\omega}\right)^{1+g}4\cos(g\pi)\frac{\Gamma(2+2g)^2}{g+2}\,{}_3F_2\left(g+1,2g+2,2g+3;2,g+3;-\frac{\omega}{\bar\omega}\right)\right\}\\
&+(\omega\to\bar\omega)\ ,
\end{aligned}
\tag{D.16}
$$

where we have introduced the constants that appear in the initial condition in Eq. (4.33). In the same way, we obtain

$$
\begin{aligned}
&F^2(\mu')\,T(\omega,\bar\omega,\mu,\mu';\,{}^1S_0) = F^2(\mu'_c)\frac{C_F}{2N_c^2}\frac{4\pi\alpha_s(\mu'_c)}{m_b}\exp\left[V(\mu'_c,\mu')\right]\,\theta(\bar\omega-\omega)\\
&\left(\frac{\mu_c'^2\bar n\cdot v n\cdot v'}{\omega\,\bar\omega}\right)^g\left\{2\frac{\Gamma(1+g)\Gamma(2+g)}{\Gamma(1-g)\Gamma(2-g)}\frac{\omega}{\bar\omega}\,{}_3F_2\left(1,g+1,g+2;1-g,2-g;-\frac{\omega}{\bar\omega}\right)\right.\\
&\left.+\frac{\Gamma^2(1+g)}{\Gamma^2(1-g)}-\left(\frac{\omega}{\bar\omega}\right)^{1+g}4\cos(g\pi)\Gamma(1+2g)\Gamma(2g+2)\,{}_2F_1\left(2g+2,2g+1;2;-\frac{\omega}{\bar\omega}\right)\right\}\\
&-(\omega\to\bar\omega)\ .
\end{aligned}
\tag{D.17}
$$

In Eqs. (D.16) and (D.17) we renamed the initial scale $\mu'_0=\mu'_c$ to denote its connection to the scale m_c. Setting $\mu'=\mu'_c$ or, equivalently, $g=0$, it can be explicitly verified that the solutions Eqs. (D.16) and (D.17) satisfy the initial conditions Eq. (4.33).

APPENDIX E

BOOST TRANSFORMATION OF THE D-MESON DISTRIBUTION AMPLITUDE

We derive in this Appendix the relation between the distribution amplitudes in the D-meson and in the bottomonium rest frames, as given in Eq. (4.60). In the D-meson rest frame, characterized by the velocity label $v_0 = (1, 0, 0, 0)$, the local heavy-light matrix element is defined as

$$\langle 0|\bar{\xi}_n^{\bar{l}}(0)\frac{\bar{n}\!\!\!/}{2}\gamma_5\, h_n^c(0)|D\rangle_{v_0} = -iF(\mu')\frac{\bar{n}\cdot v_0}{2}\ . \tag{E.1}$$

The matrix element of the heavy- and light-quark fields at a light-like separation $z_0^\mu = n\cdot z_0\,\bar{n}^\mu/2$ defines the light-cone distribution $\tilde{\phi}_0(n\cdot z_0,\mu')$ in coordinate space:

$$\langle 0|\bar{\chi}_n^{\bar{l}}(n\cdot z_0)\,\frac{\bar{n}\!\!\!/}{2}\gamma_5\,\mathcal{H}_n^c(0)|D\rangle_{v_0} = -iF(\mu')\frac{\bar{n}\cdot v_0}{2}\,\tilde{\phi}_0(n\cdot z_0,\mu')\ . \tag{E.2}$$

Eqs. (E.1) and (E.2) imply $\tilde{\phi}_0(0,\mu') = 1$. In the definitions (E.1) and (E.2) the subscript 0 is used to denote quantities in the D-meson rest frame. This convention is used in the rest of this Appendix. In the bottomonium rest frame, where the velocity label in light-cone coordinates is $v = (n\cdot v, \bar{n}\cdot v, 0)$ and the light-like separation is $z^\mu = n\cdot z\,\bar{n}^\mu/2$, we define

$$\langle 0|\bar{\xi}_n^{\bar{l}}(0)\frac{\bar{n}\!\!\!/}{2}\gamma_5\, h_n^c(0)|D\rangle_{v} = -iF(\mu')\frac{\bar{n}\cdot v}{2} \tag{E.3}$$

and

$$\langle 0|\bar{\chi}_n^{\bar{l}}(n\cdot z)\,\frac{\bar{n}\!\!\!/}{2}\gamma_5\,\mathcal{H}_n^c(0)|D\rangle_{v} = -iF(\mu')\frac{\bar{n}\cdot v}{2}\,\tilde{\phi}(n\cdot z,\mu')\ . \tag{E.4}$$

Suppose that Λ is some standardized boost that takes the D meson from v, its velocity in the bottomonium rest frame, to rest. It is straightforward to find the relations between the D-meson momenta in the two frames:

$$n\cdot p_0 = \bar{n}\cdot v\, n\cdot p \quad \text{and} \quad \bar{n}\cdot p_0 = n\cdot v\,\bar{n}\cdot p\ .$$

There is a similar relation for the light-cone coordinates,

$$n \cdot z_0 = \bar{n} \cdot v \, n \cdot z \; .$$

With $U(\Lambda)$, the unitary operator that implements the boost Λ, one can write

$$U(\Lambda)|D\rangle_v = |D\rangle_{v_0} \; .$$

We choose Λ such that, for the Dirac fields,

$$U(\Lambda)\xi_n^{\bar{l}}(x)\, U^{-1}(\Lambda) = \Lambda_{1/2}^{-1}\, \xi^{\bar{l}}(\Lambda x) \quad \text{and} \quad U(\Lambda)h_n^c(x)\, U^{-1}(\Lambda) = \Lambda_{1/2}^{-1}\, h^c(\Lambda x) \; ,$$

where

$$\Lambda_{1/2} = \cosh\frac{\alpha}{2} + \frac{\vec{\not{n}}\not{\bar{n}} - \not{\bar{n}}\vec{\not{n}}}{4} \sinh\frac{\alpha}{2} \; ,$$

with α related to v by $e^{\alpha} = \bar{n} \cdot v$ and $e^{-\alpha} = n \cdot v$.

Now we can write the matrix element in Eq. (E.3) as

$$\begin{aligned} &\langle 0|\, \bar{\xi}_n^{\bar{l}} \frac{\vec{\not{n}}}{2} \gamma_5 h_n^c(0)|D\rangle_v \\ &\quad = \langle 0|U^{-1}(\Lambda) \left(U(\Lambda)\bar{\xi}_n^{\bar{l}}(0)U^{-1}(\Lambda) \right) \frac{\vec{\not{n}}}{2}\gamma_5 \left(U(\Lambda)h_n^c(0)U^{-1}(\Lambda) \right) U(\Lambda)|D\rangle_v \\ &\quad = \langle 0|\bar{\xi}^{\bar{l}}(0)\Lambda_{1/2}\frac{\vec{\not{n}}}{2}\gamma_5\Lambda_{1/2}^{-1}h^c(0)|D\rangle_{v_0} = \bar{n}\cdot v\, \langle 0|\bar{\xi}^{\bar{l}}(0)\frac{\vec{\not{n}}}{2}\gamma_5 h^c(0)|D\rangle_{v_0} \\ &\quad = -iF(\mu')\frac{\bar{n}\cdot v}{2}\bar{n}\cdot v_0 = -iF(\mu')\frac{\bar{n}\cdot v}{2} \; . \end{aligned} \tag{E.5}$$

where, in the last step, we have used $\bar{n} \cdot v_0 = 1$. Eq. (E.5) is thus in agreement with the definition in Eq. (E.3). Applying the same reasoning to Eq. (E.4), one finds

$$\begin{aligned} \langle 0|\bar{\chi}_n^{\bar{l}}(n\cdot z)\, \frac{\vec{\not{n}}}{2}\gamma_5\, \mathcal{H}_n^c(0)|D\rangle_v &= \bar{n}\cdot v\, \langle 0|\bar{\chi}^{\bar{l}}(\bar{n}\cdot v\, n\cdot z)\, \frac{\vec{\not{n}}}{2}\gamma_5\, \mathcal{H}^c(0)|D\rangle_{v_0} \\ &= -iF(\mu')\frac{\bar{n}\cdot v}{2}\, \tilde{\phi}_0(n\cdot z_0, \mu') \; . \end{aligned} \tag{E.6}$$

Comparing Eq. (E.6) with (E.4), we see that $\tilde{\phi}(n \cdot z, \mu') = \tilde{\phi}_0(\bar{n} \cdot v\, n \cdot z, \mu')$. Note that in the bottomonium rest frame the normalization condition for the distribution amplitude is also $\tilde{\phi}(0, \mu') = 1$.

In the main text of this chapter we have used the D-meson distribution amplitudes in momentum space,

$$\phi_0(\omega_0,\mu') \equiv \frac{1}{2\pi}\int dn\cdot z_0\, e^{i\omega_0 n\cdot z_0}\tilde{\phi}_0(n\cdot z_0,\mu')\;,$$
$$\phi(\omega,\mu') \equiv \frac{1}{2\pi}\int dn\cdot z\, e^{i\omega n\cdot z}\tilde{\phi}(n\cdot z,\mu')\;.$$

Using Eq. (E.6), we can relate the two distributions:

$$\begin{aligned}\phi(\omega,\mu') &= \frac{1}{2\pi}\int dn\cdot z\, e^{i\omega n\cdot z}\tilde{\phi}(n\cdot z,\mu') = \frac{1}{2\pi}\int dn\cdot z\, e^{i\omega n\cdot z}\tilde{\phi}_0(\bar{n}\cdot v\, n\cdot z,\mu')\\ &= \frac{1}{2\pi}\frac{1}{\bar{n}\cdot v}\int dn\cdot z\, e^{i\frac{\omega}{\bar{n}\cdot v}n\cdot z}\tilde{\phi}_0(n\cdot z,\mu') = \frac{1}{\bar{n}\cdot v}\phi_0\left(\frac{\omega}{\bar{n}\cdot v},\mu'\right)\;,\end{aligned}$$

as stated in Eq. (4.60). The D-meson light-cone distribution is normalized to 1 in both frames,

$$\int d\omega_0\phi_0(\omega_0,\mu') = \int d\omega\phi(\omega,\mu') = 1,$$

as can be easily proved using $\tilde{\phi}_0(0,\mu') = \tilde{\phi}(0,\mu') = 1$.

REFERENCES

[1] H. Georgi, Ann. Rev. Nucl. Part. Sci. **43**, 209 (1993).

[2] A. V. Manohar, [arXiv:hep-ph/9606222].

[3] D. B. Kaplan, [arXiv:nucl-th/0510023], [arXiv:nucl-th/9506035].

[4] U. van Kolck, Prog. Part. Nucl. Phys. **43**, 337 (1999).

[5] U. van Kolck, Nucl. Phys. A **699**, 33c (2002); Nucl. Phys. A **790**, 39c (2007); U. van Kolck, L. J. Abu-Raddad and D. M. Cardamone, [arXiv:nucl-th/0205058].

[6] C. A. Bertulani, H.-W. Hammer, and U. van Kolck, Nucl. Phys. A **712**, 37 (2002); P. F. Bedaque, H. -W. Hammer, and U. van Kolck, Phys. Lett. B **569**, 159 (2003).

[7] B. Long and U. van Kolck, Nucl. Phys. A **840**, 39 (2010).

[8] V. Pascalutsa and D. R. Phillips, Phys. Rev. C **67**, 055202 (2003).

[9] A. Nogga, R. G. E. Timmermans, and U. van Kolck, Phys. Rev. C **72**, 054006 (2005).

[10] K. Fujikawa, Phys. Rev. Lett. **42**, 1195 (1979).

[11] E. Jenkings and A. V. Manohar, Phys. Lett. B **255**, 558 (1991).

[12] H. Georgi, Phys. Lett. B **240**, 447 (1990).

[13] M. Luke and A. V. Manohar,, Phys. Lett. B **286**, 348 (1992).

[14] K. Nakamura *et al.* [Particle Data Group], J. Phys. G **37**, 075021 (2010); partial update edition (2012).

[15] A. Hosaka and H. Toki, "Quarks, Baryons and Chiral Symmetry", World Scientific Publishing Co. Pte. Ltd., Singapore (2001).

[16] H. Georgi, *Weak Interactions*, an updated online version (2008).

[17] S. Coleman, J. Wess, and B. Zumino, Phys. Rev. **177**, 2239 (1969); C. Callan, S. Coleman, J. Wess, and B. Zumino, Phys. Rev. **177**, 2247 (1969).

[18] S. Weinberg, Physica **96A**, 327 (1979).

[19] P. F. Bedaque and U. van Kolck, Phys. Lett. B **428**, 221 (1998).

[20] U. van Kolck, Nucl. Phys. A **645**, 273 (1999).

[21] J. W-. Chen, G. Rupak, and M. J. Savage, Nucl. Phys. A **653**, 386 (1999).

[22] S. Weinberg, Phys. Lett. B **251**, 288 (1990); Nucl. Phys. B **363**, 3 (1991).

[23] D. B. Kaplan, M. J. Savage, and M. B. Wise, Nucl. Phys. B **478**, 629 (1996); Nucl. Phys. B **534**, 329 (1998); Phys. Lett. B **424**, 390 (1998).

[24] E. Epelbaum and U. -G. Meißner,[arXiv:nucl-th/9903046]; X. Kong and F. Ravndal, Nucl. Phys. A **656**, 421 (1999); Phys. Lett. B**450**, 320 (1999); Phys. Lett. B**470**, 1 (1999); D. B. Kaplan, M. J. Savage, and M. B. Wise, Phys. Rev. C **59**, 617 (1999); J. -W. Chen *at. al.*, Nucl. Phys. A **644**, 221 (1998); J. -W. Chen, G. Rupak, and M. J. Savage, Phys. Lett. B**464**, 1 (1999); J. -W. Chen, H. W. Griesshammer, M. J. Savage, and R. P. Springer, Nucl. Phys. A **644**, 245 (1998); J. -W. Chen, Nucl. Phys. A **653**, 375 (1999); M. Butler and J. -W. Chen, Nucl. Phys. A **675**, 575 (2000); M. J. Savage, K. A. Scaldeferri, and M. B. Wise, Nucl. Phys. A **652**, 273 (1999); D. B. Kaplan, M. J. Savage, and R. P. Springer, Phys. Lett. B**449**, 1 (1999); M. J. Savage and R. P. Springer, Nucl. Phys. A **644**, 235 (1998); P. F. Bedaque and H. W. Griesshammer, Nucl. Phys. A **671**, 357 (2000).

[25] S. Fleming, T. Mehen, and I. W. Stewart, Phys. Rev. C **61**, 044005 (2000); Nucl. Phys. A **677**, 313 (2000).

[26] W. M. Frank and D. J. Land, Rev. Mod. Phys. **43**, 36 (1971); S. R. Beane, P. F. Bedaque, L. Childress, A. Kryjevski, J. McGuire, and U. van Kolck, Phys. Rev. A **64**, 042103 (2001);

[27] S. R. Beane, P. F. Bedaque, M. J. Savage, and U. van Kolck, Nucl. Phys. A **700**, 377 (2002).

[28] C. W. Bauer, S. Fleming, D. Pirjol, and I. W. Stewart, Phys. Rev. D **63**, 114020 (2001).

[29] C. W. Bauer and I. W. Stewart, Phys. Rev. B **516**, 134 (2001).

[30] C. W. Bauer, D. Pirjol and I. W. Stewart, Phys. Rev. D **66**, 054005 (2002).

[31] C. W. Bauer, D. Pirjol and I. W. Stewart, Phys. Rev. D **65**, 054022 (2002).

[32] R. van der Leeuw, *Soft-Collinear Effective Theory*, Universiteit Utrecht, Utrecht, The Netherlands (2008).

[33] J. Chay and C. Kim, Phys. Rev. D **65**, 114016 (2002).

[34] M. Beneke, A. P. Chapovsky, M. Diehl and T. Feldmann, Nucl. Phys. B **643**, 431 (2002); M. Beneke and T. Feldmann, Phys. Lett. B **553**, 267 (2003).

[35] R. J. Hill and M. Neubert, Nucl. Phys. B **657**, 229 (2003).

[36] R. S. Azevedo, B. Long and E. Mereghetti, Phys. Rev. **D80**, 074026 (2009).

[37] A. Manohar and H. Georgi, Nucl. Phys. B **234**, 189 (1984).

[38] J. Gasser and H. Leutwyler, Ann. Phys. **158**, 142 (1984); Nucl. Phys. B **250**, 465 (1985).

[39] V. Bernard, N. Kaiser, and U.-G. Meißner, Int. J. Mod. Phys. E **4**,193 (1995); V. Bernard, Prog. Part. Nucl. Phys. **60**, 82 (2008).

[40] E. Epelbaum, Prog. Part. Nucl. Phys. **57**, 654 (2006).

[41] J. F. Donoghue, C. Ramirez, and G. Valencia, Phys. Rev. D **39**, 1947 (1989).

[42] J. Borges, Nucl. Phys. B **51**, 189 (1973); J. Sá Borges, J. Soares Barbosa, and V. Oguri, Phys. Lett. B **393**, 413 (1997).

[43] T. N. Truong, Phys. Rev. Lett. **61**, 2529 (1988) 2529; A. Dobado, M.J. Herrero, and T.N. Truong, Phys. Lett. B **235**, 134 (1990).

[44] S. R. Beane and C. B. Chiu, [arXiv:hep-ph/9303254]; J. Nieves and E. Ruiz Arriola, Nucl. Phys. A **679**, 57 (2000).

[45] A. Dobado and J. R. Peláez, Phys. Rev. D **56**, 3057 (1997); A. Gómez Nicola, F. J. Llanes-Estrada, and J. R. Peláez, Phys. Lett. B **606**, 351 (2005).

[46] J. A. Oller and E. Oset, Phys. Rev. D **60**, 074023 (1999); J. A. Oller, E. Oset, and J. E. Palomar Phys. Rev. D **63**, 114009 (2001).

[47] S. Weinberg, Phys. Rev. **166**, 1568 (1968).

[48] S. Gasiorowicz and D. Geffen, Rev. Mod. Phys. **41**, 531 (1969).

[49] J. J. Sakurai, *Currents and Mesons*, University of Chicago Press, Chicago (1969).

[50] M. Bando, T. Kugo, and K. Yamawaki, Phys. Rept. **164**, 217 (1988).

[51] G. Ecker, J. Gasser, A. Pich, and E. de Rafael, Nucl. Phys. B **321**, 311 (1989).

[52] M. C. Birse, Z. Phys. A **355**, 231 (1996).

[53] H. B. O'Connell, B. C. Pierce, A. W. Thomas, and A. G. Williams, Prog. Part. Nucl. Phys. **39**, 201 (1997).

[54] I. Rosell, J. J. Sanz-Cillero, and A. Pich, JHEP **0408**, 042 (2004); A. Pich, I. Rosell, and J. J. Sanz-Cillero, JHEP **1102**, 109 (2011); S. Leupold, Phys. Rev. D **73**, 085013 (2006).

[55] H. Georgi, Phys. Rev. Lett. **63**, 1917 (1989); Nucl. Phys. B **331**, 311 (1990).

[56] G. E. Brown and M. Rho, Phys. Lett. B **338**, 301 (1994).

[57] S. Weinberg, "Unbreaking Symmetries", in *Trieste 1993, Proceedings, Salam-festschrift.*

[58] M. Piai, A. Pierce, and J. G. Wacker, [arXiv:hep-ph/0405242].

[59] K. Kawarabayashi and M. Suzuki, Phys. Rev. Lett. **16**, 255 (1966); Riazuddin and Fayyazuddin, Phys. Rev. **147**, 1071 (1966).

[60] P. Cho, Nucl. Phys. B **358**, 383 (1991).

[61] N. M. Kroll, T. D. Lee, and B. Zumino, Phys. Rev. **157**, 1376 (1967).

[62] A. R. Zerwekh, Acta Phys. Polon. **38**, 2077 (2007).

[63] S. Weinberg, Phys. Rev. Lett. **63**, 2333 (1989).

[64] S. Scherer, Adv. Nucl. Phys. **27**, 277 (2003).

[65] M. Kaku, *Quantum Field Theory A Modern Introduction*, Oxford University Press, New York (1993).

[66] G. t' Hooft, Nucl. Phys. B **33**, 173 (1971a); G. t' Hooft, Nucl. Phys. B **35**, 167 (1971b).

[67] B. R. Martin, D. Morgan and G. Shaw, *Pion-Pion Interactions in Particle Physics*, Academy Press Inc. (London)Ltd., London (1976); S. Weinberg, *The Quantum Theory of Fields, Vol. 1 Foundations*, Cambridge University Press, Revised Edition, Cambridge (2002).

[68] M. E. Peskin and D. V. Schoeder, *An Introduction to Quantum Field Theory*, Westview Press (1995).

[69] J. Bijnens, G. Colangelo, and P. Talavera, JHEP **9805**, 014 (1998).

[70] S. Weinberg, Phys. Rev. Lett. **17**, 616 (1966).

[71] F. Jegerlehner and R. Szafron, [arXiv:hep-ph/1101.2872].

[72] Akmetshin 07, Phys. Lett. B **648**, 28 (2007).

[73] Achasov 06, ZETF **130**, 437 (2006).

[74] Barkov 85, Nucl. Phys. B **256**, 365 (1985).

[75] S. D. Protopopescu, M. Alston-Garnjost, A. Barbaro-Galtieri, S. M. Flatte, J. H. Friedman, T. A. Lasinski, G. R. Lynch, M. S. Rabin, || and F. T. Solmitz, Phys. Rev. D **7**, 1279 (1973).

[76] P. Estabrooks and A. D. Martin, Nucl. Phys. B **79**, 301 (1974).

[77] S. Dubinsky, A. Korchin, N. Merenkov, G. Pancheri, O. Shekhovtsova, Eur. Phys. J. C **40**, 41 (2005).

[78] E. Epelbaum, H. Kamada, A. Nogga, H. Witala, W. Glöckle and U. - G. Meißner, Nucl. Phys. A **689**, 111 (2001).

[79] P. F. Bedaque, M. J. Savage, R. Seki and U. van Kolck, *Nuclear Physics with Effective Field Theory*, ISBN 981-02-4181-X, World Scientific (2000).

[80] T. Frederico, V. S. Timóteo, and L. Tomio, Nucl. Phys. A **653**, 209 (1999); M. P. Valderrama and E. R. Arriola, Phys. Rev. C **70**, 044006 (2004); Phys. Rev. C **72**, 054002 (2005).

[81] J. Schwinger, Phys. Rev. **61**, 387 (1942).

[82] W. Pauli and S. Kusaka, Phys. Rev. **63**, 400 (1943); J. M. Jauch and N. Hu, Phys. Rev. **65**, 289 (1944); J. M. Jauch, Phys. Rev. **67**, 125 (1945); F. C. Barker, Proc. Phys. Soc. A **63**, 898 (1950).

[83] G. Araki, Phys. Rev. **74**, 985 (1948); Prog. Theor. Phys. **3**, 442 (1948); Prog. Theor. Phys. **4**, 34 (1949).

[84] M. Sasaki, S. Nakamura, and S. Hayakawa, Prog. Theor. Phys. **3**, 454 (1948).

[85] S. Hiroishi and H. Tanaka, Prog. Theor. Phys. **4**, 231 (1949).

[86] S. Weinberg, Phys. Rev. **177**, 2604 (1969).

[87] D. B. Kaplan and M. J. Savage, Phys. Lett. B **365**, 244 (1996); D. B. Kaplan and A. V. Manohar, Phys. Rev. C **56**, 76 (1997); M. K. Banerjee, T. D. Cohen, and B. A. Gelman, Phys. Rev. C **65**, 034011 (2002); D. O. Riska, Nucl. Phys. A **710**, 55 (2002).

[88] M. M. Nagels, T. A. Rijken, and J. J. de Swart, Phys. Rev. D **17**, 768 (1978); C. Ordóñez, L. Ray, and U. van Kolck, Phys. Rev. C **53**, 2086 (1996).

[89] R. Machleidt, Adv. Nucl. Phys. **19**, 189 (1989).

[90] J. Schwinger, Phys. Rev. Lett. **18**, 923 (1967).

[91] J. Schwinger, Phys. Lett. B**24**, 473 (1967).

[92] E. Wigner, Phys. Rev. **51**, 160, 947 (1937); **56**, 519 (1939).

[93] A. Calle Cordón and E. Ruiz Arriola, [arXiv:0807.2918v1].

[94] P. F. Bedaque and U. van Kolck, Ann. Rev. Nucl. Part. Sci **52**, 339 (2002).

[95] R. Jackiw, *Delta-function potentials in two- and three- dimensional quantum mechnics. M. A. B. Beg memorial volume*, World Scientific, Singapore (1991).

[96] V. L. Chernyak and A. R. Zhitnitsky, Phys. Rept. **112**, 173 (1984).

[97] S. J. Brodsky and G. P. Lepage, Adv. Ser. Direct. High Energy Phys. **5**, 93 (1989).

[98] N. Brambilla *et al.* [Quarkonium Working Group], arXiv:hep-ph/0412158.

[99] G. T. Bodwin, E. Braaten, and G. P. Lepage, Phys. Rev. D **51**, 1125 (1995) [Erratum-ibid. D **55**, 5853 (1997)].

[100] C. W. Bauer, S. Fleming, and M. E. Luke, Phys. Rev. D **63**, 014006 (2000).

[101] C. W. Bauer, S. Fleming, D. Pirjol, I. Z. Rothstein, and I. W. Stewart, Phys. Rev. D **66**, 014017 (2002).

[102] A. K. Leibovich, Z. Ligeti, and M. B. Wise, Phys. Lett. B **564**, 231 (2003).

[103] A. Pineda and J. Soto, Nucl. Phys. Proc. Suppl. **64**, 428 (1998).

[104] N. Brambilla, A. Pineda, J. Soto, and A. Vairo, Nucl. Phys. B **566**, 275 (2000).

[105] N. Brambilla, A. Pineda, J. Soto, and A. Vairo, Rev. Mod. Phys. **77**, 1423 (2005).

[106] B. Grinstein, Nucl. Phys. B **339**, 253 (1990).

[107] E. Eichten and B. R. Hill, Phys. Lett. B **234**, 511 (1990).

[108] M. Beneke, A. P. Chapovsky, A. Signer, and G. Zanderighi, Phys. Rev. Lett. **93**, 011602 (2004).

[109] M. Beneke, A. P. Chapovsky, A. Signer, and G. Zanderighi, Nucl. Phys. B **686**, 205 (2004).

[110] S. Fleming, A. H. Hoang, S. Mantry, and I. W. Stewart, Phys. Rev. D **77**, 074010 (2008).

[111] S. Fleming, A. H. Hoang, S. Mantry, and I. W. Stewart, Phys. Rev. D **77**, 114003 (2008).

[112] G. T. Bodwin, E. Braaten, D. Kang, and J. Lee, Phys. Rev. D **76**, 054001 (2007).

[113] D. Kang, T. Kim, J. Lee, and C. Yu, Phys. Rev. D **76**, 114018 (2007).

[114] V. V. Braguta, A. K. Likhoded, and A. V. Luchinsky, arXiv:0902.0459 [hep-ph].

[115] V. V. Braguta and V. G. Kartvelishvili, arXiv:0907.2772 [hep-ph].

[116] B. Aubert *et al.* [BABAR Collaboration], Phys. Rev. Lett. **101**, 071801 (2008) [Erratum-ibid. **102**, 029901 (2009)].

[117] D. M. Asner *et al.*, Phys. Rev. D **78**, 091103 (2008).

[118] R. A. Briere *et al.* [CLEO Collaboration], Phys. Rev. D **78**, 092007 (2008).

[119] R. J. Hill, Phys. Rev. D **73**, 014012 (2006).

[120] M. E. Luke and A. V. Manohar, Phys. Rev. D **55**, 4129 (1997).

[121] M. E. Luke, A. V. Manohar, and I. Z. Rothstein, Phys. Rev. D **61**, 074025 (2000).

[122] A. V. Manohar and I. W. Stewart, Phys. Rev. D **62**, 014033 (2000).

[123] A. H. Hoang and I. W. Stewart, Phys. Rev. D **67**, 114020 (2003).

[124] A. Manohar and M. Wise, *Heavy Quark Physics*, Cambridge University Press, Cambridge (2000).

[125] A. V. Manohar and I. W. Stewart, Phys. Rev. D **76**, 074002 (2007).

[126] G. P. Korchemsky and A. V. Radyushkin, Nucl. Phys. B **283**, 342 (1987).
I. A. Korchemskaya and G. P. Korchemsky, Phys. Lett. B **287**, 169 (1992).

[127] B. I. Eisenstein *et al.* [CLEO Collaboration], arXiv:0806.2112 [hep-ex].

[128] B. O. Lange and M. Neubert, Phys. Rev. Lett. **91**, 102001 (2003).

[129] C. Amsler *et al.* [Particle Data Group], Phys. Lett. B **667**, 1 (2008).

[130] R. Barbieri, R. Gatto, R. Kogerler, and Z. Kunszt, Phys. Lett. B **57**, 455 (1975).
W. Celmaster, Phys. Rev. D **19**, 1517 (1979).

[131] G. T. Bodwin, D. K. Sinclair, and S. Kim, Phys. Rev. D **65**, 054504 (2002).

[132] E. J. Eichten and C. Quigg, Phys. Rev. D **52**, 1726 (1995).

[133] W. Buchmuller and S. H. H. Tye, Phys. Rev. D **24**, 132 (1981).

[134] V. M. Braun, D. Y. Ivanov, and G. P. Korchemsky, Phys. Rev. D **69**, 034014 (2004).

[135] A. G. Grozin and M. Neubert, Phys. Rev. D **55**, 272 (1997).

[136] M. Beneke, G. Buchalla, M. Neubert, and C. T. Sachrajda, Phys. Rev. Lett. **83**, 1914 (1999).

[137] S. J. Lee and M. Neubert, Phys. Rev. D **72**, 094028 (2005).

[138] V. Pilipp, arXiv:hep-ph/0703180.

[139] A. H. Hoang, Z. Ligeti, and A. V. Manohar, Phys. Rev. Lett. **82**, 277 (1999).

[140] Z. Ligeti, I. W. Stewart, and F. J. Tackmann, Phys. Rev. D **78**, 114014 (2008).

[141] G. T. Bodwin, E. Braaten, and G. P. Lepage, Phys. Rev. D **46**, R1914 (1992).

[142] N. Brambilla, D. Eiras, A. Pineda, J. Soto, and A. Vairo, Phys. Rev. Lett. **88**, 012003 (2002).

[143] N. Brambilla, D. Eiras, A. Pineda, J. Soto, and A. Vairo, Phys. Rev. D **67**, 034018 (2003).

[144] A. Vairo, Mod. Phys. Lett. A **19**, 253 (2004).

[145] F. Maltoni and A. D. Polosa, Phys. Rev. D **70**, 054014 (2004).

[146] S. Stracka, private communication.

[147] I. M. Gelfand and G. E. Shilov, *Generalized Functions, Vol. 1*, Academic Press, New York (1964).